THE GEOCHEMISTRY AND GEOCHRONOLOGY OF THE BONG URANIUM DEPOSIT, THELON BASIN, NUNAVUT, CANADA

by

Ryan Sharpe

A Thesis
Submitted to the Faculty of Graduate Studies of
The University of Manitoba
In Partial Fulfillment of the Requirements
For the Degree of

MASTER OF SCIENCE

Department of Geological Sciences
University of Manitoba
Winnipeg, Manitoba

Abstract

The Thelon basin, Nunavut, is similar to the uranium-producing Athabasca Basin, Saskatchewan; however, the uranium deposits associated with the Thelon Basin are poorly understood. The objective of this research is to develop a genetic model for the Bong uranium deposit, located in the Northeast Thelon region on the Kiggavik project of AREVA Resources Canada Inc. The Bong deposit formed in four stages. The first stage involved silicification of the host rocks. Stage 2 is characterized by pervasive argillization of the host rock and the formation of Stage A uraninite in veins and coating graphite (~1120 Ma). This stage is characterized by ~225°C fluids with calculated $\delta^{18}O$ and δD values of -7.9‰ and -100.9‰, respectively. During Stage 3, organic matter formed, along fractures in permeable clay-rich alteration zones. At ~1040 Ma, an oxidizing fluid event (Stage 4) reconcentrated uraninite into redox fronts (Stage B) and altered Stage A uraninite to uranophane.

Acknowledgements

I would like to extend my appreciation to everyone involved in the preparation of this thesis. First and foremost I would like to thank my advisor, Dr. Mostafa Fayek, who kept me on track and provided much insight into my work, without him this thesis would not have happened. Thank you to Dave Quirt (AREVA Resources Canada Inc.) and Charlie Jefferson (Geological Survey of Canada) who were always available for questions and provided me with pertinent literature and figures. The EPMA work was carried out under the direction of Ravinder Sidhu, who was always very helpful.

Funding for the project was from the Natural Sciences and Engineering Research Council of Canada (NSERC), Natural Resources Canada (NRCan), AREVA Resources Canada Inc., and the Canadian Foundation for Innovation (CFI).

Finally, I owe much gratitude to my wonderful friends and family, a special thanks to Shaun Gallagher for editing some of the figures. However, most important of all is my wife Lindsey, without her continual motivation I would not have finished this thesis as soon as I did, thank you for all your love and support.

Dedication

This thesis is dedicated to Margaret Trotter who passed away during the final stages of writing. You always had a keen interest in my work and helped me to stay positive during the entire process. I had hoped so dearly that you would be able to see me complete this work. However, I know that you would tell me that the process and the lessons we take away from it are more important than the end result. That is the way you lived your life. I am very grateful for the time we were able to spend together. You will be missed.

Table of Contents

List of Tables

List of Figures

List of Copyrighted Material for which Permission was Obtained

Chapter 1: Introduction

Canada is an important global supplier of uranium and currently second to Kazakhstan in uranium production (WNA, 2011). Currently, all of Canada's uranium production is from the unconformity-type uranium deposits of the Athabasca Basin in Saskatchewan. However, with new mines nearly in production (e.g., Cigar Lake), combined with increased production from existing mines such as McArthur River, Canada's production will no doubt increase production substantially in the coming years. The Canadian unconformity-type uranium deposits of the Athabasca Basin are extremely high-grade, averaging up to ~20% U (e.g., Cigar Lake, McArthur River) and they commonly average in excess of 2% U, which has led to increased exploration in areas with similar geologic and fluid histories.

The Paleoproterozoic era was marked by the formation of many economically important sedimentary basins, including the Athabasca, McArthur, and Espinhaço basins (Kyser, 2007). In terms of uranium production, the most significant of these basins is the Athabasca Basin. The Thelon Basin shares a spatial and temporal relationship to the Athabasca Basin and may prove to share similar geological relationships and, ultimately, economic potential. Although the fluid history of the Athabasca Basin has been thoroughly studied by many researchers (Hoeve & Sibbald, 1978; Hoeve & Quirt, 1984; Sibbald, 1985; Quirt, 1989; Kotzer & Kyser, 1993, 1995; Fayek & Kyser, 1997; Hecht & Cuney, 2000; Kyser *et al*., 2000; Quirt, 2001; Alexandre *et al*., 2005; Cloutier *et al*., 2009), the fluid history of the

Thelon Basin and associated basement rocks is poorly known (Renac, 2002; Hiatt *et al*., 2003; Rainbird *et al*., 2003; Hiatt *et al*., 2010; Pehrsson *et al*., 2010).

1.1 History

The Kiggavik project area (formerly called Lone Gull), which is proximal to the edge of the Thelon Basin, hosts a number of uranium deposits and prospects with an estimated uranium content of 51,000 tonnes U (AREVA, 2011). The Kiggavik deposit (Main Zone, Centre Zone, East Zone) and exploration camp are located approximately 80 km west of Baker Lake, Nunavut (Figs. 1.1, 1.2). The original prospect was discovered in 1974 when a systematic airborne radiometric survey by Urangesellschaft Canada detected mineralization at surface near the edge of the Thelon Basin (Fuchs *et al.*, 1986). The original survey was followed up by ground resistivity and gravity surveys to delineate alteration zones associated with mineralization (Hasegawa *et al.,* 1990). The Main and Centre zones of the Kiggavik deposit were drilled in 1977 (Fig. 1.3) and a pre-feasibility study was conducted in 1986 with positive results. In the late 1980s, the Bong, End, and Andrew Lake deposits were discovered. In 1993, the COGEMA Group became operator of the project. A second, more detailed, pre-feasibility study was completed in 1997 and this study concluded that the mineralization was sub-economic and would continue to be so over the medium term (Blaise *et al.*, 1997). Following this report, there was a hiatus in exploration work until 2006 when AREVA Resources Canada (formerly COGEMA Resources Inc.) decided to evaluate areas outside of the main deposits, and over the past six years, other prospective areas have been located.

Figure 1.1: Map of Canada displaying the location of the Kiggavik camp in Nunavut (Google Maps, 2012).

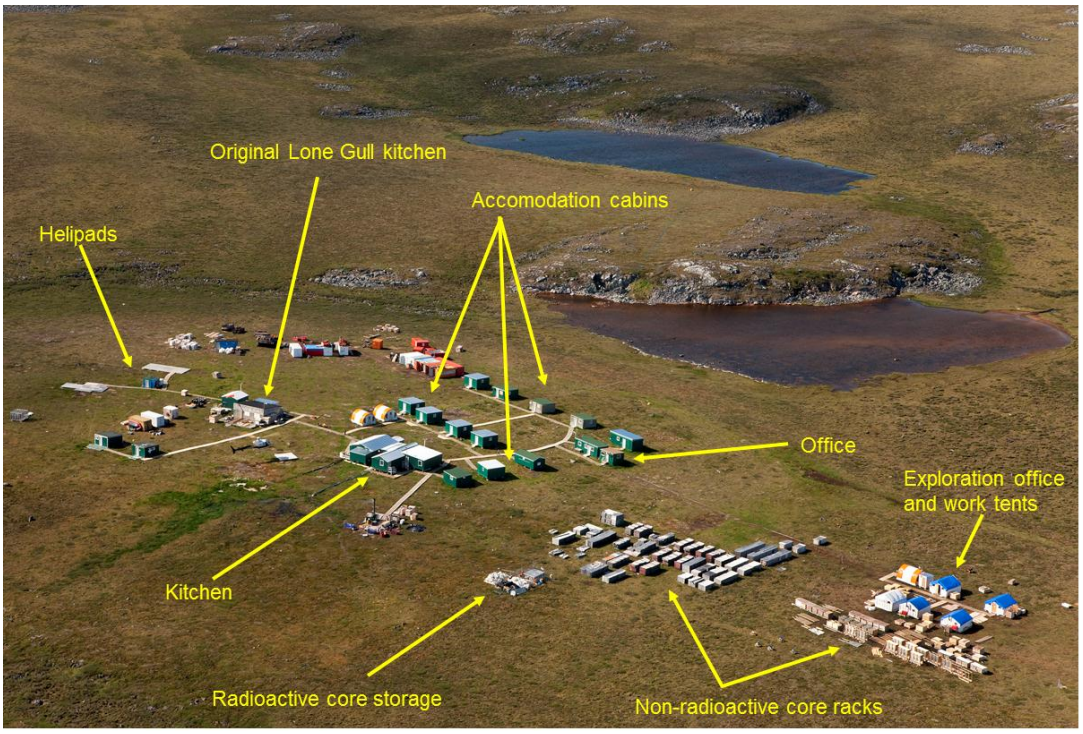

Fig. 1.2: Kiggavik camp of AREVA Resources Canada in 2010 (Quirt, 2011).

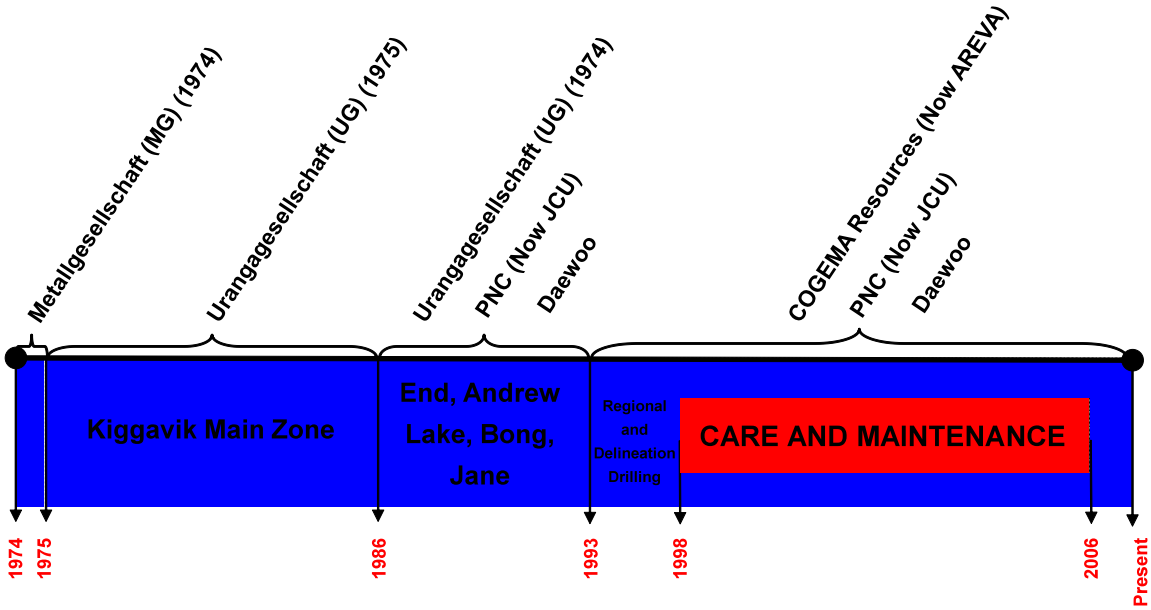

Figure 1.3: Kiggavik project history (Quirt, 2011).

1.2 Previous Work

Donaldson (1965) worked in the Thelon Basin, defining the Dubawnt Supergroup, of which the Thelon sediments are part. Since that time, much work has been done on the basin fill itself including sequence stratigraphy, diagenesis, and fluid history (Renac *et al*., 2002; Hiatt *et al.*, 2003; Rainbird *et al.,* 2003; Hiatt *et al.,* 2010; Rainbird *et al.,* 2010). However, the majority of these studies have had a very large scope, generally including the entire basin and the surrounding units.

There are few published studies that focus on the Kiggavik area (Farkas, 1984, Fuchs *et al*., 1986; Weyer *et al.,* 1987; Fuchs & Hilger, 1989). The uranium mineralization is described as being composed of pitchblende surrounded and replaced by coffinite, indicating that the deposit has been subject to remobilization (Fuchs *et al.*, 1986). Previous studies noted chlorite, hematite, and illite alteration, which highlighted the importance of redox reactions in the formation of the deposits (Fuchs *et al.,* 1986; Fuchs & Hilger, 1989). Fuchs *et al*. (1986) report K-Ar ages of 1358 Ma and 1073 Ma from intensely altered samples associated with mineralization. Farkas (1984) separated pitchblende, coffinite, and galena using a microscope, analyzed the minerals for their U/Pb isotopic ratios, and reported ages that group around 1400 Ma and 1000 Ma. Both studies concluded that the older ages are from primary mineralization and the younger ages represent a remobilization event.

1.3 Purpose and Scope of Study

The Thelon Basin has been the subject of much uranium exploration interest over the past several years. The similarities between the Thelon and Athabasca Basins, both in terms of geologic history and age, suggest that the Thelon Basin could host high-grade unconformity-type deposits similar to those in the Athabasca Basin. The Thelon Basin near the Kiggavik Project area is relatively understudied and poorly understood when compared to the Athabasca Basin. Age constraints on the mineralization are rare (Section 1.2; Farkas, 1984; Fuchs *et al.*, 1986) and no modern geochronology has been done on the mineralization. There are only brief mentions of a genetic model for these deposits (e.g., Fredrich *et al.*, 1989; Weyer *et al.*, 1987) and a complete genetic model has not been proposed (Friedrich *et al.*, 1989).

The overall purpose of this thesis is to develop an exploration model for the Bong deposit, Thelon Basin. Specific objectives include: (1) characterize the mineral paragenesis of barren and mineralized samples, including the ore minerals and alteration minerals; (2) determine the fluid history and temperature of formation of the deposits using oxygen and hydrogen isotopes; (3) identify the mechanisms of uranium precipitation; and (4) determine the age(s) of uranium mineralization. Samples collected for this research consist of outcrop and drill-core samples. However, due to the lack of outcrop exposure in the vicinity of the Bong deposit, the majority of samples used for this study come from drill core. Detailed investigations of the mineralogy and textures of the samples were done with particular attention

to the uranium minerals and their paragenetic relation with other minerals. Barren and mineralized holes were systematically sampled. In addition, graphite and organic matter were studied to investigate the conditions for uranium-mineral precipitation. Oxygen and hydrogen isotopes were used to determine the source and temperature of the mineralizing fluids, while select samples were used for U-Pb and Pb-Pb geochronology to constrain absolute timing of mineralization.

Chapter 2: Geologic Setting

2.1 Regional Geology

2.1.1 Western Churchill Province

The western Churchill Province is the part of the Churchill craton that is exposed north and west of Hudson Bay. Variably reworked Archean continental crust and early Paleoproterozoic sedimentary cover comprise the Province. The Thelon-Taltson Orogen (2.0-1.9 Ga), the product of east-dipping subduction-related magmatism resulting from the collision between the western Churchill and Slave provinces at ~1970-1960 Ma (Hoffman, 1988; Tirrul & Grotzinger, 1990), defines the border to the west. The Trans-Hudson Orogen (2.0-1.8 Ga), a product of subduction beneath the western Churchill province prior to the terminal collision with the Archean Superior province at ~1830 Ma, forms the border to the south (Stern *el al.,* 1995; Sanborn-Barrie *et al.,* 2001). The province has two major domains, the Rae and Hearne provinces. Geophysical analysis has defined the Snowbird tectonic zone as the boundary between the Rae and Hearne (Ross *et al.*, 1995). The province hosts a number of intracratonic sedimentary basins, containing orthoquartzite, that are both spatially-related and temporally-related (Fig. 2.1).

Intracratonic sedimentary basins located in the western Churchill Province include the Athabasca, Thelon and Hornby Bay basins. These basins are all early Proterozoic and consist of thick sequences of sedimentary rocks such as the Athabasca Group in the Athabasca Basin and the Dubawnt Supergroup, which includes the Thelon Formation, in the Thelon Basin and Baker Lake Basin.

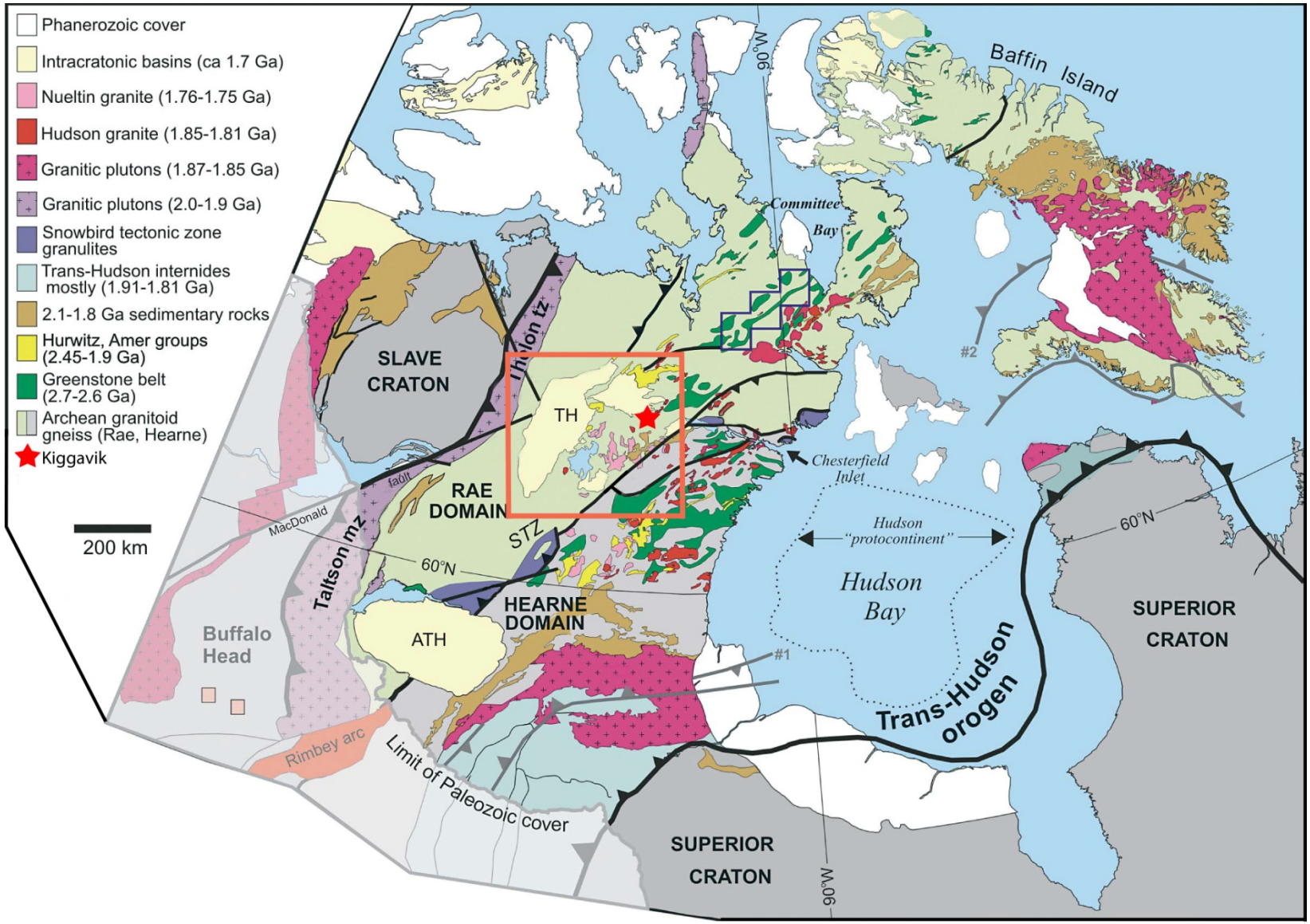

Figure 2.1: Regional geology of the western Churchill Province. Abbreviations: TH: Thelon Basin, ATH: Athabasca Basin, STZ: Snowbird Tectonic Zone. Orange box is the location of Figure 2.3 (From Berman *et al.*, 2005).

2.1.2 Dubawnt Supergroup

Early Proterozoic sedimentary cover in the central portion of the western Churchill Province is dominated by the Dubawnt Supergroup. The succession covers ~200,000 km^2 and contains predominately continental clastic rocks and intercalated volcanic rocks (Rainbird *et al.*, 2003). The Dubawnt Supergroup unconformably overlies metasedimentary rocks and anorthosite-gabbro Paleoproterozoic rocks, which unconformably overlie granitic and supracrustal rocks of the late Archean.

Three main groups comprise the Dubawnt Supergroup, the basal Baker Lake Group, the Wharton Group, and the Barrensland Group (Fig. 2.2). Rainbird *et al.* (2003) and Peterson (2006) describe these groups in detail. The combined thickness of the Supergroup is estimated to be ~15 km, although the sequence is nowhere observed in its entirety. Each succession is separated by an unconformity. The Baker Lake Group (ca. 1.83 Ga; Peterson, 2006) is the most extensive succession of the three. The lowermost formations in the Baker Lake Group are the South Channel and Kazan Formations that are composed of coarse-grained alluvial red-bed sandstone overlain by finer-grained equivalents, and reach maximum thicknesses of ~650 m and ~600 m, respectively. Lava flows and volcaniclastic deposits of the Christopher Island Formation overlie these units. The Christopher Island Formation has a maximum thickness of ~2 km and is composed of subaerial alkaline mafic to felsic volcanic rocks that are typically ultrapotassic (Miller *et al.*, 1989; Peterson, 2006). The group is capped by the Kunwak Formation, which

contains sedimentary rocks similar to the South Channel and Kazan Formations. The Wharton Group unconformably overlies the Baker Lake Group.

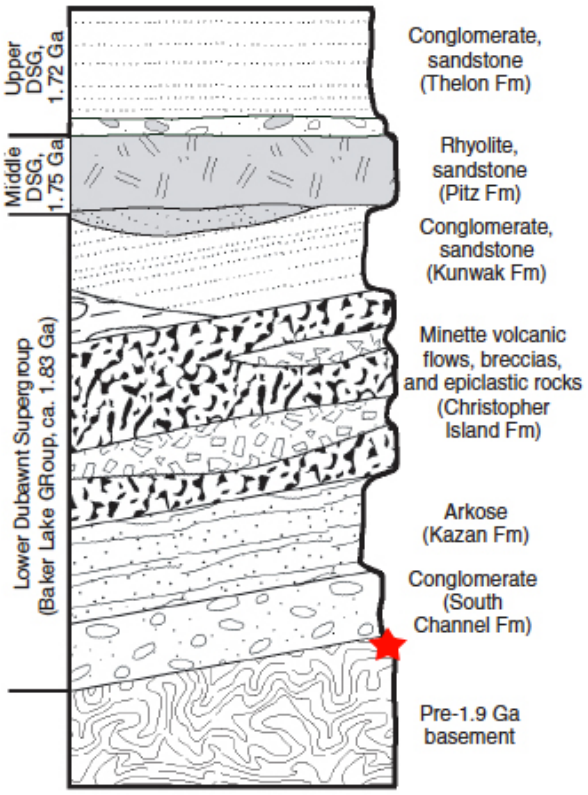

Figure 2.2: Simplified stratigraphic section of the Dubawnt Supergroup. Red star denotes the relative position of the Bong deposit (From Peterson, 2006)

The Wharton Group comprises the Amarook and Pitz Formations. The Amarook Formation is a well-indurated sandstone unit. Porphyritic rhyolite lava flows, the extrusive flow equivalent of the 1765 to 1750 Ma Nueltin granites, and pyroclastic and epiclastic sedimentary rocks of the Pitz Formation, are the uppermost lithologies in the Wharton Group.

The Thelon Formation of the Barrensland Group unconformably overlies the Pitz Formation.

The Thelon Formation (1.72 Ga; Peterson, 2006) is the dominant unit in the Thelon Basin and consists of mainly quartz-rich sandstones and conglomerates. The Kuungmi Formation, a thin and spatially-restricted unit of altered basaltic flows, overlies the Thelon Formation. A U-Pb baddelyite age of 1540 ± 30 Ma has been obtained from this unit (Chamberlain *et al.*, 2010). In turn, the Kuungmi Formation

is overlain by the Lookout Point Formation, a thin unit of stomatolite-bearing siliceous dolostone. Hiatt *et al.* (2003) used the presence of the Kuungmi Formation basalt to indicate late tectonic activity during basin evolution and used the presence of dolomite to suggest that a marine transgression occurred.

2.1.3 Thelon Basin

The Thelon Basin is a Paleoproterozoic intracratonic basin located in northern Canada. The basin lies within the Rae domain of the western Churchill Province and straddles the border between the Northwest Territories and Nunavut (Fig. 2.1). The Thelon Basin is contemporaneous with other intracratonic basins such as the uranium-rich Athabasca basin (Orrell *et al*., 1999; Ramaekers, 2004; Rainbird *et al*., 2007), as well as the McArthur Basin in Australia (Polito *et al*., 2006), and Espinhaço Basin in Brazil (Martins-Neto, 2000). These basins are characterized by thick sequences of mature quartz sandstone, conglomerate, and minor siltstone that were deposited unconformably over a paleoregolith developed on basement lithologies (Needham, 1988; Rainbird *et al*., 2003; Ramaekers *et al*., 2007). The basins in the Churchill Province formed as a consequence of the Trans-Hudson Orogen (2.0–1.8 Ga; Hiatt *et al.,* 2003).

The timing of the onset of basin formation in the Thelon is constrained by dating of diagenetic phosphate minerals in the basal units (U-Pb 1720 Ma; Miller *et al.*, 1989), the emplacement of fluorite-bearing granites into the Amer group (ca. 1753 Ma; Miller, 1995), and primary zircon from the underlying Pitz formation rhyolite flows (1753 Ma; Rainbird & Davis, 2007). Therefore, the initiation of deposition in the Thelon basin is constrained to between 1753 and 1720 Ma, which is similar to the Athabasca Basin (1740 to 1730 Ma; Orrell *et al*., 1989; Rainbird *et al*., 2007) and possibly younger than the Kombolgie Formation (~1790 Ma; Polito *et al.*, 2006).

The dominant basin fill in the Thelon Basin is the Thelon Formation of the Barrensland Group (Fig. 2.3). The Thelon Formation has been described by numerous authors, including Miller *et al*. (1989), Hiatt *et al.* (2003), and Rainbird *et al.* (2003), and consists of quartz-dominated sandstones and conglomerates. In the western Thelon, the Barrensland Group also includes the small, spatially-restricted outcrops of Kuungmi Formation, a thin basaltic unit, and the Lookout Point formation, marine dolostones, which overlie the Thelon formation. The Pitz and Amarook Formations of the Wharton Group lie stratigraphically beneath the Thelon formation.

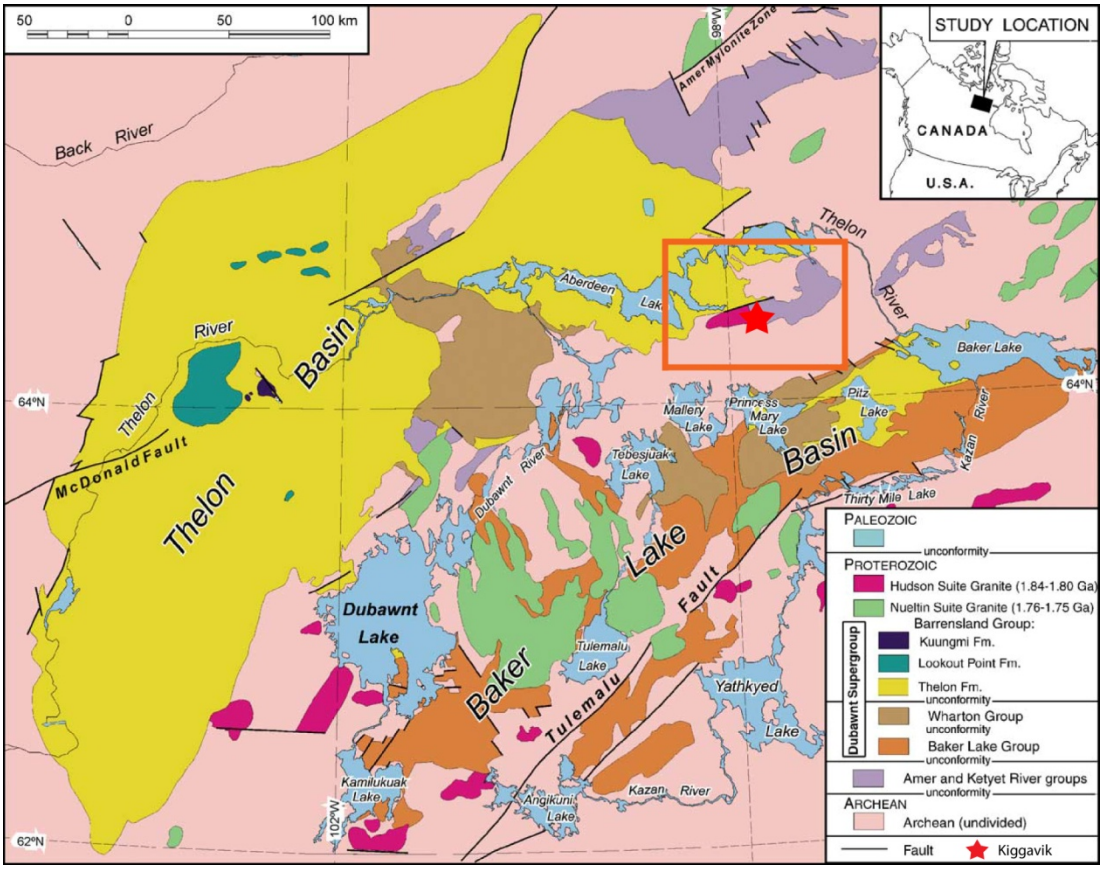

Figure. 2.3: Regional geology of the Thelon basin and distribution of the Dubawnt Supergroup with the location of the Kiggavik camp. Orange box is the location of Figure 2.5 (From Rainbird *et al.*, 2003).

2.2 Local Geology

The northeastern portion of the Thelon Basin is known as the NE Thelon sub-basin. The Kiggavik project area is located about 5 km SSE of the southeastern terminus of the NE Thelon sub-basin, near the fault contacts between the basin sediments and basement rock. The dominant basement lithology is the Woodburn Lake Group, which consists of metasedimentary, metavolcanic and volcaniclastic strata. More specifically, the Bong deposit is hosted in the greywackes of the Woodburn Lake Group's Pipedream Assemblage, which have been intruded by the hybrid Lone Gull granite (1.83 + 1.57 Ga; Scott *et al.*, 2011) and smaller lamprophyre and syenite dikes.

2.2.1 Local Basement Geology

The basement geology in the region consists mainly of highly deformed metasedimentary, metavolcanic and volcaniclastic strata of the Neoarchean Woodburn Lake Group (WLG), ~2.6 Ga mylonitized rhyolite (quartz eye rhylolite), and the hybrid Lone Gull granite (1.83 + 1.75 Ga; Scott *et al.* 2011). The granite, composed of the Hudson and Nueltin Suites, contains disseminated pitchblende (Weyer *et al*., 1987). The close association of the granite with the Kiggavik uranium deposits has spurred research on the granite itself including petrography, geochronology and geochemistry studies (Miller & LeCheminant, 1985; LeCheminant *et al*., 1987; Peterson & Van Breemen, 1999; Peterson *et al*., 2002; Turner, 2003; Scott *et al*., 2011). The exact role the granite plays in the formation is unknown, however potassic metasomatism resulting from the Nueltin event has

been proposed as an exploration guide to U-Au-Ag deposits in the Area (Peterson *et al*., 2012).

Zaleski *et al.* (2000) divided the WLG into upper and lower Archean packages. The upper package includes a quartzite that was believed to be interbedded with a ca. 2630 Ma felsic volcanic rock. However, re-evaluation by Pehrsson *et al.* (2010) led to the removal of the quartzite from the Woodburn Lake group based on field relationships. More recently, the Woodburn Lake group has been divided into six discrete assemblages (Pehrsson *et al*., 2010; Jefferson *et al*., 2011; Fig. 2.4).

The uppermost succession is composed of the Amarulik wackes, which are quartz-feldspar wackes with quartz eyes and locally volcaniclastic textures. The Wading Lake (Meadowbank River in the SE) assemblage underlies the Amarulik wackes. Mafic to intermediate amygdaloidal plagioclase-phyric flows and volcaniclastic rocks comprise the Meadowbank River assemblage. This sequence is in turn underlain by a sequence of felsic to intermediate volcanic to volcaniclastic rocks interbedded with grey wacke turbidite and slate, known as the Pipedream assemblage. This assemblage is host to the Kiggavik uranium deposits and the Meadowbank gold deposit. The North Meadowbank River assemblage underlies the Pipedream assemblage. This sequence consists of felsic volcanic flows and volcaniclastic rocks and is underlain by the Half Way Hills greenstone belt that is composed of mafic aphyric pillowed flows. The lowermost assemblage is the

Marjorie Lake assemblage. The rocks of the Marjorie Lake assemblage are highly metamorphosed graded psammitic turbidites, banded iron formation and felsic volcanics. This assemblage appears to be host to the Tatiggaq and Qavvik uranium prospects located west of Kiggavik. The Woodburn Lake group lies unconformably on Mesoarchean granites via a thrust contact (Jefferson *et al*., 2011).

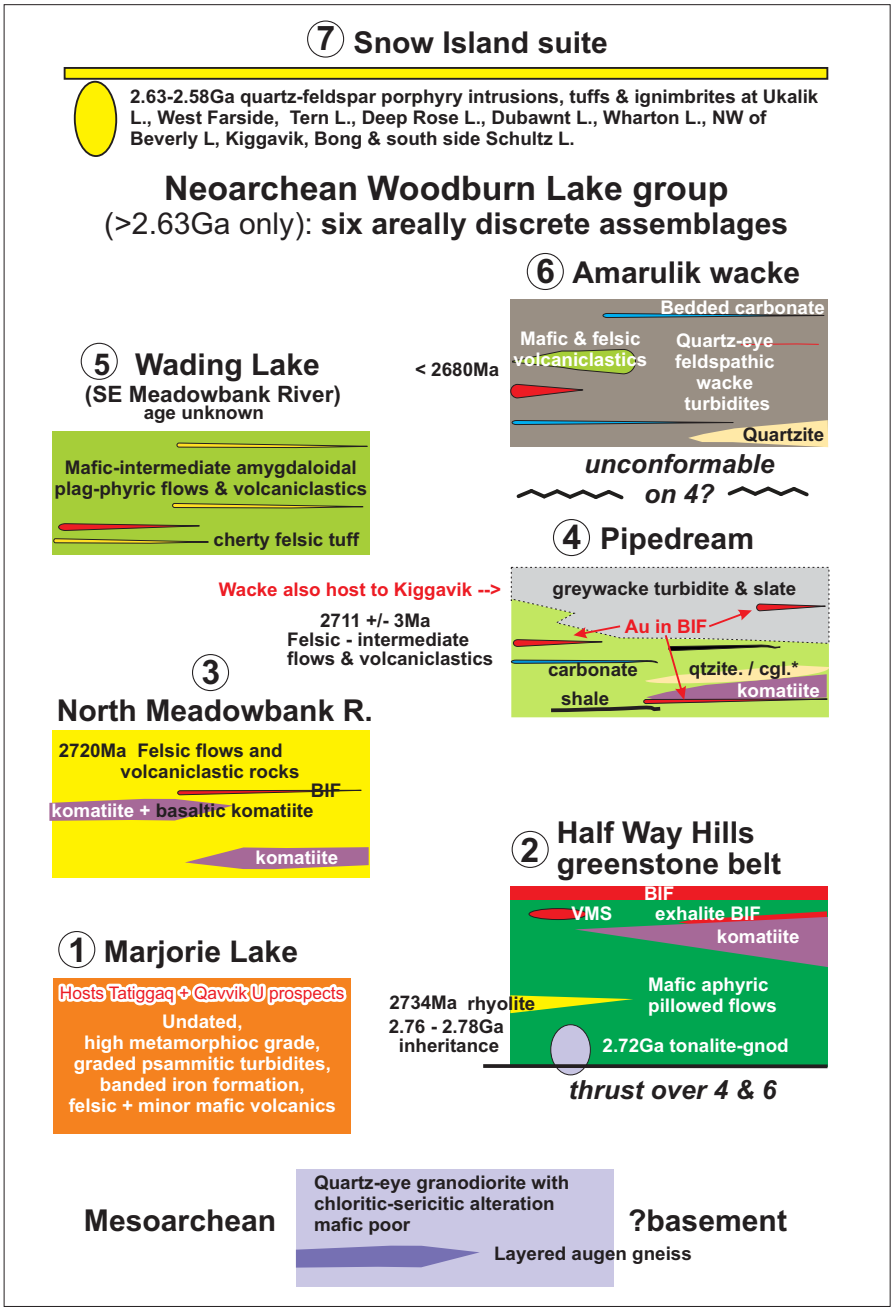

*Quartzite documented on NE shore of Pipedream Lake has fuchsitic clasts including komatiite. Also documented in drilling: quartzite/cobble conglomerate between komatiite and intermediate volcaniclastics

Figure 2.4: Woodburn Lake Group assemblage relationships (Jefferson *et al.*, 2011).

2.3 Uranium Mineralization

Several uranium deposits and showings lie along a southwest-northeast trend in the Kiggavik area (Andrew Lake-Kiggavik Trend; Fig. 2.5). The Bong deposit itself is located approximately 3 km south of the faulted contact between the Thelon and the underlying basement. All deposits and showings in the area are hosted solely in the basement and are located along roughly E-W trending faults that exhibit intense alteration associated with hydrothermal activity. Alteration generally consists of a strong bleaching of the host rock as well as minor hematization (Fuchs & Hilger, 1987). The uranium mineralization is described as pitchblende surrounded and replaced by coffinite, indicating that the deposit has been subject to remobilization (Fuchs *et al.,* 1986). Average grade is on the order of 0.5% U for the deposits (AREVA, 2011). Geochronology of mineralization and associated alteration report ages that group at ~1400 Ma and ~1000 Ma (Fuchs *et al*., 1986; Farkas, 1984). Both studies concluded that the older ages are from primary mineralization and the younger ages represent a remobilization event.

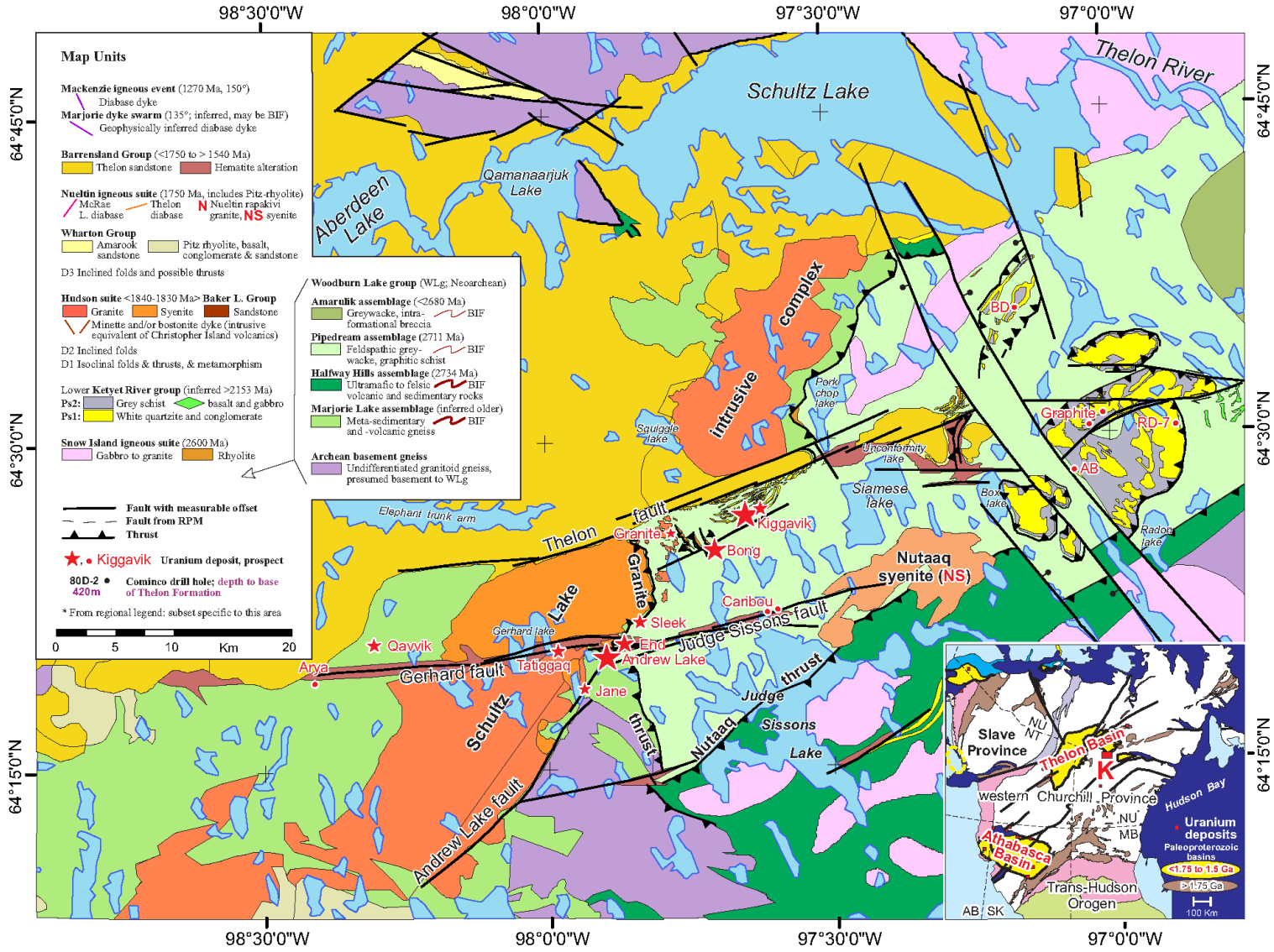

Figure 2.5: Kiggavik area geology compilation map with the location of the major uranium deposits in the Kiggavik Camp. The Bong deposit is located ~3 km south of the faulted contact between the Thelon Formation and the underlying basement, inset is the location of the Thelon Basin relative to the Athabasca Basin in the Western Churchill Province (Jefferson *et al.*, in prep).

Chapter 3: Methodology

3.1 Sampling

Fieldwork consisted of sampling outcrop and drill core between July 4th and July 17th, 2011. In total, 192 samples were collected from 17 drill holes and numerous outcrops. Eighteen mineralized samples were collected from drill core all other samples were unmineralized. The samples were collected for petrographic, geochemical and isotopic analyses. Polished thin sections were made from 75 of the unmineralized samples and the 18 mineralized samples. Polished thin sections were examined using optical and scanning electron microscopy to determine the paragenetic relation between minerals. Detailed descriptions of drill core and thin sections referenced in figures are included in Appendix A. An electron microprobe was used to quantify the chemistry of oxide, silicate, and sulphide minerals in the samples. Seven samples containing carbonaceous material were sent for carbon-isotope analysis. A total of 52 samples were taken from two drill holes - one mineralized and one barren - to determine the oxidation state of the iron in the samples. A secondary ion mass spectrometer (SIMS) was used to measure both U-Pb and stable-isotope ratios in selected minerals.

3.2 Optical Microscopy and Scanning Electron Microscope (SEM)

Thin sections were examined using a Nikon Eclipse 50i POL polarizing microscope. Selected samples were carbon-coated and examined using a Cambridge Stereoscan 120 scanning electron microscope (SEM). The SEM is equipped with a back-scattered electron detector and an energy dispersive X-ray spectroscopy (EDS)

detector with digital-imaging capabilities. The SEM was used to characterize the samples in greater detail at higher magnification than possible with optical methods. The backscatter-electron (BSE) images were used in the selection of samples for electron microprobe and SIMS analysis.

3.3 Electron-Probe Microanalysis (EPMA)

Electron-probe microanalysis (EPMA) was done using a Cameca SX100 Universal EPMA equipped with five wavelength-dispersive spectrometers and a Princeton Gamma-Tech (PGT) energy-dispersive spectrometer. Quantitative analyses of oxide, silicate and sulphide minerals from 16 samples were obtained. The EPMA used a beam size between 1 and 10 μm, depending on the size of the areas being analyzed, with an acceleration voltage of 15 keV and a 20 nA current. In total, 21 elements were analyzed. The elements analyzed for and the standards used are listed in Appendix B. Elemental detection limits were 1000 ppm for all elements except for Pb, Th, U, and F. These elements had detection limits of 1500 ppm, 1300 ppm, 6000 ppm and 2200 ppm, respectively.

Chemical-lead (Pb) ages of uraninite grains were calculated using the EMPA data and the Cameron-Schiman (1978) equation:

$$t = Pb \times 10^{10} / (1.612U + 4.95\ Th) \quad [1]$$

where Pb, U and Th are in atomic percent and t is given in years.

3.4 Geochemical Analyses

Fifty drill-core samples were selected for the determination of Fe_2O_3 and FeO, as well as the other major element oxides and trace elements. Samples were sent to ActLabs Canada and pulverized so that 95% passed through a 105µ sieve. Aliquots of the powdered material were then fused prior to whole-rock analysis. The analyses were done on samples prepared and analyzed in a batch system, using inductively coupled plasma mass spectroscopy (ICP-MS, Package 4B; ActLabs, 2012). Each batch contained a method reagent blank, certified reference material and 17% replicates. Samples were mixed with a flux of lithium metaborate and lithium tetraborate and fused in an induction furnace. The molten melt was immediately poured into a solution of 5% nitric acid containing an internal standard, and mixed continuously until completely dissolved (~30 minutes). The samples were analyzed for major oxides and selected trace elements on a combination simultaneous/sequential Thermo Jarrell-Ash ENVIRO II ICP or a Varian Vista 735 ICP. Calibration was performed using 7 prepared USGS and CANMET certified reference materials. One of the 7 standards was used during the analysis for every group of ten samples (Act Labs, 2012).

The ICP-MS data comprised the total iron in the samples, expressed as Fe_2O_3-total. Ferrous iron, as FeO, was then determined by titration (Package 4F; ActLabs, 2012). The method of titration used is a modified method from Wilson (1955). During titration FeO was determined using a cold acid digestion of ammonium metavanadate and hydrofluoric acid in an open system. Ferrous ammonium

sulphate was added after digestion and potassium dichromate was the titrating agent. When titrating, the endpoint was determined by colour. The contribution of ferrous iron, as FeO, was then subtracted from the total iron value and the balance computed as ferric iron (Fe_2O_3). Detection limits for both ICP-MS Fe_2O_3-total and titration FeO were 0.01 wt% (Act Labs, 2012).

3.5 Isotope-Ratio Mass Spectrometry (IRMS)

Gas-source Isotope-Ratio Mass Spectrometry (IRMS) was used to determine the $^{13}C/^{12}C$ ratios of seven samples, five mineralized and 2 unmineralized samples containing organic carbon. Material from the five mineralized samples was drilled out using a Fordom DP-95 drill press. The material removed by the drill was split into two halves. Half of the sample was tested for the presence of inorganic carbon (i.e. carbon as carbonate) with HCl and half was sent to the G.G. Hatch Stable Isotope Laboratory at the University of Ottawa for analysis using IRMS. The two altered but unmineralized samples containing organic carbon were crushed and pulverized so that 95% passed through a 105µ sieve. Aliquots of powdered material were placed in a beaker, well-mixed with distilled water, and placed in an ultrasonic bath for 60 minutes to allow all of the material except for the carbon to settle to the bottom of the bath. After the ultrasonic bath, the top 2.5 cm of water plus suspended material was poured into a separate beaker and allowed to dry overnight in an oven. A small amount of this concentrated material was taken to test for the presence of inorganic carbon (carbonate) with HCl, while the rest was sent to the University of Ottawa laboratory for carbon-isotope analysis.

For carbon-isotope analysis, the samples and standards were weighed into tin capsules and loaded into an Elemantar Isotope Cube Elemental Analyzer interfaced to a Thermo Delta Advantage Isotope-Ratio Mass Spectrometer (IRMS). The samples and standards were flash-combusted at about 1800°C using the Dumas combustion method, where a sample of known mass is combusted in a high-temperature chamber in the presence of oxygen. This leads to the release of carbon dioxide, water and nitrogen. The resulting gas products were carried by helium through columns of oxidizing chemicals optimized for CO_2, so that other products (water and nitrogen) were absorbed, and sent via a continuous flow column (Thermo Conflo III) to the IRMS. Analytical precision was ~0.2%.

All carbon-isotope data are presented in the δ-notation. The $\delta^{13}C$ values are reported in units of per mil (‰) relative to Vienna PeeDee Belemnite (V-PDB) standard and are calculated using the following equation:

$$\delta^{13}C = [(^{13}C/^{12}C)_{sample} / (^{13}C/^{12}C)_{V\text{-}PDB}] * 10^3 \quad [2]$$

where $^{13}C/^{12}C$ is the ratio of the abundance of the heavy to the light isotope.

3.6 In Situ Secondary Ion Mass Spectrometry (SIMS)

Prior to Secondary Ion Mass Spectrometry (SIMS) analysis, the polished thin sections were cleaned with ethanol and polished with a 1-mircon diamond-cleaning compound to remove the carbon coating that was used for the SEM and EMPA. Each section was subsequently cleaned using soap, then immersed in a dilute soap solution in an ultrasonic cleaner. The sections were immersed three more times in

the ultrasonic cleaner, first using tap water, then purified water, and finally ethanol. Once cleaning was complete, the sections were sputtered-coated with a thin layer of gold to provide a conductive surface. Isotopic ratios of radiogenic and stable isotopes were obtained from uraninite, illite and muscovite.

During measurement, a mass-dependent bias, referred to as instrumental mass fractionation (IMF), is introduced. It typically favors the light isotope. The observed IMF results from a variety of processes, including secondary atom ionization (sputtering) and extraction (Sigmund, 1969; Shroeer *et al.,* 1973; Yu & Lang, 1986), secondary ion transmission (Shimizu & Hart, 1982), and detection (Lyon *et al.,* 1994; Riciputi *et al.,* 1998). Sputtering and ionization, which depend strongly on sample characteristics (i.e., chemical composition), are the greatest contributors to variability in IMF. Therefore, accurate isotopic analysis by SIMS requires calibration using a mineral standard that is compositionally similar to the mineral under analysis to correct for IMF. Ion-microprobe results from the standard are compared to its accepted isotopic composition in order to calculate a correction factor that is applied to the data obtained during the same analytical session (Holliger, 1988).

Quite commonly, the minerals of interest (e.g., uraninite, muscovite, etc.) vary considerably in their chemical composition or are chemically zoned at the micrometer-scale; however, it is impractical to find standards that match the wide range in chemical compositions of these minerals. Therefore, a mass-bias model

that accounts for variation in IMF with chemical composition for the minerals of interest is necessary. These models are developed using a suite of standards with chemical compositions that cover the range of compositions of the minerals from which a working calibration curve is developed (Fayek *et al*., 2002b). In addition, the relative ion-yields of two elements and their isotopes, such as U and Pb, may vary as function of chemical composition, producing incorrect measurements of elemental and isotopic ratios. For example, the $^{206}Pb/^{238}U$ ratio measured by SIMS may deviate significantly from their "true" $^{206}Pb/^{238}U$ value because Pb ionizes more readily than U. In addition, the $^{206}Pb/^{238}U$ ratio also may vary as a function of chemical composition of the sample because other elements present (e.g., Si, Ca, etc.) may enhance the ion-yield of Pb^+ or U^+. Therefore, an ion-yield normalizing coefficient (α_{SIMS}) that accounts for variation in relative ion-yields with chemical composition for the mineral of interest is necessary (Holliger, 1991; Fayek *et al.,* 2002b).

The standard and minerals of interest were analyzed during the same analytical session. The value of the standard was used to correct for IMF using the equation:

$$\alpha_{SIMS} = R_{SIMS} / R_{STD} \quad [3]$$

where R the a measured isotopic ratio (e.g., $^{207}Pb/^{235}U$ or $^{18}O/^{16}O$), SIMS denotes the samples and STD denotes the standard.

The normalizing coefficient (α) was applied to the measured ratios from the minerals to obtain "true" isotopic ratios:

$$R_{true} = \alpha * R_{SIMS} \quad [4]$$

where R is the measured isotopic ratio.

3.6.1 Radiogenic Isotopes

The SIMS analytical protocol for U-Pb measurements in uranium minerals using the CAMECA 7f ion microprobe is as follows. A ~2 nA primary ion beam of O^-, accelerated at 12.5 kV, was focused to a 15 x 30 μm spot using a 750 μm aperture in the primary column. The sample accelerating voltage was +7.95 kV, with electrostatic analyzer in the secondary column set to accept +8.00 kV. The entrance and exit slits were narrowed to obtain flat-top peaks at a mass resolving power of about 1400. Ions were detected with a Balzers SEV 1217 electron multiplier coupled with an ion-counting system with an overall deadtime of 25 ns. The following species were detected sequentially by switching the magnetic field: $^{204}Pb^+$, $^{206}Pb^+$, $^{207}Pb^+$, $^{208}Pb^+$, $^{235}U^+$, and $^{238}U^+$. A 50-volt energy offset suppressed hydride isobaric interferences. A typical analysis lasted ~11 minutes, comprising 40 cycles of analysis. Negligible common Pb ($^{204}Pb^+$) was detected.

Ratios corrected for mass bias (Equation 4) were used to calculate U-Pb isotopic ages using the ISOPLOT program (Ludwig, 1993). Pb-Pb ratios were used to iteratively calculate ages of uraninite using the following equation:

$$^{207}Pb/^{206}Pb = {}^{235}U/^{238}U * e^{\lambda 2t} - 1 \,/\, e^{\lambda 1t} - 1 \quad [5]$$

where $^{207}Pb/^{206}Pb$ is the ratio measured by SIMS and corrected for mass bias, $^{235}U/^{238}U$ is 1/137.88, λ_2 and λ_1 are the decay constants for ^{235}U ($9.8485E^{-10}$ y^{-1}) and ^{238}U ($1.55125E^{-10}$ y^{-1}) and t is time in years.

3.6.2 Stable Isotopes

Hydrogen-isotope compositions of illite and muscovite were determined using the CAMECA 7f ion microprobe. A ~25 nA primary beam of O^-, accelerated at 12.5 kV, was focused to a 10 x 15 μm spot using a 750 μm aperture in the primary column. A 50-volt offset was used to eliminate molecular ion interferences (Riciputi *et al.,* 1998; Fayek *et al*., 2002a). The entrance and exit slits were narrowed to obtain flat-top peaks at a mass-resolving power of about 800. Ions were detected with a Balzers SEV 1217 electron multiplier coupled with an ion-counting system with an overall deadtime of 52 ns. During analysis, the magnetic field was alternated to switch between the detection of hydrogen and deuterium molecules. A typical analysis lasted ~9 minutes, comprising 60 cycles of analysis.

Oxygen-isotope compositions of illite, muscovite and uraninite were also measured using the CAMECA 7f ion microprobe. A ~2 nA primary beam of Cs^+ was accelerated at 10kV and focused to a 10 x 15 μm spot using a 100 μm aperture in the primary column. An offset of 200-volts was used to eliminate molecular ion interferences. Ions were detected with a Balzers SEV 1217 electron multiplier coupled with an ion-counting system using an overall deadtime of 52 ns. Two

isotopes of oxygen, $^{16}O^-$ and $^{18}O^-$, were detected by switching the magnetic field. Analyses comprised 70 cycles and lasted ~10 minutes.

All stable-isotope data are presented in the δ-notation relative to the appropriate standard. Both hydrogen and oxygen are reported relative to Vienna Standard Mean Ocean Water (V-SMOW) in units of per mil (‰) and are calculated using the following equation:

$$\delta^2D \text{ or } \delta^{18}O\ (‰) = (R_{sample} / R_{V\text{-}SMOW} - 1) * 10^3 \quad [6]$$

where R_{sample} is the ratio of the abundance of the heavy to the light isotope of the sample that has been normalized to obtain "true" isotopic ratios (see equation 4) and $R_{V\text{-}SMOW}$ is the ratio of the abundance of the heavy to the light isotope of the standard.

Chapter 4: Results

4.1 Petrography

Petrography was done on 93 thin sections, with particular attention being given to the mineralogy of the host rock, the alteration of the host rock minerals and the uranium minerals (Appendix A). A scanning electron microscope was used for more detailed petrography on select sections. The mineral paragenesis is summarized in Figure 4.1. The ore-bearing lithology is the Woodburn Lake Group, which consists of metasedimentary, metavolcanic and volcaniclastic strata. In other deposits in the Kiggavik area, minor amounts of mineralization are hosted in the ~2.6 Ga mylonitized rhyolite and the mixed Lone Gull granite (1.83 + 1.75 Ga; Scott *et al.,* 2011). These rocks have been intruded by lamprophyre and syenite dikes.

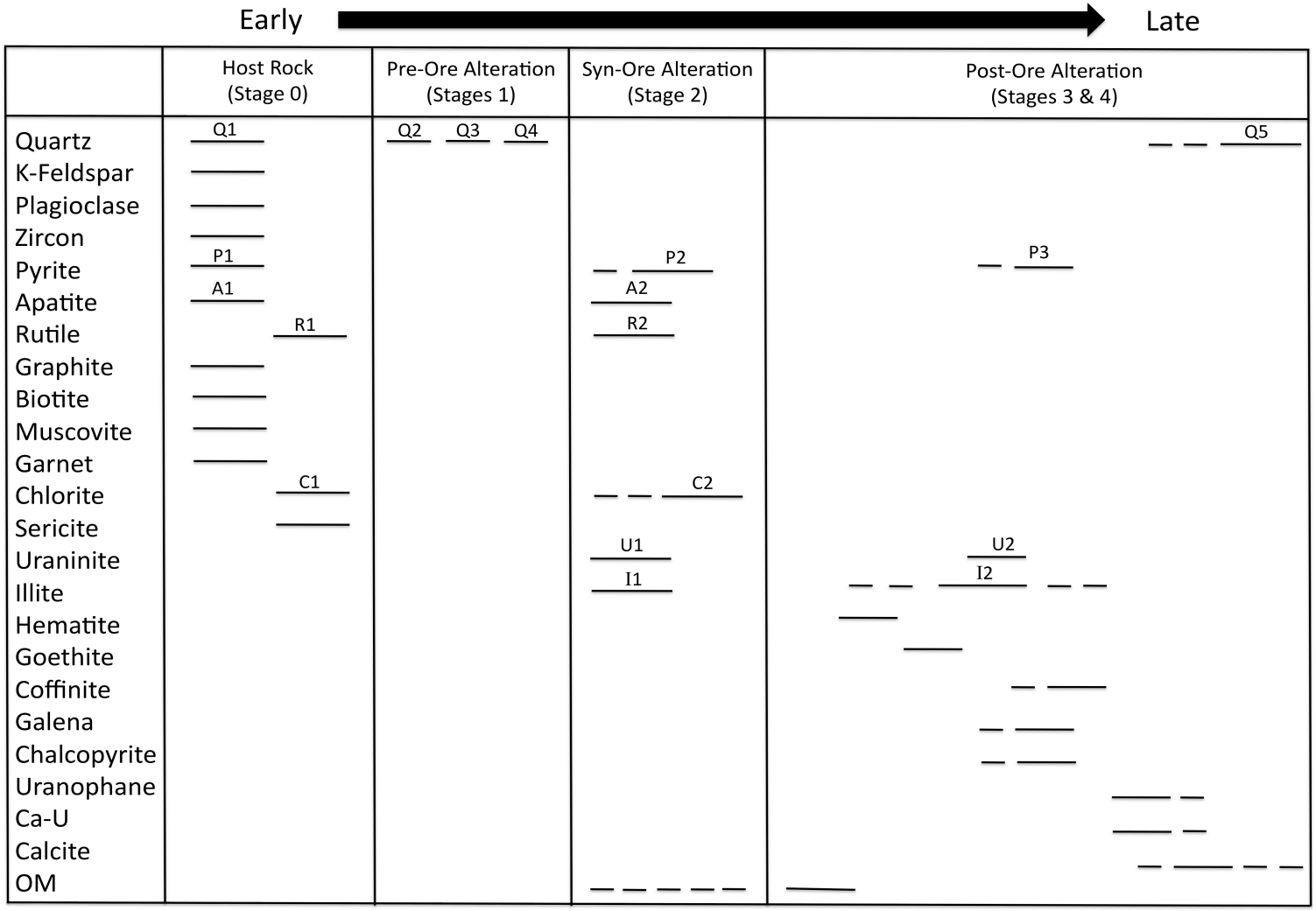

Figure 4.1: Paragenetic sequence of the Bong uranium deposit, broken into metamorphic host rock, pre-ore alteration, syn-ore alteration and post-ore alteration assemblages. Abbreviations: Ca-U = calcium-rich uranium mineral, OM = unidentified organic matter.

4.1.1 Host Rock

In the Bong part of the Kiggavik area, the Woodburn Lake Group (WLG) is composed primarily of Pipedream Assemblage metasedimentary rocks, ranging lithologically from arkose to wacke, and has been subsequently altered by distinct fluid events. The metasediments are green-grey, fine to medium grained and display a sub-horizontal foliation (Fig. 4.2A). The primary minerals are 0.1 to 0.4 mm size quartz (60-70%) and feldspar (15-25%) grains with minor amounts of 0.1 to 0.3 mm size muscovite and biotite (5%). The dominant feldspar is K-feldspar with minor plagioclase. Quartz and feldspar grains are generally sub-rounded to rounded and muscovite is tabular, forming as laths between quartz and feldspar grains. Locally, there are layers that contain euhedral garnet porphyroblasts (up to 2.5 mm wide) along with tabular biotite formed during peak metamorphism (Fig. 4.2B). Biotite is often altered to chlorite (C1; Fig. 4.2C) and the feldspars are altered to sericite (Fig. 4.2D & E). Chloritization proceeds as a pseudomorphic replacement of biotite, while sericitization involves the breakdown of the feldspars along grain boundaries and fractures. This form of alteration is interpreted to be the result of retrograde metamorphism. Pyrite (P1; Fig. 4.2E) occurs as 0.1 to 0.2 mm size, subhedral to euhedral, disseminated grains. Accessory minerals include zoned and highly fractured rare zircon (Fig. 4.2F), apatite (A1) and rutile (R1). Rutile is more abundant in areas where ferromagnesian minerals (i.e., biotite, garnet) are present and is likely related to retrograde metamorphism of these minerals. Rare graphite-rich material occurs mainly as nodules and blebs that are 0.5-3 cm in diameter.

Muscovite, biotite and garnet formation is indicative of medium temperatures and pressures during peak metamorphic conditions and are related to amphibolite-grade metamorphism. The subsequent alteration of peak metamorphic minerals (e.g., chloritization of biotite) is related to retrograde metamorphism (Greenschist facies) that occurred when the rocks cooled during uplift and exhumation.

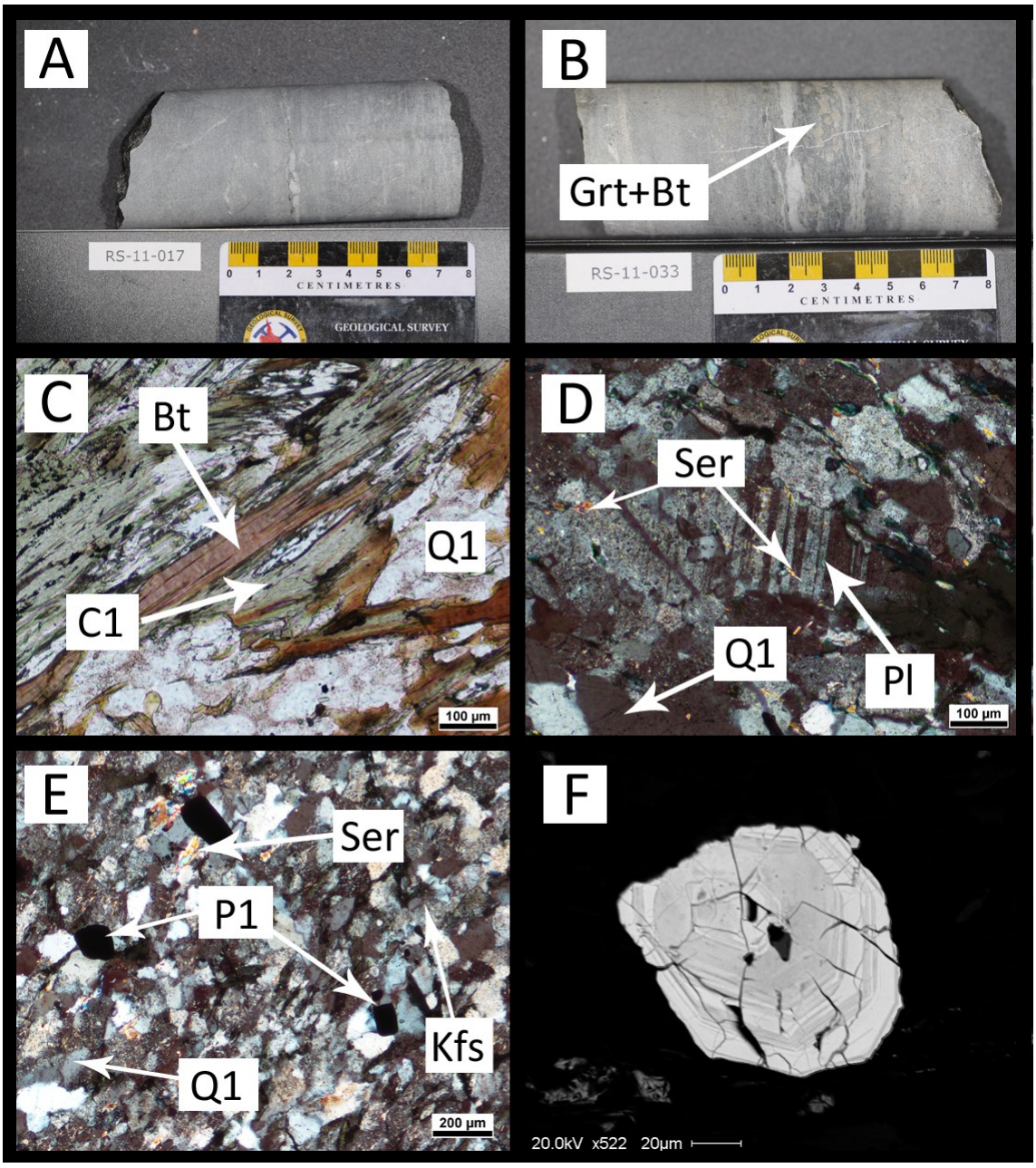

Figure 4.2: Images of pipedream assemblage (PDA) of the WLG metasedimentary rocks. A) Typical WLG host rock (Sample RS-11-017). B) Garnet and biotite layer (Sample RS-11-033). C) Pseudomorphic chloritization of biotite (Sample RS-11-058). D) Sericitization of feldspars (Sample RS-11-067). E) First generation of pyrite and minor sericitization (Sample RS-11-072). F) Zoned detrital zircon (Sample RS-11-030). Abbreviations: Grt = Garnet, Bt = Bioitite, C1 = First generation of chlorite, Q1 = First generation of quartz, Ser = Sericite, Pl = Plagioclase, Kfs = K-feldspar, P1 = First generation of pyrite.

4.1.2 Alteration Minerals

The main alteration mineral assemblages can be divided into pre-ore, syn-ore, and post-ore. The pre-ore alteration mineral is quartz, while syn-Stage A mineralization alteration minerals include illite, pyrite, rutile, apatite and chlorite. Syn-Stage B mineralization alteration minerals include illite, sulphides, rutile, apatite, chlorite, goethite, hematite and organic matter, while illite, calcite and drusy quartz fill late, post-mineralization veins.

Pre-ore Alteration Minerals

Pre-ore alteration consists of the addition of quartz, in the form of silicification, brecciation and veins. The silicification event, which precipitated quartz (Q2), flooded the host rock with silica, silicifying the host rock (Fig. 4.3A). Silicification is characterized by the precipitation of microcrystalline quartz in fractures and along grain boundaries. Breccia zones formed in areas where the fluid pressure exceeded the confining pressure of the host rock. These breccia zones are generally at a high angle to the core axis, oblique to foliation, and consist of fragments of host rock that are cemented by quartz (Fig. 4.3B). Breccia zones are 1 cm to 5 cm wide.

There are two distinct generations of quartz veins (Q3, Q4; Fig. 4.3C & 4.3D), which crosscut each other in thin section (Fig. 4.3E). Quartz veins also crosscut previously brecciated areas (Fig. 4.3F).

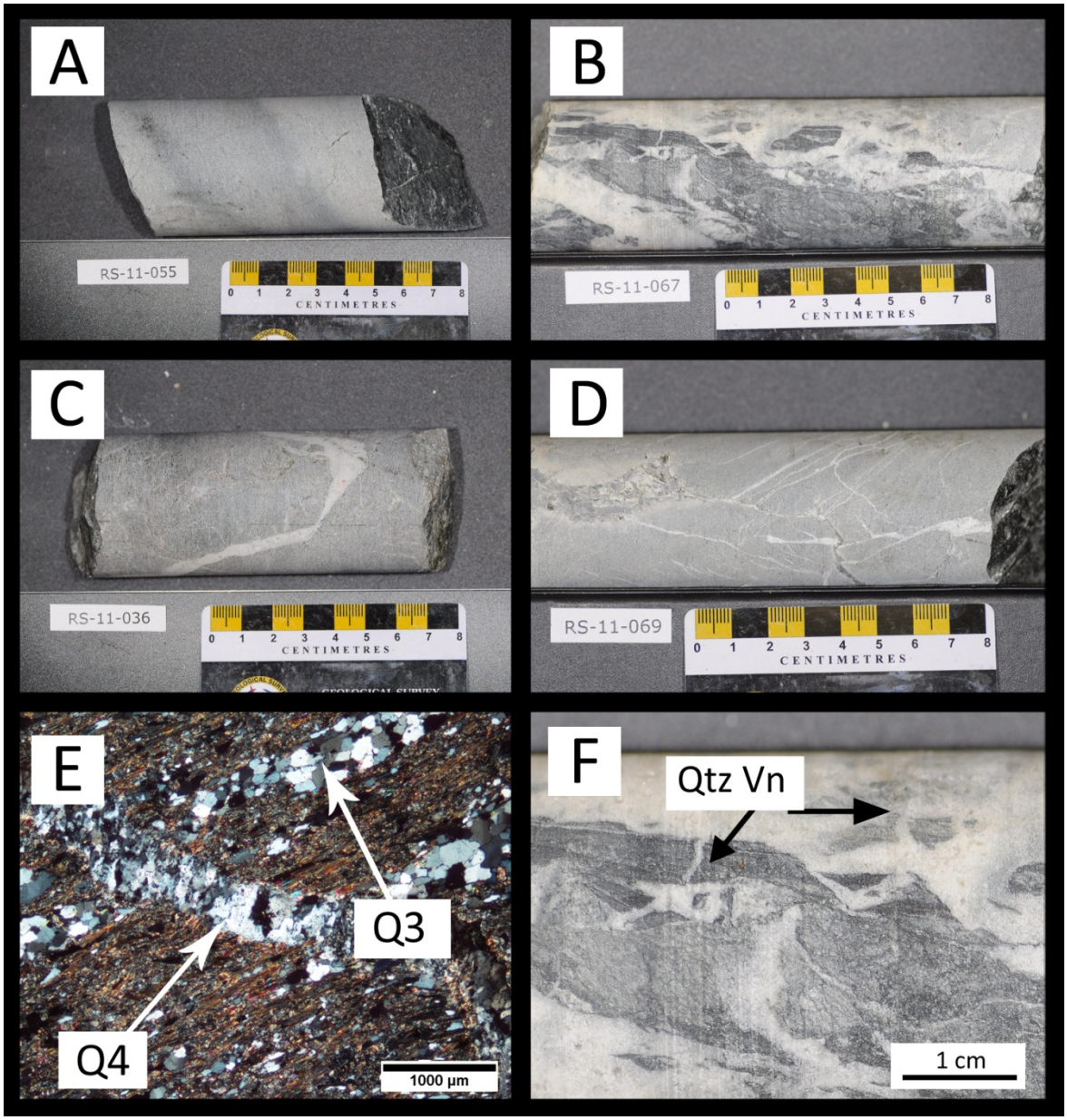

Figure 4.3: Pre-ore alteration of the WLG metasediments. A) Silicified WLG (Sample RS- 11-055). B) Brecciated WLG (Sample RS-11-067). C) Quartz vein at high angle to core axis (Sample RS-11-036). D) Quartz veinlets (Sample RS-11-069). E) Two generations of quartz veins (Sample RS-11-072). F) Quartz veins cross cutting a brecciated portion of the host rock (Sample RS-11-067). Abbreviations: Q3 = Second generation of alteration quartz, Q4 = Third generation of alteration quartz, Qtz Vn = Quartz veins (unknown generation).

Syn-Stage A Alteration Minerals

Macroscopic alteration observed in drill-core includes a strong bleaching of the host rock (Fig. 4.4), argillization and desilicification. The bleaching is the result of the breakdown of ferromagnesian minerals (biotite, Fe-Mg chlorite), while argillization is the result of the breakdown of the original host rock (e.g., feldspars, muscovite, biotite, chlorite). This results in a pervasive cream off white coloration and a change in rheology of the host rock. The alteration zone is centered on fault zones and generally extends 100 to 200 m in the vertical direction and extends a few hundred metres laterally. There is a fairly rapid transition from macroscopically unaltered greenish-grey WLG metasediment to bleached WLG metasediment (Fig. 4.4).

Microscopically, there is an increase in the degree of alteration. Unaltered metasediments (Fig. 4.5A & a) consist of primary rock-forming minerals (e.g., feldspars, muscovite, quartz), which make-up the entirety of the rock. Weakly to moderately altered zones (Fig. 4.5B, b, C & c) consist of feldspars and micas that are partially altered to illite, and quartz has been partially dissolved. Finally, there are intensely altered zones (Fig. 4.5D & d) that are composed almost entirely of illite. Despite the intense alteration (e.g., argillization, desilicification), primary foliation remains visible.

The dominant syn-ore alteration mineral is illite (I1). At the thin-section scale, illite forms as a result of the breakdown of muscovite, biotite, garnet, and K-

feldspar (Fig. 4.6). Also associated with the formation of illite is a desilification of the host rock where quartz grains are partially corroded (Fig. 4.5b & c). Although alteration of the host-rock is intense (Fig. 4.6A & B), primary rock-forming minerals (e.g., quartz, muscovite) in the alteration zone are sometimes preserved (Fig. 4.6 C-H). Chlorite (Fig. 4.6E & F) and garnet (Fig. 4.6G & H) are also altered to illite.

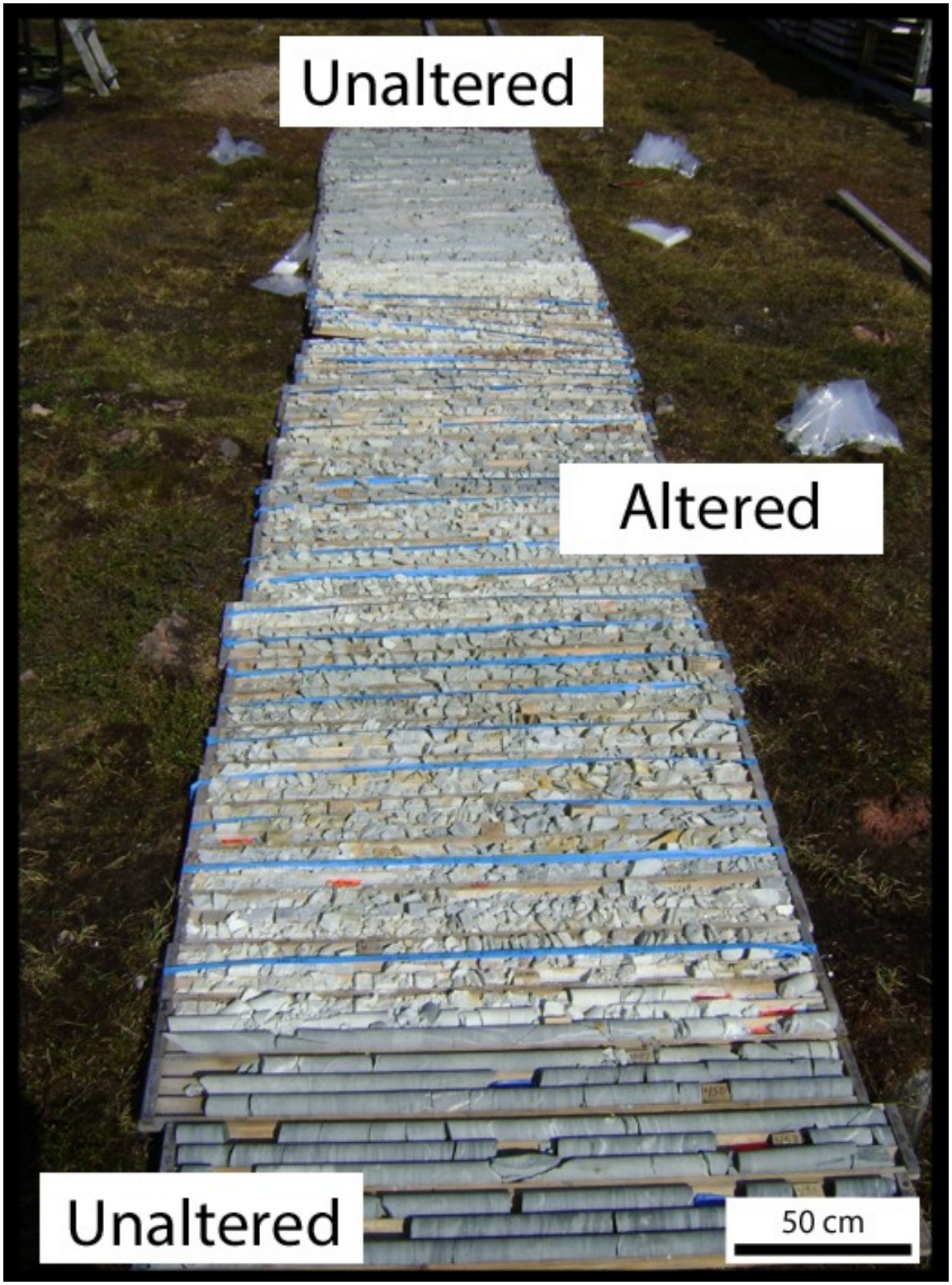

Figure 4.4: Strong bleaching of the host rock observed down hole in Bong-42. The zone is approximately 130 m in core and composed predominately of illite and quartz.

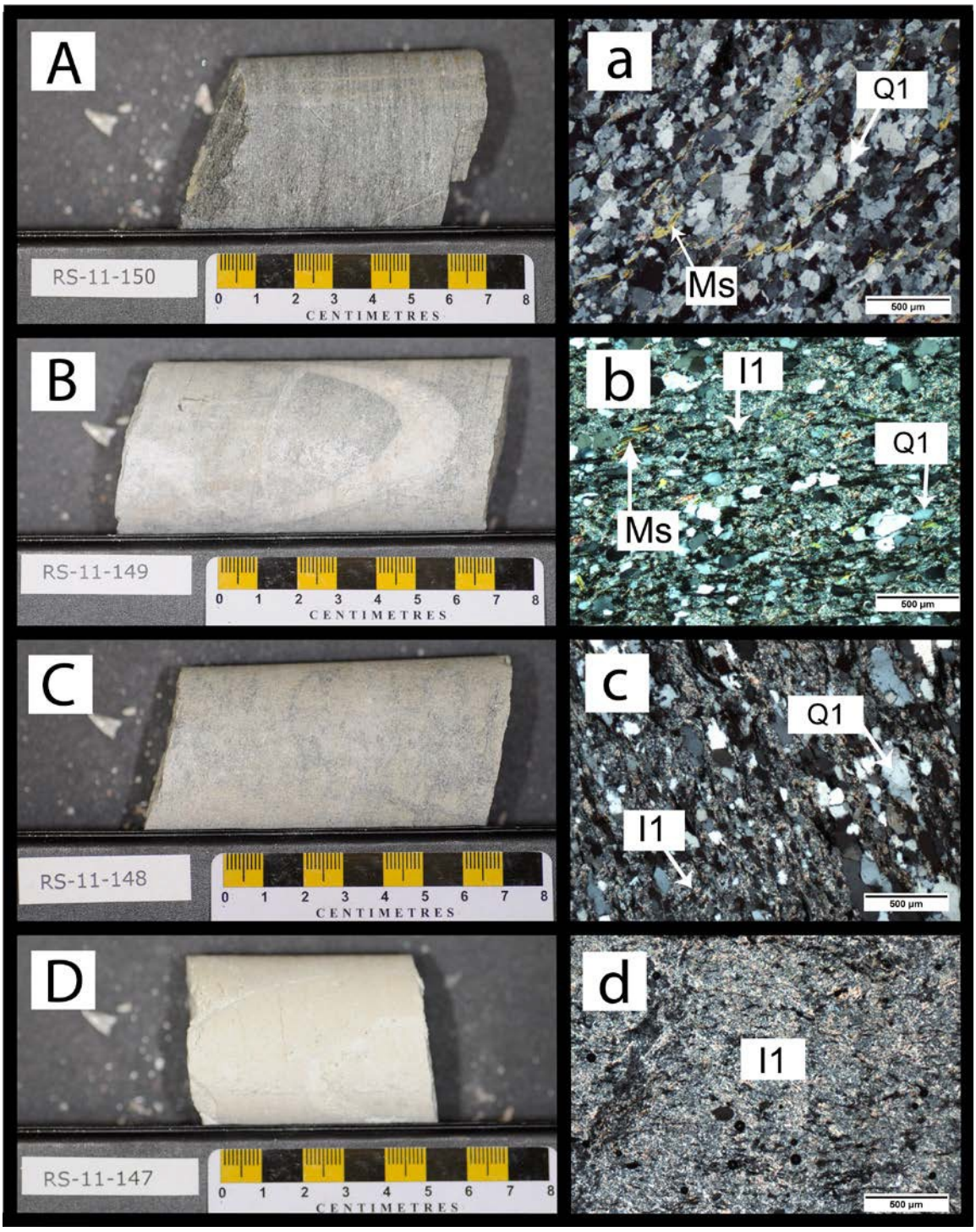

Figure 4.5: Drill core samples (RS-11-147 to 150) and corresponding thin-sections. A) Unaltered WLG. a) The unaltered rock is composed predominately of quartz with minor muscovite. B) Weakly altered WLG b) Illite has begun to replace some of the minerals, but all components of the rock are still present. C) Moderately altered WLG c) Muscovite is completely broken down leaving partially dissolved quartz grains in a matrix composed of illite. D) Highly altered WLG. d) The dominant mineral is illlite. Abbreviations: Q1 = First generation of quartz, Ms = Muscovite, I1 = First generation of illite.

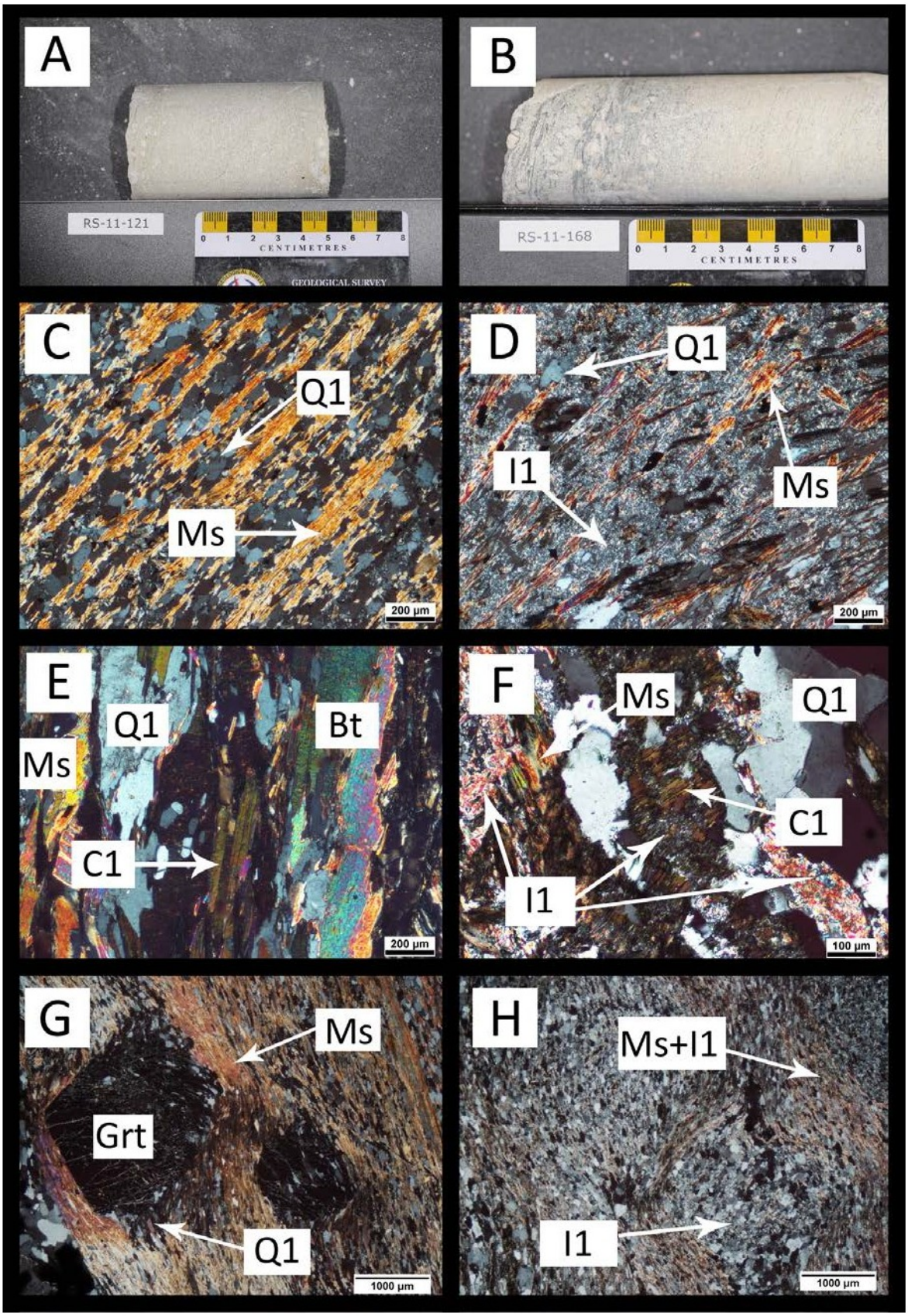
A
RS-11-121
CENTIMETRES
GEOLOGICAL SURVEY
B
RS-11-168
CENTIMETRES
C
Q1
Ms
200 µm
D
Q1
I1
Ms
200 µm
E
Q1
Bt
Ms
C1
200 µm
F
Ms
Q1
C1
I1
100 µm
G
Ms
Grt
Q1
1000 µm
H
Ms+I1
I1
1000 µm

Figure 4.6: Syn-ore hydrothermal alteration of the Pipedream assemblage metasediments. A) Illitized WLG (Sample RS-11-121), comparable to its unaltered equivalent in Fig. 4.2A. B) Altered garnet and biotite layer (Sample RS-11-168), comparable to its unaltered equivalent in Fig. 4.2B. C) Unaltered area composed of quartz and muscovite in the WLG (Sample RS-11-030). D) Alteration of an area similar to that shown in C, muscovite is broken down to illite (Sample RS-11-168). E) Unaltered area composed of quartz, muscovite, biotite and chlorite in the WLG (Sample RS-11-058). F) Alteration of an area similar to that shown in E, micas have been partially illitized, quartz remains relatively unaltered (Sample RS-11-160). G) Garnets surrounded by muscovite and quartz (Sample RS-11-076). H) Alteration of an area similar to that shown in G, garnets have been almost completely dissolved and muscovite is altering to illite (Sample RS-11-168). Abbreviations: Q1 = First generation of quartz, Ms = Muscovite, I1 = First generation of illite, Bt = Biotite, C1 = First generation of chlorite, Grt = Garnet.

A plot of illite, muscovite, and chlorite compositions on an MR^3-$2R^3$-$3R^2$ diagram (Fig. 4.7; Velde, 1975, 1977) show that these minerals have a range of compositions. The illite and muscovite can be clearly identified based on chemical composition (Fig. 4.8A). However, the composition of illite formed from the alteration of these minerals is sometimes phengitic (Fig. 4.8B & C).

Altered muscovite generally has lower K, Fe and Mg contents and higher Al and Si contents relative to unaltered muscovite. Illite generally has higher Si, Ca and Mg and lower Al and K than both unaltered and altered muscovite (Table 4.1; Appendix B). Plots of illite from the Bong deposit (Fig. 4.8) show highly variable chemical compositions. Illite forming at the expense of chlorite and muscovite may have a more phengitic composition than illite forming at the expense of feldspars.

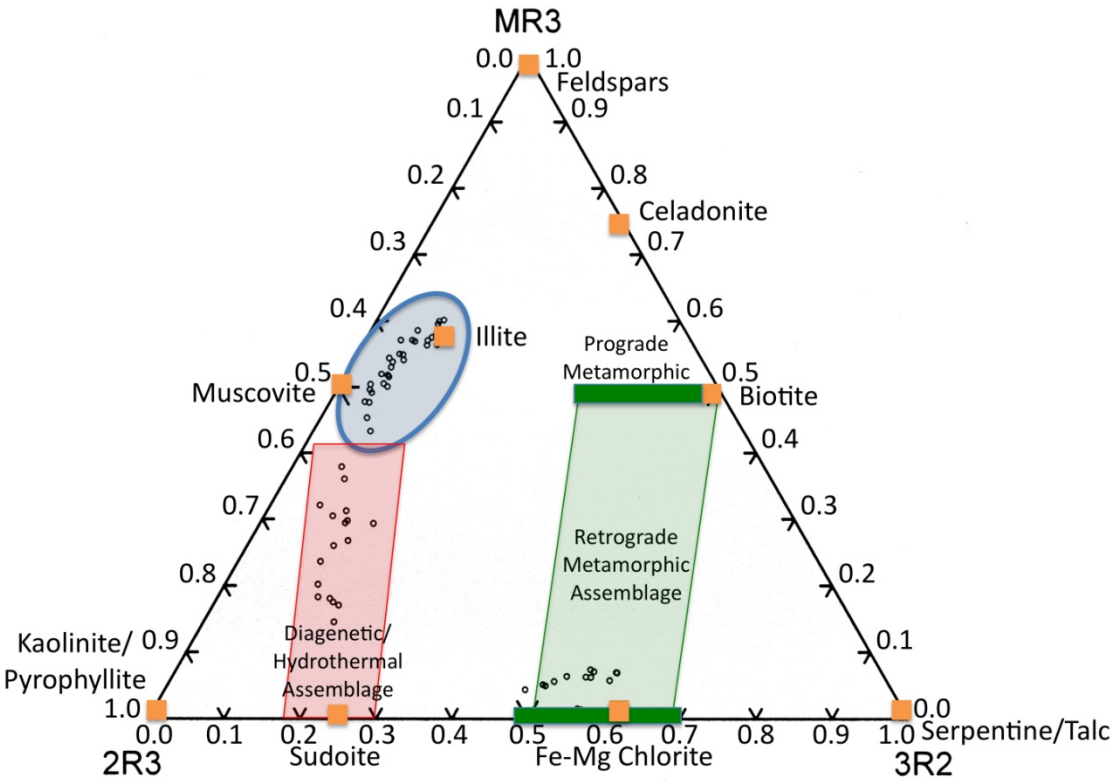

Figure 4.7: A simplified chemiographic representation of the assemblages formed during metamorphism and hydrothermal alteration. Data has been plotted on a MR^3-$2R^3$-$3R^2$ diagram (Velde, 1975, 1977), where $MR^3 = Na^+ + K^+ + 2Ca^{2+}$, $2R^3 = ((Fe^{3+} + Al^{3+} + Ti^{4+}) - MR^3) / 2$ & $3R^2 = ((Fe^{2+} + Mg^{2+} + Mn^{2+} + Ni^{2+}) / 3$. The blue box highlights the area where the muscovite and illite plot. While the red and green boxes represent the hydrothermal assemblage and metamorphic assemblage of minerals, respectively (Quirt, Pers. Comm. Jan 29, 2012)

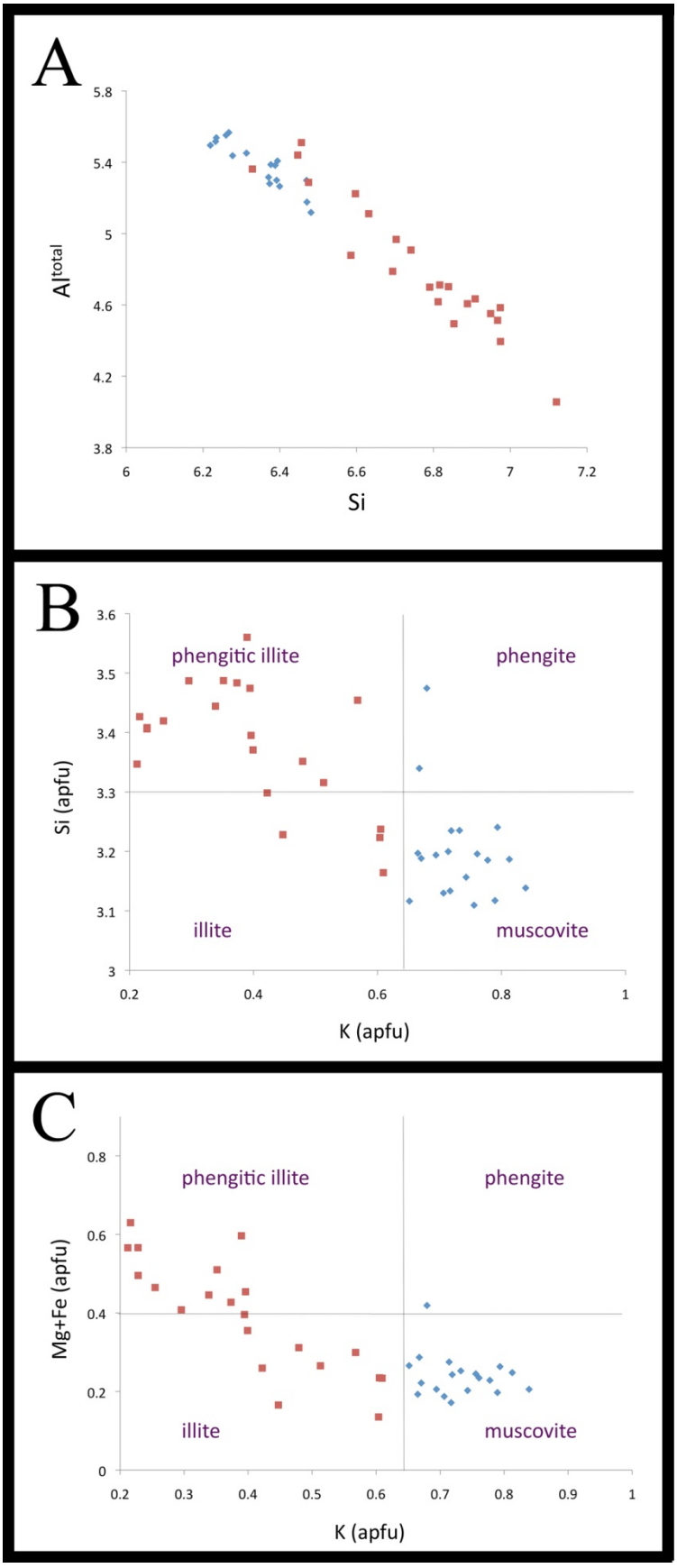

Figure 4.8: A) Plot of Al^{total} vs. Si. Muscovite* has a tighter grouping than illite*, which has a more variable composition. B) Plot of Si vs. K. Illite* has highly variable Si and K contents. Muscovite* is much more constrained in its Si and K content. C) Plot of Mg + Fe vs. K. Illite* has a highly variable Fe + Mg content. Muscovite* has slightly elevated Fe + Mg content.

*Illite = Red, Muscovite = Blue (based on petrography)

Table 4.1: Sample EMPA data for phyllosilicates from the Bong deposit (see Appendices B and C for full data set).

Sample	Mineral	SiO_2	Al_2O_3	K_2O	CaO	FeO	MgO	Total
RS-11-072	Muscovite	45.76	29.60	10.21	0.02	3.87	1.52	90.99
RS-11-072	Muscovite	45.41	30.81	10.00	0.05	4.79	1.77	92.84
RS-11-072	Muscovite	46.42	30.38	10.15	0.05	4.35	2.01	93.36
RS-11-072	Muscovite	47.04	31.63	10.15	0.03	4.11	1.48	94.44
RS-11-072	Muscovite	46.09	31.51	10.23	0.00	4.29	1.53	93.64
RS-11-072	Muscovite	45.93	30.88	10.22	0.01	4.53	1.61	93.16
RS-11-072	Muscovite	46.78	30.24	10.58	0.01	4.08	1.51	93.19
RS-11-072	Muscovite	49.16	28.14	10.30	0.07	4.37	1.81	93.84
RS-11-072	Muscovite	45.96	31.12	10.85	0.00	4.49	1.58	94.00
RS-11-072	Muscovite	45.57	31.41	10.33	0.05	4.48	1.58	93.42
Average	**Muscovite**	**46.41**	**30.57**	**10.30**	**0.03**	**4.33**	**1.64**	**93.29**
303GC	Alt. Muscovite	46.68	35.00	8.89	0.01	2.52	1.05	94.16
303GC	Alt. Muscovite	47.47	35.73	8.40	0.01	2.00	0.79	94.39
303GC	Alt. Muscovite	48.24	34.49	8.22	0.02	1.94	0.99	93.90
303GC	Alt. Muscovite	48.31	34.63	7.97	0.01	2.05	1.10	94.08
303GC	Alt. Muscovite	47.46	35.77	8.52	0.01	1.73	0.77	94.27
303GC	Alt. Muscovite	45.20	33.95	7.41	0.05	2.99	0.91	90.51
301GC	Alt. Muscovite	47.45	34.77	8.76	0.00	1.80	1.04	93.81
302GC	Alt. Muscovite	47.27	33.25	8.82	0.04	1.90	1.26	92.54
302GC	Alt. Muscovite	46.86	33.69	7.07	0.08	1.98	1.21	90.89
302GC	Alt. Muscovite	47.65	33.27	8.34	0.02	2.13	1.56	92.97
Average	**Altered**	**47.26**	**34.45**	**8.24**	**0.03**	**2.10**	**1.07**	**93.15**
303GC	Illite	51.92	29.55	6.69	0.30	1.51	2.17	92.15
303GC	Illite	51.51	28.63	4.58	0.45	2.05	2.79	90.00
303GC	Illite	50.00	33.59	5.02	0.11	2.24	1.38	92.34
301GC	Illite	50.14	30.98	4.66	0.19	2.79	1.98	90.73
301GC	Illite	51.02	28.78	3.72	0.29	2.62	3.15	89.57
301GC	Illite	50.85	24.58	4.36	0.53	4.77	3.04	88.12
302GC	Illite	50.64	29.74	4.63	0.24	3.90	2.35	91.51
302GC	Illite	50.24	32.52	6.83	0.08	2.29	1.77	93.74
303GC	Illite	52.27	28.91	6.26	0.07	2.66	2.64	92.81
302GC	Illite	50.03	28.39	3.86	0.38	3.83	2.20	88.68
Average	**Illite**	**50.86**	**29.57**	**5.06**	**0.26**	**2.87**	**2.35**	**90.96**

Temperature estimates were calculated from illite chemical compositions using equation [7] (Battaglia, 2004):

$$T\ (°C) = 267.95x + 31.50 \qquad [7]$$

where x = K+|Fe-Mg| and K, Fe and Mg are expressed in cations per 11 oxygen atoms.

Based on chemical compositions provided in Appendix C and equation 7, the Bong illite has formation temperatures that range from 124°C to 214°C with an average value of 163°C. The complete data set of the illite chemical compositions can be found in Appendix C.

Other minerals in the syn-ore assemblage are pyrite (P2), rutile (R2), apatite (A2) and chlorite (C2). Although others have observed the presence of APS minerals in the Kiggavik area (Davis *et al*., 2011), no APS minerals were observed in the current study. Furthermore, compared to the other deposits in the Andrew Lake-Kiggavik trend (e.g., End, Andrew Lake), APS minerals are much more rare in the Bong deposit (Riegler. Pers. Com. Jan 23, 2013). Pyrite occurs as subhedral-euhedral grains that are 0.05-0.2 mm wide (Fig. 4.9A) and is more abundant in areas of mineralization than in unaltered host rock. Pyrite is sometimes observed in close proximity to rutile. Rutile is composed of subhedral-anhedral grains that are 0.05-0.3 mm wide (Fig. 4.9A & B) and is more abundant in areas that were previously rich in biotite and garnet. Syn-ore apatite fills fractures in the rock and is generally composed of 0.1-0.2 mm anhedral grains (Fig. 4.9 C). Chlorite occurs as laths that are 0.2-0.6 mm long within the illite matrix. Chlorite that formed at this stage is distinct from earlier generations of chlorite because it is not altered to illite (e.g., Fig. 4.6 F vs. Fig. 4.9 D).

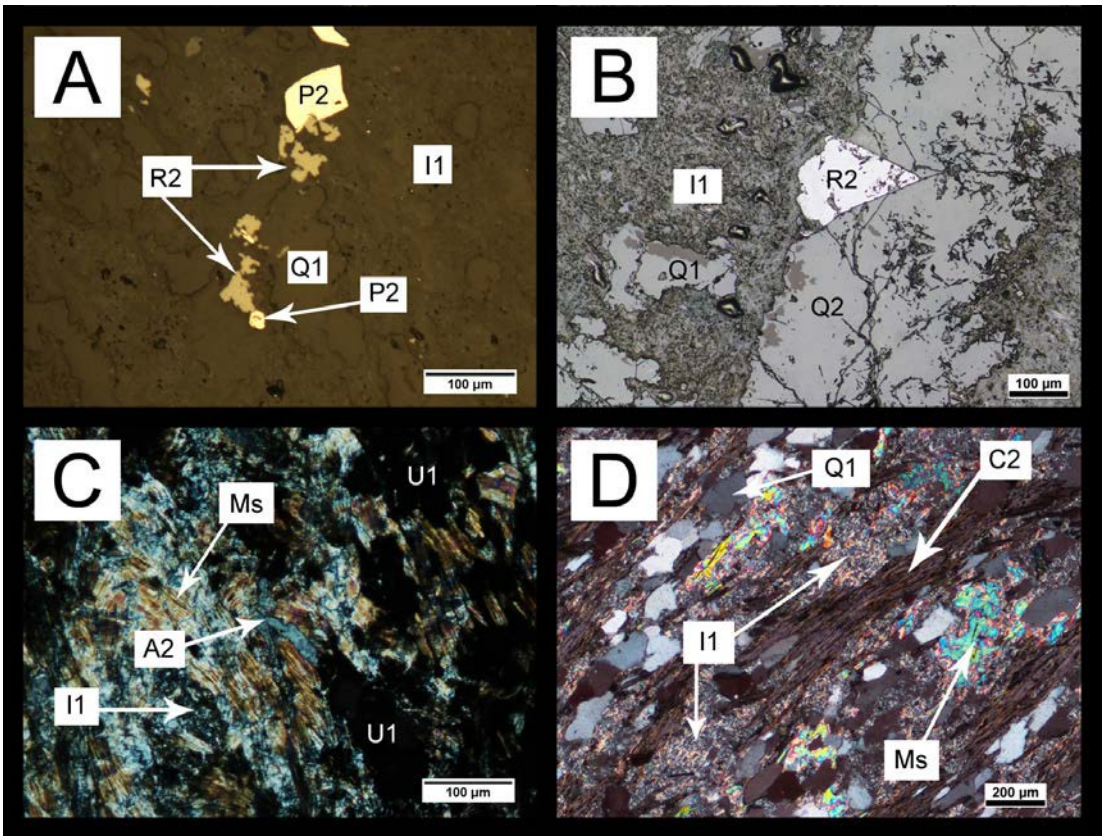

Figure 4.9: Reflected and transmitted light images of minerals in the main ore assemblage. A) Pyrite and rutile forming together (Sample 302GC). B) Hydrothermal rutile forming in a fracture of a pre-ore quartz vein (Sample RS-11-162). C) Hydrothermal apatite forming along with illite and uraninite (Sample RS-11-142). D) Syn-ore chlorite that is unaltered by syn-ore illite, pre-ore muscovite is highly altered (Sample RS-11-139). Abbreviations: Q1 = First generation of quartz, P2 = Second generation of pyrite, R2 = Second generation of rutile, I1 = First generation of illite, Ms = Muscovite, U1 = Stage A uraninite, C2 = Second generation of chlorite.

Organic matter is also present in the Bong deposit (Fig. 4.10A). The organic matter is restricted to the host-rock alteration zone and is disseminated and fills fractures in core (Fig. 4.10B). At the thin-section scale, organic matter fills fractures and pore space, as well as between cleavage planes in mica minerals (Fig. 4.10C). Finely disseminated organic matter is also present with the roll-front style of mineralization (U2; Fig. 10D & E).

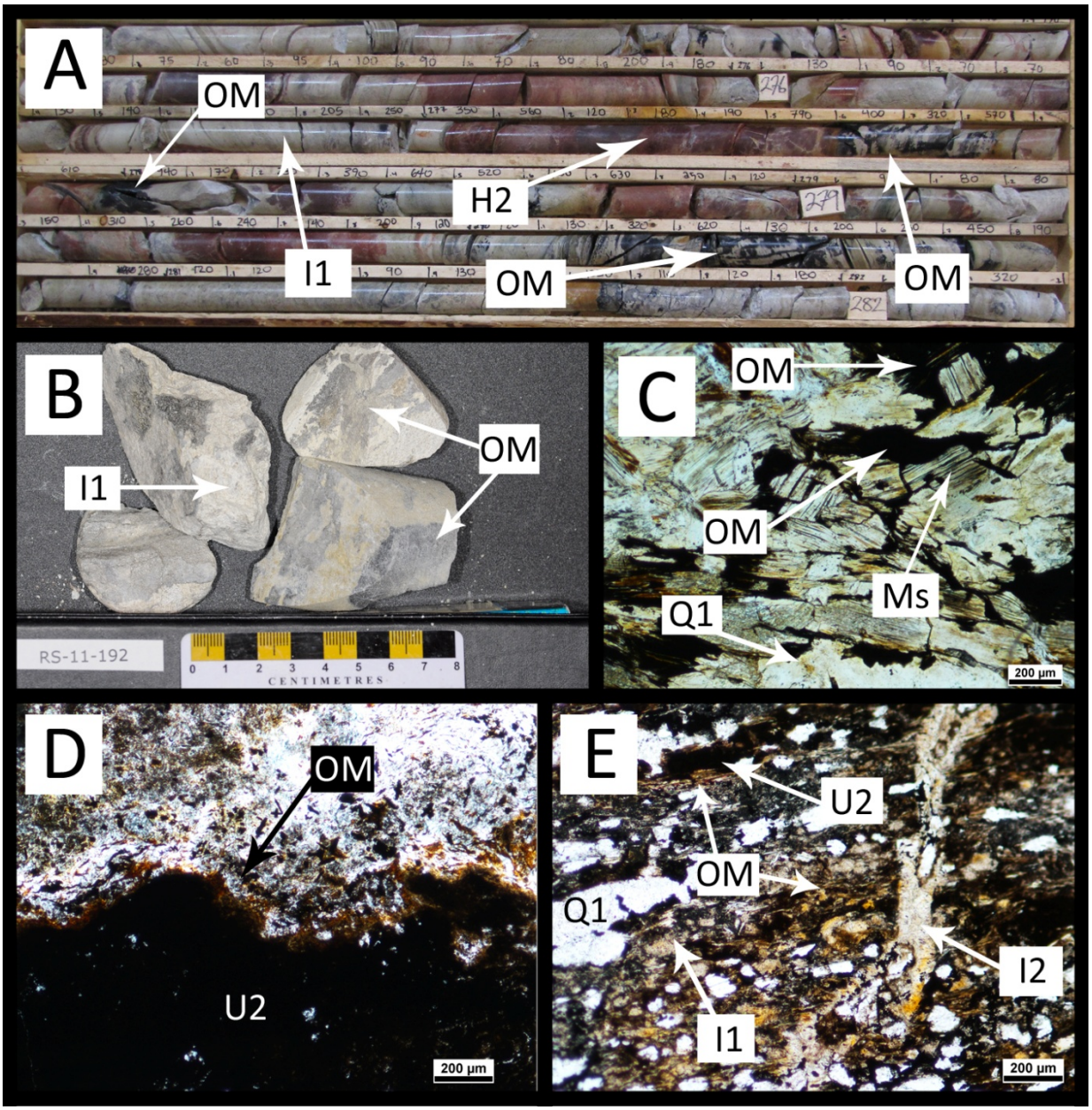

Figure 4.10: Organic matter in the Bong Deposit. A) Organic matter along fractures in core (Hole Bong-50). B) Drill core sample of organic matter in the altered zone (Sample RS-11-192). C) Transmitted light image of organic matter within fractures, filling pore space and in cleavage planes in muscovite. (Sample RS-11-158). D) Organic matter associated with Stage B uraninite (Sample RS-11-160). E) Organic matter filling fractures and pore space and associated with Stage B uraninite. A late generation of illite crosscuts all these features. (Sample RS-11-176). Abbreviations: OM = Organic matter, I1 = First generation of illite, H2 = Second generation of hematite, U2 = Stage B uraninite, Q1 = First generation of quartz, I2 = Second generation of illite.

Syn-Stage B Alteration Minerals

Post-ore alteration features and minerals consist of mini-redox fronts (illite, chlorite, sulphides, uraninite, carbonaceous material, goethite and hematite), illite, calcite and drusy quartz.

The most striking feature is the presence of mini-roll fronts or redox fronts (Fig. 4.11), where an oxidized zone is separated from a reduced zone by a front that is often mineralized. Three distinct zones characterize the redox fronts. These zones are similar to those observed by Mercadier *et al*. (2011) at Eagle Point and P-Patch:

1) A bleached (reduced) zone consisting of illite ± chlorite.
2) A brownish/black zone containing goethite and uraninite, which represents the uranium redox front.
3) A hematized (oxidized) zone rich in hematite.

The redox fronts are both barren (Fig. 4.11A) and mineralized (Fig. 4.11B), and fronts sometimes terminate on contact with organic matter (Fig. 4.11C).

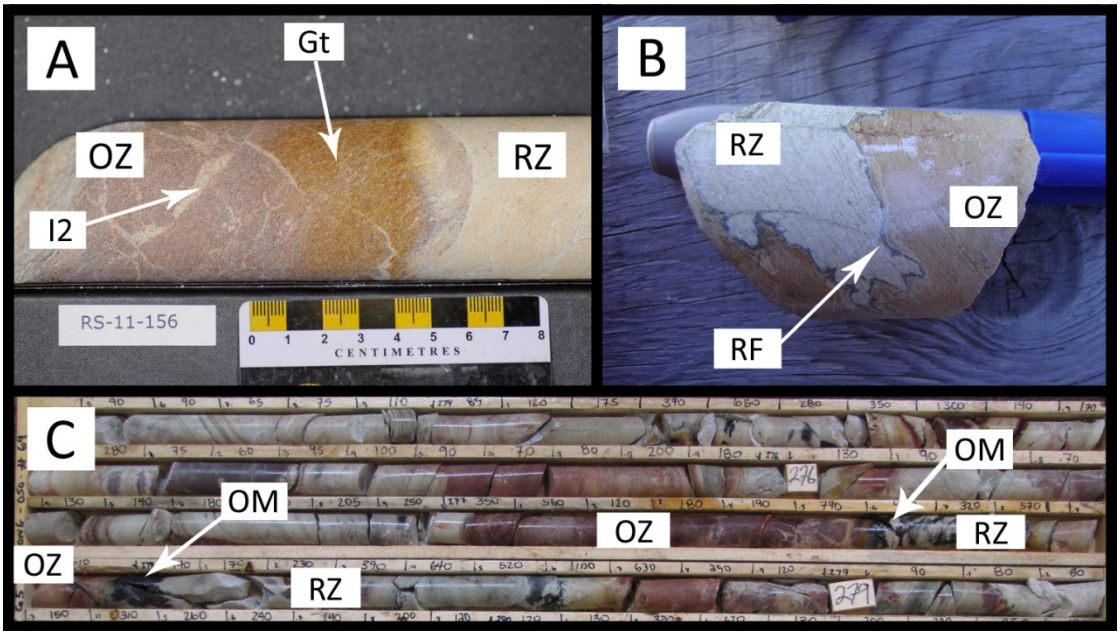

Figure 4.11: Redox fronts from the Bong deposit. A) A barren redox front (Sample RS-11-156). B) A mineralized redox front (Sample RS-11-176). C) Redox fronts terminating upon contact with organic matter (Hole Bong-50). Abbreviations: OZ = Oxidized zone, RF = Redox front, RZ = Reduced zone, Gt = Goethite, OM = Organic matter I2 = Second generation of illite.

The bleached zone consists mainly of a microcrystalline matrix of illite. Chlorite (0.2-0.4 mm) is locally present as tabular grains within the illite matrix. Primary rock-forming minerals (e.g., quartz, muscovite) are sometimes observed, but are rare. The bleached zone just beyond the uranium redox front and, to a lesser extent the redox front itself, are generally enriched in sulphides.

The redox front itself is composed of uraninite (U2) that occurs in voids and as coatings around previous minerals (e.g., rutile, apatite, pyrite). Goethite is also present at the redox front (Fig. 4.11A) and occurs as disseminated grains in the illite matrix.

The sulphides associated with the redox fronts consist of pyrite, galena and chalcopyrite. Pyrite occurs in veins that crosscut Stage A uraninite (Fig. 4.12A), subhedral-euhedral grains forming around Stage A uraninite (Fig. 4.12B), cementing Stage A uraninite (Fig. 4.12C) and intergrown with chalcopyrite (Fig. 4.12D). The veins are small (<20 μm wide) and rare; however the subhedral-euhedral grains (~0.1 mm in diameter) are common near the redox fronts, which contrast to the metamorphic and ore- stage pyrite that is much less common and generally larger. Galena occurs as subhedral to euhedral grains that are generally <100 μm (Fig. 4.12E & F). The galena is generally observed in close proximity (filling fractures) or exsolved in Stage A uraninite (e.g., 4.12A & F).

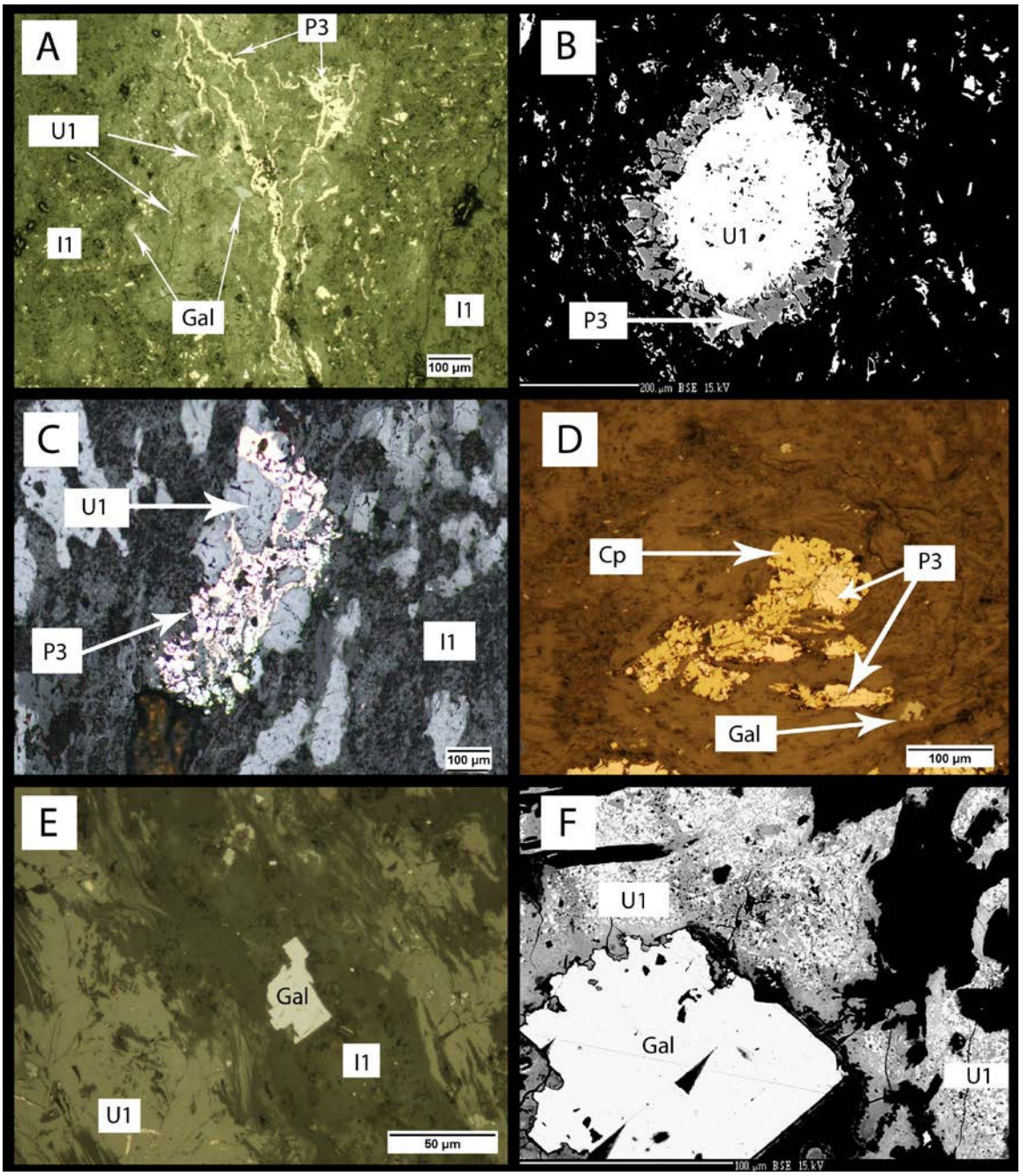

Figure 4.12: Reflected light and BSE images of sulphides in the Bong deposit. A) Pyrite veins crosscutting uraninite and exsolved galena in a grain of uraninite (Sample 302GC). B) Pyrite forming around a grain a uraninite (Sample 303GC). C) Pyrite cementing grains from the first generation of uraninite (Sample 303GC). D) Chalcopyrite intergrown with pyrite, subhedral galena grain is also present (Sample RS-11-142). E) Subhedral galena grain forming near altered Stage A uraninite (Sample RS-11-172). F) Galena forming within an altered grain of uraninite (Sample RS-11-143). Abbreviations: P3 = Third generation of pyrite, Gal = Galena, I1 = First generation of illite, U1 = Stage A uraninite Cp = Chalcopyrite.

In the oxidized zone, hematite is disseminated throughout (Fig. 4.11). However, apart from the hematite overprint, the oxidized zone displays the same alteration and primary mineralogy as the bleached zone, which is composed mainly of illite, chlorite, altered muscovite and quartz (Fig. 4.13A & B). Hematite can range from sparsely (Fig. 4.13C) to pervasively (Fig. 4.13D) disseminated throughout. There are no sulphides or uranium minerals observed in the oxidized zone.

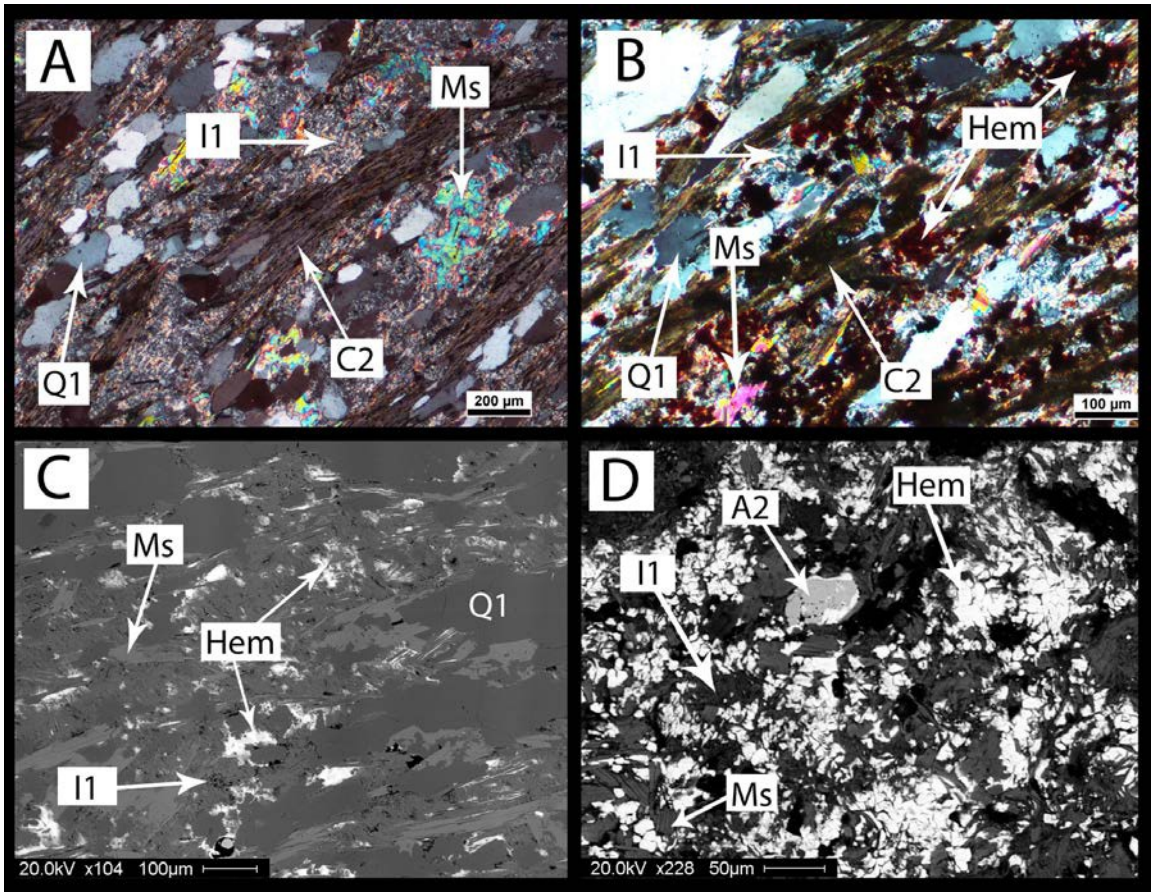

Figure 4.13: Late-stage hematite in the oxidized zone in the Bong deposit. A) Quartz, muscovite, chlorite and illite in the bleached zone (Sample RS-11-139). B) Quartz, muscovite, chlorite and illite with a hematite overprint in the oxidized zone (Sample RS-11-140). C) Sparsely disseminated hematite (Sample RS-11-140). D) Pervasive disseminated hematite (Sample RS-11-162). Abbreviations: Q1 = First generation of quartz, Ms = Muscovite, C2 = Second generation of chlorite, I1 = First generation of illite, Hem = Hematite, A2 = Second generation of apatite.

Post-mineralization Alteration Minerals

Illite, calcite and drusy quartz post-date the U-Fe redox fronts of the Stage B mineralization. The illite (I2) crosscuts the earlier generation of matrix illite (I1) and occurs in veins that are 1 to 6 mm wide (Fig. 4.14). Calcite occurs in veins that are 1 to 5 mm wide (Fig. 4.15). Drusy quartz crystals infill 2 cm wide fractures in the altered metasediments (Fig. 4.16). Individual quartz crystals are perfectly euhedral and are up to 8 mm long.

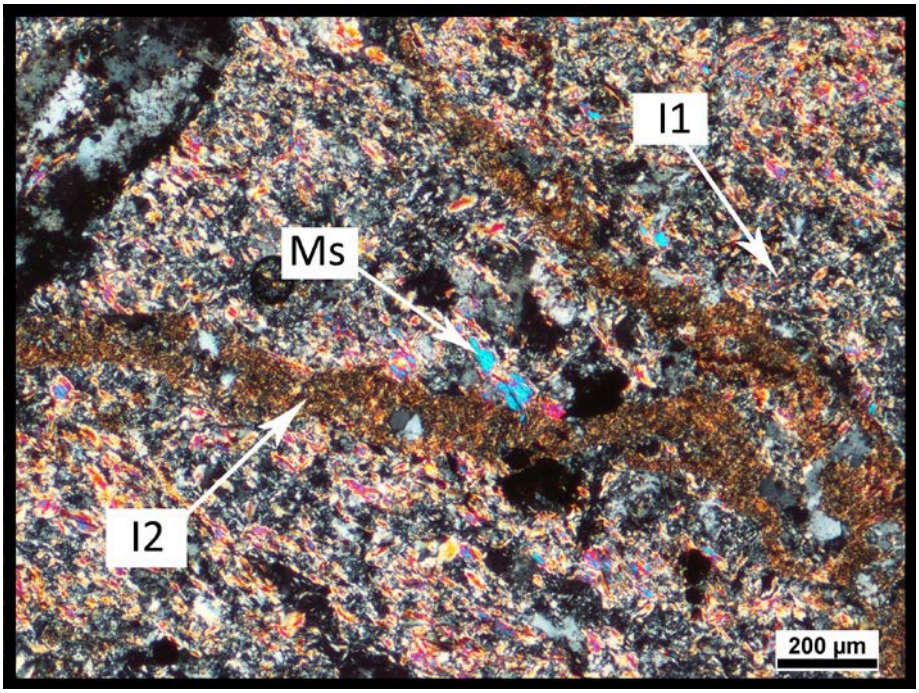

Figure 4.14: Late illite veins crosscutting the first generation of illite (Sample RS-11-191). Abbreviations: Ms = Muscovite, I1 = First generation of illite, I2 = Second generation of illite.

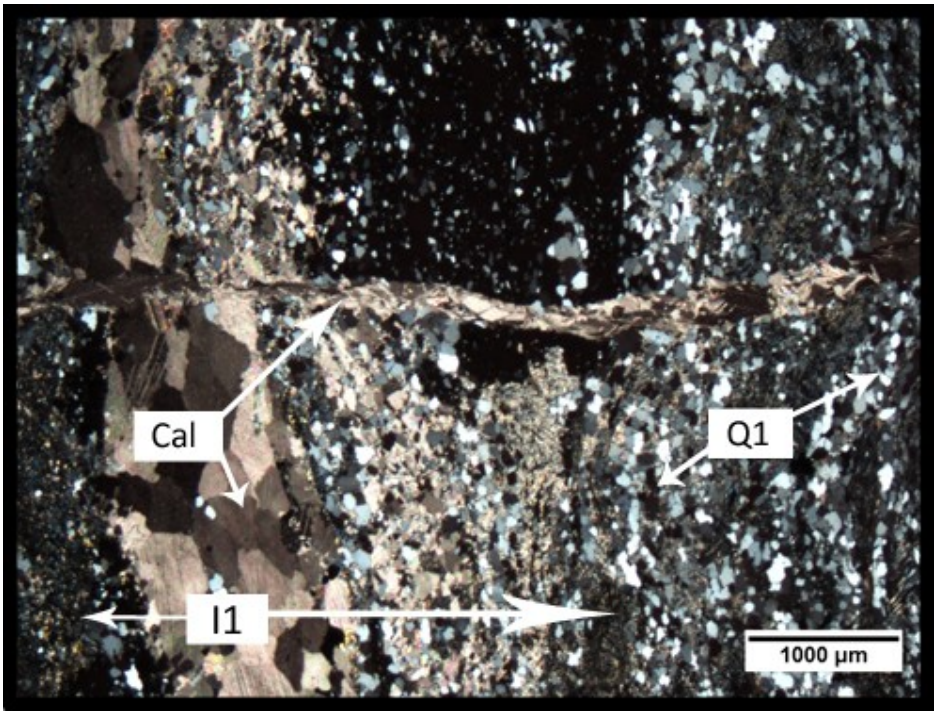

Figure 4.15: A 1mm wide calcite vein being crosscut by a second, smaller calcite vein. The calcite veins crosscut areas that have been altered to illite (Sample RS-11-170). Abbreviations: Q1 = First generation of quartz, I1 = First generation of illite, Cal = Calcite.

Figure 4.16: Late drusy quartz (up to 8 mm) forming in a fracture (~2 cm wide) in strongly bleached basement rock (Sample RS-11-155).

4.1.3 Uranium Minerals

There are three main styles of uranium mineralization observed in the Bong deposit; (1) uraninite in veins parallel to foliation (U1a; Fig. 4.17A), (2) uraninite coating and filling fractures in graphite nodules (U1b; Fig. 4.17B) and (3) uraninite in roll-fronts (U2; Fig. 4.17C & D). Vein and graphite-associated uraninite are Stage A uraninite, while mini-roll-fronts are Stage B uraninite.

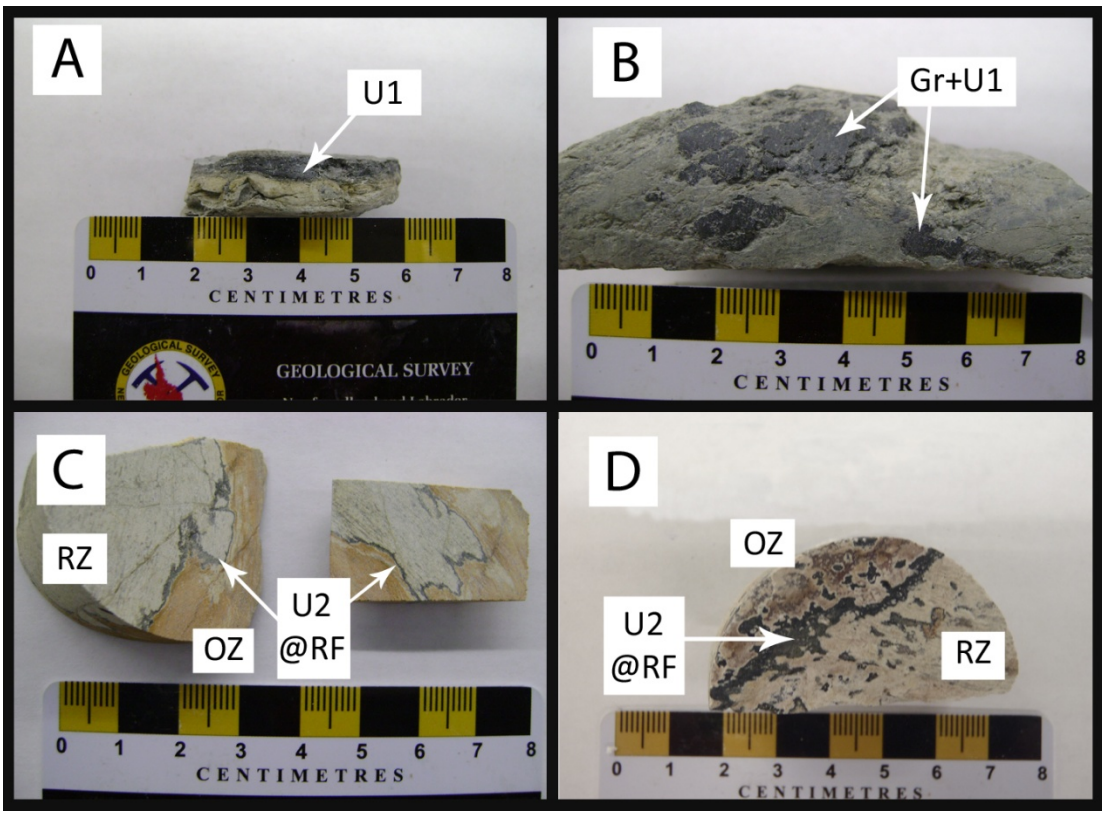

Figure 4.17: Styles of uranium mineralization in the Bong deposit. A) Foliation parallel fracture filling vein-type uraninite (Sample RS-11-172). B) Graphitic nodules with uraninite coating and filling fractures (Sample 302GC). C) Roll-front uraninite with well defined redox front (Sample RS-11-176). D) Roll-front uraninite with a less well-developed redox front (Sample RS-11-162). Abbreviations: U1 = Stage A uraninite, Gr = Graphite, U2 = Stage B uraninite, RZ = Reduced zone, OZ = Oxidized zone, RF = Redox front.

The vein-type mineralization occurs roughly along the foliation of the host rock in the illitized zone, although the mineralized areas are often enriched in

chlorite (Fig. 4.18A). Individual veins are narrow, less than 5 mm wide (Fig. 4.18B & C) and consist of uraninite filling fractures and voids along the plane of foliation (Fig. 4.18D & E). This style of mineralization will be referred to as vein-type.

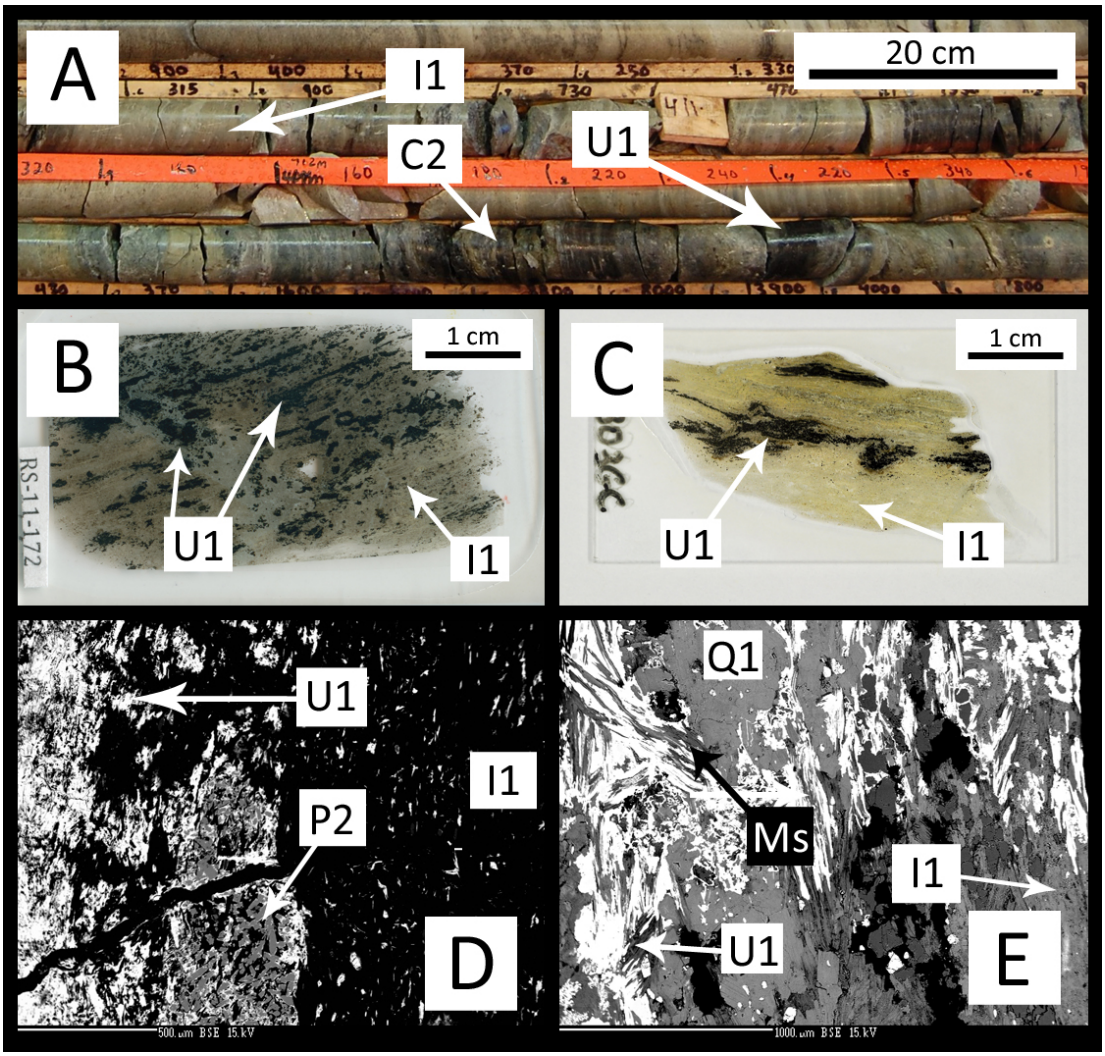

Figure 4.18: Vein-type uraninite from the Bong Deposit. A) Uraninite forming along foliation (perpendicular to core axis) with illite and chlorite (Hole Bong-39). B) Thin section of RS-11-172 showing uraninite forming within the plane of foliation. C) Thin section of sample 303GC displaying the same style of uraninite as B. D) BSE image of uraninite forming in fractures parallel to foliation (Sample 303GC) E) BSE image of uraninite filling fractures between quartz and muscovite. (Sample RS-11-172). Abbreviations: U1 = Stage A uraninite, I1 = First generation of illite, C2 = Second generation of chlorite, P2 = Second generation of pyrite, Ms = Muscovite, Q1 = First generation of quartz.

Two types of carbonaceous material are present in the Bong deposit: 1) graphite and 2) unidentified organic matter. Graphite occurs mainly as nodules and blebs, while the organic matter occurs filling fractures, within voids and in cleavage planes of previous minerals (e.g., muscovite). The graphite is much more competent than the organic matter which is very soft and has a distinct sulphur smell.

Rare graphite-rich material is observed in core (Fig. 4.19A). Individual nodules and blebs are 0.5-3 cm in diameter (Fig. 4.19B-D). Uraninite is observed rimming and filling fractures within the nodules and blebs (Fig. 4.19E & F).

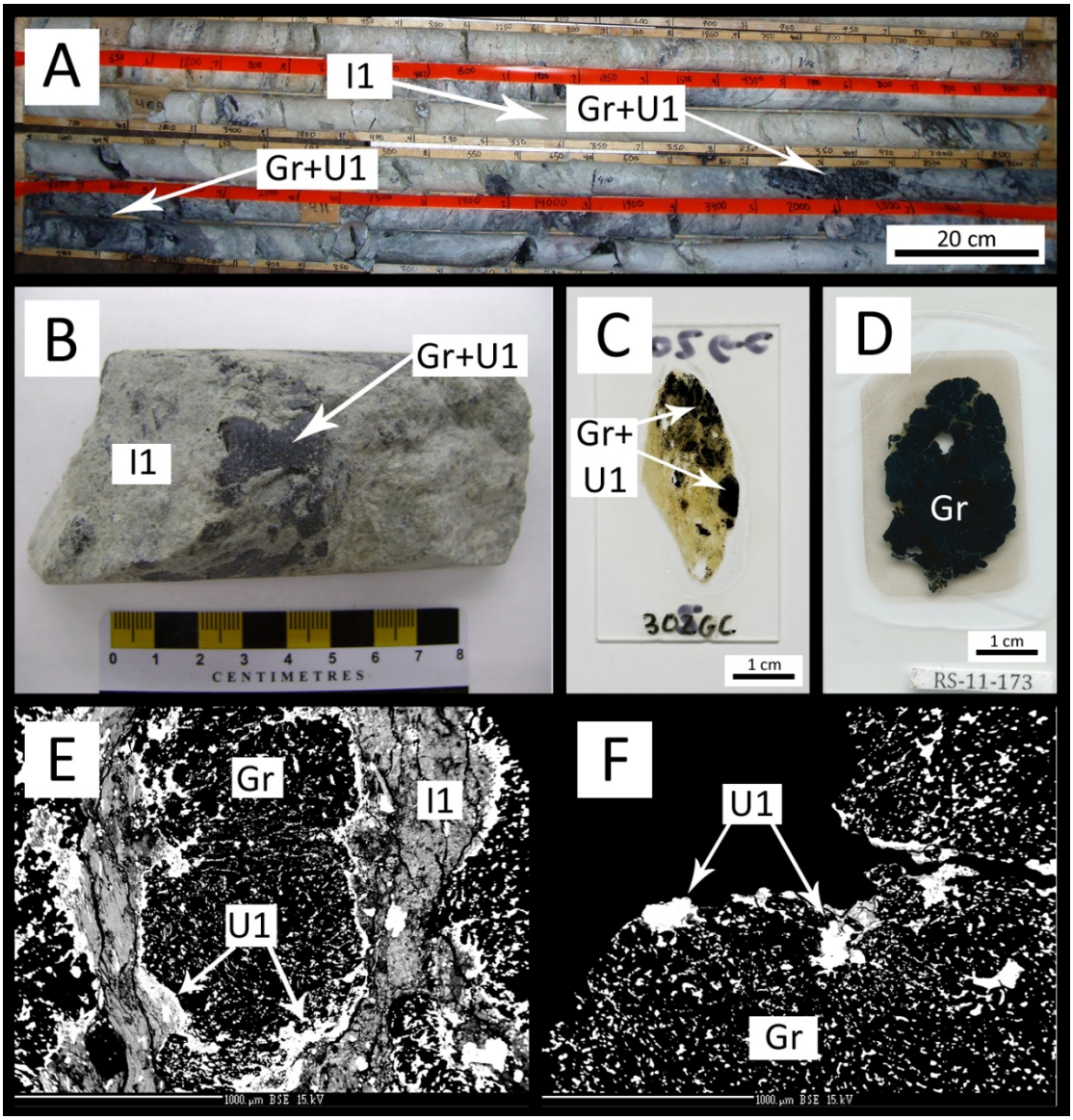

Figure 4.19: Graphitic material in the Bong deposit. A) Mineralized graphitic zones in drill core. B) Graphite nodules in drill core (Sample 302GC). C) Thin section of sample 303GC, showing graphite nodules in a clay-rich matrix. D) Thin section of a large graphite nodule (Sample RS-11-173). E) BSE image of uranium filling fractures and coating graphite nodules (Sample 302GC). F) Close up of the edge of a graphite nodule, uraninite is observed filling all pore space. (Sample RS-11-173). Abbreviations: U1 = Stage A uraninite, Gr = Graphite, I1 = First generation of illite.

The uraninite in the roll-fronts occurs at redox boundaries ("fronts"; Fig. 4.20A) between an oxidized zone that is rich in hematite (plus illite) and a reduced ("bleached") zone composed of almost entirely illite (Fig. 4.11). The uraninite occurs along redox fronts that range from 1 mm to 1 cm in width (Fig. 4.20B & C). The

uraninite occurs along the front as matrix cement (Fig. 4.20B) and as blebby grains (Fig. 4.20C) up to 3 mm wide. The uraninite associated with the roll-fronts is observed to cement alteration minerals from the first stage of mineralization (Fig. 4.20D & E), such as apatite (A2), rutile (R2), and illite (I1).

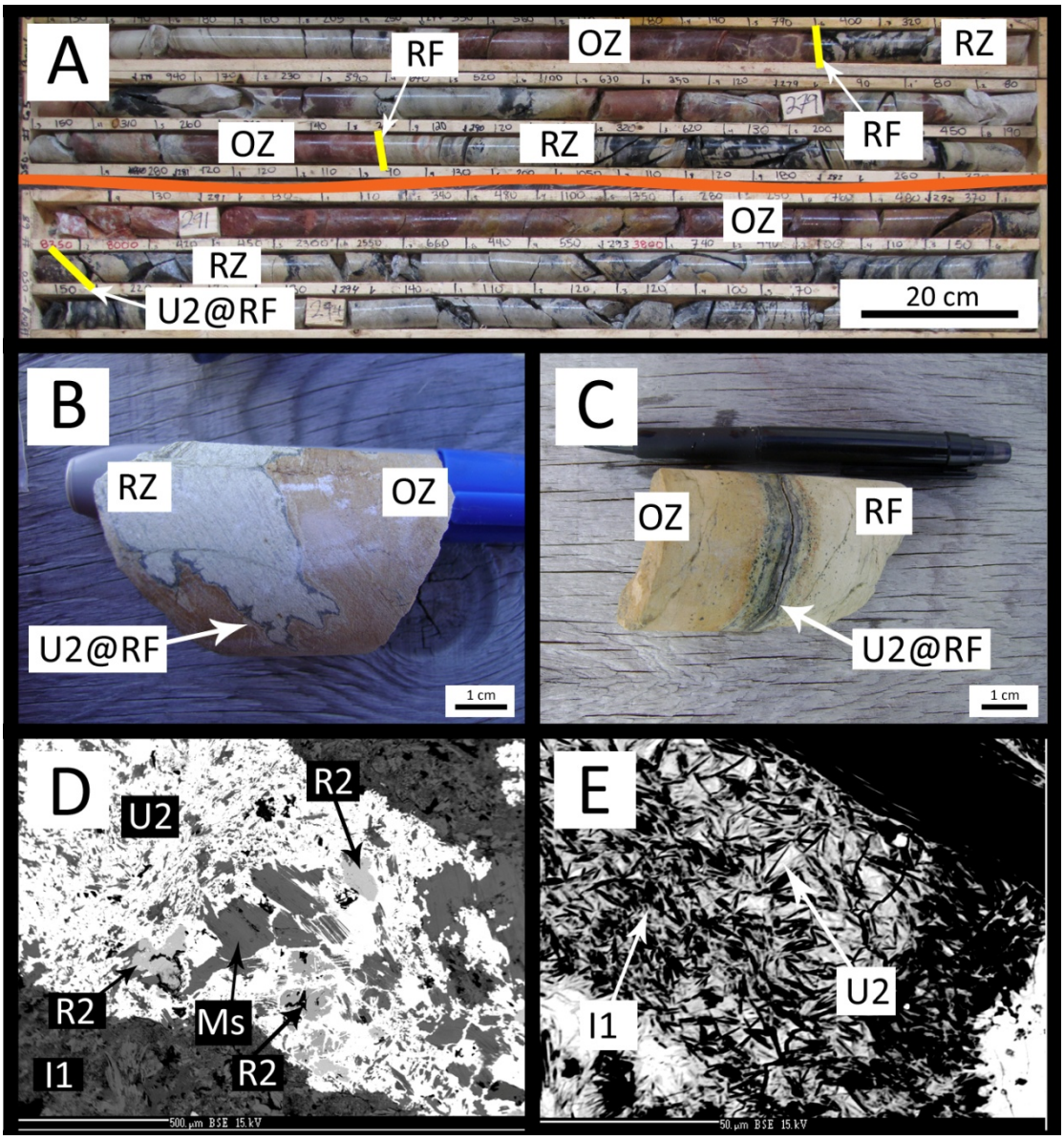

Figure 4.20: Roll-front uraninite in the Bong deposit. A) Roll-fronts consisting of oxidized and reduced zones in core (Hole Bong-50). B) Mineralized redox front with a sharp contact between oxidized and reduced zones (Sample RS-11-1760 C) Mineralized redox front with small blebs of uraninite surrounding the redox front (Sample RS-11-191). D) Stage B uraninite cementing minerals associated with Stage A uraninite. (Sample RS-11-162). E) Stage 1 illite cemented by Stage B uraninite (Sample RS-11-191). Abbreviations: OZ = Oxidized zone, RF = Redox front, RZ = Reduced zone, U2 = Stage B uraninite, I1 = First generation of illite, R2 = Second generation of rutile, Ms = Muscovite.

The uraninite in the three styles of mineralization has undergone varying degrees of alteration that is reflected by the mineral chemistry. Vein-type uraninite (U1a) is the most visibly altered and is composed of grains that are generally less

than a few hundred microns in size that are highly fractured and altered (Fig. 4.21). The mineral alteration is characterized by lower reflectance on back-scattered electron images due to the incorporation of elements like Si and Ca into the uraninite structure (Fig. 4.21A- D). Vein-type uraninite contains variable amounts of Pb (3.4-13.1 wt.% PbO), silica (SiO_2 up to 6.2 wt.%), and Ca (CaO <1.6 wt.%). The higher Si and Ca contents in the uraninite are generally linked to the areas that have been visibly altered. U1 is also altered to uranophane and a Ca-rich uranium mineral, possibly becquerelite (Fig. 4.21; Table 4.2).

Uraninite associated with graphite (U1b) is also characterized by variable amounts of Pb (2.4-10.2 wt.% PbO), silica (1.3-13.7 wt.% SiO_2), and Ca (0.7-1.2 wt.% CaO), while the roll-front uraninite (U2) is characterized by low Pb (<2.1 wt.% PbO) and silica (1.24-1.71 wt.% SiO_2), but higher Ca contents (1.4-6.8 wt % CaO).

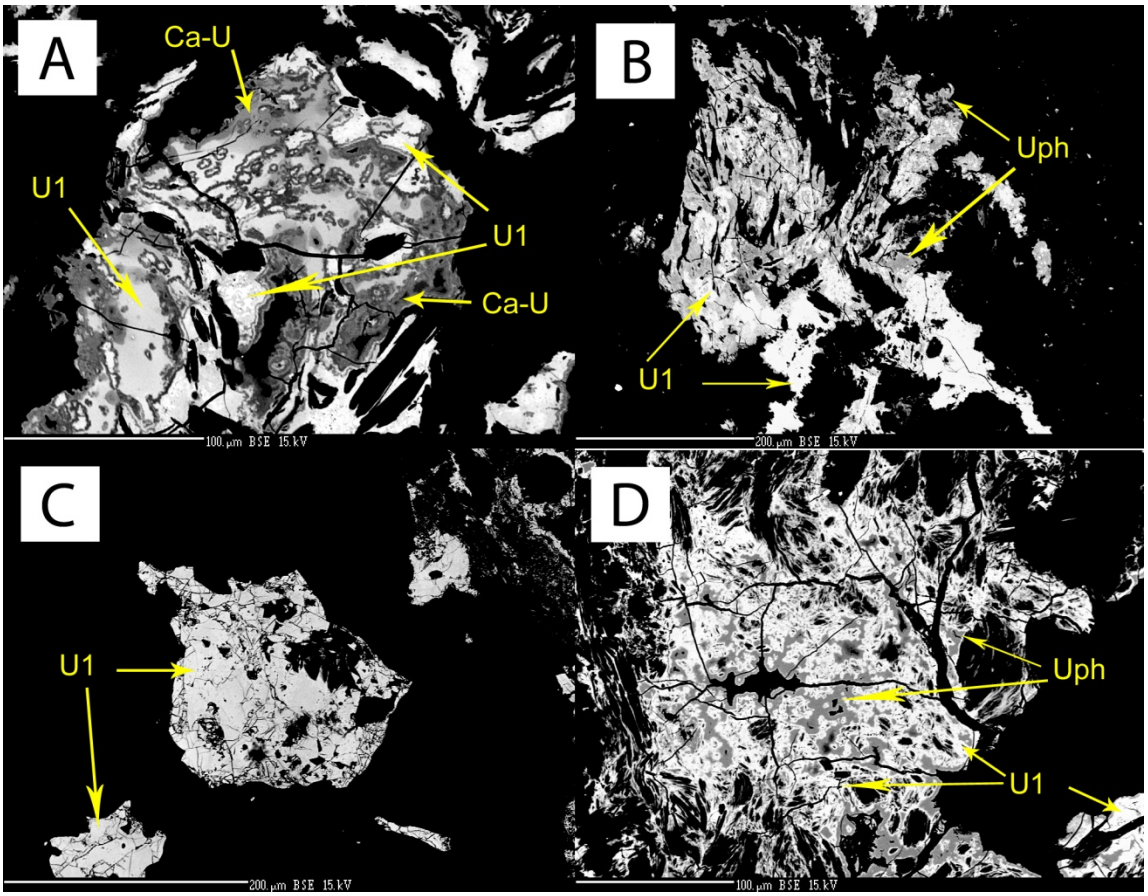

Figure 4.21: BSE images of uraninite grains from the Bong deposit. Lighter areas represent more pristine uraninite and darker areas are indicative of alteration. A) Uraninite that has been altered to Ca-rich uranium minerals (Sample RS-11-143). B) Uraninite that has been altered to uranophane (Sample 303GC) C) Formerly subhedral grains that are now highly fractured and altered (Sample RS-11-172). D) Alteration to uranophane along fractures in the uraninite grain (Sample 301GC). Abbreviations: U1 = Stage A uraninite, Uph = Uranophane, Ca-U = Calcium-rich uranium mineral.

Table 4.2: Sample EMPA data (wt. %) for alteration phases after uraninite from the Bong deposit.

Sample	Mineral	UO_2	SiO_2	CaO	PbO	FeO	Al_2O_3	Total
RS-11-143	Uranophane	58.91	22.17	2.65	<DL	0.85	2.51	87.09
RS-11-172	Uranophane	49.73	20.31	3.71	<DL	0.64	3.48	77.87
303GC	Uranophane	57.19	16.13	2.58	1.96	0.88	1.65	80.39
RS-11-143	Ca-U	80.89	1.49	5.11	0.36	<DL	0.14	87.99
RS-11-143	Ca-U	81.27	1.43	5.05	0.37	0.03	0.11	88.26
RS-11-143	Ca-U	81.43	1.65	5.24	0.40	0.02	0.27	89.01
RS-11-172	Ca-U	83.77	1.71	5.39	0.61	0.01	0.17	91.66
RS-11-172	Ca-U	85.19	1.68	5.27	0.52	0.03	0.16	92.85
RS-11-172	Ca-U	83.67	1.61	5.53	0.56	<DL	0.16	91.53
RS-11-172	Ca-U	81.45	1.33	5.65	0.48	<DL	0.13	89.04

Uraninite in the mini-roll-fronts is also observed coating earlier rutile (TiO_2; Fig. 4.22A), apatite (Fig. 4.22B) and pyrite (Fig. 4.22B & C). The coating is generally 5-20 μm thick and it sometimes contains illite that is associated with Stage A uraninite (Fig. 4.22B). Sulphide minerals that have uranium coatings are corroded (Fig. 4.22C). Coffinite is observed filling fractures in quartz grains (Fig. 4.22D). Coffinite is characterized by variable silica content (9.8-19.2 wt.% SiO_2), low Pb (<3.0 wt.% PbO), and moderate Ca (1.0-3.6 wt.% CaO).

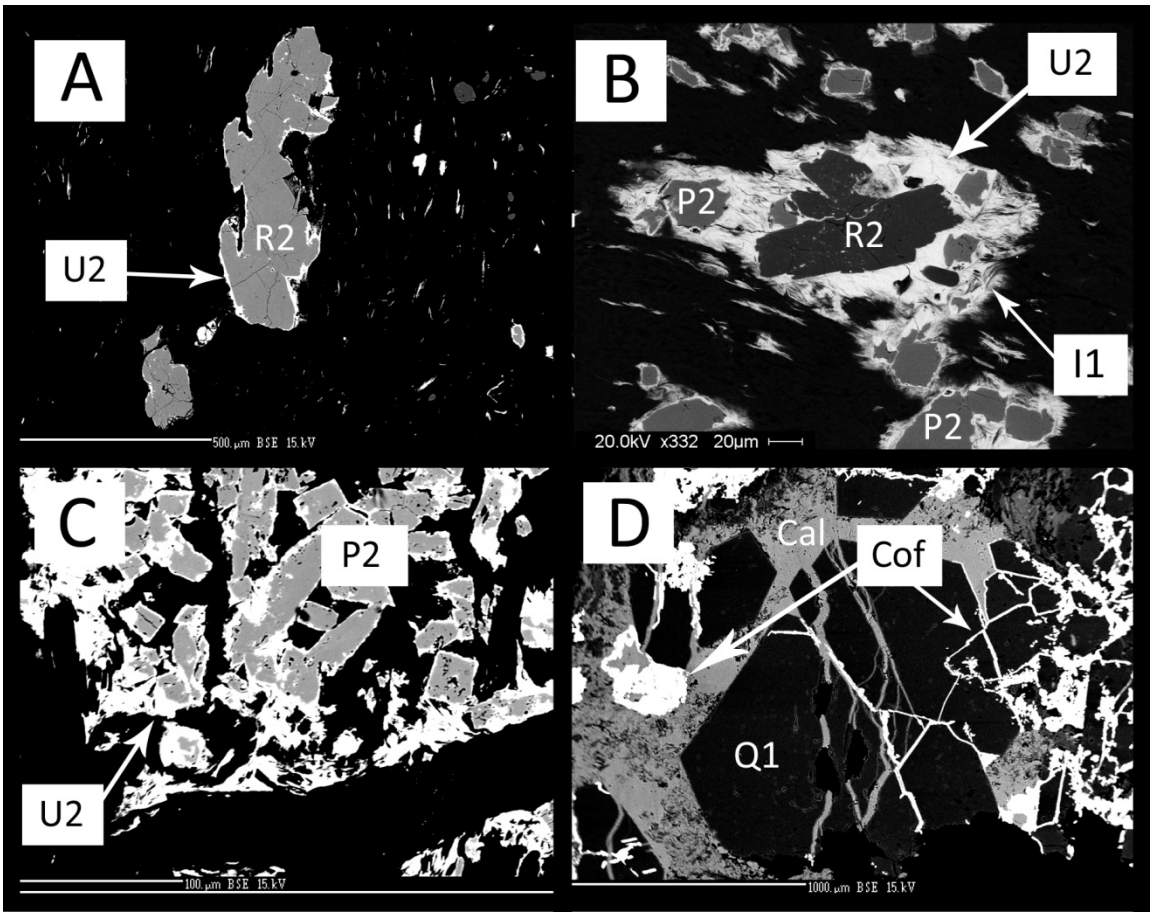

Figure 4.22: BSE images of remobilized uranium minerals from the Bong uranium deposit. A) Uraninite coating hydrothermal rutile (Sample RS-11-162). B) Uraninite coating rutile and pyrite as well as incorporating fine-grained illite from the first stage of mineralization (Sample 303GC). C) Uraninite forming around corroded sulphides (Sample 301GC). D) Coffinite filling fractures in quartz and crosscut by paragenetically late calcite (Sample RS-11-144). Abbreviations: U2 = Stage B uraninite, R2 = Second generation of rutile, P2 = Second generation of pyrite, I1 = First generation of illite, Q1 = First generation of quartz, Cal = Calcite, Cof = Coffinite.

4.2 Iron Speciation

Samples from one barren and one mineralized hole, Bong-49 and Bong-42, respectively, were taken at 20 m intervals and were analyzed to determine the oxidation state of the iron. The quantities of total iron and ferrous iron (FeO) in the samples were determined by ICP-MS and titration, respectively. The quantity of ferric iron (Fe_2O_3) was then back calculated. The results are listed in Appendix D. Total iron was plotted verses depth for both the mineralized and unmineralized holes (Fig. 4.23). From the iron chemical data, the mole percent for each iron species was determined and normalized. These values were then used to calculate the Fe^{2+}/Fe^{3+} ratio of each sample. The Fe^{2+}/Fe^{3+} ratios were plotted verses depth for the two holes (Fig. 4.24A & B). The area shaded in green is the altered zone in the mineralized hole and the "expected" depth of alteration in the unmineralized hole. The expected depth in the unmineralized hole is the depth where alteration in the mineralized hole is observed.

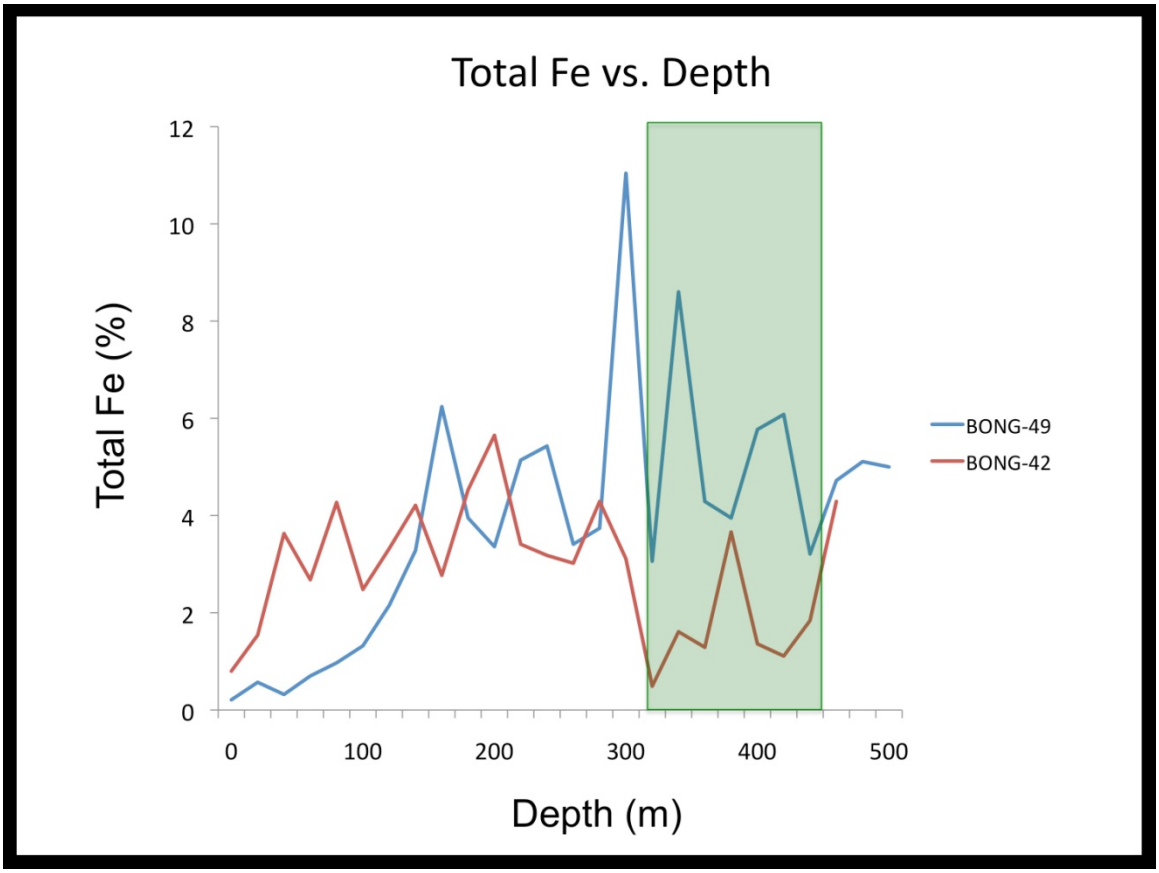

Figure 4.23: Graphical representation of the total iron (%) vs. depth in the mineralized (Bong-42) and unmineralized holes (Bong-49). The green box represents the alteration zone in the mineralized hole and the expected depth of alteration in the unmineralized hole.

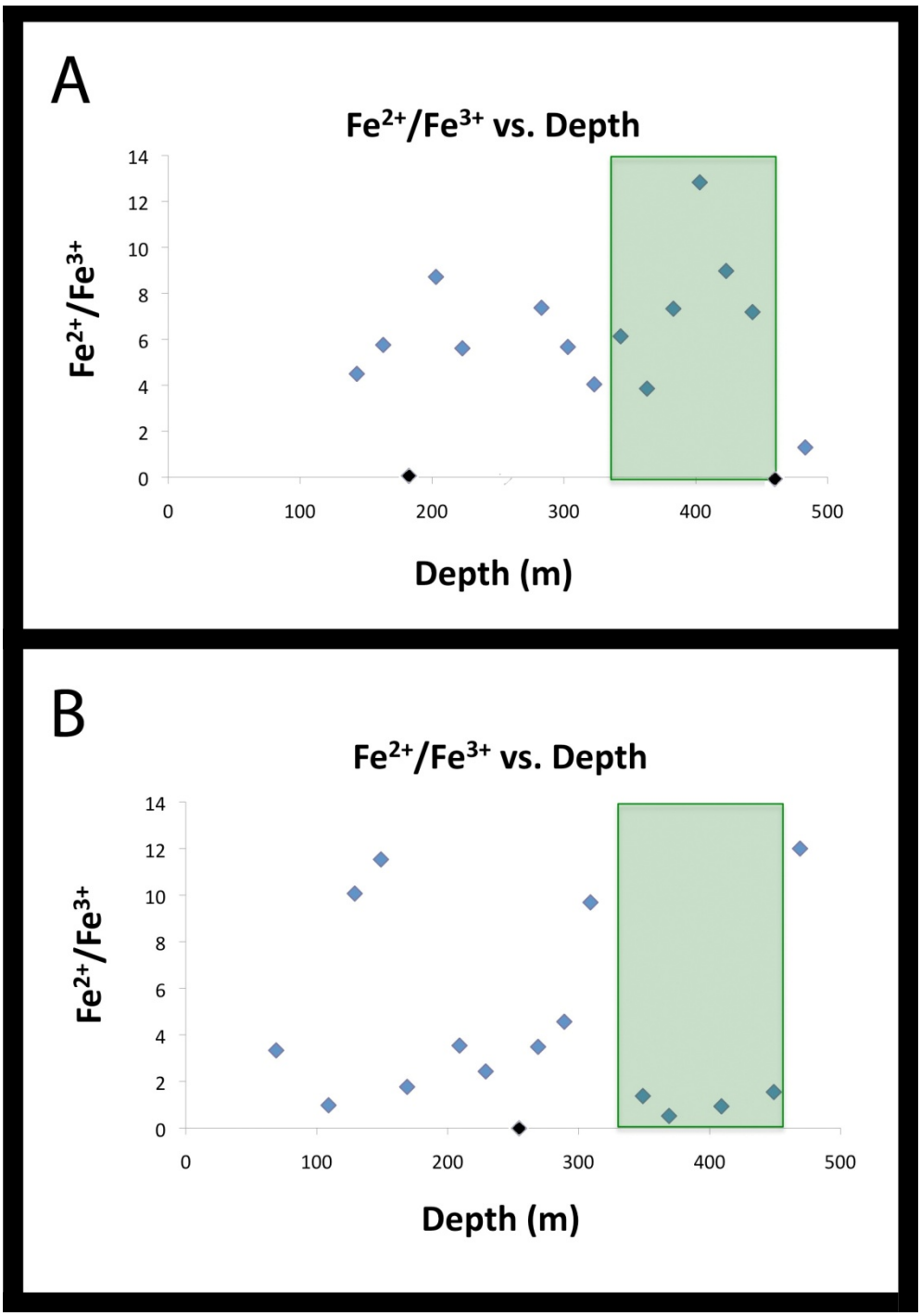

Figure 4.24: Graphical representation of iron oxidation state vs. depth. A) Fe^{2+}/Fe^{3+} ratio vs. depth in an unmineralized hole (Bong-49). The green box represents the depth where mineralization would be "expected" to occur. B) Fe^{2+}/Fe^{3+} ratio vs. depth in a mineralized hole (Bong-42). The green box represents the alteration zone in the hole. Black dots represent depths where the amount of ferric iron was below the ICP-MS detection limit (0.01%).

The amount of total iron in the unaltered portions of the two holes is very similar (Fig. 4.23). It is only in the altered zone of the mineralized hole (Bong-42) that a marked decrease in the amount of total iron is observed. The amount of Fe^{3+} is also constant in the unaltered portion of both holes, averaging 0.49 mol.% in the unaltered barren hole and 0.48 mol.% in the unaltered portion of the mineralized hole. In the alteration zone of the mineralized hole, the amount of Fe^{3+} is still fairly constant, averaging 0.42 mol.%. The main difference between the unaltered and altered portions is the amount of Fe^{2+}. The amount of Fe^{2+} in the barren hole averages 3.36 mol.%, while the unaltered portion of the mineralized hole averages 2.31 mol.%. The altered portion of the mineralized hole averages 0.57 mol.% Fe^{2+}, which is much lower than the unaltered zones. Therefore, the lower amount of total iron in the mineralized hole is due to the decrease in ferrous iron and thus the Fe^{2+}/Fe^{3+} ratio in the altered zone is much lower than the unaltered rock. This is evident when the mol. % of Fe^{3+} and Fe^{2+} are plotted with depth for each hole (Fig. 4.25A & B).

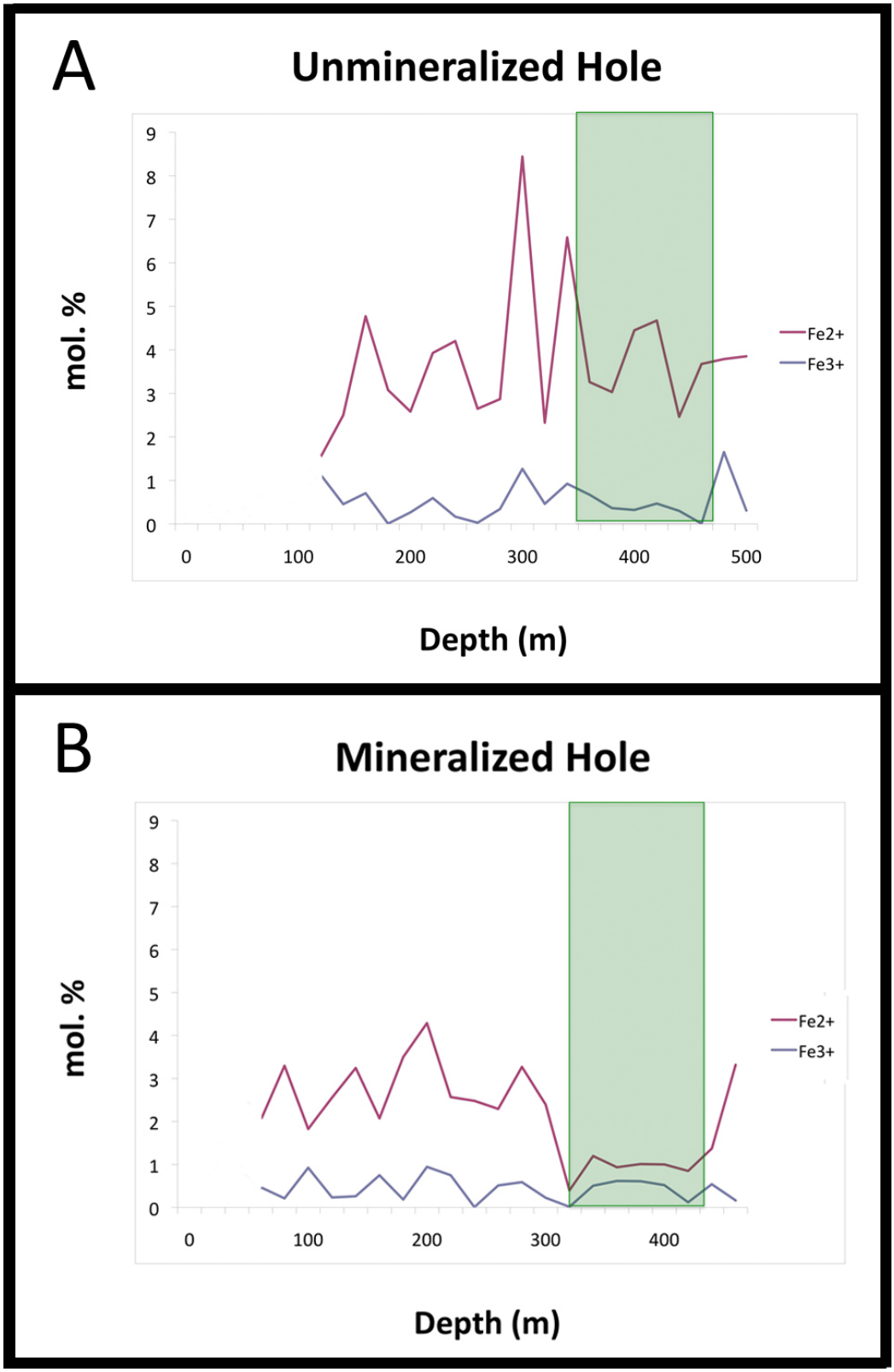

Figure 4.25: Graphical representation of mol. % (Fe^{2+} & Fe^{3+}) vs. depth. A) Unmineralized hole, Bong-49. B) Mineralized hole, Bong-42. The green box represents the alteration zone in Bong-42 and the expected depth of alteration in Bong-49.

4.5 Stable Isotopes

Uranium and phyllosilicate minerals were analyzed for their oxygen-isotope compositions and phyllosilicate minerals were analyzed for their hydrogen-isotope compositions (Appendix E). These analyses were done *in situ* by SIMS (Section 3.6) Bulk carbon isotopic compositions of graphite and organic matter were analyzed by gas-source Isotope-Ratio Mass Spectrometer (IRMS; Section 3.5; Appendix F).

4.5.1 Hydrogen Isotopes

Metamorphic muscovite (unaltered and altered) and hydrothermal illite were analyzed for their δD values (Table 4.3). Metamorphic muscovite has δD values that range from -69.5 ± 3.2‰ to -29.8 ± 3.2‰ and average -50.0 ± 14.5‰. The illite has δD values that range from -123.0 ± 5.4‰ to -75.1 ± 5.4‰ and average -99.7 ± 21.1‰. The (altered) muscovite in the alteration zones has δD values that are similar to those from illite, ranging from -125.5 ± 5.4‰ to -93.4 ± 5.4‰ and averaging -106.5 ± 13.9‰.

Table 4.3: Secondary ion mass spectrometry (SIMS) data depicting δD values from various mica minerals in the Bong deposit.

Sample	Mineral	δD V-SMOW (‰)	1σ
RS-11-148-2	Illite	-92.2	3.1
RS-11-148-5	Illite	-119.7	3.2
RS-11-172-1	Illite	-75.1	3.2
RS-11-172-3	Illite	-123.0	3.2
RS-11-172-4	Illite	-117.7	3.0
303GCB-2	Illite	-76.6	3.0
303GCB-3	Illite	-116.7	3.0
	Average:	**-99.7**	**3.1**

Sample	Mineral	δD V-SMOW (‰)	1σ
303GCB-4	Altered Muscovite	-101.6	3.1
RS-11-172-5	Altered Muscovite	-125.5	3.2
RS-11-172-6	Altered Muscovite	-101.3	3.1
RS-11-172-9	Altered Muscovite	-93.4	3.2
	Average:	**-106.5**	**3.1**

Sample	Mineral	δD V-SMOW (‰)	1σ
RS-068A-1	Muscovite	-29.8	3.1
RS-068A-2	Muscovite	-66.7	3.1
RS-068C-1	Muscovite	-57.9	3.2
RS-068C-2	Muscovite	-36.7	3.1
RS-068C-3	Muscovite	-69.5	3.2
RS-068B-1	Muscovite	-42.9	3.2
RS-068B-2	Muscovite	-55.7	3.2
RS-068B-3	Muscovite	-40.5	4.2
	Average:	**-50.0**	**3.3**

4.5.2 Oxygen Isotopes

Vein-type and roll-front uraninite were analyzed for $\delta^{18}O$ values (Table 4.4). Vein-type uraninite has $\delta^{18}O$ values that range from -27.4 ± 0.5‰ to -11.9 ±0.5‰ and average -19.1 ± 4.5‰, whereas altered vein-type uraninite range from -7.4 ± 0.5‰ to 3.9 ± 0.5‰ and average -2.2‰. ± 3.9‰. Roll-front uraninite has $\delta^{18}O$ values that range from -44.7 ± 1.4‰ to -30.6 ± 1.4‰ and average -37.8 ± 5.0‰.

Table 4.4: Secondary ion mass spectrometry (SIMS) data depicting $\delta^{18}O$ values from various uranium minerals in the Bong deposit.

Sample	Mineral	$\delta^{18}O$ V-SMOW (‰)	1σ
RS-143BO-1	Vein-Type Uraninite	-18.4	1.2
RS-143BO-2	Vein-Type Uraninite	-23.2	1.2
RS-143BO-3	Vein-Type Uraninite	-26.3	1.2
RS-143BO-4	Vein-Type Uraninite	-19.8	1.2
RS-143BO-5	Vein-Type Uraninite	-19.0	1.2
RS-143BO-6	Vein-Type Uraninite	-23.5	1.2
303GCO-1	Vein-Type Uraninite	-16.8	1.2
303GCO-2	Vein-Type Uraninite	-11.9	1.2
303GCO-3	Vein-Type Uraninite	-17.4	1.2
RS-172O-2	Vein-Type Uraninite	-13.1	1.2
RS-172O-3	Vein-Type Uraninite	-17.0	1.2
RS-172O-4	Vein-Type Uraninite	-19.5	1.2
RS-172O-5	Vein-Type Uraninite	-12.8	1.2
303GCB-1	Vein-Type Uraninite	-27.4	1.2
303GCB-2	Vein-Type Uraninite	-21.4	1.2
303GCB-3	Vein-Type Uraninite	-21.3	1.2
303GCB-4	Vein-Type Uraninite	-16.0	1.2
	Average:	**-19.1**	**1.2**

Sample	Mineral	$\delta^{18}O$ V-SMOW (‰)	1σ
303GCO-4	Alt. Vein-Type Uraninite	-0.2	1.2
RS-143AO-1	Alt. Vein-Type Uraninite	-1.8	1.2
RS-143AO-2	Alt. Vein-Type Uraninite	3.9	1.2
RS-143AO-3	Alt. Vein-Type Uraninite	0.3	1.2
RS-143AO-4	Alt. Vein-Type Uraninite	-4.0	1.2
RS-172O-6	Alt. Vein-Type Uraninite	-7.4	1.2
RS-172O-1	Alt. Vein-Type Uraninite	-6.1	1.2
	Average:	**-2.2**	**1.2**

Sample	Mineral	$\delta^{18}O$ V-SMOW (‰)	1σ
RS-176CO-1	Roll-Front Uraninite	-41.7	1.2
RS-176CO-2	Roll-Front Uraninite	-44.7	1.2
RS-176CO-3	Roll-Front Uraninite	-38.3	1.2
RS-176CO-4	Roll-Front Uraninite	-35.4	1.2
RS-176CO-5	Roll-Front Uraninite	-30.6	1.2
RS-176CO-6	Roll-Front Uraninite	-35.9	1.2
	Average:	**-37.8**	**1.2**

The $\delta^{18}O$ values of the altered uraninite are on average ~17‰ higher than those of the relatively unaltered uraninite. A plot of $\delta^{18}O$ values versus the (Si + Ca) content of the uraninite shows good correlation ($R^2 = 0.84$; Fig. 4.26). The $\delta^{18}O$ values of the uraninite increase with the increasing amount of silica and calcium in the uraninite structure.

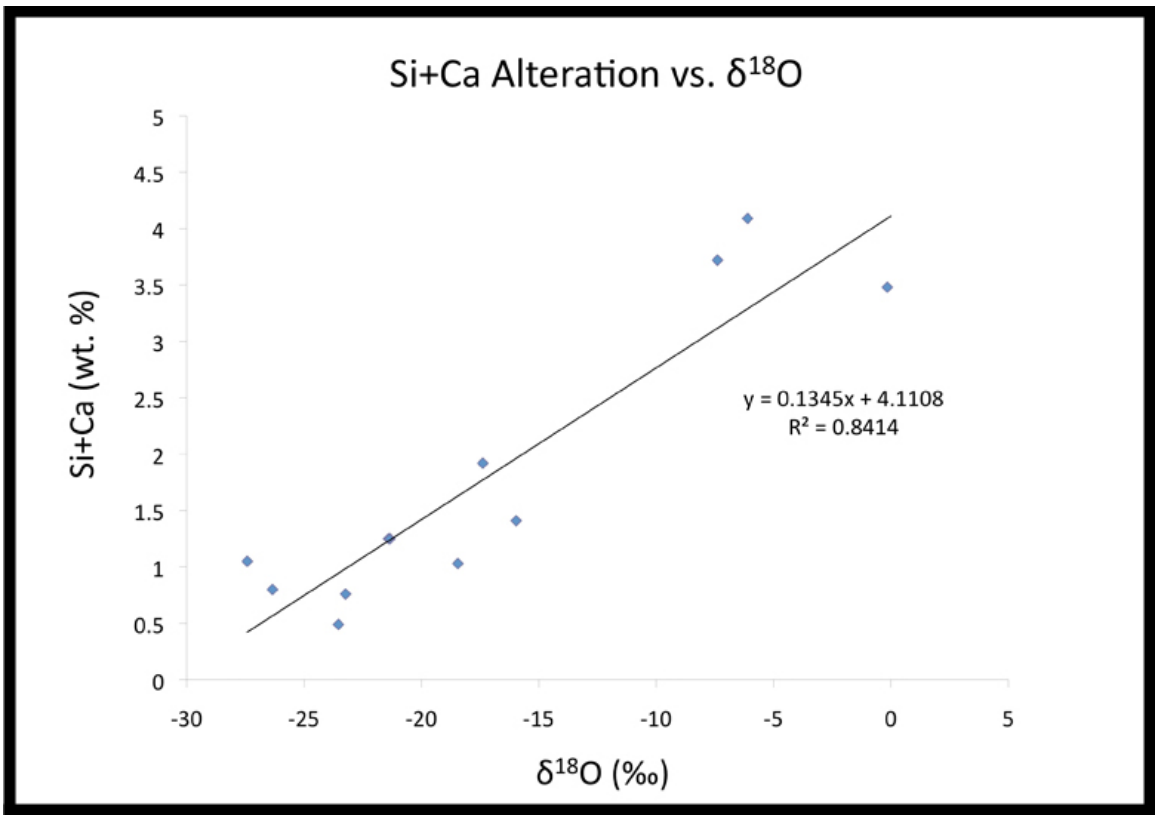

Figure 4.26: Relationship between Si and Ca content (wt. %) of uraninite and $\delta^{18}O$ values.

Metamorphic muscovite and hydrothermal illite were also analyzed for their $\delta^{18}O$ values (Table 4.5). Metamorphic muscovite from relatively unaltered metasediment samples has $\delta^{18}O$ values that range from 5.3 ± 1.2‰ to 13.3 ± 1.2‰ (average 9.2 ± 2.7‰), whereas muscovite from highly-altered equivalent material

has lower $\delta^{18}O$ values that range from 0.9 ± 0.8‰ to 6.2 ± 0.8‰ with an average value of 3.1 ± 1.5‰. Illite has $\delta^{18}O$ values that range from -5 ± 0.8‰ to 3.7 ± 0.8‰ (average -2.1 ± 3.5‰).

Table 4.5: Secondary ion mass spectrometry (SIMS) data depicting $\delta^{18}O$ values from various mica minerals in the Bong deposit.

Sample	Mineral	$\delta^{18}O$ V-SMOW (‰)	1σ
RS-147-3	Illite	-4.0	1.2
RS-147-4	Illite	-5.0	1.2
RS-147-5	Illite	-4.6	1.2
RS-147-8	Illite	3.7	1.3
RS-147-9	Illite	0.8	1.3
RS-147-10	Illite	-3.3	1.3
	Average:	**-2.1**	**1.3**

Sample	Mineral	$\delta^{18}O$ V-SMOW (‰)	1σ
RS-142O-2	Altered Muscovite	6.2	1.3
RS-142O-3	Altered Muscovite	2.2	1.3
RS-142O-4	Altered Muscovite	3.1	1.3
RS-142O-6	Altered Muscovite	3.7	1.3
RS-142O-7	Altered Muscovite	0.9	1.3
RS-142O-9	Altered Muscovite	2.8	1.2
RS-142O-10	Altered Muscovite	3.5	1.3
RS-142O-11	Altered Muscovite	2.3	1.3
	Average:	**3.1**	**1.3**

Sample	Mineral	$\delta^{18}O$ V-SMOW (‰)	1σ
RS-136O-2	Muscovite	11.3	1.2
RS-136O-3	Muscovite	8.8	1.2
RS-136O-4	Muscovite	7.7	1.3
RS-136O-5	Muscovite	13.2	1.3
RS-136O-6	Muscovite	13.3	1.2
RS-136O-7	Muscovite	5.3	1.2
RS-136O-8	Muscovite	7.7	1.2
RS-136O-9	Muscovite	8.0	1.3
RS-136O-10	Muscovite	7.8	1.2
	Average:	**9.2**	**1.2**

Based on petrography, Stage A uraninite is in textural equilibrium with the illite. Therefore, an equilibrium temperature can be calculated using the illite-H_2O [8] and uraninite-H_2O [9] fractionation factors from Sheppard & Gilg (1996) and Fayek & Kyser (2000):

$$1000 * \ln \alpha_{illite\text{-}H_2O} = A * 10^6 / T^2 + B * 10^3 / T + C \quad [8]$$

where A = 2.39, B = 0.00 and C = -3.76

&

$$1000 * \ln \alpha_{U_2O\text{-}H_2O} = A * 10^6 / T^2 + B * 10^3 / T + C \quad [9]$$

where A = 16.58, B = -77.52 and C = 77.48

Using the average isotopic values, the calculated equilibrium temperature for Stage A uraninite and illite is 227°C. The overall range for the data is 155°C to 244°C. Using the calculated equilibrium temperature and the theoretical fraction factor between uraninite and H_2O of Fayek & Kyser ([9]; 2000), the average calculated $\delta^{18}O$ value for the fluid that precipitated the Stage A uraninite and coeval illite is -7.9‰, with an overall range from 6.0‰ to 8.7‰.

Using the calculated equilibrium temperature and the theoretical fractionation factor between illite and H_2O of Capuano ([10]; 1992), the average calculated δD value of the fluid that precipitated the illite and coeval Stage A uraninite is -103.8‰, with an overall range of -106.8‰ to -88.6‰.

$$1000 * \ln \alpha_{illite\text{-}H_2O} = B * 10^3 / T + C \quad [10]$$

where B = -45.30 and C = 94.70

4.5.3 Carbon Isotopes

The $\delta^{13}C$ values range from -48.3‰ to -21.1‰ (Table 4.6; Appendix F). The results can be separated into two significantly distinct groups; 1) Organic matter associated with roll-front uraninite, that has $\delta^{13}C$ values that range from -27.9‰ to -21.1‰ and an average value of -24.2 ± 3.1‰, and 2) A mineralized graphite nodule and unmineralized organic matter, that have $\delta^{13}C$ values that range from -48.3‰ to -39.0‰ and an average value of -42.5 ± 5.1‰.

Table 4.6: Carbon-isotope analyses of graphite and organic matter in the Bong deposit

Sample ID	Sample Description	Weight (mg)	% Carbon	$\delta^{13}C$ V-PBD (‰)
RS-11-142	OM associated with roll front	3.505	0.494	-25.5
RS-11-145	OM associated with roll front	10.790	0.206	-27.9
RS-11-159	Unmineralized OM	50.540	0.167	-48.3
RS-11-160	OM associated with roll front	10.370	0.369	-22.2
RS-11-173	Mineralized graphite nodule	0.260	55.150	-39.0
RS-11-190	OM associated with roll front	9.788	0.247	-21.1
RS-11-192	Unmineralized OM	56.013	0.138	-40.2

* Abbreviations: OM = Organic matter

4.6 Geochronology

Chemical-Pb ages, and Pb-Pb and U-Pb isotopic ages, were calculated for both stages of uraninite and chemical Pb ages were calculated for coffinite. Chemical Pb ages were calculated from electron microprobe analyses, while Pb-Pb and U-Pb geochronology was done using U-Pb and Pb-Pb isotopic ratios measured by SIMS (Section 3.6).

4.6.1 Chemical Lead Ages

Chemical-Pb ages (Fig. 4.27) were calculated for the uraninite and coffinite using equation [1]. The EPMA data, along with the corresponding chemical lead ages, are in Appendices B and G, respectively.

Chemical-Pb ages for least-altered vein-type Stage A uraninite range from 840 Ma to 1195 Ma and have an average age of 1041 Ma. However, altered vein-type uraninite generally gives much younger ages, ranging between 17 Ma and 1108 Ma, with a much lower average age of 293 Ma. Chemical-Pb ages from Stage A uraninite associated with graphite have ages that range from 289 Ma to 960 Ma and average 637 Ma. Roll-front Stage B uraninite has very young ages from 33 Ma to 63 Ma (average age 46 Ma), while coffinite gives a similar average chemical-Pb age of 98 Ma.

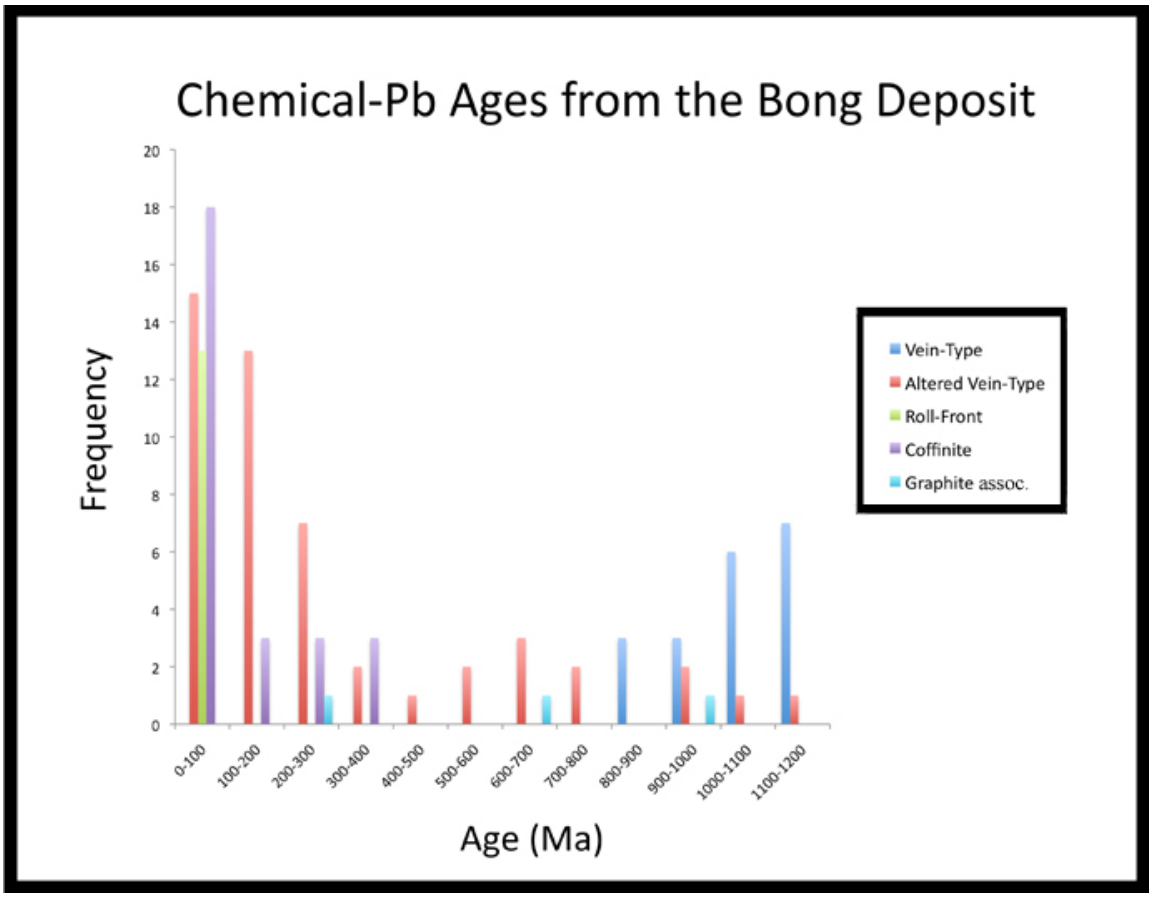

Figure 4.27: Distribution of chemical-Pb ages from the various styles of mineralization.

Two main assumptions are made when calculating chemical-Pb ages. The first is that any Pb present in the sample is presumed to be radiogenic in origin (i.e. the result of U decay). The second is that the U-Pb system has remained closed since the formation of the uranium minerals, which means that no gain or loss of U or Pb occurred after crystallization (Bowles, 1990). However, it is very unusual to obtain concordant U-Pb data from uraninite and the degree of discordance is often much greater than 5% because Pb diffusion in uraninite is a rapid process (Janeczek & Ewing, 1995). Therefore, chemical-Pb ages are generally unreliable for determining the initial age of crystallization, but can provide valuable information on tectonic events that can cause Pb remobilization (Fayek *et al.*, 2000).

4.6.2 Pb-Pb Isotope Geochronology

Lead-isotope analyses were done by SIMS on vein-type and roll-front uraninite (Fig 4.28). Data were obtained from the least-altered uraninite in these environments (Fig. 4.29). The Pb-isotope data was used to calculate $^{207}Pb/^{206}Pb$ ages using equation [5] (Appendix H). The $^{207}Pb/^{206}Pb$ ages for the vein-type uraninite range from 529 Ma to 1177 Ma, with an average age of 1030 Ma. The $^{207}Pb/^{206}Pb$ ages from the roll-front style of mineralization are more highly variable and range from 691 Ma to 1853 Ma, averaging 1345 Ma. A number of the ages from the roll-front style of uraninite were >1100 Ma. These points were observed to be tightly grouped and extremely discordant (>75%, Fig. 4.30) and the analyses had very low $^{206}Pb/^{204}Pb$, which indicate that they have incorporated common lead. Therefore, the artificially high Pb-Pb ages from some of the roll-front uranium sample points are unreliable. These ages were removed from subsequent plots.

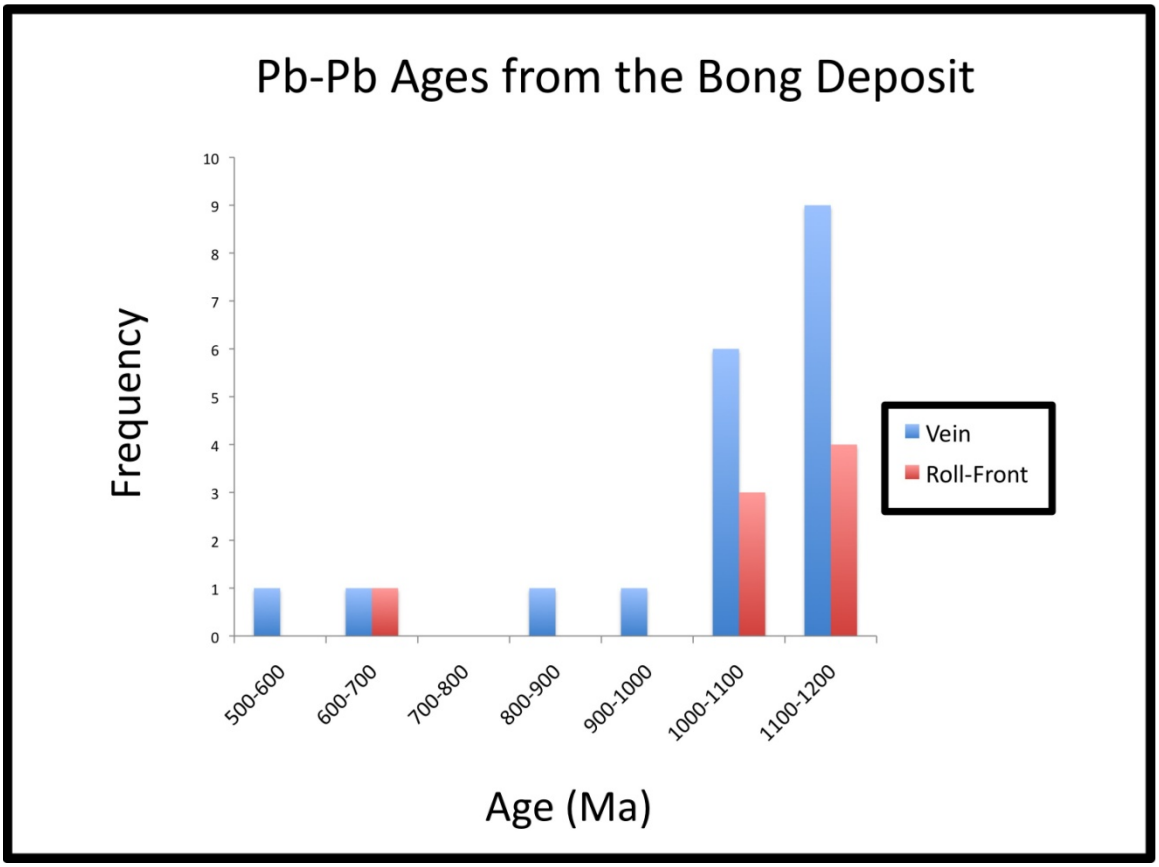

Figure 4.28: Distribution of Pb-Pb ages from vein-type and roll-front uraninite. Distinct groups are observed ~1050 Ma & ~1150 Ma.

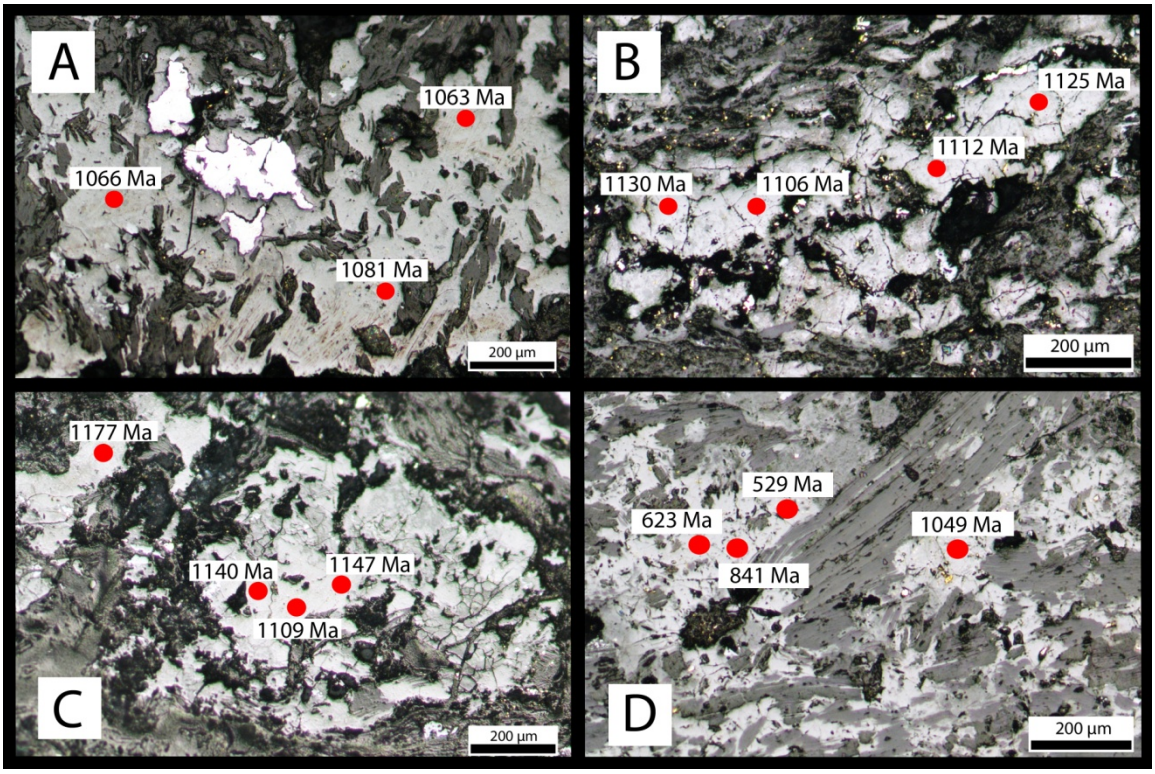

Figure 4.29: Reflected light images showing locations of SIMS analysis points. A) Fairly pristine uraninite with homogeneous ages (Sample RS-11-143). B) Fractured uraninite with older ages on more pristine larger areas (Sample 303GC). C) The unaltered uraninite in the top left has an older age than the fractured grain in the centre (Sample 303GC). D) Highly altered and fractured disseminated uraninite exhibiting a large range of ages (Sample RS-11-172).

4.6.3 U-Pb Isotope Geochronology

Uranium- and lead-isotope ratios, $^{206}Pb/^{238}U$ and $^{207}Pb/^{235}U$, for the vein-type and roll-front uraninite were plotted on Concordia diagrams (Fig. 4.30). Only data from least-altered uraninite with negligible common Pb were considered (see Section 4.6.2). Vein-type uraninite data give an upper intercept at 1117 ± 15 Ma and an MSWD of 1.9 (Fig. 4.30A). The data for the roll-front uraninite give an upper intercept at 1040 ± 39 Ma and an MSWD of 34 (Fig 4.30B). The points for the roll-front uraninite are tightly grouped and plot very near to the origin of the concordia diagram, resulting in the high MSWD value. A high MSWD value indicates that the value has a large amount of scatter. This can result either from the underestimation

of analytical uncertainties or indicate that another source of scatter, sometimes called “geological” scatter, is present.

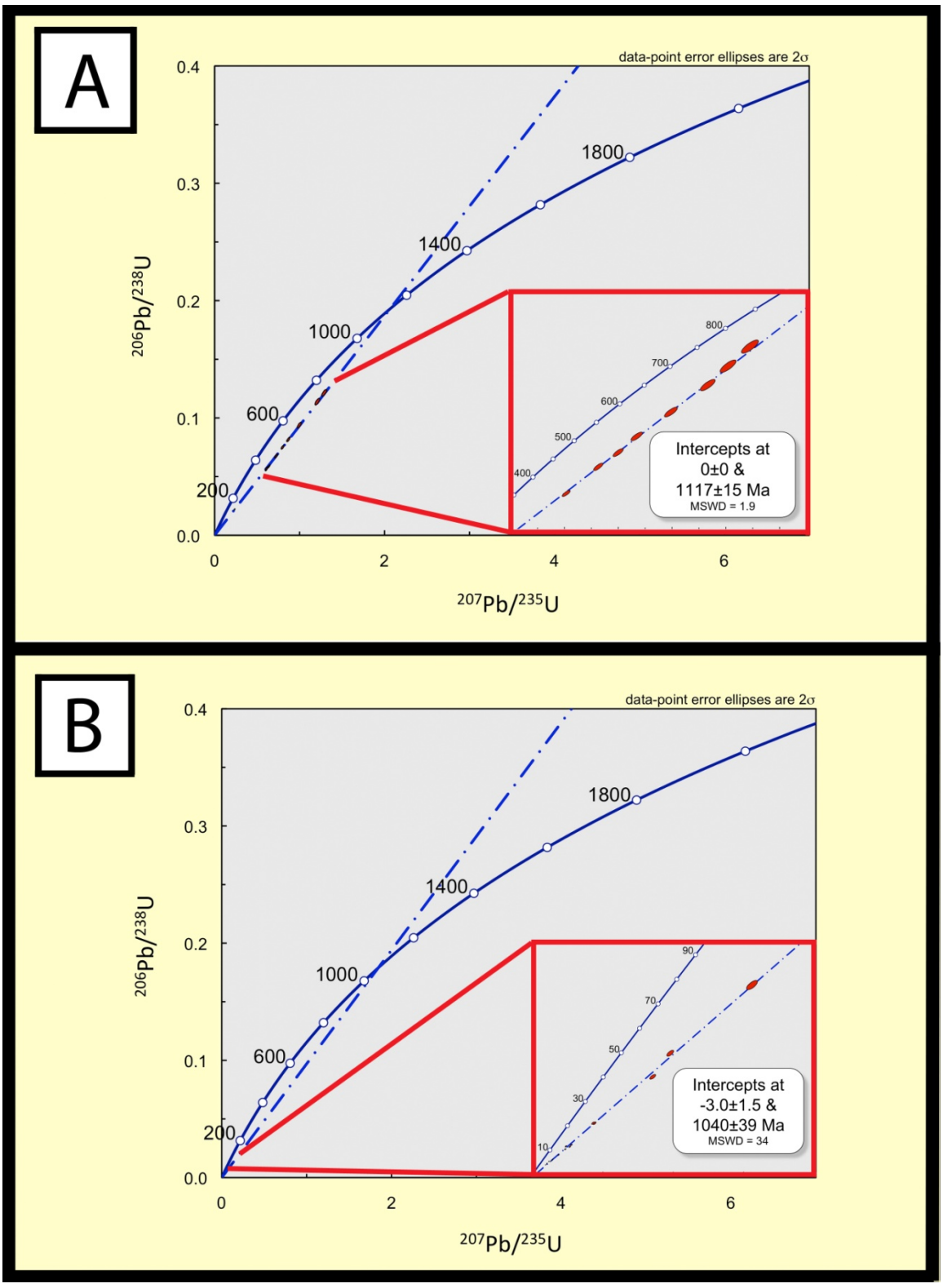

Figure 4.30: U-Pb results from *in situ* isotopic analysis. A) Vein-type uraninite. B) Roll-front uraninite.

Chapter 5: Discussion

The Athabasca Basin, Saskatchewan, Canada, and the McArthur Basin (Kombolgie Formations), Northern Territory, Australia, are host to some of the largest and richest unconformity-type uranium deposits in the world (Jefferson *et al*., 2007a,b). The Thelon basin shares spatial and temporal relations with these basins, seems to share similar geological relations, and may ultimately prove to have similar economic potential. Although the fluid histories of the Athabasca Basin (Hoeve & Sibbald, 1978; Hoeve & Quirt, 1984; Sibbald, 1985; Quirt, 1989; Kotzer & Kyser, 1993, 1995; Fayek & Kyser, 1997; Hecht & Cuney, 2000; Kyser *et al*., 2000; Quirt, 2001; Alexandre *et al.*, 2005; Cloutier *et al*., 2009) and McArthur Basin (Needham *et al*., 1988; Mernagh *et al*., 1998; McKay & Mieztis, 2001; Polito *et al*., 2006, 2011) have been thoroughly studied, the fluid histories of the Thelon Basin, associated basement rocks, and uranium deposits are relatively poorly constrained (Renac, 2002; Hiatt *et al*., 2003; Rainbird *et al*., 2003; Hiatt *et al*., 2010; Pehrsson *et al*., 2010). Outstanding questions related to the Thelon Basin deposits include: (1) Are the uranium showings and deposits associated with the Thelon Basin of the unconformity-type? (2) If they are not unconformity-type deposits, what type of uranium deposits are associated with the Thelon Basin and what is their genetic history? To answer these questions it is important to compare the uranium-deposit models that currently exist for the well-studied Athabasca and Kombolgie deposits to the uranium deposits from the Thelon Basin. For this study, the fluid history and genetic model of the basement-hosted Bong deposit, located adjacent to the Thelon

Basin, will be compared to the basement-hosted deposits from the Athabasca and Kombolgie regions.

5.1 The Athabasca Basin Unconformity-type Deposits

The salient features of the Thelon, Kombolgie, and Athabasca deposits are summarized in Table 5.1. Although the exact age of the Athabasca Basin is still debated, most recent studies suggest that sedimentation in the Athabasca Basin began between 1740 and 1730 Ma in the eastern Athabasca (Orrell *et al*., 1999; Ramaekers, 2004; Rainbird *et al*., 2007; Ramaekers *et al*., 2007). Uranium mineralization is generally related to major Hudsonian-age brittle faults that cut the unconformity between the Archean-Paleoproterzoic crystalline basement rocks and the Proterozoic Athabasca Group sandstone (Hoeve & Sibbald, 1978; Macdonald, 1980; Hoeve & Quirt, 1984; Sibbald, 1985; Quirt, 1989; Kotzer & Kyser, 1993, 1995; Fayek & Kyser, 1997; Hecht & Cuney, 2000; Kyser *et al*., 2000; Quirt, 2001; Alexandre *et al*., 2005; Cloutier *et al*., 2009). Jefferson *et al.* (2007b) summarized the empirical models for the formation of Athabasca Basin unconformity-type uranium deposits (Fig. 5.1). Two sub-types of uranium deposits were identified: (1) generally mono-metallic basement-hosted uranium deposits, and (2) poly-metallic sandstone-hosted deposits. Although some basement deposits contain minor amounts of Au, Cu and V. Individual deposits can range from purely sandstone-hosted to entirely basement-hosted with hybrids of both basin- and basement-hosted deposits being common (e.g., Key Lake, Shea Creek; Fig. 5.2).

Table 5.1: Comparison of the Thelon, Kombolgie and Athabasca Basin Basement Hosted Uranium Deposits (Data from Jefferson *et al.*, 2007b, Polito *et al.*, 2004, 2005)

Geologic Attribute	Thelon	Kombolgie	Athabasca
Maximum Age of Sedimentation (Ma)	ca. 1720	ca. 1790	ca. 1750-1720
Max. Hydrothermal Temperatures	~220°C	~200°C	~225°C
Clay Alteration Halo	Yes	Yes	Yes
Average Grade	0.40%	0.32%	~1.8%
Dominant Clay Alteration Mineral	Illite	Illite	Illite
Oxidation of U-minerals	Yes	Yes	Yes
Graphite Present	Rare	Variable	Common

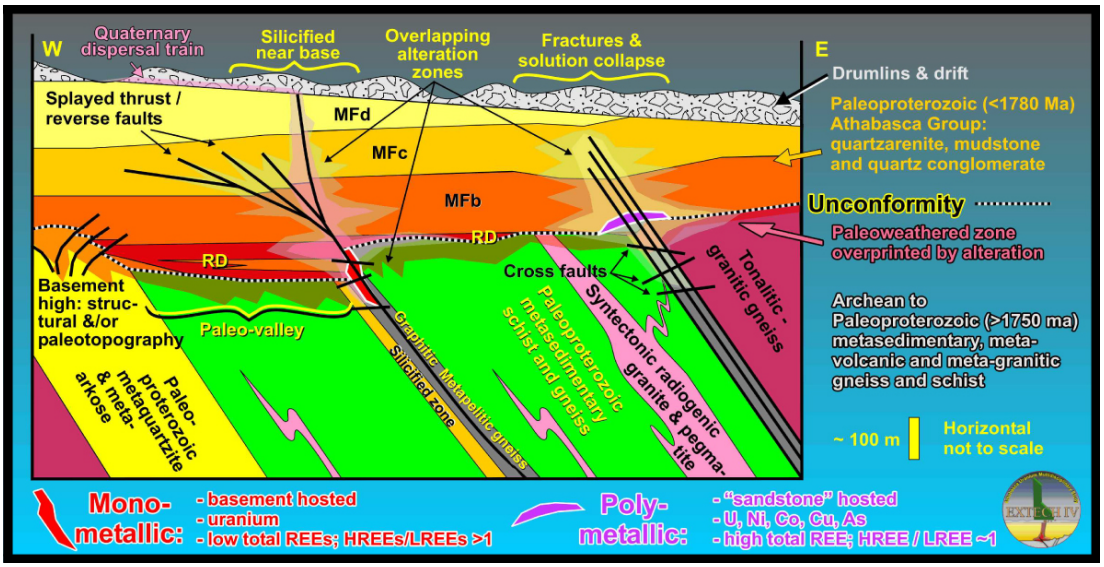

Figure 5.1: Generalized geologic context of sandstone- (poly-metallic) and basement hosted (mono-metallic) unconformity-type uranium deposits (from Jefferson *et al.*, 2007b).

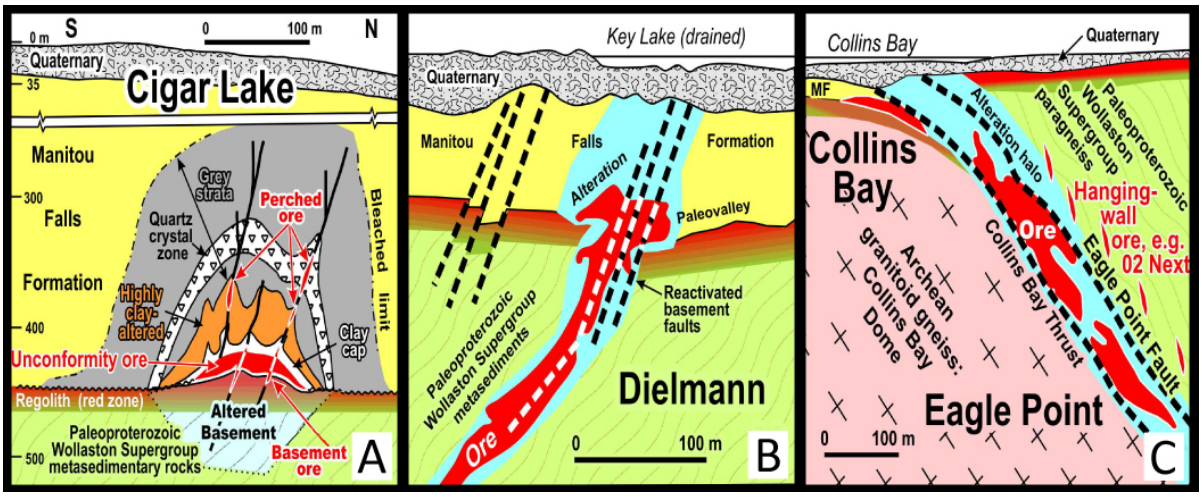

Figure 5.2: Examples of three end-member unconformity-type uranium deposit styles. A) Sandstone-hosted B) Sandstone- and basement-hosted. C) Basement-hosted (from Jefferson *et al.*, 2007b).

Alteration minerals associated with the unconformity-type deposits from the Athabasca Basin can vary between deposits (Hoeve & Quirt, 1984; Quirt, 1989; Quirt, 2003), but generally they are zoned. Alteration haloes around basement deposits consist of an inner zone of illite ± sudoite, then sudoite ± illite grading to Fe-Mg chlorite ± sudoite, then to unaltered biotite + Fe-Mg chlorite in fresh rock (Fig. 5.3; Hoeve & Quirt, 1984). Fluids flowing from the basement were reducing; fluids from the red beds were oxidizing and contained U. Models invoke mixing of such fluids at the unconformity (egress-style) and fluid-rock interaction (ingress-style) to precipitate U. The shear zones and fluid flows along them may have been linked (Hoeve & Quirt, 1984; Quirt, 1989; Jefferson et al., 2007b). A generalized paragenesis of basement-hosted deposits from the Athabasca Basin (Alexandre *et al.,* 2009) is presented in Figure 5.4.

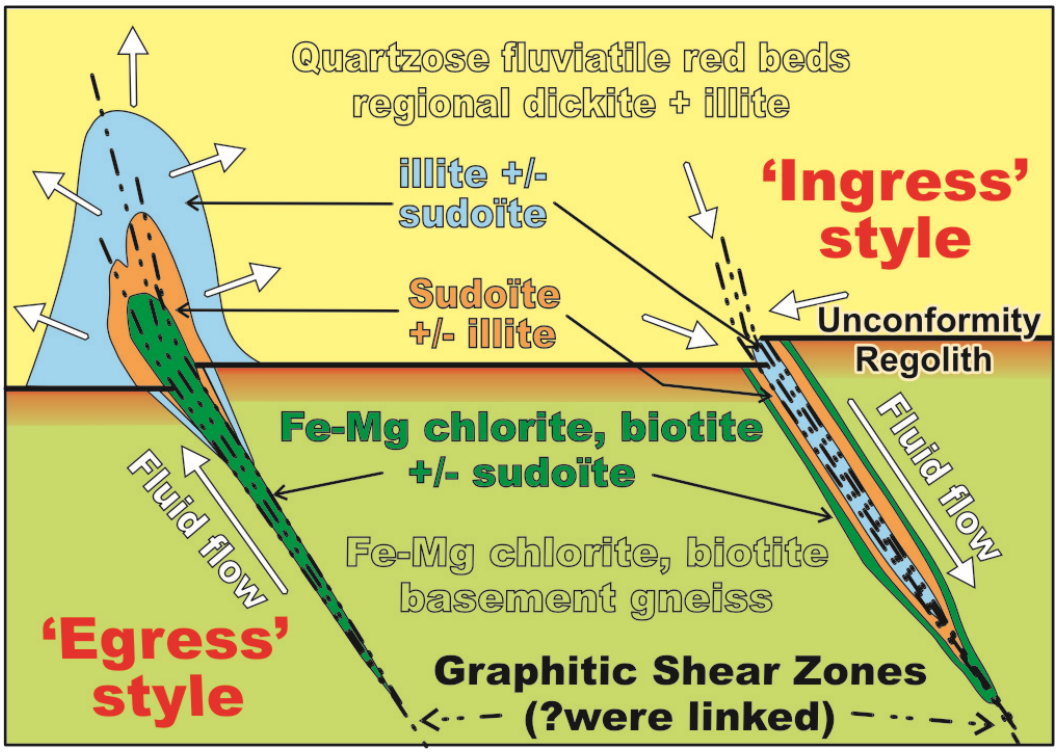

Figure 5.3. Diagrammatic explanation of 'egress'- versus 'ingress'-style alteration zones for unconformity associated uranium deposits (from Jefferson et al., 2007b; after Hoeve & Quirt, 1984; Sibbald, 1985; Fayek & Kyser, 1997; Quirt, 1989, 2003).

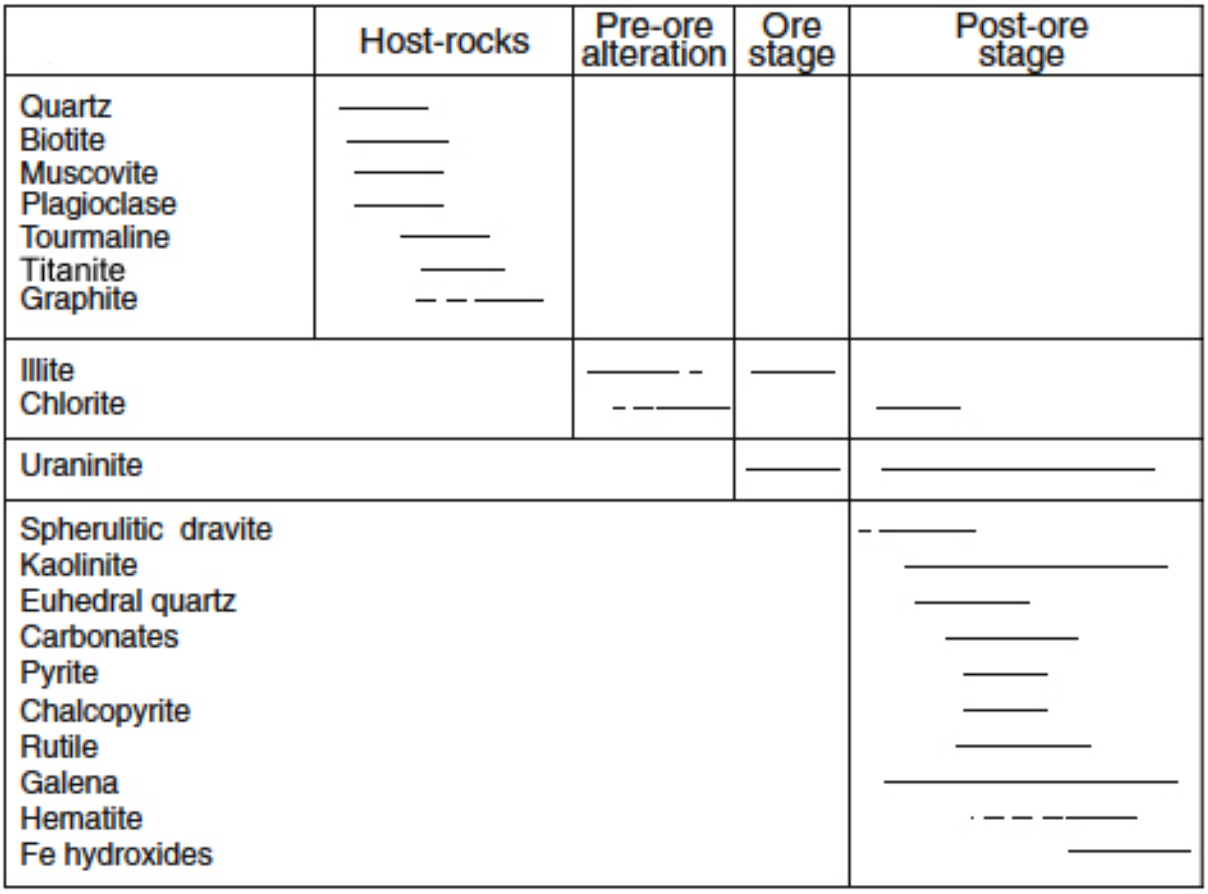

Figure 5.4: Simplified paragenesis for basement-hosted unconformity-type uranium deposits in the Athabasca basin (modified after Alexandre et al., 2007).

Uraninite from the Athabasca Basin basement-hosted deposits occurs in five main forms: disseminations, veins, blebby grains, massive replacement and mini-roll-fronts. Coffinite is locally present and uranyl-minerals are generally only rarely observed. Although the age(s) of primary uranium mineralization in the Athabasca Basin is (are) controversial, studies have reported ages from ~1600 to 1460 Ma (Fayek *et al.*, 2002a; Alexandre *et al.*, 2003) with secondary ore-forming or remobilizing events at ~1350, ~1150, ~900, and ~300 Ma (Hoeve & Quirt, 1984; Cumming & Kritic, 1992; McGill *et al.*, 1993; Fayek & Kyser, 1997; Kyser *et al.*, 2000; Fayek *et al.*, 2002a; Boulanger, 2012). The fluids associated with uranium

mineralization are generally interpreted to be 180-225°C basinal brines (Pagel, 1975; Pagel et al., 1980; Kotzer & Kyser, 1990, 1992, 1993; Kyser *et al.,* 2000; Alexandre *et al*., 2005; Cloutier *et al*., 2009). Hydrogen- and oxygen-isotope compositions of fluids that formed basement-hosted unconformity type deposits in the Athabasca basin have δD values that range from -100‰ to -10‰ and $\delta^{18}O$ values that range from -25‰ to 11‰ (Kotzer & Kyser, 1990, 1992, 1993; Kyser *et al.,* 2000; Alexandre *et al*., 2005; Cloutier *et al*., 2010). Typically, very low δD and $\delta^{18}O$ values have been interpreted to be the result of a complete or partial reset by recent meteoric waters infiltrating into the deposits (Kotzer & Kyser, 1990, 1993). Therefore, $\delta^{18}O$ values of ~2‰ to 11‰ and δD values ~-60‰ to -10‰ are most commonly accepted for the fluids that formed these deposits (Kyser *et al*., 2000).

Three mechanisms for uranium deposition have been suggested for the unconformity-related deposits from the Athabasca Basin: (1) Fe-U redox couple (Hoeve & Sibbald, 1978; Wallis *et al.,* 1983; Hoeve & Quirt, 1984; Fayek & Kyser, 1997; Holk *et al.,* 2003), (2) interaction with reduced graphite/bitumen and chemical precipitation of the uraninite (Hoeve & Sibbald, 1978; Hoeve & Quirt, 1984), and (3) mixing between two fluids, an uraniferous oxidizing basinal brine and a reducing basement-source fluid (Hoeve & Quirt, 1984; Wilson & Kyser, 1987; Kotzer & Kyser, 1993, 1995; Fayek & Kyser, 1997). Currently, mechanisms 1 and 3 are considered to be more likely and part of one process (Quirt, 1989, 2003; Jefferson et al., 2007 a,b).

The role that graphite plays in the reduction of uranium is unclear and its role in the formation of unconformity-related uranium deposits been studied extensively (Hoeve & Sibbald, 1978; Hoeve & Quirt, 1984; Leventhal *et al.,* 1987; Kyser *et al*., 1989; Landais *et al.,* 1993; McCready *et al.,* 1999; Sangley *et al*., 2007; Wilson *et al*., 2007). Graphite has been proposed as a reductant for uranium because of the close association between graphite and uranium mineralization (Hoeve & Sibbald, 1978; Hoeve & Quirt, 1984). Graphitic zones also play other roles in uranium deposition. They are often the site of reactivated faults (Jefferson *et al*., 2007) and may also drive convection by conducting heat from deep heat sources (Hoeve & Quirt, 1984). Many researchers have studied carbon isotopes to try and understand the relation between graphite and uranium (e.g., Leventhal *et al.,* 1987; Kyser *et al*., 1989; Landais *et al.,* 1993; Sangley *et al*., 2007). Graphite collected from unaltered and altered basement rock around the Key Lake Deposit has a limited range of $\delta^{13}C$ values (-25 ± 5‰), while carbon 'buttons' at Key Lake have a $\delta^{13}C$ value of -53‰ (Kyser *et al*., 1989). Leventhal *et al.* (1987) observed a similar trend where $\delta^{13}C$ values were ~-26 ± 3‰ in graphite-bearing metasediments while the carbon 'buttons' in the mineralized zones had $\delta^{13}C$ values of ~-44 ± 3‰. Bitumen and graphite at Cigar Lake are restricted to values between -31.2‰ and -27.3‰ (Landais *et al.,* 1993). Sangley *et al*. (2007) measured *in-situ* carbon-isotope compositions in bitumen from the Athabasca basin and observed a large range of $\delta^{13}C$ values ranging from -51‰ to -23‰. The study concluded that the organic matter has an abiogenic origin.

5.2 The McArthur Basin Unconformity-type Deposits

The McArthur Basin, Australia, which began to form at ~1790 Ma (Polito *et al*., 2006), seems to be slightly older than the Athabasca Basin. The unconformity-type uranium deposits (e.g., Koongarra, Nabarlek, Ranger, and Jabiluka) in the basin are not as well studied as the Athabasca deposits. Uranium mineralization is associated with major faults that cut the Paleoproterozoic sandstone and the unconformably-underlying paleo-weathered, carbonaceous, Fe-rich basement rock. Basement lithologies of the Nimbuwah Domain, most notable of which is the Lower Cahill Formation, host most of the uranium mineralization (Polito *et al*., 2011). The regional metamorphic grade of the basement rocks is amphibolite facies and all the basement rocks are folded. Peak metamorphism occurred during the Barramundi Orogeny, between 1870 and 1855 Ma (Needham *et al*., 1988), similar to the age of the Trans-Hudson Orogeny in western Canada that affected the basement rocks of the eastern Athabasca region. Like some of the Athabasca basement-hosted deposits, which are generally monometallic, with locally significant Cu, V or Au, many Australian deposits also contain significant quantities of gold- and platinum-group elements (PGE) that are paragenetically associated with the uranium mineralization (Mernagh *et al*., 1998).

Alteration associated with most of the uranium deposits can be divided into two zones: an outer zone characterized by replacement of metamorphic biotite, garnet, amphibole, feldspar and sillimanite by chlorite and fine-grained sericite, and an inner zone (proximal to the main ore zone) characterized by intense

chloritization and sericitization/illitization of the host rock, as well as hematite ± kaolinite ± tourmaline ± quartz (Nutt, 1989; Mernaugh *et al.,* 1998; *Polito et al.,* 2004; Polito *et al.,* 2011). At the Jabiluka deposit, widespread chloritization is observed in the sandstone (Gustafson & Curtis, 1983). The chloritization seems to be identical to that in the basement rock; however, mineralization is not present in the sandstone. Strong desilicification occurs at the unconformity (Mernagh *et al*., 1998). Post-ore alteration consists mainly of late-stage Mg-rich chlorite and quartz-carbonate veins, with minor sulphides and secondary uranium minerals (Polito *et al*., 2011). A generalized paragenesis of basement-hosted deposits in the McArthur Basin (from Polito *et al.,* 2011) is presented in Figure 5.5.

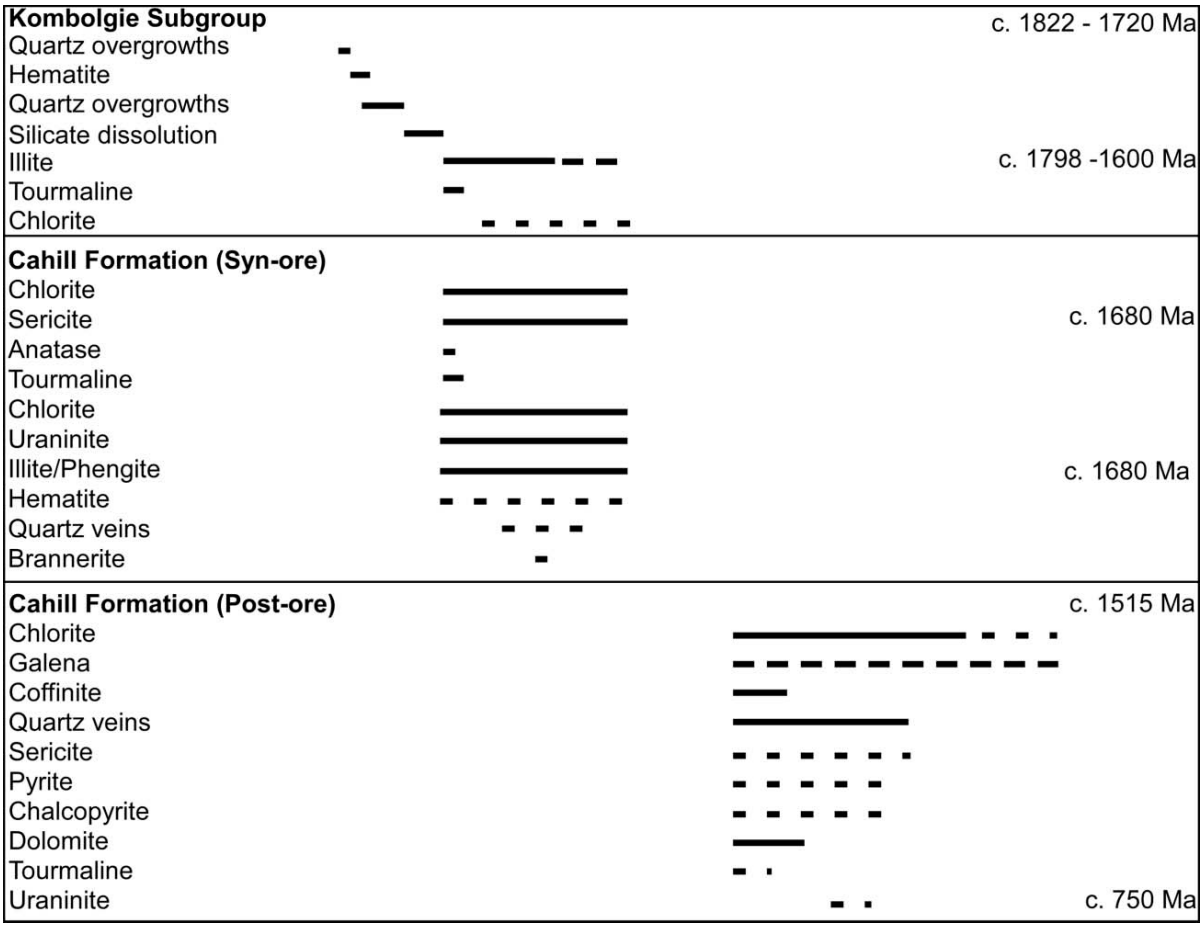

Figure 5.5: Simplified paragenesis for unconformity-type uranium deposits in the McArthur basin (from Polito *et al*., 2011).

Uraninite is the most common primary uranium mineral, although minor amounts of brannerite and coffinite also occur (Mernagh *et al*., 1998). The uraninite occurs in three main styles: veins, breccia-fill and as disseminated uraninite. In the Jabiluka deposit, disseminated grains of uraninite characterize stage-one mineralization, whereas stage-two uraninite occurs in veins (Polito *et al*., 2005). Reported ages from primary uraninite are ~1675-1650 Ma, whereas second-stage uraninite formed at ~870, ~750 & ~600 Ma (Maas, 1989; Polito *et al*., 2004, 2005). Mineralization at the Ranger deposit has an age of~1737 Ma (Maas, 1989), which

pre-dates the overlying Kombolgie Subgroup sandstones (Ludwig *et al*., 1987; Maas, 1989).

Hydrogen- and oxygen-isotope compositions of fluids that formed basement-hosted unconformity-type deposits in the McArthur basin have δD values that range from around -45‰ to -10‰ and $\delta^{18}O$ values that range from around 0‰ to 8‰ (Polito *et al*., 2004; 2005, 2011). The fluids are generally interpreted to be 200°C basinal brines from the McArthur Basin that flowed into the underlying basement rock via reactivated pre-Kombolgie Subgroup faults, very similar to the metallogenesis proposed for the Athabasca deposits. The brines were initially highly oxidizing, acidic and Ca-rich (Mernagh *et al.,* 1998).

Most studies on the uranium deposits from the McArthur Basin have suggested that the dominant mechanisms for uranium reduction were: (1) mixing between an uraniferous oxidizing fluid and a reducing fluid, or (2) Fe-oxidation by uraniferous oxidizing fluids that interacted with Fe-rich host lithologies (Wilde *et al.,* 1989; Jaireth, 1992; Mernagh *et al*., 1994; Komninou & Sverjensky, 1996; Mernagh *et al*., 1998), again very similar to the metallogenesis proposed for the Athabasca deposits.

Three models have been proposed for the formation of unconformity-related deposits from the McArthur Basin. Model I suggests that oxidized meteoric fluids interacted with the Kombolgie Supergroup as they descended along dilatational

structures and faults and became uranium-rich, acidic and Ca-rich brines. These brines either mixed with reducing fluids or interacted with Fe-rich, reducing basement lithologies, and precipitated uraninite at or below the unconformity (Johnston & Wall, 1984; Wilde *et al*., 1989; Jaireth, 1992; Solomon & Groves, 1994; Mernagh *et al*., 1994; Komninou & Sverjensky, 1996). Model II suggests similar depositional mechanisms for uraninite as model I; however, the source for the fluids is a uranium-bearing, oxidizing basinal brine formed during peak diagenesis (Hoeve *et al*., 1980; Sibbald & Quirt, 1987; Ruzicka, 1993; Polito *et al*., 2011). Model III invokes supergene processes (Knipping, 1974; Ruzicka, 1975; Crick & Muir, 1980; Donnelly & Ferguson, 1980; Furguson *et al*., 1980; Ewers *et al*., 1984; Needham, 1988) where uranium is leached from Paleoproterozoic rocks by surface waters and precipitated in reducing environments as a result of pH change. These three models are similar to those proposed, over time, for the Athabasca deposits (Quirt, 1989; Jefferson et al., 2007b).

5.3 The Bong Deposit, Thelon Basin

The age of the Thelon basin is between 1750 and 1720 Ma (Miller *et al*., 1989; Rainbird *et al*., 2003), which is similar to the Athabasca Basin (1740 to 1730 Ma; Orrell *et al*., 1989; Rainbird *et al*., 2007) and possibly younger than the McArthur basin (~1790 Ma; Polito, 2006). The Bong deposit is hosted entirely in the basement rocks (Woodburn Lake Group metasediments) because the Thelon Basin sandstone cover has been completely removed in the Kiggavik area. Therefore, the geological setting of the Bong deposit is similar in setting to the basement-hosted deposits from the Athabasca Basin, such as the Rabbit Lake, Eagle Point, Cluff Lake and Millennium deposits and the Ranger, Jabiluka, and Naberlek deposits from the McArthur Basin.

The Rabbit Lake, Eagle Point and Millennium deposits are hosted in the basement rocks of the Wollaston lithostructural domain (Sibbald *et al.,* 1977; Hoeve & Sibbald, 1978; Sibbald, 1985; Annesley et al., 2005). The domain comprises three main groups: ca. 2.80-2.95 Ga Archean orthogneiss, overlain by pre-1.92 Ga Paleoproterozoic metasedimentary rocks that are locally graphitic and intruded by 1.80-1.84 Ga granitoids, gabbros and associated pegmatites related to the Trans-Hudson Orogen (Lewry & Sibbald, 1977; Annesley *et al*., 2005). The basement rocks hosting mineralization in the Australian deposits consist of metamorphic psammopelitic sedimentary rocks and various schists (Cuney & Kyser, 2009). Graphitic units are present beneath the Jabiluka deposit, but not the Nabarlek (Polito *et al*., 2005, 2004). The basement rocks beneath the McArthur Basin are

intruded by the Zamu dolerite (1884 Ma) and later intrusions, such as the Jimbu microgranite and the Oenpelli dolerite, around 1720 Ma (Dodson *et al*., 1974; Rawlings & Page, 1999). Similar to the rocks that host the basement-hosted deposits of the Athabasca and McArthur Basins, the Bong deposit is hosted by the Woodburn Lake Group metasedimentary rocks, which are intruded by the hybrid 1830 to 1750 Ma Lone Gull granites (Scott *et al.,* 2011) and numerous smaller intrusive rocks. Graphitic material is only a minor component of the rocks associated with the Bong deposit. The paucity of graphitic units in the basement rocks from the Kiggavik area suggests that graphite may not be a major component in the formation of basement-hosted unconformity-type uranium deposits from the Thelon Basin. Graphite is also rare or absent around the Nabarlek uranium deposit (Polito *et al*., 2004). Although graphite is associated with the majority of deposits from the Athabasca basin, a few lower-grade deposits have formed without significant amounts of graphite being present (Jefferson *et al*., 2007a,b).

The alteration associated with the Bong deposit can be divided into pre-ore, syn-ore, and post-ore alteration. Pre-ore alteration of the Woodburn Lake Group metasediments consists of retrograde metamorphic chloritization of biotite, sericitization of muscovite and feldspars, silicification and brecciation. The main alteration minerals associated with the main ore-forming stage are illite and chlorite, which are accompanied by minor amounts of pyrite, rutile, and apatite (Fig. 4.1). The formation of mini-roll-fronts with distinct zones (reduced, oxidized, redox front; Section 4.1.2), a second generation of illite, and late quartz and carbonate

veins are characteristic of post-main-stage ore alteration. This alteration sequence produced an outer zone characterized by the replacement of muscovite, biotite, garnet and feldspar by chlorite and fine-grained sericite, and an inner zone (proximal to the main ore zone) characterized by intense illitization ± chloritization of the host rock. This style of alteration is similar to alteration associated with basement-hosted uranium deposits of the McArthur basin and the Athabasca Basin (Hoeve & Sibbald, 1978; Hoeve & Quirt, 1984; Sibbald, 1985; Quirt, 1989; Kotzer & Kyser, 1995; Fayek & Kyser, 1997; Quirt, 2001, 2003; Alexandre *et al*., 2005, 2009).

Uranium mineralization of the Bong deposit occurs in three styles: vein-type, graphite-associated, and mini-roll-fronts. Stage A uraninite from the Bong deposit is associated with illite and occurs as veins and coating and filling fractures in graphite, whereas Stage B uraninite occurs in mini-roll-fronts. Vein-type uraninite is more characteristic of the Nabarlek and Jabiluka deposits (Polito *et al*., 2004, 2005). Primary uraninite in the Athabasca Basin basement-hosted uranium deposits also occurs as fracture filling and in veins, with the addition of massive replacement-style uraninite (Hoeve & Sibbald, 1978; Hoeve & Quirt, 1984; Quirt, 1989; Fayek & Kyser, 1997; Cloutier *et al*., 2009). There are also deposits from the Athabasca Basin (Millennium, Eagle Point, P-Patch) that show evidence for late-stage mini-roll front-style mineralization (Beshears, 2009; Mercadier et al., 2011). At the Eagle Point and P-Patch deposits, redox fronts may represent more than 80% of the U resource (Mercadier *et al*., 2011), highlighting the importance of the roll-front style of mineralization within basement-hosted unconformity-type deposits.

5.3.1. Geochronology of uranium minerals

There are very few reported ages on uranium minerals from the Thelon Basin. Farkas (1984) reported U-Pb isotopic ages of 1403 ± 10 Ma and 1000 ± 10 Ma for uranium minerals from the Kiggavik deposit. However, the fine-grained nature of pitchblende and coffinite made separation of the two minerals difficult. Fuchs *et al.* (1986) reported whole rock K-Ar ages from relatively unaltered and altered Woodburn Lake metasediments and from the Lone Gull Granite. The unaltered samples gave ages of 1648 Ma and 1563 Ma, whereas the altered samples gave ages of 1358 Ma and 1073 Ma. Fuchs *et al.* (1986) interpreted the older ages to be related to uplift and erosion of Woodburn Lake Group and Lone Gull basement rocks after the Hudsonian Orogeny. Alternatively, the older ages may represent the age of deep burial and diagenesis. The younger ages, 1358 Ma and 1073 Ma, were interpreted to be the age of primary mineralization and the age of a resetting event that remobilized uranium, respectively.

Chemical-Pb ages from least altered vein-type uraninite from the Bong deposit range from 838 Ma to 1192 Ma, with an average age of 1031 Ma. Altered vein-type uraninite consistently gave much younger ages between 575 Ma and 668 Ma, with an average age of 591 Ma. Chemical-Pb ages from uraninite associated with graphite range from 289 Ma to 960 Ma and average 637 Ma. The mini-roll-front uraninite has a wide range of ages, from 10 Ma to 113 Ma with an average of 50 Ma, whereas coffinite gave an average chemical-Pb age of only 19 Ma.

Chemical-Pb ages have been used to infer formation ages of uraninite (Bowles, 1990). This is only possible when the U-Pb system has remained closed over the grain's entire history. Uraninite is known to be highly susceptible to alteration by circulating fluids, including Pb loss due to diffusion (Kotzer & Kyser, 1993; Janeczek & Ewing, 1995) and Pb loss due to episodic precipitation of secondary minerals (Evins *et al.,* 2005). Therefore, the ranges in chemical-Pb ages from the Bong deposit likely represent different Pb-loss events. For example, chemical-Pb ages of unaltered vein-type uraninite correlate with the timing of the Grenville Orogeny (~1090-950 Ma; Rivers, 2008) whereas the alteration of vein-type uraninite may be related to the breakup of the supercontinent Rodinia (~750-580 Ma; Powell *et al*., 1993). Chemical-Pb ages from the Bong deposit are similar to those that have been obtained from deposits of the Athabasca and McArthur Basins (Fayek & Kyser, 1997, Polito *et al*., 2004, 2005).

In situ, U-Pb isotope micro-analysis of vein-type and mini-roll-front uraninite from the Bong deposit gave similar upper intercept ages of 1117 ± 15 Ma and 1040 ± 39 Ma, respectively, on Concordia plots. Therefore ~1120 Ma and ~1040 Ma are interpreted to be the minimum age of crystallization for Stage A and Stage B uraninite, respectively, in the Bong deposit. These ages are relatively young compared to the ages reported for primary ore from the Athabasca and McArthur Basins (~1600-1500 Ma and ~1670-1650 Ma, respectively). However, these ages are similar to later stage 2 and 3 uraninite from the Athabasca and McArthur Basins (e.g. Kyser *et al*., 1990; Fayek *et al.,* 2002a, 2002b; Polito *et al.,* 2004) and basement-

hosted uranium deposits along the periphery of the Athabasca Basin (e.g., Roughrider deposit; Boulanger, 2012).

5.3.2 Temperature and fluid composition

A temperature for the fluid associated with the main stage of ore deposition at the Bong deposit was calculated using the $\delta^{18}O$ values of illite and Stage A uraninite, and the illite-H_2O [8] and uraninite-H_2O [9] fractionation factors from Sheppard and Gilg (1996) and Fayek and Kyser (2000), respectively. The average calculated equilibrium isotopic temperature for uraninite and illite is 227°C, which differs by ~65°C from the average temperature calculated using illite chemistry (163°C; Section 4.2.1 eq. [7]; Battalgia, 2004). The range in temperatures for the equilibrium isotopic method is 155°C to 244°C, while the range in temperatures using illite chemistry is 124°C to 214°C. The range in temperatures differs only by ~30°C.

Clay-mineral thermometry has been a topic of debate (Essene & Peacor, 1995) and therefore temperature estimates using this method are generally approached with caution. There are many different types of clay thermometers, including estimates using illite and chlorite crystallinity (Frey, 1987), chlorite and illite compositions (Cathelineau & Nieva, 1985; Cathelineau, 1988; Battaglia, 2004) and smectite/illite reactions (Hower *et al.,* 1976; Hoffman & Hower, 1979). The method of Battaglia (2004) was chosen because it was developed using only illite

and at temperatures that were expected for the formation of the Bong deposit (~200°C).

In order for a stable isotope thermometer to work, a few conditions must be met: (1) the isotopic compositions of the minerals (i.e. uraninite and illite) must be measured with the necessary precision (e.g., SIMS), (2) the minerals need to be in isotopic equilibrium, which in this study was determined through petrographic characterization of hand samples and thin sections, and (3) a suitable fractionation factor that varies as a function of temperature is required (See equations [8] & [9]). Therefore, using both the clay mineral and stable isotope thermometry methods, the temperature for the deposit has been restricted to a range from ~160°C to ~230°C. However, for the purposes of this discussion the isotopic equilibrium temperature of 227°C will be used, because it is based on stable isotope thermometry, which is considered more reliable than clay mineral thermometry. The average $\delta^{18}O$ and δD value of the fluid that formed Stage A uraninite and coeval illite was calculated to be -7.9‰ and -101‰, respectively. These values are consistent with hydrothermal water of meteoric origin (Fig. 5.6) heated by the geothermal gradient.

Although the temperature of the mineralizing fluid from the Bong deposit is similar to mineralizing fluids associated with uranium deposits from the Athabasca and McArthur basins (e.g., ~200°C; Pagel, 1975; Hoeve & Quirt, 1984; Kotzer & Kyser, 1990, 1992, 1993; Kyser *et al.,* 2000; Alexandre *et al*., 2005; Cloutier *et al*., 2009; Polito *et al*., 2004, 2005), the isotopic composition of the fluid is significantly

different from the fluids associated with the basement-hosted, unconformity-related deposits from the Athabasca and McArthur Basins (Fig. 5.6). Typical $\delta^{18}O$ values for the Athabasca and Kombolgie basins are between 0‰ and 10‰, while δD values range from -60‰ to -10‰ and the fluids that formed these deposits have been interpreted as basinal brines (Kotzer & Kyser, 1993; Kyser *et al.,* 2000; Alexandre *et al*., 2005; Polito *et al*., 2004, 2005; Cloutier *et al*., 2010). The $\delta^{18}O$ and δD values for the fluids that formed the Bong deposit are -7.9‰ and -101‰, respectively, and represent meteoric-sourced hydrothermal fluids. Therefore, if basinal brine is not required for the formation of the Bong deposit the unconformity is not considered a critical factor.

The lower values in the Bong deposit could represent a more isotopically depleted meteoric source for the fluids, although paleocontinent reconstructions of the Earth place the Thelon basin closer to the equator than both the Athabasca and McArthur basins ~1100 Ma, when Stage A uraninite formed (Weil *et al*., 1998). Therefore, based on the latitude effect, it would be expected that the $\delta^{18}O$ and δD values for meteoric-sourced fluid in the Thelon would be higher than that for the McArthur and Athabasca. However, the Thelon basin would have been the farthest from the ocean at this time, so Rayleigh fractionation may have played a role in the depletion of ^{18}O and D. It is also possible that the $\delta^{18}O$ and δD values for the uraninite and illite have been affected by recent meteoric water.

Previously reported low values have been interpreted as earlier isotopic systematics having been reset by interactions with meteoric water. If this were the case, then it would be expected that uraninite from both stages of mineralization would have similar $\delta^{18}O$ values. However, uraninite from Stage A mineralization has $\delta^{18}O$ values that are ~19‰ higher than that of Stage B (Table 4.4). Also, the correlation between $\delta^{18}O$ values and alteration (i.e., the amounts of Si and Ca in uraninite; Fig. 4.26) show that uraninite with higher $\delta^{18}O$ values (~-7‰ to ~4‰) is the most altered, while uraninite with lower $\delta^{18}O$ values is the least altered. This is because the incorporation of SiO_2 and CaO into the uraninite structure should result in an overall $\delta^{18}O$ enrichment (Kotzer & Kyser, 1990, 1993). The lack of petrographically observable alteration in uraninite having low $\delta^{18}O$ values would require that uranium-oxide minerals exchange O isotopes with fluids with only minor disturbances in their chemical compositions and original textures (Kotzer & Kyser, 1993; Fayek et al., 2011).

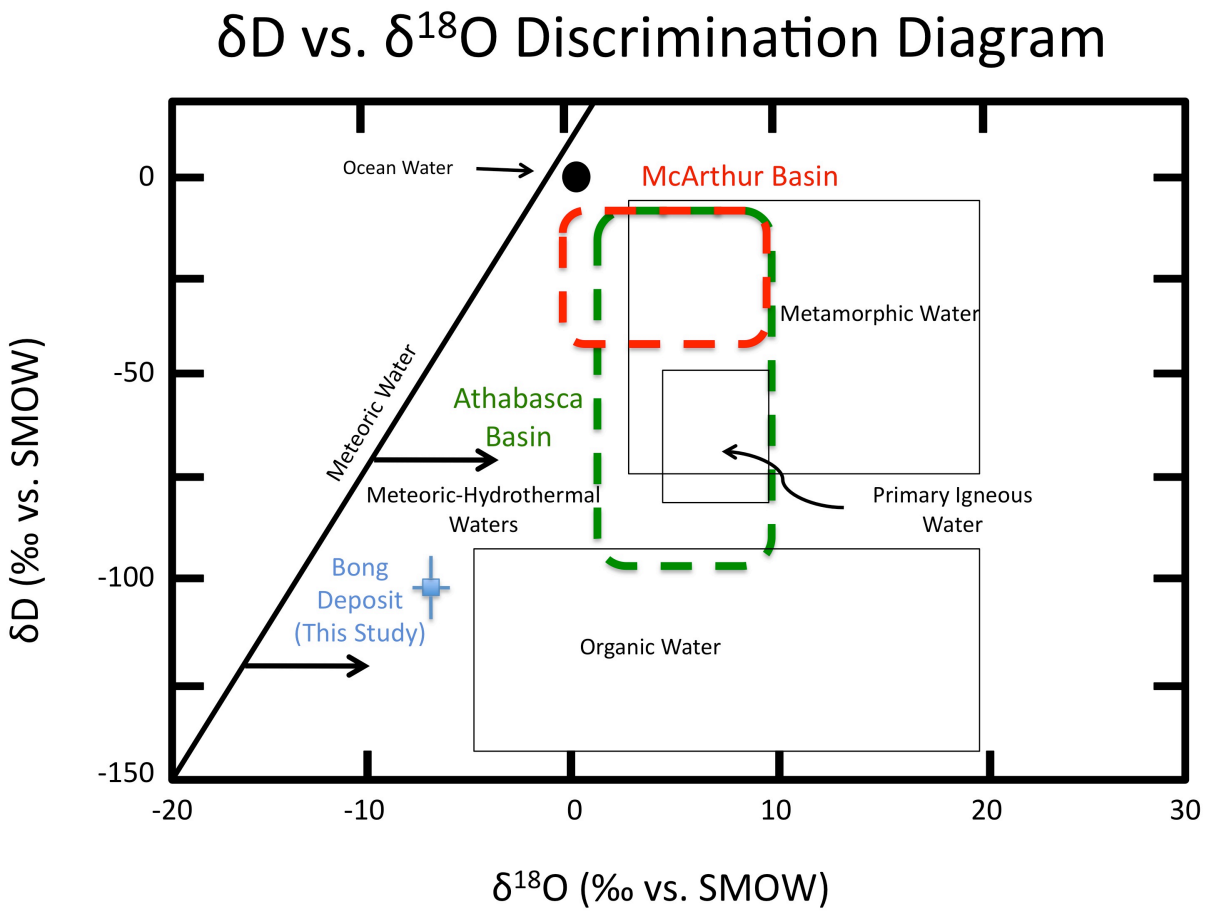

Figure 5.6: Oxygen and hydrogen discrimination diagram for various fluid sources. The values from the Bong deposit plot to the right of the meteoric water line in the meteoric-hydrothermal water area (diagram after Sheppard 1986, Sharp 2007). The green and red boxes represent observed values for basement-hosted unconformity related deposits in the Athabasca and McArthur basins, respectively (data from Kotzer & Kyser, 1993; Kyser *et al.*, 2000; Alexandre *et al.*, 2005; Polito *et al.*, 2004, 2005; Cloutier *et al.*, 2010).

5.3.3 Mechanism for uranium precipitation

There are several mechanisms for the precipitation of uranium, some of which include boiling, dilution, cooling and reduction. Many of these processes are related to changes in temperature and pressure. There is no evidence of any intrusions contemporaneous with formation of the Bong deposit, therefore, drastic changes in temperature or pressure are unlikely to have occurred. Based on hand sample observations, petrography, and Fe speciation analyses reduction is mostly likely the main mechanism for uranium precipitation at the Bong deposit. In addition, reduction is also the favored mechanism of precipitation in the Athabasca and Kombolgie deposits (Jefferson *et al.,* 2007a, b; Polito *et al.,* 2004, 2005).

With reduction being the favored mechanism of uranium precipitation, three possible processes for uranium reduction at the Bong deposit include: (1) iron-uranium oxidation-reduction couple, (2) change in fluid chemistry (e.g., pH and Eh), and (3) fluid interaction with hydrocarbons (graphite and organic matter).

The lack of ferric iron in the illitized zone (Fig. 4.24) suggests that iron oxidation did not play a key role in the formation of Stage A uraninite. The main processes during this stage are then more likely to be changes in fluid chemistry and/or fluid interaction with graphite. The presence of disseminated organic matter and hematite (Section 4.1.2; Figs. 4.10 & 4.13) associated with the stage-B uraninite suggests that oxidation of residual Fe (e.g., sulphides) and interaction with organic

matter was the mechanism for the reduction of uranium during the formation of mini-roll-fronts.

Based on stable isotope-geochemistry, Stage A uraninite and illite precipitated from a ~225°C meteoric-hydrothermal fluid. The presence of illite at 225°C suggest that the pH of the fluid was between 5 and 6 (Romberger, 1984; Kotzer & Kyser, 1995). If the initial fluid (meteoric) was oxidizing and acidic (pH 2-4; Fig. 5.7), Fe^{2+} would be the dominant Fe species and U^{6+} would be in dominant uranium species in solution. Through interaction with reducing basement lithologies (containing sulphides (P1) and graphite; Fig. 4.1) the fluid would become increasingly reduced. Continued interaction of the fluid with the host rock and the alteration of silicate minerals would increase the pH to 5-7, which would be accompanied with a reduction in fO_2 that would precipitate uraninite and illite.

A second, less-pervasive fluid event facilitated local remobilization and concentration of the uranium into mini-roll-fronts. Three characteristic zones comprise the roll-fronts:

1) A bleached (reduced) zone consisting of illite ± chlorite that is enriched in sulphides.
2) A brownish zone containing goethite and uraninite, which represents the uranium redox front (Fe-U redox couple with goethite + uraninite as reaction products).

3) A hematized (oxidized) zone rich in hematite and devoid of sulphides and uranium minerals.

The reaction to precipitate uranium at the roll-front involves the oxidation of iron and reduction of uranium, ultimately forming uraninite and goethite at the redox front:

$$6H_2O + U^{6+} + 2Fe^{2+} \rightarrow UO_2 + 2FeO(OH) + 10H^+ \quad [11]$$

The initial fluid was oxidizing (pH ~4.5; Fig. 5.7) and therefore would have dissolved any uranium minerals and sulphides it encountered. However, through interaction with organic matter and the oxidation of residual Fe^{2+} (Fig. 4.24), there would have been a decrease in the amount of dissolved oxygen. This decrease would cause uraninite to precipitate at the redox front (Fig. 4.10) and sulphides to precipitate in the reduced area just beyond the redox front.

Figure 5.7: Pourbaix diagram for the U-F-S-O system with a Fe-O and clay system overlays @ 200°C, 10 ppm Fe, 100 ppm F, 1000 ppm S, 1000 ppm K, 1.0 m NaCl, P_{CO2} = 10 atm. The diagram shows the fO_2 and pH condition of each species' stability. The evolution of the fluids that precipitated Stage A uraninite (Fluid 1) and Stage B uraninite (Fluid 2) has been plotted on the diagram (modified after Romberger, 1984).

Graphite is locally present in unaltered material, and graphite and organic matter are both present in the alteration zone of the Bong deposit. Uraninite coats and fills fractures within graphite nodules and blebs (Stage A uraninite; Section 4.1.3). Organic matter is disseminated with Stage B uraninite (Section 4.1.3). Therefore, it is likely that this material acted as a reductant to facilitate uranium deposition. The $\delta^{13}C$ values of the graphite and organic matter were measured and the values range from -48.3‰ to -21.1‰ (Table 4.6; Appendix F). The results can be separated into two distinct groups; 1) Organic matter associated with mini-roll-front uraninite, that has $\delta^{13}C$ values that range from -27.9‰ to -21.1‰ and an average value of -24.2 ± 3.1‰, and 2) a mineralized graphite nodule and unmineralized organic matter, that have $\delta^{13}C$ values that range from -48.3‰ to -39.0‰ and an average value of -42.5 ± 5.1‰. Similar $\delta^{13}C$ values have been observed in graphite, bitumen and carbon nodules in the Athabasca Basin (Section 5.1).

The graphite and organic matter in the Bong deposit have very different characteristics, $\delta^{13}C$ values, and different relation to the ore. Therefore, it is likely that the two represent distinct sources of carbon. No unmineralized counterpart for the mineralized graphite nodule was obtained. Therefore carbon isotopes cannot be used to determine the role of graphite in mineralization. However, mineralized samples of organic matter have $\delta^{13}C$ values ~20‰ higher than unmineralized samples.

Samples of unmineralized organic matter in the bleached zone have $\delta^{13}C$ values of ~-43‰, while samples of organic matter associated with Stage B uraninite have $\delta^{13}C$ values of ~-24‰. During alteration of carbon-rich material (i.e., organic matter), enrichment in ^{13}C occurs because ^{12}C-^{12}C bonds are weaker than, and therefore easier to break, than the bonds formed by ^{13}C (Faure & Mensing, 2005). Consequently, the alteration (breakdown) of organic matter by hydrothermal fluids will lead to an increase in $\delta^{13}C$ values in the remaining material. As the mineralizing fluid that precipitated Stage B uraninite has further altered organic matter associated with the roll-fronts, the $\delta^{13}C$ values should be higher than that of unmineralized organic matter. The observed ~20‰ increase in ^{13}C in mineralized samples relative to barren samples is consistent with hydrothermal alteration of the organic matter.

5.3.4 Origin of the Organic Matter

The origin of the organic matter in the Bong deposit is difficult to determine as petrographic descriptions and carbon isotopes are the only techniques used in the current study. The organic matter differs from the graphite in a number of ways. The graphite generally forms nodules and blebs, and is mineralized (uraninite coating and filling fractures; e.g., Fig. 4.19). The organic matter fills fractures, is disseminated in the host rock and is sometime associated with roll-fronts. It has a characteristic sulphur smell when encountered in freshly drilled core. Organic matter that was an original constituent of the host rock could have been converted to graphite or destroyed during metamorphism, because the process of metagenesis

is destructive and hydrocarbons are converted to methane or graphite (Selley, 1998). Therefore, the organic matter at the Bong deposit, likely posted-dated metamorphism of the host rock. The material must have either (1) migrated into the basement or (2) been produced *in situ* in the alteration zone by the alteration/remobilization of pre-existing graphite material.

In order for the material to migrate into the basement, there would need to be a source of the material independent from the basement. The overlying Thelon basin is the most likely source, yet bitumen is currently not part of the Thelon basin paragenesis (Rainbird *et al*., 2003; Peterson, 2006). However, the Thelon basin is not as well studied as the Athabasca and Kombolgie basins and a large portion of the basin, including that above the deposits in the Kiggavik area, has been eroded. Therefore, it is possible that bitumen is present but yet to be observed or was eroded away with the overlying basin in the area surrounding the Bong deposit.

A second possibility for the origin of the organic matter is that it was produced *in situ* by the alteration or remobilization of pre-existing graphite material. Although graphite alteration and depletion is observed at other uranium deposits (e.g., Midwest, Cigar Lake, Rabbit Lake; Hoeve & Quirt, 1984; Landais *et al*., 1993) the exact mechanism has not been identified. One such mechanism is Fischer-Tropsch synthesis (Riegler, Pers. Comm., Jan 21, 2012). Fischer–Tropsch synthesis can produce hydrocarbons *in situ* (Röper, 1983). Fischer–Tropsch synthesis is a process that is used to generate hydrocarbons from abiogenic sources, whereby a

mixture of carbon monoxide and hydrogen are converted into liquid hydrocarbons. The Fischer–Tropsch process involves a series of chemical reactions that produce a variety of hydrocarbon molecules according to the equation:

$$(2n + 1)\ H_2 + nCO \rightarrow C_nH_{(2n+2)} + nH_2O \quad [12]$$

Stage A uraninite precipitated from a fluid when the fluid encountered graphitic material according to the equation:

$$U^{6+} + 3H_2O + C \rightarrow UO_2 + CO + 6H^+ \quad [13]$$

Carbon monoxide and hydrogen produced during the interaction of graphite with hydrothermal fluids could then be used in the Fischer-Tropsch process to generate hydrocarbon molecules. Fischer-Tropsch synthesis reactions generally take place in excess of 500°C (Selley, 1998), while the mineralizing fluid that formed the Bong deposit has a temperature of only ~227°C. Therefore, there may be another mechanism responsible for hydrocarbon formation.

5.3.5 Genetic Model

Based on the mineral paragenesis, redox reactions, stable isotopes and geochronology, a genetic model for the Bong deposit can be developed. This model consists of four stages (Fig. 5.8). The host rocks associated with Bong deposit consist of Woodburn Lake Group (WLG) metasediments. The WLG is intruded by the Lone Gull Granite and also by various dykes and smaller scale intrusives (Stage 0; Fig. 5.8A).

Stage 1 (Fig. 5.8B) involved a silica-rich fluid event that silicified and brecciated the WLG but not the quartzite and rhyolite. This suggests that the silica-rich fluid may have been derived from below in association with intruding magmas, such as the mixed Lone Gull Granite (at ~ 1.83 Ga & ~1.75 Ga; Scott *et al.,* 2011) and flowed upward along faults and between rheological contacts. Fluid over-pressuring caused localized brecciation.

Stage 2 (Fig. 5.8C) in the formation of the deposit is characterized by the infiltration of fluids into the basement rocks along pre-existing faults at ~1120 Ma. The fluids were oxidizing and highly acidic, and likely scavenged uranium from the detrital phases (i.e., monazite, zircon) in the metasediments or the overlying Thelon sediments. This fluid is associated with widespread illitization and desilification, resulting in bleaching and a loss of coherence of the host rock. Through continued interaction with reduced basement rocks containing sulphides and graphite, the

oxidizing fluid was reduced and precipitated uraninite. The uraninite formed during this stage is both vein-type, and coating and fracture fillings in graphite.

Stage 3 (Fig. 5.8D) is characterized by the formation of organic matter, the origin of which is unknown. Possibilities for the origin of this material include the migration of bitumen into the basement or production *in situ* by the alteration/remobilization of pre-existing graphite material.

The final stage (Stage 4; Fig. 5.8E) in the formation of the Bong deposit is defined by post-ore alteration by oxidizing fluids. Stage 4 occurred at ~1040 Ma and is characterized by hematization and remobilization of uranium into mini-roll-fronts. Three characteristic zones comprise this stage:

1) A bleached (reduced) zone consisting of illite ± chlorite that is enriched in sulphides.
2) A brownish zone containing goethite and uraninite, which represents the uranium redox front (Fe-U redox couple with goethite + uraninite as reaction products).
3) A hematized (oxidized) zone rich in hematite and devoid of sulphides and uranium minerals.

The reaction to precipitate uranium at the roll-front involves the oxidation of iron and reduction of uranium ultimately forming uraninite and goethite at the redox front:

$$6H_2O + U^{6+} + 2Fe^{2+} \rightarrow UO_2 + 2FeO(OH) + 10H^+ \quad [11]$$

The addition of organic matter (Stage 3) added another possible reductant for the reduction of uranium. The enrichment of organic matter in ^{13}C associated with mineralization relative to barren samples is consistent with oxidation of organic matter that may have been involved in the uranium reduction process.

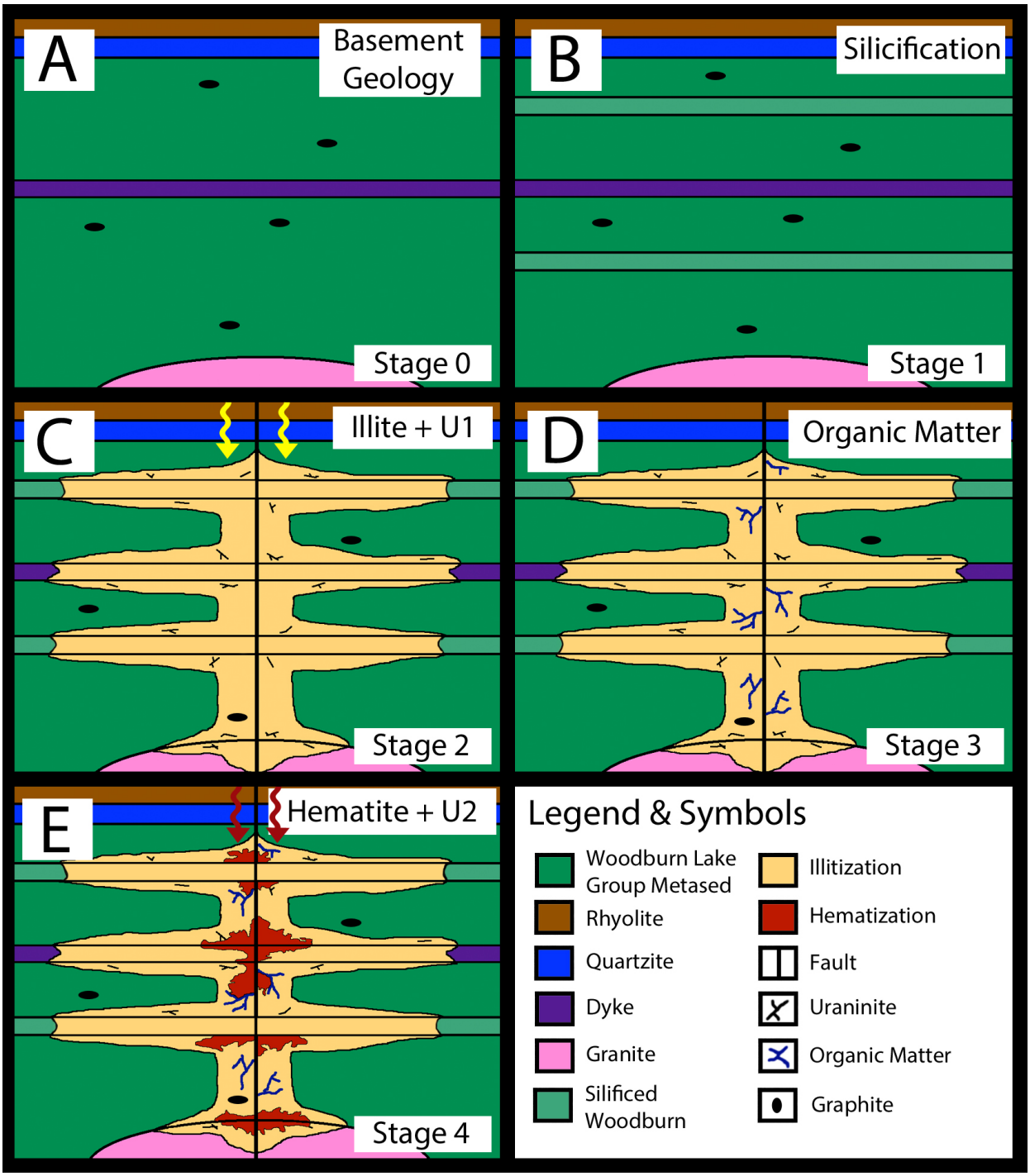

Figure 5.8: Genetic model for the Bong deposit. A) Stage 0: Idealized geology of the area. B) Stage 1: Silicification of areas of the host rock. C) Stage 2: A highly acidic, oxidizing fluid moves along a fault causing pervasive bleaching. Changes in geochemical conditions cause precipitation of uraninite as vein-type and graphite associated uraninite (Stage A uraninite) at ~1120 Ma. D) Stage 3: Formation/introduction of organic matter in the deposit (possibly syn-stage 2). E) Stage 4: Remobilization of uraninite into roll-fronts (Stage B uraninite) by an oxidizing fluid at ~1040 Ma.

Chapter 6: Conclusions

6.1 Conclusions

Various petrographic, geochemical and isotopic techniques were used to characterize the Paleoproterozoic Bong uranium deposit that has historically been considered to be unconformity-type. The major conclusions from this work relate to the source and temperature of the fluids carrying the uranium, the mechanism of deposition of the uranium, and the timing of the events. The main conclusions of this study are:

1. The deposit has three main styles of uranium mineralization that occurred in two stages. Stage A uraninite (vein-type and graphite-associated) formed during a fluid event that produced pervasive argillization in the basement host rock. A later, less-pervasive oxidizing fluid remobilized and concentrated the uranium into mini-roll-fronts (Stage B uraninite).

2. *In-situ* U-Pb geochronology of Stage A uraninite gave an age of 1117 ± 15, while *in situ* U-Pb geochronology of Stage B uraninite gave an age of 1040 ± 39. These ages are taken to be the minimum ages of crystallization for Stage A and Stage B uraninites, respectively. Furthermore, the U-Pb systematics of these samples have been variably reset by major tectonic events, probably related to the Grenville Orogeny (~1090-950 Ma) and the breakup of the supercontinent Rodinia (~750-580 Ma), and are reflected in the Pb-Pb and

chemical-Pb ages of the uraninite. Ages <100 Ma are related to uraninite alteration resulting from interaction with recent meteoric water.

3. Using the oxygen isotopic composition of uraninite and illite, and uraninite-water and illite-water fractionation factors, the fluid associated with Stage A uraninite had a temperature of 227°C. This fluid had an average $\delta^{18}O$ value of -7.9‰ and an average δD value of -100.9‰, which is consistent with a hydrothermal fluid sourced from meteoric waters. This is in contrast mineralizing fluids that formed both the Athabasca Basin and McArthur Basin deposits, which have isotopic compositions characteristic of basinal brines.

4. Carbon-rich material acted as a reductant for both stages of uraninite. Stage A uraninite is observed coating graphite and filling pore space. Based on petrographic relation and carbon-isotope values, organic matter also acted as a reductant during the formation of Stage B uraninite.

5. The Fe-U redox couple was important in the precipitation of Stage B uraninite. However, it did not play a significant role in the precipitation of Stage A uraninite because the concentration of Fe^{2+} is lower in the alteration zone compared to unaltered WPG, the concentration of Fe^{3+} is unchanged. This suggests that a change in pH likely caused the precipitation of Stage A uraninite.

6. The Bong deposit formed in four stages. Stage 1 involved silicification of the host rocks. Stage 2 is characterized by pervasive argillization of the host rock and the formation of Stage A uraninite in veins and coating graphite (~1120 Ma). This stage is characterized by ~225°C fluids with calculated $\delta^{18}O$ and δD values of -7.9‰ and -100.9‰, respectively. During Stage 3, organic matter formed along fractures in permeable clay-rich alteration zones. At ~1040 Ma, an oxidizing fluid event (Stage 4) reconcentrated uraninite into redox fronts (Stage B) and altered Stage A uraninite to uranophane.

7. Based on temperature, geochemistry, isotopic composition and age, the mineralization in the Bong deposit is meteoric-hydrothermal in origin. The geology, alteration and timing of the uranium mineralization in the Bong deposit shows similarities to both the McArthur Basin in Australia and the Athabasca Basin in Canada. However, based on isotopic composition the mineralizing fluid that formed the Bong deposit is meteoric-hydrothermal in origin (see point 3). Basinal brines are not required to form this deposit and, therefore, the unconformity is not a critical factor for the current proposed genetic model.

6.2 Recommendations for Future Work

To fully characterize the fluid history of the Bong deposit, further analysis is necessary, these include:

- More detailed study of the graphite and organic matter in the deposit
  to determine the origin of the material and the role it played in the precipitation of uranium minerals, as the graphite and organic matter was involved in the formation of both stages of uranium mineralization and are likely an important factor in the genesis of the deposit.
- *In-situ* U-Pb age dating of the uraninite associated with the graphite, as well as the uraninite rims on the rutile, apatite, and sulphides.
- Ar-Ar age dating of the clay alteration minerals associated with the first generation of uraninite.
- Rare earth element (REE) compositions of the uraninite
  to help in the determination of the source of uranium and to compare REE patterns to other deposit types.
- Sulphur isotopes on all generations of sulphides
  to determine the source of sulphur for the sulphides.
- Oxygen isotopes on all generations of quartz
  to isotopically separate the different generations of quartz and, combined with fluid inclusions, obtain information on the isotopic composition of the fluids that formed the quartz.

- Fluid inclusions on the different generations of quartz

  to determine the minimum temperature of formation and composition of the fluids associated with each generation of quartz and relate these compositions to uranium metallogenesis.

References

ActLabs (2012): The 2012 Canadian schedule of services and fees*; ActLabs Canada*, 30 p.

Adler, H.H. (1974): Concepts of uranium-ore formation in reducing environments in sandstones and other sediments; *Formation of uranium ore deposits*, IAEA Conference, Athens, Greece, 141-167.

Alexandre, P., Kyser, K. & Polito, P. (2003): Geochronology of the Paleoproterozoic basement-hosted unconformity-type uranium deposits in northern Saskatchewan, Canada; Uranium Geochemistry 2003, International Conference, Université Henri Poincaré, Nancy, France, April 13-16, 2003, Proceedings, 37-40.

Alexandre, P., Kyser, K. & Polito, P. (2005): Alteration mineralogy and stable isotope geochemistry of Paleoproterozoic basement-hosted unconformity-type uranium deposits in the Athabasca Basin, Canada; *Society of Economic Geologist*, **100**, 1547-1563.

Alexandre, P., Kyser, K., Thomas, D., Polito, P. & Marlatt, J. (2007): Geochronology of the unconformity-related uranium deposits in the Athabasca Basin, Saskatchewan, Canada and their integration in the evolution of the basin; *Mineralium Deposita*, **44**, 41-59.

Annesley, I.R., Madore, C. & Portella, P. (2005): Geology and thermotectonic evolution of the western margin of the Trans-Hudson Orogen: evidence from the eastern sub-Athabasca basement, Saskatchewan; Canadian Journal of Earth Sciences, **42**, 573-597.

AREVA Resources Canada Inc. (2011): Kiggavik Project EIS: Popular Summary; Tier 1, Volume 1, p. 51.

Battaglia, S. (2004): Variations in the chemical composition of illite from five geothermal fields: a possible geothermometer; *Clay Minerals*, **39**, 501-510.

Berman, R.G., Sanborn-Barrie, M., Stern, R.A. & Carson, C.J. (2005): Tectonometamorphism at ca. 2.35 and 1.85 Ga in the Rae Domain, western Churchill Province, Nunavut, Canada: Insights from structural, metamorphic and *in situ* geochronological analysis of the southwestern Committee Bay Belt; *The Canadian Mineralogist*, **43**, 409-442.

Beshears, C. (2009): The geology and geochemistry of the Millennium uranium deposit, Athabasca Basin, Saskatchewan, Canada; MSc. Thesis, University of Manitoba, Winnipeg, Manitoba.

Blaise, J.R., Bouf, F., Heurley, P., Roussel, V., Ruhlmann, F., and Tiers, P. (1997): Prefeasibility study – Kiggavik-Sissons. COGEMA, internal report number 97.189/GF, dated 12/10/97, 201 p.

Boulanger, R. (2012): Geological, petrographic & geochemical characterization of the Roughrider west zone unconformity-type uranium deposit, Athabasca Basin, Saskatchewan; MSc. Thesis, University of Regina, Regina, Saskatchewan.

Bowles, J.F.W. (1990): Age Dating of Individual Grains of Uraninite in Rocks from Electron Microprobe Analyses; *Chemical Geology*, **83**, 47-53.

Cameron-Schiman, M. (1978): Electron microprobe study of uranium minerals and its application to some Canadian deposits; Ph.D. Thesis, University of Alberta, Edmonton, Alberta.

Capuano, R.M. (1992) The temperature dependence of hydrogen isotope fractionation between clay minerals and water: Evidence from a geopressured system; *Geochimica et Cosmochimica Acta*, **56**, 2547-2554.

Cathelineau, M. (1988): Cation site occupancy in chlorites and illites as a function of temperature; *Clay Minerals*, **23**, 471-485.

Cathelineau, M., & Nieva D. (1985): A chlorite solid solution geothermometer: The Los Azufres (Mexico) geothermal system; *Contributions to Mineral Petrology*, **91**, 235-244.

Chamberlain, K.R., Schmitt, A.K., Swapp, S.M., Harrison, T.M., Swoboda-Colberg ,N., Bleeker, W., Peterson, T.D., Jefferson, C.W., & Khudoley, A.K. (2010): *In-situ* U-Pb (IN_SIMS) micro-baddeleyite dating of mafic rocks: Method with examples; *Precambrian Research*, **183**, 379-387.

Cloutier, J., Kyser, K., Olivo, G.R., Alexandre, P. & Halaburda, J. (2009): The Millennium uranium deposit, Athabasca Basin, Saskatchewan, Canada: An atypical basement-hosted unconformity-related uranium deposit; *Economic Geology*, **104**, 815-840.

Cloutier, J., Kyser, K., Olivo, G.R. & Alexandre, P. (2010): Contrasting patterns of alteration at the Wheeler River area, Athabasca Basin, Saskatchewan, Canada: Insights into the apparently uranium-barren Zone K alteration system; *Economic Geology*, **105**, 303-324.

Crick I.H. & Muir M.D. (1980): Evaporites and uranium mineralization in the Pine Creek Geosyncline. In: Uranium in the Pine Creek Geosyncline (editors Ferguson J. & Goleby A.B.). International Atomic Energy Agency, Vienna; 531–542.

Cumming, G.L., & Krstic, D. (1992): The age of unconformity-associated uranium mineralization in the Athabasca Basin, northern Saskatchewan; *Canadian Journal of Earth Sciences*, **29**, 1623-1639.

Cuney, M. & Kyser, K. (2009): Recent and not-so-recent developments in uranium deposits and implications for exploration; Mineralogical Association of Canada, Short Course Series Volume 39, 257 p.

DeVoto, R.H. (1978): Uranium in Phanerozoic sandstone and volcanic rocks. Short course in uranium deposits: Their mineralogy and origin; *Mineralogical Association of Canada Short Course Handbook* **3**, 293-305.

Dodson, R.G., Needham, R.S., Wilkes, P.G., Page, R.W., Smart, P.G. & Watchman, A.L. (1974): Uranium mineralization in the Rum Jungle-Alligator Rivers Province, Northern Territory, Australia; In International Atomic Energy Agency (ed.), *Formation of Uranium Ore Deposits*; Proceedings of a Symposium, Athens, 551-568.

Donaldson, J.A. (1965): The Dubawnt Group, District of Keewatin and Mackenzie; *Geological Survey of Canada*, Paper 64-20.

Donnelly T.H. & Ferguson J. (1980): A stable isotope study of three deposits in the Alligator Rivers Uranium Field, NT. In: Uranium in the Pine Creek Geosyncline (editors Ferguson J. & Goleby A.B.). International Atomic Energy Agency, Vienna; 397–406.

Essene, E.J. & Peacor, D.R. (1995): Clay mineral thermometry: A critical perspective; *Clays and clay minerals*, 43, **5,** 540-553.

Evins, L.Z., Jensen, K.A. & Ewing R.C. (2005): Uraninite Recrystallization and Pb Loss in the Oklo and Bangombé Natural Fission Reactors, Gabon; *Geochimica et Cosmochimica Acta*, **69**, 1589**-**1606.

Ewers G.R., Ferguson J., Needham R.S. & Donnelly T.H. (1984): Pine Creek Geosyncline NT. In: Proterozoic Unconformity and Stratabound Uranium Deposits (editor Ferguson J.); International Atomic Energy Agency, Vienna; Tecdoc 315: 135–206.

Farkas, A. (1984): Mineralogy and host rock alteration of the Lone Gull deposit; *Internal Report*, Urangesellschaft.

Faure, G. & Mensing, T.M. (2005): Isotopes: Principles and applications; *John Wiley & Sons Inc.,* Hoboken, New Jersey, 897 p.

Fayek, M. & Kyser, T.K. (1997): Characterization of multiple fluid events and rare-earth-element mobility associated with formation of unconformity-type uranium deposits in the Athabasca Basin, Saskatchewan; *The Canadian Mineralogist*, **35**, 627-658.

Fayek M. & Kyser T.K. (2000): Low temperature oxygen isotopic fractionation in the uraninite-UO_3-CO_2-H_20 system; *Geochimica et Cosmochimica Acta*, **64**, 2185-2197.

Fayek, M, Harrison, T.M., Grove, M. & Coath, C.D. (2000): A rapid *in situ* method for determining ages of uranium oxide minerals: Evolution of the Cigar Lake deposit, Athabasca Basin; *International Geology Review*, **42**, 163-171.

Fayek, M., Harrison, T.M., Ewing, R.C., Grove, M., & Coath, C.D. (2002a): O and Pb isotope analyses of uranium minerals by ion microprobe and U-Pb ages from the Cigar Lake deposit; *Chemical Geology*, **185**, 205-225.

Fayek, M., Kyser, T.K. & Riciputi, L.R. (2002b): U and Pb isotope analysis of uranium minerals by ion microprobe and the geochronology of the McArthur River and Sue Zone uranium deposits, Saskatchewan, Canada; *The Canadian Mineralogist*, **40**, 1553-1569.

Fayek, M., Horita, J. & Ripley, E.M. (2011): The oxygen isotopic composition of uranium minerals: A review; *Ore Geology Review*, **41**, 1-21.

Ferguson, J., Ewers, G.R. & Donnelly, T.H. (1980): Model for the development of economic uranium mineralization in the Alligator Rivers Uranium Field. In: Uranium in the Pine Creek Geosyncline (editors Ferguson J. & Goleby A.B.). International Atomic Energy Agency, Vienna; 563–574.

Fischer, R.P. (1950): Uranium bearing sandstone deposits of the Colorado Plateau; *Economic Geology*, **45**, 1-11.

Frey, M. (1987): Low temperature metamorphism; Glasgow (Blackie), 351 p.

Friedrich, G., Weyer, H.J., & Bechtel, A. (1989): The Lone Gull uranium deposit: New geochemical and petrological data as evidence for the nature of the ore-bearing solutions; In: Proceedings of an IAEA Technical Committee Meeting on Metallogenesis of Uranium Deposits, March 9-12 1987, IAEA TC-542.

Fuchs, H. & Hilger, W. (1989): Kiggavik (Lone Gull): an unconformity related uranium deposit in the Thelon Basin, Northwest Territories, Canada, in Uranium Resources and Geology of North America, Proceedings of a Technical Committee Meeting, Saskatoon, 1-3 September, 1987: International Atomic Energy Agency, TECDOC-500, Vienna, 429-454.

Fuchs, H.D., Hiliger, W. and Prosser, E. (1986): Geology and exploration history of the Lone Gull property; *Uranium Deposits of Canada*, CIM Special Volume 33.

Google Maps (2012): Map of Canada, retrieved on Oct 2nd, 2012, from http://maps.google.ca/.

Gustafson, L.B. and Curtis, L.W. (1983): Post-Kombolgie Metasomatism at Jabiluka, Northern Territory, Australia, and its significance in the formation of high-grade uranium mineralization in lower Proterozoic rocks; *Economic Geology*, **78**, 26-56.

Harshman, E.N. (1972): Geology and uranium deposits, Shirley Basin area, Wyoming, U.S. *Geological Survey Professional Paper* **745**, 82 p.

Hasegawa, K. Davidson, G.I., Wollenberg, P. and Yoshimasa, I. (1990): Geophysical exploration for unconformity-related uranium deposits in the northeastern part of the Thelon Basin, Northwest Territories, Canada; *Mining Geology*, **40**, 83-95.

Hecht, L. & Cuney, M. (2000): Hydrothermal alteration of monazite in the Precambrian crystalline basement of the Athabasca Basin (Saskatchewan, Canada): Implications for the formation of unconformity-related uranium deposits; *Mineralium Deposita*, **35**, 791-795.

Hiatt, E.E., Kyser, T.K. & Dalrymple, R.W. (2003): Relationships among sedimentology, stratigraphy and diagenesis in the Proterozoic Thelon Basin, Nunavut, Canada: implications for paleo-aquifers and sedimentary-hosted mineral deposits; *Journal of Geochemical Exploration*, **80**, 221-240.

Hiatt, E.E., Palmer, S.E., Kyser, T.K. & O'Connor, T.K. (2010): Basin evolution, diagenesis and uranium mineralization in the Paleoproterozoic Thelon Basin, Nunavut, Canada; *Basin Research*, **22**, 302-323.

Hoeve, J. & Quirt, D. (1984): Mineralization and host rock alteration in relation to clay mineral diagenesis and evolution of the Middle-Proterozoic, Athabasca Basin northern Saskatchewan, Canada; *Saskatchewan Research Council*, Technical Report 187, 187 p.

Hoeve J. & Sibbald, T.I. (1978): On the genesis of Rabbit Lake and other unconformity-type uranium deposits in northern Saskatchewan, Canada; *Economic Geology*, **73**, 1450-1473.

Hoeve, J., Sibbald, T.I.I., Ramaekers, P. & Lewry, J.F. (1980): Athabasca Basin unconformity-type uranium deposits: A special class of sandstone-type deposits. In: Ferguson, J. & Goleby, A.B. (eds), Uranium in the Pine Creek geosyncline; Proceedings of International Uranium Symposium on the Pine Creek Geosyncline, Sydney, Australia. International Atomic Energy Agency, Vienna, 575-594.

Hoffman, P.F. (1988): United plates of America, the birth of a carton: Early Proterozoic assembly and growth of Laurentia; *Annual Review of Earth and Planetary Sciences*, **16**, 543-603.

Hoffman, J. & Hower. J. (1979): Clay mineral assemblages as low-grade metamorphic geothermometer: Application to the thrust faulted disturbed belt of Montana. In: Aspects of Diagenesis, P. A. Scholle & P. S. Schluger, (eds); SEPM Special Publication 26, 55-79.

Holk, G.J., Kyser, T.K., Chipley, D., Hiatt, E.E. & Marlatt, J. (2003): Mobile Pb-isotopes in Proterozoic sedimentary basins as guides for exploration of uranium deposits; *Journal of Geochemical Exploration*, **80**, 297-320.

Holliger, P. (1988): Ages U/Pb defines in situ sur oxides d'uranium a l'analyseur ionique: methodologie et consequences geochimiques; *Comptes rendus de l'Académie des Sciences Paris,* **307**, 367–373.

Holliger, P. (1991): SIMS isotope analyses of U and Pb in uranium oxides: geological and nuclear applications; *8th International SIMS Conference Program*, 719-722.

Hower, J., Eslinger, E.V., Hower, M.E. & Perry E.A. (1976): Mechanism of burial metamorphism of argillaceous sediments: I. Mineralogical and chemical evidence; *Geological Society of America Bulletin*, **87**, 725-737.

Jaireth S. (1992): Hydrothermal transport of platinum and gold in the unconformity-related uranium deposits, a preliminary thermodynamic investigation; *Mineralium Deposita*, **27**, 42–54.

Janeczek, J. & Ewing, R.C. (1995): Mechanisms of Lead Release from Uraninite in Natural Fission Reactors in Gabon; *Geochimica et Cosmochimica Acta*, **59**, 1917– 1931.

Jefferson, C.W., Thomas, D.J., Gandhi, S.S., Ramaekers, P., Delaney, G., Brisbin, D., Cutts, C., Quirt, D., Portella, P., and Olson, R.A. (2007a) Unconformity-associated uranium deposits of the Athabasca Basin, Saskatchewan and Alberta, *in* Goodfellow, W.D., ed., Mineral Deposits of Canada: A Synthesis of Major Deposit-Types, District Metallogeny, the Evolution of Geological Provinces, and Exploration Methods; *Geological Association of Canada, Mineral Deposits Division*, Special Publication No. 5, 273-305.

Jefferson, C.J., Thomas, D., Quirt, D.H., Mwenifumbo, C.J., and Brisbin, D. (2007b) Empirical models for unconformity-associated uranium deposits. In: "Proceedings of Exploration 07: Fifth Decennial International Conference on Mineral Exploration", edited by B. Milkereit, p. 741-769.

Jefferson, C.W., Chorlton. L.B., Pehrsson, S.J., Peterson, T.D.,. Wollenberg, P., Scott, J., Tschirhart, V., McEwan, B., Bethune, K., Calhoun, L., White, J.C., Leblon, B. LaRocque, A. Shelat, Y., Lentz, D., Patterson, J., Riegler, T., Skulski, T., Robinson, S., Paulen, R., McClenaghan, M.B., Layton-Matthews, D., MacIsaac, D., Riemer, W., Stieber, C., and Tschirhart, P. (2011): Northeast Thelon Region: Geomapping for Uranium in Nunavut; Geological Survey of Canada, Open File 6962, 1 CD-ROM. doi:10.4095/289037.

Jefferson, C.W., Pehrsson, S., Peterson, T., Wollenberg, P., Tschirhart, V., Riegler, T., McEwan, B., Tschirhart, P., Scott, J., Chorlton, L., Davis, W., Bethune, K., Riemer, W., Patterson, J., and Stieber, C (in prep.): Bedrock geology of the western Tehek-Marjorie supracrustal belt and Northeast Thelon Basin margin in parts of NTS 66A and 66B, Nunavut; Geological Survey of Canada, Open File.

Johnston J.D. & Wall V.J. (1984): Why unconformity-related U deposits are unconformity related; Geological Society of Australia, Abstracts 12, 285–287.

Knipping, H.D. (1974): The concepts of supergene versus hypogene emplacement of uranium at Rabbit Lake, Saskatchewan, Canada; *Canadian Institute of Minning and Metallurgy*, Bulletin 73, **818**, 84-90.

Komninou A. & Sverjensky D.A. (1996): Geochemical modeling of the formation of an unconformity type uranium deposit; *Economic Geology*, **91**, 590–606.

Kotzer, T.G. & Kyser, T.K. (1990): Fluid history of the Athabasca Basin and its relation to uranium deposits; *in* Summary of Investigations 1990, Saskatchewan Energy and Mines, *Saskatchewan Geological Survey*, Miscellaneous Report, 90-4, 153-157.

Kotzer, T.G. & Kyser, T.K. (1992): Isotopic, mineralogic and chemical evidence for multiple episodes of fluid movement during prograde and retrograde diagenesis in a Proterozoic Basin; *Proceedings of the 7th International Symposium on Water-Rock Interaction*, Park City, Utah, July 13-18, 1177-1181.

Kotzer, T.G. & Kyser, T.K. (1993): O, U, and Pb isotopic and chemical variations in uraninite: Implications for determining the temporal and fluid history of ancient terrains; *American Mineralogist*, **78**, 1262-1274.

Kotzer, T.G. & Kyser, T.K. (1995): Petrogenesis of the Proterozoic Athabasca Basin, northern Saskatchewan, Canada, and its relation to diagenesis, hydrothermal uranium mineralization and paleohydrogeology; *Chemical Geology*, **120**, 45-89.

Kyser, T.K. (2007): Fluids, basin analysis and mineral deposits; *Geofluids*, **7**, 238-257.

Kyser, T.K, Wilson, M.R. & Rutherman, G. (1989): Stable isotope constraints on the role of graphite in the genesis of unconformity-type uranium deposits; *Canadian Journal of Earth Sciences*, **26**, 490-498.

Kyser, T.K., Kotzer, T. & Sibbald, T.I.I. (1990) Oxygen, U-Pb and Pb-Pb isotope systematics in uraninite from complex U-Au-PGE vein-type and unconformity-type uranium deposits in northern Saskatchewan; *in* Summary of Investigations 1990, Saskatchewan Energy and Mines, *Saskatchewan Geological Survey*, Miscellaneous Report, 90-4, 64-69.

Kyser, K., Hiatt, E., Renac, C., Durocher, K., Holk, G., & Deckart, K. (2000): Diagenetic fluids in Paleo- and Mesoproterozoic sedimentary basins and their implications for long protracted fluid histories, Chapter 10 in Kyser, K., ed., Fluids and Basin Evolution, Short Course Series Volume 28 (Series editor Robert Raeside); *Mineralogical Association of Canada*, 225-262.

Landais, P., Dubessy, J., Dereppe, J. & Philp, R.P. (1993): Characterization of graphite alteration and bitumen genesis in the Cigar Lake deposits (Saskatchewan, Canada); *Canadian Journal of Earth Sciences*, **30**, 743-753.

LeCheminant, A.N., Miller, A.R., & LeCheminant, G.M. (1987): Early Proterozoic alkaline igneous rocks, District of Keewatin, Canada: petrogenesis and mineralization; *In*: Geochemistry and Mineralization of Proterozoic Volcanic Suites, T.C. Pharoah, R.D. Beckinsdale, Rickard D. (eds). Geological Society Special Publication 33, 219-240.

Leventhal, J.S., Grauch, R.I, Threlkeld, C.N., Liche, F.E. & Harper, C.T. (1987): Unusual organic matter associated with uranium from the Claude deposit, Cluff Lake, Canada*; Economic Geology*, **82**, 1169- 1176.

Lewry, J.F. & Sibbald, T.I.I. (1977): Variation in lithology and tectonometamorphic relationships in Precambrian basement of northern Saskatchewan; *Canadian Journal of Earth Sciences*, **14**, 1453-1477.

Ludwig, K. (1993): ISOPLOT, Excel Based Program for Plotting Radiogenic Isotopes; USGS, Open File Report, no. 91-445, 1-42.

Ludwig, K.R., Grauch, R.J., Nutt, C.J., Nash, J.T., Frishman, D. & Simmons, K.R. (1987): Age of uranium mineralization at the Jabiluka and Ranger deposits, Northern Territory, Australia: New U-Pb evidence; *Economic Geology*, **84**, 64-90.

Lyon, I.C., Saxton, J.M. & Turner, G. (1994): Isotopic fractionation in secondary ionization mass spectrometry; *Rapid Communications in Mass Spectrometry,* **8**, 837– 843.

Maas, R. (1989): Nd-Sr isotope constraints on the age and origin of unconformity-type uranium deposits in the Alligator Rivers Uranium Field, Northern Territory, Australia; *Economic Geology*, **82**, 857-875.

Macdonald, C. (1980): Mineralogy and geochemistry of a Precambrian regolith in the Athabasca Basin, M.Sc. Thesis, University of Saskatchewan, 151 p.

Martins-Neto, M.A. (2000): Tectonics and sedimentation in a Paleo-Mesoproterozoic rift-sag basin (Espinaço basin, southeastern Brazil); *Precambrian Research,* **103**, 147–173.

McCready, A.J., Annesley, I.R., Parnell, J. & Richardson, L.C. (1999): Uranium-bearing carbonaceous matter, McArthur River uranium deposit, Saskatchewan; *in* Summary of Investigations 1999, **2**, Saskatchewan Geological Survey, Sask. Energy & Mines, Misc. Report 99-4, 110-120.

McGill, B., Marlatt, J., Matthews, R., Sopuck, V., Homeniuk, L., & Hubregtse, J., 1993, The P2 North uranium deposit Saskatchewan, Canada; *Exploration Mining Geology*, **2**, 321-331.

McKay, A.D. & Miezitis, Y. (2001): Australia's uranium resources, geology and development of deposits; *AGSO-Geoscience Australia*, Mineral Resource Report 1, 184 p.

Mercadier, J., Cuney, M., Cathelineau, M. & Lacorde, M. (2011): U redox fronts and kaolinisation in basement-hosted unconformity-related U ores of the Athabasca Basin (Canada): late remobilization by meteoric fluids; *Mineralium Deposita*, **46**, 105-135.

Mernagh, T.P., Heinrich, C.A., Leckie, J.F., Carville, D.P., Gilbert, D.J., Valenta, R.K. & Wyborn, L.A.I. (1994): Chemistry of low temperature hydrothermal gold, platinum, and palladium (±uranium) mineralization at Coronation Hill, Northern Territory, Australia; *Economic Geology*, **89**, 1053-1073.

Mernagh, T.P., Wyborn, L.A.I. & Jagodzinski, E.A. (1998): Unconformity-related U ± Au ± platinum-group-element deposits; *Journal of Australian Geology & Geophysics*, **17**, 197-205.

Miller, A.R. (1995): Polymetallic unconformity-related uranium veins in lower Proterozoic Amer group, Pelly Lake map area, northern Thelon Basin, Churchill Province, Northwest Territories. *In Current Research 1995-C; Geological Survey of Canada*. 151–161.

Miller, A.R. & LeCheminant, A.N. (1985): Geology and uranium metallogeny of Proterozoic supracrustal successions, central District of Keewatin, N.W.T. with comparisons to northern Saskatchewan; *In*: Geology of uranium deposits. *Edited by* T.I.I. Sibbald and W. Petruk. Canadian Institute of Mining and Metallurgy, Special Vol. 32, 167-185.

Miller, A.R., Cumming, G., & Krstic, D. (1989): U-Pb, Pb-Pb and K-Ar isotopic study and petrography of uraniferous phosphate bearing rocks in the Thelon Formation, Dubawnt Group, Northwest Territories, Canada; *Canadian Journal of Earth Sciences*, **26**, 867-880.

Needham R.S. (1988): Geology of the Alligator Rivers Uranium Field, Northern Territory; Bureau of Mineral Resources, Australia; Bulletin 224.

Needham R.S., Stuart-Smith P.G. & Page R.W. (1988): Tectonic evolution of the Pine Creek Inlier, Northern Territory; *Precambrian Research*, **40/41**, 543–564.

Nutt, C.J. (1989): Chloritization and associated alteration at the Jabiluka unconformity-type uranium deposit, Northern Territory, Australia; *Canadian Mineralogist*, **27**, 41-58.

Orrell, S.E., Bickford, M.E., & Lewry, J.F. (1999): Crustal evolution and age of thermotectonic reworking in the western hinterland of Trans-Hudson Orogen, northern Saskatchewan; *Precambrian Research*, **95**, 187-223.

Pagel, M. (1975): Détermination des conditions physico-chimiques de la silicification diagénétique des grès Athabasca (Canada) au moyen des inclusions fluids; *Académie des Sciences Paris*, **280**, Comptes Rendus, Série D, 2301-2304.

Pagel, M., Poty, B. & Sheppard, S.M.F. (1980): Contributions to some Saskatchewan uranium deposits mainly from fluid inclusion and isotopic data, in Ferguson, S., and Goleby, A., eds., Uranium in the Pine Creek Geosyncline: *International Atomic Energy Agency (IAEA)*, 639-654.

Pehrsson, S., Jefferson, C.W., Peterson, T., Scott, J., Chorlton, L., & Hillary, B. (2010): Basement to the Thelon Basin, Nunavut – Revisited. *Geoscience Canada 2010 [Abstract]*. May 10th-14th, 2010.

Peterson, T.D. (2006): Geology of the Dubawnt Lake area, Nunavut-Northwest Territories; Geological Survey of Canada, Bulletin 580, 51 p.

Peterson, T.D., & Van Breemen, O. (1999): Review and progress report of Proterozoic granitoid rocks of the western Churchill Province, Northwest Territories (Nunavut); Current Research 1999-C; Geological Survey of Canada, 119-127

Peterson, T.D., Scott, J.M.J., Jefferson, C.W. & Tschirhart, V. (2012): Regional potassic alteration corridors spatially related to the 1750 Ma Nueltin Suite in the northeast Thelon Basin region, Nunavut – guides to uranium, gold and silver?; *GAC-MAC 2012 [Abstract]*. May 27-29, 2012.

Peterson, T.D., Van Breemen, O., Sandeman, H., & Cousens, B. (2002): Proterozoic (1.85-1.75Ga) igneous suites of the Western Churchill Province: granitoid and ultrapotassic magmatism in a reworked Archean hinterland; Precambrian Research, **119**, 73-100.

Polito, P.A., Kyser, T.K., Marlatt, J., Alexandre, P., Bajwah, Z., & Drever, G. (2004): Significance of alteration assemblages for the origin and evolution of the Proterozoic Nabarlek unconformity-related uranium deposit, Northern Territory, Australia; *Economic Geology*, **99**, 111–139.

Polito, P.A, Kyser, T.K., Thomas, D., Marlatt, J. & Drever, G. (2005): Re-evaluation of the petrogenesis of the Proterozoic Jabiluka unconformity-related uranium deposit, Northern Territory, Australia; *Mineralium Deposita*, **40**, 257-288.

Polito, P.A., Kyser, T.K., Southgate, P.N. & Jackson, M.J. (2006): Sandstone diagenesis and aquifer evolution in the Mt Isa Basin: the isotopic and fluid inclusion history of fluid flow in the Mt Isa Basin; *Economic Geology*, **101**, 1159-1188.

Polito, P.A., Kyser, T.K., Alexandre, P., Hiatt, E.E. & Stanley, C.R. (2011): Advances in understanding the Kombolgie Subgroup and unconformity-related uranium deposits in the Alligator River Uranium Field and how to explore for them using lithogeochemical principles; *Australian Journal of Earth Sciences*, **58**, 453-474.

Powell, C.M., Li, Z.X., McElhinny, M.W., Meert, J.G. & Park, J.K. (1993): Paleomagnetic constraints on tioming of the Neoproterozoic breakup of Rodinia and the Cambrian formation of Gondwana; *Geology*, **21**, 889-892.

Quirt, D.H. (1989): Host-rock alteration at Eagle Point South; *Saskatchewan Research Council*, Publication No. R-855-1-E-89, 95 p.

Quirt, D.H. (2001): Kaolinite and dickite in the Athabasca sandstone, northern Saskatchewan, Canada; *Saskatchewan Research Council*, Publication No. 10400-16D01, 27 p.

Quirt, D.H. (2003): Athabasca unconformity-type uranium deposits: One deposit type with many variations. In: Uranium Geochemistry (Cuney, M., ed.), International Conference Proceedings, Nancy 2003, 309-312.

Quirt, D.H. (2011): The Kiggavik uranium deposits; AREVA Resources Canada Inc. Power point presentation, March 2011.

Rainbird, R.H. & Davis, W.J. (2007): U-Pb detrital zircon geochronology and provenance of the late Paleoproterozoic Dubawnt Supergroup: linking sedimentation with tectonic reworking of the western Churchill Province, Canada; *Geological Society of America Bulletin,* **119**, 314-328.

Rainbird, R.H., Hadlari, T., Aspler, L.B, Donaldson, J.A., LeCheminant, A.N., & Peterson, T. D. (2003): Sequence stratigraphy and evolution of the Paleoproterozoic intracontinental Baker Lake and Thelon basins, western Churchill Province, Nunavut, Canada; *Precambrian Research*, **125**, 21-53.

Rainbird, R.H., Stern, R.A., Rayner, N., & Jefferson, C.W. (2007): Age, provenance, and regional correlation of the Athabasca Group, Saskatchewan and Alberta, constrained by igneous and detrital zircon geochronology, in Jefferson, C.W., and Delaney, G., eds., EXTECH IV: Geology and Uranium EXploration TECHnology of the Proterozoic Athabasca Basin, Saskatchewan and Alberta: Geological Survey of Canada, Bulletin 588, (also Geological Association of Canada, Mineral Deposits Division, Special Publication 4; Saskatchewan Geological Society, Special Publication 18), 193-210.

Rainbird, R.H., Davis, W.J., Pehrsson, S.J., Wodicka, N., Rayner, N. & Skulski, T. (2010): Early Paleoproterozoic supracrustal assemblages of the Rae domain, Nunavut, Canada: Intracratonic basin development during supercontinent break-up and assembly; *Precambrian Research*, **181**, 167-186.

Ramaekers, P. (2004): Development, Stratigraphy and Summary Diagenetic History of the Athabasca Basin, Early Proterozoic of Alberta and Its Relation to Uranium Potential; Alberta Geological Survey, Alberta Energy and Utilities Board, Special Report 62 (PDF), 85 p.

Ramaekers, P., Jefferson, C.W., Yeo, G.M., Collier, B., Long, D.G.F., Catuneanu, O., Bernier, S., Kupsch, B., Post, R., Drever, G., McHardy, S., Jiricka, D., Cutts, C., & Wheatley, K. (2007): Revised geological map and stratigraphy of the Athabasca Group, Saskatchewan and Alberta, in Jefferson, C.W., and Delaney, G., eds., EXTECH IV: Geology and Uranium EXploration TECHnology of the Proterozoic Athabasca Basin, Saskatchewan and Alberta; Geological Survey of Canada, Bulletin 588, (also Geological Association of Canada, Mineral Deposits Division, Special Publication 4; Saskatchewan Geological Society, Special Publication 18) p. 155-192.

Rawlings, D.J. & Page, R.W. (1999): Geology, geochronology and emplacement structures associated with the Jimbu Microgranite, McArthur Basin, northern Australia; *Australian Journal of Earth Sciences*, **46**, 703-723.

Renac, C., Kyser, T.K., Durocher, K., Dreaver, G. & O'Connor, T. (2002): Comparison of diagenetic fluids in the Proterozoic Thelon and Athabasca Basins, Canada: Implications for protracted fluid histories in stable intracratonic basins; *Canadian Journal of Earth Sciences*, **39**, 113-132.

Riciputi, L.R., Paterson, B.A. & Ripperdan R.L. (1998): Measurement of light stable isotope ratios by SIMS: Matrix effects for oxygen, carbon, and sulfur isotopes in minerals; *International Journal of Mass Spectrometry*, **178**, 81-112.

Rivers, T. (2008): Assembly and preservation of lower, mid, and upper orogenic crust in the Grenville Province – Implications for the evolution of large hot long-duration orogens; *Precambrian Research*, **167**, 237-259.

Romberger, S.B. (1984): Transport and deposition of uranium in hydrothermal systems at temperatures up to 300°C: geological implications; *in* Uranium geochemistry, mineralogy, geology, exploration and resources, De Vivo, B., Ippolito, F., Capaldi, G. and Simpson, P.R. (eds), *The Institution of Mining and Metallurgy,* 201 p.

Röper, M. (1983) Fischer-Tropsch synthesis; *Catalysis by Metal Complexes*, **4**, 41-88.

Ross, G.M., Milkereit, B., Eaton, D., White, D., Kanasewich, R.E. & Burianyk, M.J.A. (1995) Paleoproterozoic collisional orogen beneath the western Canada sedimentary basin imaged by Lithoprobe crustal seismic-reflection data; *Geology*, **23**, 195-199.

Ruzicka V. (1975): Some metallogenic features of the 'D' uranium deposit at Cluff Lake, Saskatchewan; Geological Survey of Canada, Paper 75-1C: 279–283.

Ruzicka V. (1993): Unconformity-associated uranium deposits. In: Mineral Deposit Modeling (Kirkham R.V., Sinclair W.D., Thorpe R.I. & Duke J.M.); Geological Association of Canada, Special Paper 40: 125–149.

Sanborn-Barrie, M., Carr, R. & Thériault, R. (2001): Geochonological contraints on metamorphism, magmatism and exhumation of deep-crustal rocks of the Kramanituar Complex, with implications for the Paleoproterozoic evolution of the Archean western Chruchill Province, Canada; *Contributions to Mineralogy and Petrology,* **141**, 592-612.

Sangely, L., Chaussidon, M., Michels, R., Brouand, M., Cuney, M., Hualut, V. & Landais, P. (2007): Micrometer scale carbon isotopic study of bitumen associated with Athabasca uranium deposits: Constraints on the genetic relationship with petroleum source-rocks and the abiogenic origin hypothesis; *Earth and Planetary Science Letters*, **258**, 378-396.

Scott, J.M.J, Davis, W.J., Peterson, T.D. & Jefferson, C.W. (2011): U-Pb Shrimp geochronology of the Paleoproterozoic granite in the Kiggavik area of the northeast Thelon Basin, Nunavut; *Geological Association of Canada - Mineralogical Association of Canada, joint annual meeting 2011, Ottawa*, 198-199.

Selley, R.C. (1998): Elements of petroleum geology; 2nd Edition, *Academic Press Ltd*, London, England, 470 p.

Sharp, Z (2007): Principles of stable isotope geochemistry; 1st Edition, Pearson Education Inc., Upper Saddle River, NJ, 344 p.

Shawe, D.R. & Granger, H.C. (1965): Uranium ore rolls: an analysis; *Economic Geology*, **60**, 240-250.

Sheppard, S.M.F. (1986): Characterization and isotopic variations in natural waters; *Reviews in Mineralogy and Geochemistry*, **16**, 165-183.

Sheppard, S.M.F. & Gilg, H.A. (1996): Characterization and isotopic variations in natural waters; *Reviews in Mineralogy and Geochemistry*, **16**, 165-183.

Shrestha, B. (2010): Kiggavik Project Annual Report 2009 Field Season; *Internal Report*, AREVA Resources Canada Inc.

Shimizu, N. & Hart, S.R. (1982): Applications of the ion-microprobe to geochemistry and cosmochemistry; *Annual Review of Earth and Planetary Science*, **10**, 483-526.

Shroeer, J.M., Rhodin, T.N. & Bradley, R.C. (1973): A Quantum-mechanical model for the ionization and excitation of atoms during sputtering; *Surface Science*, **34**, 571– 580.

Sibbald, T.I.I. (1985): Geology and genesis of the Athabasca uranium deposits, *in* Summary of Investigations 1985; *Saskatchewan Geological Survey*, Miscellaneous Report 85-4, 45 p.

Sibbald, T.I.I. & Quirt, D. (1987): Uranium deposits of the Athabasca Basin; Saskatchewan Research Council, Publication #R-855-5G-87, 72 p.

Sibbald, T.I.I., Munday, R.J.C. & Lewry, J.F. (1977): The geological setting of uranium mineralization in northern Saskatchewan, *in* Dunn, C.E. (ed.), Uranium in Saskatchewan; *Geological Society of Saskatchewan*, Special Publication 3, 51-98.

Sigmund, P. (1969): Theory of sputtering. I. Sputtering yield of amorphous and polycrystalline targets; *Physical Review*, **184**, 386-416.

Solomon M. & Groves D.I. (1994): The geology and origin of Australia's mineral deposits; Clarendon Press, Oxford, 951 p.

Stern, R.A., Syme, E.C. & Lucas, S.B. (1995): Geochemistry of 1.9 Ga MORB- and OIB-like basalts from the Amisk collage, Flin Flon belt, Canada: evidence for an intra-oceanic origin; *Geochemicia et Cosmochimica Acta,* **59**, 3131-3154.

Tirrul, R. & Grotzinger, J.P. (1990): Early Proterozoic collisional orogeny along the northern Thelon Tectonic Zone, North- west Territories, Canada: evidence from the foreland; *Tectonics,* **9**, 1015-1036.

Turner, W.A., Heaman, L.M., & Creaser, R.A. (2003): Sm-Nd fluorite dating of Proterozoic low-sulfidation epithermal Au-Ag deposits and U-Pb zircon dating of host rocks at Mallery Lake, Nunavut, Canada; Canadian Journal of Earth Sciences, **40**, 1789-1804.

Velde, B. (1977): A proposed phase diagram for illite, expanding chlorite, corrensite and illite-montmorillonite mixed layer minerals; *Clays and Clay Minerals*, **25**, 264-270.

Wallis, R.H., Saracoglu, N., Brummer, J.J., & Golighty, J.P. (1983); The geology of the McClean Lake uranium deposits, northern Saskatchewan; *Geological Survey of Canada*, Paper 82–11, 71–110.

Weyer, H.J., Friedrich, G., Bechtel, A., & Ballhorn, R.K. (1987): The Lone Gull uranium deposit: New geochemical and petrological data as evidence for the nature of the ore bearing solutions; In: IAEA-TC542/19, 293-306.

Wilde A.R., Bloom M.S. & Wall V.J. (1989): Transport and deposition of gold, uranium, and platinum-group elements in unconformity-related uranium deposits; *Economic Geology*, **6**, 637–650.

Wilson A. D. (1955) Determination of ferrous iron in rocks and minerals; Bulletin of the Geological Survey of Great Britain. **9**, 56**–**58.

Wilson, M.R. & Kyser, T.K. (1987): Stable isotope geochemistry of alteration associated with the Key Lake uranium deposit, Canada; *Economic Geology*, **82**, 1540-1557.

Wilson, N.S.F., Stasiuk, L.D. & Fowler, M.G. (2007): Origin of organic matter in the Proterozoic Athabasca Basin of Saskatchewan and Alberta, and significance to unconformity uranium deposits; *In* Jefferson, C.W. and Delaney, G. (eds.), EXTECH IV: Geology and Uranium Exploration TECHnology of the Proterozoic Athabasca Basin, Saskatchewan and Alberta, Geological Survey of Canada, Bulliten 588/Sask. Geological Society Special Publication No. 18/Mineral Deposits Division (GAC), Special Publication 4, 325-346.

World Nuclear Association (WNA) (2011): The global nuclear fuel market: Supply and demand 2011-2030; *World Nuclear Association Biennial Report*, 196 p.

Yu, M.L. & Lang, N. (1986): Mechanisms of atomic ion emission during sputtering; *Nuclear Instruments and Methods in Physics*, **B14**, 403– 413.

Zaleski, E., Davis, W.J. & Wilkinson, L. (2000): Basement/cover relationships, unconformities and depositional cycles of the Woodburn Lake group, western Churchill Province Nunavut. *Yellowknife Geoscience Forum*, November 2000.

Appendix A
Drill-Core and Thin-Section Sample Descriptions

Table A.1: Drill hole ID and depth for drill-core and thin-section samples taken from the Bong Deposit, Thelon Basin, Nunavut, Canada

Sample	Drill Hole	Depth (m)	Sample	Drill Hole	Depth (m)
RS-11-017	Bong-49	143.0	RS-11-148	Bong-42	443.2
RS-11-130	Bong-49	137.5	RS-11-149	Bong-42	446.1
RS-11-033	Bong-49	163.5	RS-11-150	Bong-42	448.3
RS-11-036	Bong-49	193.0	RS-11-155	Bong-37	248.5
RS-11-055	Bong-49	387.0	RS-11-156	Bong-37	241.5
RS-11-058	Bong-49	413.0	RS-11-158	Bong-37	261.5
RS-11-067	Bong-49	209.8	RS-11-160	Bong-50	267.6
RS-11-069	Bong-49	311.0	RS-11-162	Bong-50	292.2
RS-11-072	Bong-49	365.8	RS-11-168	Bong-43	292.0
RS-11-076	Bong-49	430.9	RS-11-170	Bong-43	361.0
RS-11-107	Bong-42	45.5	RS-11-172	Bong-39	413.8
RS-11-121	Bong-42	319.0	RS-11-173	Bong-39	429.1
RS-11-139	Bong-42	331.0	RS-11-176	Bong-36	360.1
RS-11-140	Bong-42	349.2	RS-11-179	Bong-24	233.0
RS-11-142	Bong-42	418.3	RS-11-191	Bong-43	356.6
RS-11-143	Bong-42	414.9	RS-11-192	Bong-50	263.7
RS-11-144	Bong-42	430.9	301GC*	Bong-36	391.0
RS-11-145	Bong-42	425.1	302GC*	Bong-36	410.0
RS-11-147	Bong-42	442.5	303GC*	Bong-42	413.0

* Sampled by D. Quirt in 2009

Table A.2: Drill-core sample descriptions from the Bong Deposit, Thelon Basin, Nunavut, Canada

Sample	Mineralogy		Alteration	Structure	Comments
	Mineral	Percent			
RS-11-017	Quartz	35-45%	Chloritized	Quartz veinlets	Unaltered
	Feldspar	20-30%		~1 mm wide	Woodburn
	Chlorite	10-15%		Foliated	
RS-11-033	Quartz	30-40%	Chloritized	Foliated	Garnet-bearing
	Feldspar	15-25%			horizon
	Chlorite	10-15%			
	Garnet	3-5%			
	Biotite	3-5%			
RS-11-036	Quartz	35-45%	Chloritized	Quartz vein ~1 cm wide	
	Feldspar	20-30%			
	Chlorite	10-15%		Foliated	
RS-11-055	Quartz	35-45%	Chloritized	Foliated	Silicified Woodburn
	Feldspar	20-30%			
	Chlorite	10-15%			
RS-11-067	Quartz	60-70%	Chloritized	Brecciated at	
	Feldspar	10-20%		a high angle	
	Chlorite	5-10%		Foliated	
RS-11-069	Quartz	35-45%	Chloritized	Quartz veinets	
	Feldspar	20-30%		0.1-0.2 mm wide	
	Chlorite	10-15%		Foliated	

Table A.2: Drill-core sample descriptions from the Bong Deposit, Thelon Basin, Nunavut, Canada

Sample	Mineralogy		Alteration	Structure	Comments
	Mineral	Percent			
RS-11-121	Clay	100%	Bleached	Foliated	Despite high degree of alteration, foliation is still visible
RS-11-140	Quartz Hematite Chlorite	40-50% 20-30% 10-20%	Hematized		Hematized Woodburn
RS-11-142	Clay Uraninite Hematite	50-60% 10-20% 10-20%	1) Bleached 2) Hematized	Massive	Roll-front uraninite
RS-11-143	Clay Uraninite Chlorite	80-90% 1-5% 1-5%	Chloritized	Foliated	Vein-type uraninite
RS-11-145	Clay Uraninite Hematite	80-90% 1-5% 1-5%	1) Bleached 2) Hematized	Massive	Roll-front uraninite
RS-11-147	Clay	100%	Bleached	Foliated	Despite high degree of alteration, foliation is still visible
RS-11-148	Clay Quartz Chlorite	60-70% 10-20% 5-10%	1) Chloritized 2) Bleached	High angle quartz veins, 6 mm wide Foliated	Moderately altered

Table A.2: Drill-core sample descriptions from the Bong Deposit, Thelon Basin, Nunavut, Canada

Sample	Mineralogy		Alteration	Structure	Comments
	Mineral	**Percent**			
RS-11-149	Clay	30-40%	1) Chloritized	High angle quartz	Weakly
	Quartz	15-25%		vein, 1 cm wide	altered
	Chlorite	15-20%	2) Bleached		
	Feldspar	10-15%		Foliated	
RS-11-150	Quartz	40-50%	Chloritized	Quartz + carbonate	Unaltered
	Feldspar	20-30%		veinlets, 1 mm wide	Woodburn
	Chlorite	10-20%		Foliated	
RS-11-155	Clay	80-90%	Bleached	2 cm wide vug filled	Highly
	Quartz	5-10%		with drusy quartz	altered
				Quartz crystals up to	
				8 mm long	
				Foliated	
RS-11-156	Clay	30-40%	1) Bleached	Massive	Barren roll-front
	Hematite	35-45%			
	Goethite	10-15%	2) Hematized		
RS-11-162	Clay	60-70%	1) Bleached	Massive	Roll-front
	Uraninite	10-15%			uraninite
	Hematite	10-15%	2) Hematized		

Table A.2: Drill-core sample descriptions from the Bong Deposit, Thelon Basin, Nunavut, Canada

Sample	Mineralogy		Alteration	Structure	Comments
	Mineral	Percent			
RS-11-168	Clay	65-75%	1) Bleached	Foliated	Garnet outlines
	Muscovite	10-15%			still visible
	Quartz	5-10%			
RS-11-172	Clay	75-85%	1) Bleached	Foliated	Vein-type
	Uraninite	5-10%			uraninite
	Chlorite	1-5%	2) Chloritized		
RS-11-176	Clay	65-75%	1) Bleached	Massive	Roll-front
	Hematite	10-20%			uraninite
	Uraninite	1-5%	2) Hematized		
RS-11-191	Clay	70-80%	1) Bleached	Massive	Roll-front
	Uraninite	5-10%			uraninite
	Hematite	5-10%	2) Hematized		
RS-11-192	Clay	60-70%	1) Bleached	Foliated	Graphite horizon
	Graphite	20-30%			
302GC*	Clay	65-75%	1) Bleached	Carbon nodules	Uraninite filling
	Graphite	10-15%		up to 1.5 cm wide	fractures and
	Uraninite	3-5%	2) Chloritized		coating nodules
	Chlorite	3-5%			

* Sampled by D. Quirt in 2009

Table A.3: Thin-section descriptions from the Bong Deposit, Thelon Basin, Nunavut, Canada

Sample	Mineralogy			Alteration	Structure	Comments
	Mineral	Size	Crystal Characteristics			
RS-11-030	45-55% Quartz	0.1-0.4 mm	Subrounded-rounded	1) Minor chloritization of muscovite	Quartz + Carbonate veins up to 2 mm wide	Rock is silicified
	10-20% Muscovite	0.05-0.2 mm	Tabular			
	10-15% K-feldspar	0.1-0.2 mm	Subrounded-rounded			
	3-5% Chlorite	0.1-0.2 mm	Tabular	2) Seritization of muscovite + K-spar		
	1-5% Sericite	<0.01 mm	Tabular		Muscovite foliated	
	Accessories: pyrite rutile, apatite, zircon					
RS-11-058	35-45% Biotite	0.1-2 mm	Tabular	1) Chloritization of muscovite & biotite	Small pyrite veins >1 mm wide	Locally biotite-rich garnet-bearing horizon
	10-15% Muscovite	0.1-1 mm	Tabular			
	5-10% Quartz	0.05-0.4 mm	Subrounded-rounded			
	3-5% K-feldspar	0.1-0.2 mm	Subrounded-rounded	2) Sericitization of muscovite, biotite, K-spar & plag	Quartz veins ~0.5 mm wide	
	5-10% Chlorite	0.1-1 mm	Tabular			
	8-10% Sericite	<0.01 mm	Tabular			
	1-2% Pyrite	0.05 mm	Subhedral		Muscovite foliated	
	1% Garnet	up to 2 mm	Euhedral			
	1% Plagioclase	0.1-0.5 mm	Tabular			
	Accessories: apatite					
RS-11-067	90-95% Quartz	0.1-0.4 mm	Subrounded-rounded	1) Sericitization of plagioclase	Quartz vein 1 cm wide	Rock is silicified
	1-3% Chlorite	0.1-0.2 mm	Tabular			
	1% Plagioclase	0.1-0.3 mm	Tabular			
	1% Sericite	<0.01 mm	Tabular			
	Trace pyrite	0.05 mm	Euhedral			

Table A.3: Thin-section descriptions from the Bong Deposit, Thelon Basin, Nunavut, Canada

Sample	Mineralogy			Alteration	Structure	Comments
	Mineral	Size	Crystal Characteristics			
RS-11-072	50-60% Quartz	0.1-0.4 mm	Subrounded-rounded	1) Chloritization	Two generations of	
	10-20% K-feldspar	0.1-0.3 mm	Tabular	of muscovite	quartz veins:	
	5-10% Chlorite	0.1-0.2 mm	Tabular		1 cm wide and	
	1-5% Plagioclase	0.1-0.3 mm	Tabular	2) Sericitization of	0.7 mm wide	
	1-5% Sericite	<0.01 mm	Tabular	muscovite,		
	1-2% Muscovite	0.1-0.2 mm	Tabular	K-spar & plag	Late carbonate	
	1% Pyrite	0.1-0.2 mm	Anhedral		veins up to	
	Accessories: apatite				0.2 mm wide	
RS-11-076	30-40% Quartz	0.1-0.4 mm	Subrounded-rounded	1) Chloritization	Garnet	Garnet-bearing
	15-20% K-feldspar	0.1-0.3 mm	Tabular	of muscovite	porphyroblasts	horizon
	10-20% Muscovite	0.1-3 mm	Tabular			
	10-15% Biotite	0.1-0.2 mm	Tabular			
	1-5% Chlorite	0.1-3 mm	Tabular			
	2-3 % Garnet	0.5-1.5 cm	Euhedral			
	Accessories: apatite					
RS-11-107	30-40% Muscovite	0.2-0.6 mm	Tabular	1) Weak chloritization	Muscovite foliated	
	25-35% Quartz	0.1-0.5 mm	Subrounded-rounded			
	10-15% K-feldspar	0.1-0.3 mm	Subrounded-rounded	2) Hematite and illite		
	1-5% Illite	<0.01 mm	Tabular	areas appear to be		
	1-5% Hematite	0.01-0.02 mm	Equant	altered garnets		

Table A.3: Thin-section descriptions from the Bong Deposit, Thelon Basin, Nunavut, Canada

Sample	Mineralogy			Alteration	Structure	Comments
	Mineral	Size	Crystal Characteristics			
RS-11-139	45-55% Illite	<0.01 mm	Tabular	1) Illitization of muscovite	Massive	Muscovite is illitized but chlorite is not
	30-40% Quartz	0.1-0.2 mm	Subrounded-rounded			
	10-15% Chlorite	0.1-0.3 mm	Tabular			
	1% Muscovite	0.05-0.1 mm	Tabular			
	1% Pyrite	0.1 mm	Subhedral			
RS-11-140	35-45% Illite	<0.01 mm	Tabular	1) Weak chloritization of muscovite 2) Illitization of muscovite 3) Hematization	Veins of illite & rutile	Moderately altered
	25-35% Quartz	0.1-0.3 mm	Subrounded-rounded			
	5-10% Muscovite	0.1-0.2 mm	Tabular			
	5-10% Hematite	0.01-0.03 mm	Equant			
	1% Rutile	0.05-0.1 mm	Subhedral			
	1% Apatite	0.05-0.1 mm	Anhedral			
RS-11-142	70-80% Illite	<0.01 mm	Tabular	1) Illitization of muscovite	Massive	Highly altered Mineralized
	10-15% Uraninite	0.1-0.4 mm	Subhedral-anhedral			
	3-5% Muscovite	0.05-0.1 mm	Tabular			
	1% Rutile	0.1 mm	Subhedral			
	1% Pyrite	0.05-0.1 mm	Subhedral-euhedral			
RS-11-143	80-90% Illite	<0.01 mm	Tabular	1) Illitization	Massive	Highly altered Mineralized
	5-10% Uraninite	0-1-0.3 mm	Subhedral-anhedral			
	1% Pyrite	0.05-0.1 mm	Subhedral			
	1% Galena	0.1-0.15 mm	Anhedral			

Table A.3: Thin-section descriptions from the Bong Deposit, Thelon Basin, Nunavut, Canada

Sample	Mineralogy			Alteration	Structure	Comments
	Mineral	Size	Crystal Characteristics			
RS-11-144	40-50% Quartz	0.1-0.4 mm	Subrounded-rounded	1) Illitization	Two generations	Moderately
	20-30% Illite	<0.01 mm	Tabular		of calcite veins	altered
	5-10% Muscovite	0.05-0.1 mm	Tabular		(1 cm & 0.2 cm)	
	1-5% Coffinite	0.05-0.1 mm	Subhedral-anhedral			
	1-5% Calcite	0.1-0.4 mm	Subhedral-euhedral			
RS-11-147	90-95% Illite	<0.01 mm	Tabular	1) Illitization	Massive	Highly altered
	1-5% Quartz	0.1-0.3 mm	Subrounded-rounded			
	<1% Rutile	0.1-0.2 mm	Subhedral-anhedral			
	<1% Apatite	0.1-0.2 mm	Anhedral			
RS-11-148	50-60% Illite	<0.01 mm	Tabular	1) Illitization	Massive	Moderately
	30-40% Quartz	0.1-0.3 mm	Subrounded-rounded			altered
	<1% Rutile	0.1-0.2 mm	Subhedral-anhedral			
	<1% Apatite	0.1-0.2 mm	Anhedral			
RS-11-149	45-55% Quartz	0.1-0.3 mm	Subrounded-rounded	1) Illitization	Massive	Weakly altered
	30-40% Illite	<0.01 mm	Tabular			
	1-5% Muscovite	0.1-0.3 mm	Tabular			
	<1% Rutile	0.1-0.2 mm	Subhedral-anhedral			
	<1% Apatite	0.1-0.2 mm	Anhedral			

Table A.3: Thin-section descriptions from the Bong Deposit, Thelon Basin, Nunavut, Canada

Sample	Mineralogy			Alteration	Structure	Comments
	Mineral	Size	Crystal Characteristics			
RS-11-150	45-55% Quartz	0.1-0.4 mm	Subrounded-rounded	1) Minor chloritization	Muscovite foliated	Unaltered
	10-20% Muscovite	0.05-0.2 mm	Tabular	of muscovite		Woodburn
	10-15% K-feldspar	0.1-0.2 mm	Subrounded-rounded			
	3-5% Chlorite	0.1-0.2 mm	Tabular	2) Seritization of		
	1-5% Sericite	<0.01 mm	Tabular	muscovite + K-spar		
	Accessories: pyrite rutile, apatite, zircon					
RS-11-158	45-55% Quartz	0.1-0.4 mm	Subrounded-rounded	1) Minor chloritization	Muscovite Foliated	Weakly altered
	15-20% Illite	<0.01 mm	Tabular	of muscovite		
	5-10% Muscovite	0.05-0.2 mm	Tabular			
	3-5% Chlorite	0.01-0.03 mm	Tabular	2) Illitization		
	1-5% K-feldspar	0.1-0.2 mm	Subrounded-rounded			
	1-5% Carbonaceous Material	<0.01 mm	Equant (Disseminated)			
RS-11-160	75-80% Illite	<0.01 mm	Tabular	1) Illitization of	Massive	Highly altered
	3-5% Uraninite	0.1-0.2 mm	Anhedral	muscovite		
	1-5% Muscovite	0.1-0.2 mm	Tabular			Mineralized
	1-3% Carbonaceous Material	<0.01 mm	Equant (Disseminated)			
	1-2% Pyrite	0.05-0.1 mm	Subhedral			
	1% Galena	0.05-0.1 mm	Anhedral			

Table A.3: Thin-section descriptions from the Bong Deposit, Thelon Basin, Nunavut, Canada

Sample	Mineralogy			Alteration	Structure	Comments
	Mineral	Size	Crystal Characteristics			
RS-11-162	35-45% Illite	<0.01 mm	Tabular	1) Illitization of	Massive	Highly altered
	20-30% Quartz	0.1-0.3 mm	Subrounded-rounded	muscovite		
	10-15% Uraninite	0.05-0.1 mm	Anhedral			Mineralized
	1-5% Muscovite	0.1-0.2 mm	Tabular	2) Fracturing and		
	1-3% Carbonaceous Material	<0.01 mm	Equant (Disseminated)	alteration of uraninite		
	1-3% Rutile	0.05-0.1 mm	Anhedral			
	1-2% Apatite	0.05-0.15 mm	Anhedral			
	Trace Pyrite	0.1-0.2 mm	Subhedral			
RS-11-168	35-45% Illite	<0.01 mm	Tabular	1) Illitization of	Two generations of	
	10-20% Quartz	0.1-0.3 mm	Subrounded-rounded	muscovite	quartz veins:	
	10-15% Muscovite	0.1-0.3 mm	Tabular		2 mm wide and	
	10-15% Chlorite	0.1-0.3 mm	Tabular		0.6 mm wide	
	1-2% Apatite	0.05-0.1 mm	Anhedral			
	1% Pyrite	0.1-0.2 mm	Subhedral			
	Trace Rutile	0.05-0.1 mm	Anhedral			
RS-11-170	90-95% Illite	<0.01 mm	Tabular	1) Illitization	Two generations of	
	1-3% Pyrite	0.05-0.1 mm	Subhedral-anhedral		quartz veins:	
	1% Rutile	0.05-0.1 mm	Subhedral		0.7 mm wide and	
					0.5 mm wide	

Table A.3: Thin-section descriptions from the Bong Deposit, Thelon Basin, Nunavut, Canada

Sample	Mineralogy			Alteration	Structure	Comments
	Mineral	Size	Crystal Characteristics			
RS-11-172	60-70% Illite	<0.01 mm	Tabular	1) Illitization of	Muscovite foliated	
	10-15% Uraninite	0.05-0.1 mm	Subhedral-anhedral	muscovite		
	5-10% Muscovite	0.1-0.2 mm	Tabular			
	2-3% Pyrite	0.1 mm	Subhedral	2) Weak		
	1-2% Rutile	0.05-0.1 mm	Subhedral-anhedral	chloritization		
RS-11-173	90-95% Graphite	2 cm	Graphite Nodule			Mineralized
	1-3% Uraninite	0.05-0.1 mm	Subhedral-anhedral			graphite
	1-2% Coffinite	0.05-0.1 mm	Subhedral-anhedral			nodule
RS-11-176	40-50% Illite	<0.01 mm	Tabular	1) Illitization of	Roll-front	Mineralized
	10-20% Quartz	0.1-0.3 mm	Subrounded-rounded	muscovite		
	5-10% Muscovite	0.1-0.2 mm	Tabular			
	3-5% Hematite	0.02-0.04 mm	Equant	2) Hematization		
	3-5% Uraninite	0.01-0.03 mm	Disseminated			
	1-2% Rutile	0.05-0.1 mm	Subhedral			
	1% Pyrite	0.1-0.2 mm	Subhedral			
RS-11-179	45-55% Illite	<0.01 mm	Tabular	1) Illitization of	Brecciated:	Silicified
	30-40% Quartz	0.1-0.3 mm	Subrounded-rounded	muscovite	brecciation includes	
	1-3% Muscovite	0.1-0.2 mm	Tabular		pieces of illitized	
	1% Rutile	0.05-0.1 mm	Anhedral		rock	

Table A.3: Thin-section descriptions from the Bong Deposit, Thelon Basin, Nunavut, Canada

Sample	Mineralogy			Alteration	Structure	Comments
	Mineral	Size	Crystal Characteristics			
RS-11-191	40-50% Illite	<0.01 mm	Tabular	1) Illitization of	Roll-front	Mineralized
	10-25% Quartz	0.1-0.3 mm	Subrounded-rounded	muscovite		
	5-10% Hematite	0.1-0.2 mm	Tabular		Illite vein	
	3-5% Uraninite	0.02-0.04 mm	Equant	2) Hematization	(~0.2 mm)	
	1-5% Muscovite	0.01-0.03 mm	Disseminated			
	1-2% Rutile	0.05-0.1 mm	Subhedral			
	1% Pyrite	0.1-0.2 mm	Subhedral			
302GC*	50-60% Illite	<0.01 mm	Tabular	1) Illitization of	Massive	Carbon nodules
	10-20% Graphite	0.01 mm-2 cm	Nodules	muscovite		and fractures in
	10-15% Muscovite	0.1-0.3 mm	Tabular			nodules coated in
	1-2% Rutile	0.1-0.2 mm	Subhedral-anhedral			uraninite
	1% Apatite	0.05-0.1 mm	Anhedral			
	1% Pyrite	0.05-0.1 mm	Subhedral			Muscovite wrap
	Trace Galena	0.05 mm	Subhedral-anhedral			around nodules
301GC*	45-55% Illite	<0.01 mm	Tabular	1) Illitization of	Massive	Uraninite
	20-30% Muscovite	0.1-0.2 mm	Tabular	muscovite		associated with
	3-5% Uraninite	0.1-0.2 mm	Subhedral-anhedral			graphite
	1-5% Pyrite	0.05-0.1 mm	Subhedral			
	1-3 Rutile	0.05-0.1 mm	Subhedral-anhedral			Highly Altered
	1-2% Graphite	<0.01 mm	Equant (Disseminated)			
	1% Apatite	0.05-0.1 mm	Anhedral			Mineralized

*Sampled by D. Quirt in 2009

Table A.3: Thin-section descriptions from the Bong Deposit, Thelon Basin, Nunavut, Canada

Sample	Mineralogy			Alteration	Structure	Comments
	Mineral	Size	Crystal Characteristics			
303GC*	40-50% Illite	<0.01 mm	Tabular	1) Illitization of	Massive	Pyrite filling
	20-30% Muscovite	0.1-0.03 mm	Tabular	muscovite		fractures in
	5-10% Uraninite	0.1-0.2 mm	Anhedral			uraninite
	3-5% Graphite	<0.01 mm	Equant (Disseminated)	2) Weak		
	1-3% Pyrite	0.05-0.1 mm	Subhedral	chloritization		Uraninite assoc.
	1% Rutile	0.05-0.1 mm	Subhedral-anhedral			With graphite
	1% Apatite	0.05-0.1 mm	Anhedral			
	Trace Galena	0.05 mm	Subhedral-anhedral			

*Sampled by D. Quirt in 2009

Appendix B
Electron Probe Microanalysis (EPMA) and Standards

Table B.1: Elements and their respective standards for EMPA

Element	Standard
U	UO_2
Pb	PbTe
Si	Diopside
Al	Andalusite
K	Orthoclase
Ca	Diopside
Au	11-25C
Cl	Tugtuphite
Th	ThO_2
P	Apatite
S	Pyrite
F	Riebeckite
Fe	Pyrite
Mg	Olivine
Mn	Spessertine
Ni	Pentlandite
Cu	Chalcopyrite
As	Cobalt
Ag	11-25B
Ti	Sphene

Elements analysed for by EMPA and the respective mineral standards used for instrumental calibration. Errors associated with the EPMA measurements are <±0.1 wt%

Table B.2: Oxide weight percent data for uranium minerals from the Bong deposit, Thelon Basin, Nunavut, Canada

Sample	Mineral	SiO_2	Al_2O_3	UO_2	FeO	PbO	ThO_2	CaO	Total
RS-11-172	Vein Uraninite	0.72	<DL	84.73	0.11	10.00	<DL	1.35	97.64
RS-11-172	Altered Vein Uraninite	4.37	0.27	85.98	0.39	0.49	<DL	2.10	95.65
RS-11-172	Altered Vein Uraninite	3.95	0.18	87.47	0.58	0.52	<DL	2.37	97.63
RS-11-172	Vein Uraninite	0.64	<DL	85.13	0.00	9.98	<DL	1.44	98.14
RS-11-172	Vein Uraninite	0.42	<DL	85.42	0.00	9.56	<DL	1.13	97.90
RS-11-172	Altered Vein Uraninite	5.28	0.49	82.63	0.35	0.23	<DL	1.65	91.89
RS-11-172	Altered Vein Uraninite	4.80	0.43	84.60	0.37	<DL	<DL	1.96	92.16
RS-11-172	Altered Vein Uraninite	4.64	0.47	81.42	1.25	1.47	<DL	2.00	94.90
RS-11-172	Altered Vein Uraninite	5.25	0.56	84.29	0.39	<DL	<DL	2.01	94.08
RS-11-143	Altered Vein Uraninite	5.07	0.31	82.32	1.35	3.39	<DL	1.59	98.54
RS-11-143	Altered Vein Uraninite	3.77	0.24	87.11	0.73	<DL	<DL	1.65	96.59
RS-11-143	Altered Vein Uraninite	5.41	0.54	82.31	0.37	1.78	<DL	1.25	93.32
RS-11-143	Altered Vein Uraninite	3.69	0.22	82.69	0.86	<DL	<DL	1.44	92.38
RS-11-143	Altered Vein Uraninite	4.19	0.27	86.72	0.61	<DL	<DL	1.84	96.84
RS-11-143	Vein Uraninite	0.72	<DL	83.59	0.60	10.69	<DL	0.86	98.88
RS-11-143	Vein Uraninite	0.35	<DL	83.33	0.07	11.48	<DL	0.75	97.10
RS-11-143	Vein Uraninite	0.63	<DL	84.50	0.19	10.62	<DL	1.07	99.28
RS-11-143	Vein Uraninite	<DL	<DL	83.44	0.13	13.10	<DL	0.55	98.89
RS-11-143	Vein Uraninite	<DL	<DL	82.59	<DL	12.60	<DL	0.62	97.57
RS-11-143	Vein Uraninite	0.28	<DL	82.66	0.12	11.92	<DL	0.75	97.30
RS-11-143	Vein Uraninite	<DL	<DL	83.42	<DL	11.57	<DL	0.60	97.42
RS-11-143	Vein Uraninite	<DL	<DL	83.24	<DL	12.48	<DL	0.72	97.81
RS-11-143	Vein Uraninite	<DL	<DL	82.21	<DL	13.09	<DL	0.47	97.19
RS-11-143	Altered Vein Uraninite	1.49	0.14	80.89	<DL	<DL	<DL	5.11	92.59
RS-11-143	Altered Vein Uraninite	1.43	0.11	81.27	<DL	<DL	<DL	5.05	93.10
RS-11-143	Altered Vein Uraninite	1.65	0.27	81.43	<DL	<DL	<DL	5.24	93.67
RS-11-143	Altered Vein Uraninite	1.71	0.17	83.77	<DL	<DL	<DL	5.39	94.92
RS-11-143	Altered Vein Uraninite	1.68	0.16	85.19	<DL	<DL	<DL	5.27	96.11
RS-11-143	Altered Vein Uraninite	1.61	0.16	83.67	<DL	<DL	<DL	5.53	94.60
RS-11-143	Altered Vein Uraninite	1.33	0.13	81.45	<DL	<DL	<DL	5.65	93.32
RS-11-143	Altered Vein Uraninite	1.59	0.25	84.59	<DL	<DL	<DL	3.72	94.23
RS-11-143	Altered Vein Uraninite	2.04	0.14	84.63	<DL	<DL	<DL	3.52	93.75
RS-11-143	Altered Vein Uraninite	1.98	0.11	83.43	<DL	<DL	<DL	3.60	94.44

Table B.2: Oxide weight percent data for uranium minerals from the Bong deposit, Thelon Basin, Nunavut, Canada

Sample	Mineral	SiO_2	Al_2O_3	UO_2	FeO	PbO	ThO_2	CaO	Total
RS-11-143	Altered Vein Uraninite	2.44	0.74	83.40	<DL	<DL	<DL	3.43	94.04
301GC	Coffinite	15.04	1.61	56.93	0.62	1.59	<DL	3.09	82.91
301GC	Coffinite	15.46	2.03	62.41	0.22	<DL	<DL	2.90	90.47
301GC	Coffinite	12.77	1.21	66.07	0.12	<DL	<DL	3.34	90.40
301GC	Coffinite	10.14	0.72	64.94	0.18	0.34	<DL	5.62	92.23
301GC	Coffinite	20.31	3.48	49.73	0.64	<DL	<DL	3.71	90.19
301GC	Coffinite	10.79	0.80	66.44	0.28	0.15	<DL	5.95	95.83
301GC	Coffinite	14.95	1.17	70.48	<DL	<DL	<DL	2.25	93.31
301GC	Coffinite	15.72	1.40	68.79	0.22	<DL	<DL	2.57	94.42
301GC	Coffinite	16.11	2.23	59.07	6.76	0.18	<DL	1.84	97.73
301GC	Coffinite	15.49	1.49	71.55	0.29	<DL	<DL	1.70	92.32
301GC	Coffinite	16.12	1.71	64.65	0.32	<DL	<DL	0.90	86.02
301GC	Coffinite	17.98	2.36	65.30	0.28	<DL	<DL	3.80	91.95
301GC	Coffinite	15.87	1.45	56.51	9.60	0.27	<DL	3.45	95.82
301GC	Coffinite	22.17	2.51	58.91	0.85	<DL	<DL	2.65	90.10
RS-11-162	Roll Front Uraninite	1.28	0.10	80.76	<DL	0.40	<DL	5.82	91.29
RS-11-162	Roll Front Uraninite	1.40	0.11	80.09	<DL	0.35	<DL	5.90	90.63
RS-11-162	Roll Front Uraninite	1.56	0.13	83.83	<DL	0.57	<DL	5.69	93.68
RS-11-162	Roll Front Uraninite	1.47	0.13	84.24	<DL	0.48	<DL	5.50	93.90
RS-11-162	Roll Front Uraninite	1.62	0.16	86.36	<DL	0.55	<DL	5.43	95.92
RS-11-162	Roll Front Uraninite	1.69	0.14	85.07	<DL	0.52	<DL	5.36	94.25
RS-11-162	Roll Front Uraninite	1.54	0.19	85.85	<DL	0.59	<DL	5.71	95.32
RS-11-162	Roll Front Uraninite	1.56	0.13	85.24	<DL	0.49	<DL	5.63	94.84
RS-11-162	Roll Front Uraninite	1.65	0.18	85.96	<DL	0.56	<DL	5.58	95.34
RS-11-162	Roll Front Uraninite	1.53	0.14	84.18	<DL	0.71	<DL	5.39	93.27
RS-11-162	Roll Front Uraninite	1.42	0.10	84.32	<DL	0.45	<DL	3.76	92.07
RS-11-162	Roll Front Uraninite	1.71	0.10	84.61	<DL	0.44	<DL	3.46	92.20
RS-11-162	Roll Front Uraninite	1.24	0.12	83.45	<DL	0.51	<DL	3.79	91.42
RS-11-143	Vein Uraninite	0.96	<DL	81.05	0.26	10.23	<DL	0.83	94.68
RS-11-143	Vein Uraninite	0.67	<DL	81.22	<DL	11.22	<DL	0.84	94.96
RS-11-143	Altered Vein Uraninite	5.24	0.30	82.21	0.45	1.21	<DL	1.61	92.86
RS-11-143	Altered Vein Uraninite	5.32	0.34	80.02	0.79	1.06	<DL	1.55	92.22
RS-11-143	Altered Vein Uraninite	5.23	0.41	82.12	0.95	0.40	<DL	1.46	93.41
RS-11-143	Altered Vein Uraninite	4.49	0.33	82.65	0.55	1.98	<DL	1.51	93.28

Table B.2: Oxide weight percent data for uranium minerals from the Bong deposit, Thelon Basin, Nunavut, Canada

Sample	Mineral	SiO_2	Al_2O_3	UO_2	FeO	PbO	ThO_2	CaO	Total
RS-11-143	Altered Vein Uraninite	4.50	0.31	81.61	0.67	2.30	<DL	1.33	93.18
RS-11-143	Altered Vein Uraninite	8.35	3.50	72.82	0.89	1.23	<DL	1.50	90.99
RS-11-143	Altered Vein Uraninite	6.61	0.51	78.84	0.50	1.11	<DL	1.34	90.95
RS-11-143	Altered Vein Uraninite	6.92	0.46	75.67	0.41	2.02	<DL	1.20	89.09
RS-11-143	Coffinite	10.68	0.91	66.88	0.13	0.09	<DL	2.14	83.35
RS-11-143	Altered Vein Uraninite	7.50	0.61	75.09	0.23	0.86	<DL	1.63	87.92
RS-11-143	Coffinite	10.71	0.81	69.04	<DL	0.17	<DL	1.73	85.75
RS-11-143	Altered Vein Uraninite	3.70	0.24	82.28	0.64	1.63	<DL	1.61	91.92
RS-11-143	Altered Vein Uraninite	6.09	0.45	78.76	0.39	1.59	<DL	1.23	90.60
RS-11-143	Altered Vein Uraninite	7.12	0.64	81.73	0.17	<DL	<DL	1.07	92.66
RS-11-143	Coffinite	10.60	0.77	75.42	0.10	0.27	<DL	0.92	90.19
RS-11-143	Altered Vein Uraninite	5.59	0.54	85.12	0.33	<DL	<DL	1.42	94.29
RS-11-143	Altered Vein Uraninite	8.52	0.84	71.55	0.13	<DL	<DL	1.93	85.60
RS-11-143	Altered Vein Uraninite	5.56	0.47	82.54	0.28	<DL	<DL	1.46	91.79
RS-11-143	Altered Vein Uraninite	5.44	0.51	82.75	0.26	0.19	<DL	1.38	92.58
RS-11-143	Altered Vein Uraninite	2.94	0.20	79.72	0.29	6.69	<DL	1.48	93.14
RS-11-145	Altered Vein Uraninite	5.65	0.39	76.67	2.83	1.50	<DL	1.82	95.45
RS-11-145	Altered Vein Uraninite	5.33	0.42	80.55	1.03	3.17	<DL	1.80	96.19
RS-11-145	Coffinite	10.86	1.05	68.75	<DL	3.44	<DL	2.22	91.51
RS-11-145	Coffinite	15.77	1.22	58.76	1.76	2.56	<DL	3.32	91.16
RS-11-145	Coffinite	16.79	1.29	63.69	0.46	1.92	<DL	2.51	91.59
RS-11-172	Coffinite	12.02	2.33	70.82	0.34	<DL	<DL	3.50	90.55
RS-11-172	Coffinite	8.88	1.03	77.11	0.19	<DL	<DL	4.05	92.38
RS-11-172	Altered Vein Uraninite	5.40	0.56	81.94	0.22	<DL	<DL	2.44	91.50
RS-11-172	Altered Vein Uraninite	3.68	0.22	63.04	<DL	<DL	<DL	1.44	69.88
302GC	Altered Vein Uraninite	5.46	0.43	71.93	<DL	2.32	<DL	1.20	83.03
302GC	Altered Vein Uraninite	11.45	1.06	65.92	<DL	<DL	<DL	1.53	82.33
302GC	Altered Vein Uraninite	3.43	0.28	62.63	<DL	<DL	<DL	1.18	69.36
302GC	Altered Vein Uraninite	10.77	0.98	66.01	<DL	<DL	<DL	1.62	80.94
302GC	Coffinite	18.53	1.48	67.93	<DL	<DL	<DL	2.38	91.83
302GC	Coffinite	10.79	0.89	76.93	0.11	<DL	<DL	1.79	91.32
302GC	Coffinite	18.63	1.35	67.16	<DL	0.15	<DL	2.48	91.69
302GC	Coffinite	12.46	0.97	71.65	0.25	0.40	<DL	1.78	89.16
302GC	Coffinite	9.77	0.91	77.97	0.11	<DL	<DL	2.21	92.40

Table B.2: Oxide weight percent data for uranium minerals from the Bong deposit, Thelon Basin, Nunavut, Canada

Sample	Mineral	SiO_2	Al_2O_3	UO_2	FeO	PbO	ThO_2	CaO	Total
302GC	Coffinite	17.05	1.25	69.54	<DL	<DL	<DL	2.60	91.33
302GC	Coffinite	15.13	1.15	70.55	<DL	<DL	<DL	2.30	89.80
302GC	Coffinite	12.74	1.10	74.17	0.11	<DL	<DL	2.26	90.97
302GC	Coffinite	13.21	1.42	72.62	0.17	0.35	<DL	1.90	90.32
302GC	Coffinite	5.36	0.46	84.23	0.39	1.25	<DL	1.16	94.45
302GC	Altered Vein Uraninite	12.20	0.95	74.15	<DL	<DL	<DL	1.87	90.66
302GC	Altered Vein Uraninite	6.77	0.63	80.46	0.35	0.66	<DL	1.22	91.80
302GC	Coffinite	12.57	1.01	71.82	0.14	1.28	<DL	2.69	90.69
302GC	Altered Vein Uraninite	4.85	0.36	85.72	0.42	0.23	<DL	2.41	95.03
301GC	Altered Vein Uraninite	11.19	1.01	74.77	0.11	0.33	<DL	3.63	91.68
301GC	Coffinite	16.65	1.50	69.02	<DL	0.36	<DL	3.61	91.64
301GC	Altered Vein Uraninite	6.54	0.62	82.93	0.31	0.28	<DL	2.43	93.85
301GC	Coffinite	18.86	1.65	68.88	<DL	<DL	<DL	3.04	93.15
301GC	Coffinite	10.71	1.11	76.57	<DL	<DL	<DL	3.39	92.86
301GC	Coffinite	18.80	1.65	69.25	<DL	0.16	<DL	2.78	93.16
301GC	Coffinite	11.23	1.15	75.68	0.13	0.25	<DL	3.11	92.47
301GC	Coffinite	18.81	1.84	68.04	0.23	0.22	<DL	2.11	92.10
301GC	Coffinite	19.18	1.83	67.78	0.73	0.27	<DL	2.80	93.59
301GC	Coffinite	12.85	2.12	68.62	0.53	0.16	<DL	2.00	90.28
301GC	Coffinite	17.60	1.57	68.68	0.22	0.20	<DL	1.89	90.79
301GC	Altered Vein Uraninite	5.57	0.50	81.82	1.32	0.83	<DL	1.46	93.29
303GC	Altered Vein Uraninite	6.86	0.60	79.84	1.26	0.31	<DL	1.33	92.45
303GC	Altered Vein Uraninite	10.45	2.64	77.73	0.32	<DL	<DL	1.04	93.09
303GC	Coffinite	16.60	6.92	63.28	0.89	<DL	<DL	1.52	92.08
303GC	Vein Uraninite	0.40	0.03	83.80	<DL	11.39	<DL	1.49	97.77
303GC	Altered Vein Uraninite	5.56	0.47	82.44	0.96	1.55	<DL	1.45	94.92
303GC	Altered Vein Uraninite	6.54	0.59	78.40	1.74	2.07	<DL	1.03	95.20
303GC	Vein Uraninite	0.60	<DL	81.75	0.15	12.49	<DL	1.59	97.43
303GC	Vein Uraninite	0.32	<DL	84.00	<DL	11.35	<DL	0.93	97.40
303GC	Altered Vein Uraninite	3.34	0.23	83.85	0.25	6.21	<DL	1.30	96.90
303GC	Altered Vein Uraninite	2.55	0.18	82.99	0.20	7.43	<DL	1.02	95.84
303GC	Altered Vein Uraninite	5.25	0.41	78.94	0.83	4.51	<DL	0.92	94.42
303GC	Altered Vein Uraninite	5.31	0.33	79.02	0.22	7.08	<DL	0.92	95.94
303GC	Altered Vein Uraninite	6.21	0.39	74.50	1.88	3.55	<DL	0.86	93.52

Table B.2: Oxide weight percent data for uranium minerals from the Bong deposit, Thelon Basin, Nunavut, Canada

Sample	Mineral	SiO_2	Al_2O_3	UO_2	FeO	PbO	ThO_2	CaO	Total
303GC	Altered Vein Uraninite	5.16	0.30	74.20	2.50	6.66	<DL	0.66	96.31
303GC	Altered Vein Uraninite	6.29	0.45	76.30	0.90	5.88	<DL	0.77	95.27
303GC	Altered Vein Uraninite	3.11	0.22	78.42	0.10	11.58	<DL	1.44	95.14
303GC	Altered Vein Uraninite	8.11	0.50	67.43	1.57	2.33	<DL	0.86	85.33
303GC	Altered Vein Uraninite	1.84	0.12	76.99	0.24	10.30	<DL	0.88	92.33
303GC	Coffinite	12.13	0.75	67.67	1.14	2.78	<DL	0.76	90.30
303GC	Coffinite	14.35	0.90	66.02	0.70	0.92	<DL	0.88	87.28
303GC	Coffinite	14.75	0.86	60.82	1.53	1.54	<DL	2.51	88.81
303GC	Altered Vein Uraninite	3.52	0.30	76.33	0.34	7.20	<DL	0.76	90.39
303GC	Altered Vein Uraninite	9.50	1.62	65.55	1.93	2.47	<DL	0.89	87.82
303GC	Altered Vein Uraninite	2.07	0.14	81.16	0.13	8.15	<DL	0.97	93.94
303GC	Altered Vein Uraninite	9.30	0.71	66.56	0.85	2.00	<DL	1.26	84.64
303GC	Coffinite	13.68	1.32	62.88	0.23	2.44	<DL	0.70	84.40
RS-11-172	Coffinite	10.66	0.73	67.50	0.11	5.94	<DL	1.17	88.24
RS-11-172	Altered Vein Uraninite	4.16	0.80	69.24	<DL	1.29	<DL	2.65	80.21
RS-11-172	Altered Vein Uraninite	0.92	0.43	70.01	0.41	0.49	<DL	7.76	81.68
RS-11-144	Altered Vein Uraninite	5.71	0.61	75.23	<DL	0.33	<DL	6.27	89.69
RS-11-144	Altered Vein Uraninite	2.69	0.22	81.91	<DL	0.45	<DL	5.57	92.12
RS-11-144	Coffinite	13.14	0.88	67.93	0.44	<DL	<DL	0.60	85.03
303GC	Coffinite	10.91	2.28	61.07	0.56	10.94	<DL	1.05	91.74
303GC	Coffinite	13.72	0.94	68.13	0.17	<DL	<DL	0.58	85.26
303GC	Vein Uraninite	<DL	<DL	77.26	<DL	12.30	<DL	1.32	91.71
303GC	Altered Vein Uraninite	5.06	0.46	74.50	2.34	<DL	<DL	1.17	89.11
303GC	Vein Uraninite	0.10	<DL	79.10	0.11	11.76	<DL	0.66	92.35
303GC	Altered Vein Uraninite	2.02	0.17	76.58	0.14	9.93	<DL	0.73	90.78
RS-11-142	Coffinite	10.49	1.40	80.95	0.11	<DL	<DL	2.68	96.97
RS-11-142	Altered Vein Uraninite	6.39	0.94	84.83	0.26	<DL	<DL	2.17	95.53
RS-11-142	Coffinite	14.37	1.29	72.71	<DL	<DL	<DL	2.90	93.76
RS-11-142	Altered Vein Uraninite	4.55	0.57	85.25	0.49	<DL	<DL	3.35	95.23
RS-11-173	Uraninite in Graphite	13.68	1.32	62.88	0.23	2.45	<DL	0.70	81.26
RS-11-173	Uraninite in Graphite	10.66	0.72	67.50	0.11	5.93	<DL	1.17	86.09
RS-11-173	Uraninite in Graphite	1.28	0.14	79.59	0.03	10.18	<DL	1.04	92.26

Table B.3: Atomic weight percent data for uranium minerals from the Bong deposit, Thelon Basin, Nunavut, Canada

Sample	Mineral	Si	Al	U	Fe	Pb	Th	Ca	O	Total
RS-11-172	Vein Uraninite	1.05	<DL	27.58	0.13	3.94	<DL	2.11	64.19	100
RS-11-172	Altered Vein Uraninite	5.41	0.40	23.69	0.40	0.16	<DL	2.78	63.99	100
RS-11-172	Altered Vein Uraninite	4.83	0.26	23.79	0.59	0.17	<DL	3.10	63.63	100
RS-11-172	Vein Uraninite	0.93	<DL	27.48	0.00	3.90	<DL	2.23	63.87	100
RS-11-172	Vein Uraninite	0.61	<DL	27.77	0.00	3.76	<DL	1.76	63.13	100
RS-11-172	Altered Vein Uraninite	6.69	0.74	23.29	0.37	0.08	<DL	2.24	65.10	100
RS-11-172	Altered Vein Uraninite	5.94	0.62	23.31	0.38	<DL	<DL	2.61	64.46	100
RS-11-172	Altered Vein Uraninite	5.42	0.64	21.16	1.22	0.46	<DL	2.51	64.57	100
RS-11-172	Altered Vein Uraninite	6.43	0.80	22.96	0.40	<DL	<DL	2.63	64.28	100
RS-11-143	Altered Vein Uraninite	5.64	0.40	20.38	1.26	1.02	<DL	1.90	64.55	100
RS-11-143	Altered Vein Uraninite	4.71	0.36	24.26	0.76	<DL	<DL	2.22	64.45	100
RS-11-143	Altered Vein Uraninite	6.70	0.79	22.67	0.39	0.59	<DL	1.66	65.47	100
RS-11-143	Altered Vein Uraninite	4.79	0.34	23.88	0.93	<DL	<DL	2.00	64.80	100
RS-11-143	Altered Vein Uraninite	5.13	0.39	23.62	0.63	<DL	<DL	2.41	64.09	100
RS-11-143	Vein Uraninite	1.00	<DL	25.83	0.70	3.99	<DL	1.27	63.42	100
RS-11-143	Vein Uraninite	0.52	<DL	27.78	0.08	4.63	<DL	1.20	63.36	100
RS-11-143	Vein Uraninite	0.90	<DL	26.54	0.22	4.03	<DL	1.62	62.19	100
RS-11-143	Vein Uraninite	<DL	<DL	27.57	0.16	5.24	<DL	0.88	62.29	100
RS-11-143	Vein Uraninite	<DL	<DL	27.73	<DL	5.12	<DL	1.00	62.61	100
RS-11-143	Vein Uraninite	0.42	<DL	27.51	0.16	4.80	<DL	1.21	63.37	100
RS-11-143	Vein Uraninite	<DL	<DL	27.93	<DL	4.69	<DL	0.97	62.67	100
RS-11-143	Vein Uraninite	<DL	<DL	27.91	<DL	5.06	<DL	1.16	62.98	100
RS-11-143	Vein Uraninite	<DL	<DL	27.83	<DL	5.36	<DL	0.77	62.57	100
RS-11-143	Altered Vein Uraninite	1.86	0.20	22.49	<DL	<DL	<DL	6.84	62.73	100
RS-11-143	Altered Vein Uraninite	1.79	0.17	22.56	<DL	<DL	<DL	6.76	62.61	100
RS-11-143	Altered Vein Uraninite	2.02	0.39	22.18	<DL	<DL	<DL	6.88	62.07	100
RS-11-143	Altered Vein Uraninite	2.12	0.25	23.06	<DL	<DL	<DL	7.14	61.40	100
RS-11-143	Altered Vein Uraninite	2.07	0.23	23.29	<DL	<DL	<DL	6.93	61.17	100
RS-11-143	Altered Vein Uraninite	2.00	0.24	23.08	<DL	<DL	<DL	7.34	60.83	100
RS-11-143	Altered Vein Uraninite	1.65	0.19	22.52	<DL	<DL	<DL	7.52	61.77	100
RS-11-143	Altered Vein Uraninite	2.06	0.38	24.30	<DL	<DL	<DL	5.14	63.21	100
RS-11-143	Altered Vein Uraninite	2.67	0.22	24.56	<DL	<DL	<DL	4.92	62.93	100
RS-11-143	Altered Vein Uraninite	3.06	1.09	23.24	<DL	<DL	<DL	4.60	62.88	100

Table B.3: Atomic weight percent data for uranium minerals from the Bong deposits, Thelon Basin, Nunavut, Canada

Sample	Mineral	Si	Al	U	Fe	Pb	Th	Ca	O	Total
301GC	Coffinite	14.28	1.81	12.03	0.49	0.41	<DL	3.15	64.78	100
301GC	Coffinite	13.41	2.08	12.05	0.16	<DL	<DL	2.70	64.70	100
301GC	Coffinite	12.08	1.35	13.91	0.09	<DL	<DL	3.39	64.87	100
301GC	Coffinite	9.38	0.78	13.36	0.14	0.08	<DL	5.57	64.15	100
301GC	Coffinite	15.07	3.04	8.21	0.39	<DL	<DL	2.95	64.14	100
301GC	Coffinite	9.43	0.82	12.93	0.20	0.04	<DL	5.57	64.07	100
301GC	Coffinite	13.54	1.25	14.20	<DL	<DL	<DL	2.18	65.60	100
301GC	Coffinite	13.51	1.42	13.15	0.16	<DL	<DL	2.37	65.20	100
301GC	Coffinite	11.42	1.86	9.31	4.01	0.03	<DL	1.39	63.93	100
301GC	Coffinite	14.47	1.64	14.88	0.23	<DL	<DL	1.71	65.31	100
301GC	Coffinite	15.43	1.92	13.77	0.25	<DL	<DL	0.92	65.52	100
301GC	Coffinite	15.14	2.34	12.23	0.19	<DL	<DL	3.43	64.73	100
301GC	Coffinite	11.55	1.25	9.15	5.84	0.05	<DL	2.69	63.42	100
301GC	Coffinite	17.38	2.32	10.27	0.55	<DL	<DL	2.23	65.12	100
RS-11-162	Roll Front Uraninite	1.62	0.15	22.78	<DL	0.14	<DL	7.90	63.09	100
RS-11-162	Roll Front Uraninite	1.78	0.17	22.62	<DL	0.12	<DL	8.03	62.67	100
RS-11-162	Roll Front Uraninite	1.99	0.19	23.76	<DL	0.20	<DL	7.76	62.60	100
RS-11-162	Roll Front Uraninite	1.87	0.19	23.80	<DL	0.16	<DL	7.48	63.06	100
RS-11-162	Roll Front Uraninite	2.02	0.23	23.99	<DL	0.19	<DL	7.27	62.53	100
RS-11-162	Roll Front Uraninite	2.16	0.21	24.18	<DL	0.18	<DL	7.34	62.71	100
RS-11-162	Roll Front Uraninite	1.95	0.28	24.20	<DL	0.20	<DL	7.75	62.69	100
RS-11-162	Roll Front Uraninite	1.97	0.19	23.86	<DL	0.17	<DL	7.59	62.06	100
RS-11-162	Roll Front Uraninite	2.08	0.27	24.15	<DL	0.19	<DL	7.55	62.40	100
RS-11-162	Roll Front Uraninite	2.00	0.22	24.49	<DL	0.25	<DL	7.55	62.98	100
RS-11-162	Roll Front Uraninite	1.89	0.16	25.03	<DL	0.16	<DL	5.37	64.51	100
RS-11-162	Roll Front Uraninite	2.28	0.16	25.11	<DL	0.16	<DL	4.94	64.33	100
RS-11-162	Roll Front Uraninite	1.66	0.19	24.91	<DL	0.18	<DL	5.45	64.13	100
RS-11-143	Vein Uraninite	1.42	<DL	26.52	0.31	4.05	<DL	1.30	63.38	100
RS-11-143	Vein Uraninite	1.01	<DL	27.10	<DL	4.53	<DL	1.35	63.28	100
RS-11-143	Altered Vein Uraninite	6.46	0.44	22.54	0.46	0.40	<DL	2.13	65.08	100
RS-11-143	Altered Vein Uraninite	6.36	0.48	21.29	0.79	0.34	<DL	1.98	65.24	100
RS-11-143	Altered Vein Uraninite	6.19	0.57	21.64	0.94	0.13	<DL	1.85	64.80	100
RS-11-143	Altered Vein Uraninite	5.66	0.50	23.17	0.58	0.67	<DL	2.04	65.43	100
RS-11-143	Altered Vein Uraninite	5.58	0.46	22.53	0.70	0.77	<DL	1.77	65.17	100

Table B.3: Atomic weight percent data for uranium minerals from the Bong deposits, Thelon Basin, Nunavut, Canada

Sample	Mineral	Si	Al	U	Fe	Pb	Th	Ca	O	Total
RS-11-143	Altered Vein Uraninite	8.71	4.30	16.90	0.77	0.35	<DL	1.68	63.37	100
RS-11-143	Altered Vein Uraninite	7.91	0.72	20.98	0.50	0.36	<DL	1.72	65.24	100
RS-11-143	Altered Vein Uraninite	8.29	0.65	20.17	0.41	0.65	<DL	1.54	65.61	100
RS-11-143	Coffinite	11.70	1.17	16.29	0.12	0.03	<DL	2.51	65.01	100
RS-11-143	Altered Vein Uraninite	9.00	0.86	20.05	0.23	0.28	<DL	2.10	65.03	100
RS-11-143	Coffinite	11.60	1.03	16.63	<DL	0.05	<DL	2.00	65.53	100
RS-11-143	Altered Vein Uraninite	4.83	0.37	23.89	0.70	0.57	<DL	2.26	64.66	100
RS-11-143	Altered Vein Uraninite	7.44	0.65	21.39	0.39	0.52	<DL	1.60	65.12	100
RS-11-143	Altered Vein Uraninite	8.40	0.89	21.47	0.17	<DL	<DL	1.36	65.66	100
RS-11-143	Coffinite	11.49	0.99	18.19	0.09	0.08	<DL	1.06	65.58	100
RS-11-143	Altered Vein Uraninite	6.85	0.78	23.21	0.33	<DL	<DL	1.86	65.57	100
RS-11-143	Altered Vein Uraninite	9.83	1.14	18.36	0.13	<DL	<DL	2.38	65.28	100
RS-11-143	Altered Vein Uraninite	6.95	0.69	22.95	0.29	<DL	<DL	1.95	65.65	100
RS-11-143	Altered Vein Uraninite	6.69	0.74	22.66	0.27	0.06	<DL	1.81	65.48	100
RS-11-143	Altered Vein Uraninite	3.94	0.32	23.80	0.33	2.42	<DL	2.12	63.96	100
RS-11-145	Altered Vein Uraninite	5.85	0.47	17.68	2.45	0.42	<DL	2.02	64.70	100
RS-11-145	Altered Vein Uraninite	6.10	0.57	20.49	0.98	0.98	<DL	2.21	64.51	100
RS-11-145	Coffinite	10.88	1.24	15.33	<DL	0.93	<DL	2.38	64.89	100
RS-11-145	Coffinite	12.86	1.18	10.66	1.20	0.56	<DL	2.90	64.60	100
RS-11-145	Coffinite	14.38	1.30	12.14	0.33	0.44	<DL	2.30	65.13	100
RS-11-172	Coffinite	11.74	2.68	15.39	0.28	<DL	<DL	3.66	63.92	100
RS-11-172	Coffinite	9.55	1.30	18.46	0.17	<DL	<DL	4.67	63.97	100
RS-11-172	Altered Vein Uraninite	6.72	0.83	22.69	0.23	<DL	<DL	3.26	64.46	100
RS-11-172	Altered Vein Uraninite	6.07	0.43	23.17	<DL	<DL	<DL	2.54	65.00	100
302GC	Altered Vein Uraninite	7.40	0.68	21.70	<DL	0.85	<DL	1.74	65.08	100
302GC	Altered Vein Uraninite	12.68	1.39	16.25	<DL	<DL	<DL	1.81	65.37	100
302GC	Coffinite	5.69	0.55	23.12	<DL	<DL	<DL	2.10	64.78	100
302GC	Altered Vein Uraninite	12.42	1.33	16.94	<DL	<DL	<DL	2.00	65.38	100
302GC	Coffinite	16.17	1.53	13.19	<DL	<DL	<DL	2.22	65.37	100
302GC	Coffinite	11.65	1.13	18.48	0.10	<DL	<DL	2.07	65.30	100
302GC	Coffinite	16.13	1.38	12.94	<DL	0.03	<DL	2.30	65.01	100
302GC	Coffinite	12.83	1.18	16.42	0.21	0.11	<DL	1.97	65.39	100
302GC	Coffinite	10.62	1.16	18.86	0.09	<DL	<DL	2.57	65.46	100
302GC	Coffinite	15.70	1.35	14.25	<DL	<DL	<DL	2.56	65.47	100

Table B.3: Atomic weight percent data for uranium minerals from the Bong deposits, Thelon Basin, Nunavut, Canada

Sample	Mineral	Si	Al	U	Fe	Pb	Th	Ca	O	Total
302GC	Coffinite	14.82	1.33	15.38	<DL	<DL	<DL	2.41	65.55	100
302GC	Coffinite	13.12	1.33	16.99	0.08	<DL	<DL	2.49	65.52	100
302GC	Coffinite	13.42	1.70	16.42	0.13	0.10	<DL	2.07	65.47	100
302GC	Altered Vein Uraninite	6.57	0.67	22.98	0.36	0.41	<DL	1.53	65.63	100
302GC	Altered Vein Uraninite	12.70	1.16	17.18	<DL	<DL	<DL	2.08	65.63	100
302GC	Altered Vein Uraninite	8.10	0.89	21.41	0.32	0.21	<DL	1.57	65.57	100
302GC	Coffinite	12.80	1.21	16.27	0.11	0.35	<DL	2.94	65.14	100
302GC	Altered Vein Uraninite	5.96	0.52	23.44	0.39	0.08	<DL	3.18	65.27	100
301GC	Altered Vein Uraninite	11.66	1.24	17.32	0.09	0.09	<DL	4.05	64.92	100
301GC	Coffinite	15.21	1.61	14.03	<DL	0.09	<DL	3.53	65.07	100
301GC	Altered Vein Uraninite	7.74	0.87	21.84	0.27	0.09	<DL	3.08	65.23	100
301GC	Coffinite	16.35	1.69	13.29	<DL	<DL	<DL	2.82	65.38	100
301GC	Coffinite	11.15	1.36	17.74	<DL	<DL	<DL	3.79	64.99	100
301GC	Coffinite	16.39	1.70	13.44	<DL	0.04	<DL	2.60	65.46	100
301GC	Coffinite	11.62	1.41	17.42	0.10	0.07	<DL	3.45	65.07	100
301GC	Coffinite	16.47	1.90	13.26	0.15	0.05	<DL	1.98	65.44	100
301GC	Coffinite	16.26	1.83	12.79	0.47	0.06	<DL	2.54	65.16	100
301GC	Coffinite	12.25	2.39	14.55	0.38	0.04	<DL	2.04	65.06	100
301GC	Coffinite	16.11	1.69	13.99	0.15	0.05	<DL	1.85	65.53	100
301GC	Altered Vein Uraninite	6.67	0.70	21.80	1.19	0.27	<DL	1.88	65.59	100
303GC	Altered Vein Uraninite	7.89	0.82	20.43	1.09	0.10	<DL	1.64	65.55	100
303GC	Altered Vein Uraninite	10.92	3.25	18.08	0.25	<DL	<DL	1.17	65.41	100
303GC	Coffinite	13.47	6.62	11.43	0.54	<DL	<DL	1.32	64.18	100
303GC	Vein Uraninite	0.59	0.05	27.42	<DL	4.51	<DL	2.35	64.26	100
303GC	Altered Vein Uraninite	6.52	0.65	21.51	0.85	0.49	<DL	1.82	65.56	100
303GC	Altered Vein Uraninite	7.05	0.75	18.79	1.41	0.60	<DL	1.18	65.71	100
303GC	Vein Uraninite	0.86	0.06	26.37	0.17	4.88	<DL	2.46	64.06	100
303GC	Vein Uraninite	0.49	0.06	27.96	<DL	4.57	<DL	1.50	64.42	100
303GC	Altered Vein Uraninite	4.32	0.35	24.13	0.25	2.16	<DL	1.81	65.19	100
303GC	Altered Vein Uraninite	3.48	0.29	25.15	0.20	2.73	<DL	1.48	65.03	100
303GC	Altered Vein Uraninite	6.24	0.58	20.88	0.74	1.44	<DL	1.17	65.36	100
303GC	Altered Vein Uraninite	6.41	0.47	21.23	0.20	2.30	<DL	1.18	65.30	100
303GC	Altered Vein Uraninite	6.75	0.50	18.00	1.53	1.04	<DL	1.00	65.56	100
303GC	Altered Vein Uraninite	5.53	0.38	17.72	2.02	1.93	<DL	0.76	65.27	100

Table B.3: Atomic weight percent data for uranium minerals from the Bong deposits, Thelon Basin, Nunavut, Canada

Sample	Mineral	Si	Al	U	Fe	Pb	Th	Ca	O	Total
303GC	Altered Vein Uraninite	7.06	0.60	19.05	0.76	1.78	<DL	0.92	65.48	100
303GC	Altered Vein Uraninite	4.28	0.35	24.08	0.11	4.30	<DL	2.13	64.30	100
303GC	Altered Vein Uraninite	9.14	0.66	16.92	1.48	0.71	<DL	1.04	65.39	100
303GC	Altered Vein Uraninite	2.64	0.20	24.57	0.29	3.98	<DL	1.36	63.92	100
303GC	Coffinite	11.83	0.87	14.68	0.93	0.73	<DL	0.79	65.61	100
303GC	Coffinite	13.99	1.04	14.32	0.57	0.24	<DL	0.92	66.05	100
303GC	Coffinite	12.98	0.89	11.91	1.13	0.37	<DL	2.37	64.99	100
303GC	Coffinite	4.87	0.49	23.47	0.39	2.68	<DL	1.12	64.51	100
303GC	Altered Vein Uraninite	9.69	1.95	14.89	1.65	0.68	<DL	0.97	64.69	100
303GC	Altered Vein Uraninite	2.94	0.24	25.73	0.16	3.13	<DL	1.47	64.28	100
303GC	Altered Vein Uraninite	10.32	0.93	16.43	0.79	0.60	<DL	1.50	65.35	100
303GC	Coffinite	13.83	1.58	14.15	0.20	0.66	<DL	0.75	65.86	100
RS-11-172	Coffinite	11.73	0.94	16.52	0.10	1.76	<DL	1.38	65.37	100
RS-11-172	Altered Vein Uraninite	5.75	1.30	21.26	<DL	0.48	<DL	3.92	63.94	100
RS-11-172	Altered Vein Uraninite	1.27	0.71	21.52	0.48	0.18	<DL	11.48	61.87	100
RS-11-144	Altered Vein Uraninite	6.56	0.82	19.24	<DL	0.10	<DL	7.72	63.33	100
RS-11-144	Altered Vein Uraninite	3.40	0.32	23.08	<DL	0.15	<DL	7.55	63.05	100
RS-11-144	Coffinite	13.86	1.09	15.95	0.39	<DL	<DL	0.67	65.91	100
303GC	Coffinite	10.61	2.61	13.22	0.45	2.87	<DL	1.09	63.90	100
303GC	Coffinite	14.32	1.15	15.83	0.15	<DL	<DL	0.65	66.04	100
303GC	Vein Uraninite	<DL	<DL	27.35	<DL	5.27	<DL	2.25	62.91	100
303GC	Altered Vein Uraninite	5.89	0.64	19.26	2.28	<DL	<DL	1.46	65.12	100
303GC	Vein Uraninite	0.16	<DL	28.12	0.14	5.06	<DL	1.13	63.04	100
303GC	Altered Vein Uraninite	2.98	0.30	25.15	0.17	3.95	<DL	1.16	64.46	100
RS-11-142	Coffinite	10.60	1.66	18.21	0.10	<DL	<DL	2.90	65.03	100
RS-11-142	Altered Vein Uraninite	7.44	1.29	21.97	0.26	<DL	<DL	2.70	64.74	100
RS-11-142	Coffinite	13.25	1.40	14.92	<DL	<DL	<DL	2.86	64.99	100
RS-11-142	Altered Vein Uraninite	5.51	0.82	22.97	0.50	<DL	<DL	4.34	64.15	100
RS-11-173	Uraninite in Graphite	13.83	1.58	14.15	0.20	0.66	<DL	0.75	65.86	100
RS-11-173	Uraninite in Graphite	11.73	0.94	16.52	<DL	1.76	<DL	1.37	65.37	100
RS-11-173	Uraninite in Graphite	1.92	0.24	26.50	<DL	4.10	<DL	1.67	63.69	100

Table B.4: Oxide weight percent data for uranium alteration minerals from the Bong deposits, Thelon Basin, Nunavut, Canada

Sample	Mineral	SiO_2	Al_2O_3	UO_2	FeO	PbO	ThO_2	CaO	Total
RS-11-143	Uranophane	22.17	2.51	58.91	0.85	<DL	<DL	2.65	87.09
RS-11-172	Uranophane	20.31	3.48	49.73	0.64	<DL	<DL	3.71	77.87
303GC	Uranophane	16.13	1.65	57.19	0.88	1.96	<DL	2.58	80.39
RS-11-143	Ca-U	1.49	0.14	80.89	0	0.36	<DL	5.11	87.99
RS-11-143	Ca-U	1.43	0.11	81.27	0.03	0.37	<DL	5.05	88.26
RS-11-143	Ca-U	1.65	0.27	81.43	0.02	0.4	<DL	5.24	89.01
RS-11-172	Ca-U	1.71	0.17	83.77	0.01	0.61	<DL	5.39	91.66
RS-11-172	Ca-U	1.68	0.16	85.19	0.03	0.52	<DL	5.27	92.85
RS-11-172	Ca-U	1.61	0.16	83.67	0	0.56	<DL	5.53	91.53
RS-11-172	Ca-U	1.33	0.13	81.45	0	0.48	<DL	5.65	89.04

Table B.5: Oxide weight percent data for rutile and apatite in the Bong deposit, Thelon Basin, Nunavut, Canada

Sample	Mineral	F	SiO_2	Al_2O_3	UO_2	FeO	P_2O_5	PbO	CaO	TiO_2	Total
301GC	Fluorapatite	4.27	<DL	<DL	<DL	0.10	40.62	<DL	54.67	<DL	99.66
301GC	Fluorapatite	4.30	1.23	0.41	<DL	0.12	38.38	<DL	52.27	<DL	96.71
301GC	Rutile	<DL	<DL	0.04	<DL	0.59	<DL	<DL	0.22	98.73	99.58
301GC	Rutile	<DL	<DL	<DL	<DL	0.22	<DL	<DL	<DL	100.59	100.80
301GC	Rutile	<DL	<DL	<DL	<DL	<DL	<DL	<DL	<DL	100.40	100.40
301GC	Rutile	<DL	<DL	<DL	<DL	0.12	<DL	<DL	<DL	99.53	99.65
301GC	Fluorapatite	4.33	<DL	<DL	<DL	<DL	41.08	<DL	54.76	<DL	100.18
301GC	Fluorapatite	4.13	0.16	<DL	<DL	<DL	40.95	<DL	56.16	<DL	101.41
301GC	Rutile	<DL	<DL	<DL	<DL	<DL	<DL	<DL	<DL	99.67	99.67
301GC	Rutile	<DL	<DL	<DL	<DL	<DL	<DL	<DL	<DL	100.32	100.32
301GC	Rutile	<DL	<DL	<DL	<DL	<DL	<DL	<DL	<DL	99.78	99.78
301GC	Rutile	<DL	<DL	<DL	<DL	0.72	<DL	<DL	0.26	98.62	99.61
RS-11-172	Fluorapatite	3.68	<DL	<DL	<DL	0.03	41.23	<DL	50.71	<DL	95.65
RS-11-142	Fluorapatite	3.80	0.14	<DL	<DL	0.08	41.99	<DL	53.15	<DL	99.17
RS-11-142	Fluorapatite	3.56	<DL	<DL	<DL	0.08	42.38	<DL	53.03	<DL	99.05

Table B.6: Oxide weight percent data for silicate minerals from the Bong deposit, Thelon Basin, Nunavut, Canada

Sample	Mineral	SiO_2	Al_2O_3	K_2O	CaO	FeO	MgO	Total
RS-11-072	Fe-Mg Chlorite	27.25	18.09	0.13	2.73	22.05	14.33	84.58
RS-11-072	Fe-Mg Chlorite	26.82	19.00	0.03	0.08	24.78	16.17	86.88
RS-11-072	Muscovite	64.64	18.01	16.93	0.02	0.04	0.00	99.64
RS-11-072	Muscovite	45.76	29.60	10.21	0.02	3.87	1.52	90.99
RS-11-072	Muscovite	45.41	30.81	10.00	0.05	4.79	1.77	92.84
RS-11-072	Muscovite	46.42	30.38	10.15	0.05	4.35	2.01	93.36
RS-11-072	Muscovite	47.04	31.63	10.15	0.03	4.11	1.48	94.44
RS-11-072	Fe-Mg Chlorite	26.13	20.22	0.04	0.05	25.76	14.59	86.78
RS-11-072	Fe-Mg Chlorite	26.45	20.38	0.04	0.04	25.43	14.73	87.07
RS-11-072	Fe-Mg Chlorite	25.99	20.13	0.05	0.04	26.00	14.17	86.38
RS-11-072	Fe-Mg Chlorite	25.95	20.10	0.05	0.06	25.68	14.44	86.28
RS-11-072	Fe-Mg Chlorite	26.18	19.66	0.02	0.05	26.79	14.02	86.72
RS-11-072	Fe-Mg Chlorite	26.17	20.07	0.05	0.08	27.18	13.45	87.00
RS-11-072	Muscovite	63.01	18.59	15.83	0.01	0.08	0.00	97.52
RS-11-072	Muscovite	62.63	18.35	15.78	0.01	0.19	0.00	96.96
RS-11-072	Fe-Mg Chlorite	28.61	20.87	1.02	0.06	24.14	13.39	88.10
RS-11-072	Fe-Mg Chlorite	26.03	19.97	0.04	0.04	26.26	14.03	86.38
RS-11-072	Fe-Mg Chlorite	25.87	19.98	0.05	0.03	27.30	13.51	86.75
RS-11-072	Fe-Mg Chlorite	27.02	20.25	0.36	0.03	26.19	13.62	87.48
RS-11-072	Muscovite	46.09	31.51	10.23	0.00	4.29	1.53	93.64
RS-11-072	Muscovite	45.93	30.88	10.22	0.01	4.53	1.61	93.16
RS-11-072	Muscovite	46.78	30.24	10.58	0.01	4.08	1.51	93.19
RS-11-072	Muscovite	49.16	28.14	10.30	0.07	4.37	1.81	93.84
RS-11-072	Fe-Mg Chlorite	25.76	21.28	0.05	0.01	24.96	15.54	87.62
RS-11-072	Muscovite	45.96	31.12	10.85	0.00	4.49	1.58	94.00
RS-11-072	Muscovite	45.57	31.41	10.33	0.05	4.48	1.58	93.42
RS-11-072	Muscovite	45.50	32.98	10.19	0.02	3.04	1.06	92.79
RS-11-072	Fe-Mg Chlorite	25.53	19.84	0.04	0.02	28.30	12.69	86.42
RS-11-072	Fe-Mg Chlorite	26.64	18.81	0.05	0.02	27.71	13.96	87.18
RS-11-072	Muscovite	64.09	18.36	16.59	0.01	0.49	0.01	99.54
RS-11-072	Fe-Mg Chlorite	26.04	20.03	0.21	0.02	28.22	12.72	87.24
RS-11-072	Fe-Mg Chlorite	26.45	19.39	0.03	0.12	25.98	15.21	87.17
303GC	Altered Muscovite	46.68	35.00	8.89	0.01	2.52	1.05	94.16
303GC	Illite	50.40	26.95	3.98	0.45	4.28	2.54	88.60

Table B.6: Oxide weight percent data for silicate minerals from the Bong deposit, Thelon Basin, Nunavut, Canada

Sample	Mineral	SiO_2	Al_2O_3	K_2O	CaO	FeO	MgO	Total
303GC	Altered Muscovite	47.47	35.73	8.40	0.01	2.00	0.79	94.39
303GC	Illite	52.27	28.91	6.26	0.07	2.66	2.64	92.81
303GC	Altered Muscovite	51.01	36.53	7.49	0.21	1.27	0.72	97.22
303GC	Altered Muscovite	49.18	33.39	8.73	0.04	2.14	1.37	94.85
303GC	Altered Muscovite	47.12	29.32	7.38	0.12	1.70	1.76	87.40
303GC	Altered Muscovite	48.19	32.29	9.25	0.00	2.15	1.42	93.30
303GC	Altered Muscovite	48.24	34.49	8.22	0.02	1.94	0.99	93.90
303GC	Altered Muscovite	48.31	34.63	7.97	0.01	2.05	1.10	94.08
303GC	Altered Muscovite	47.88	33.90	9.16	0.01	2.10	1.13	94.17
303GC	Altered Muscovite	49.21	34.45	7.95	0.05	2.17	0.60	94.43
303GC	Illite	51.92	29.55	6.69	0.30	1.51	2.17	92.15
303GC	Altered Muscovite	47.46	35.77	8.52	0.01	1.73	0.77	94.27
303GC	Illite	51.51	28.63	4.58	0.45	2.05	2.79	90.00
303GC	Illite	49.33	27.12	4.14	0.32	2.34	2.75	85.99
303GC	Altered Muscovite	49.00	33.96	7.18	0.05	1.88	1.33	93.40
303GC	Altered Muscovite	45.20	33.95	7.41	0.05	2.99	0.91	90.51
303GC	Illite	50.00	33.59	5.02	0.11	2.24	1.38	92.34
303GC	Illite	48.58	35.18	5.28	0.09	1.71	0.71	91.55
303GC	Illite	49.72	32.52	6.03	0.12	2.64	1.19	92.22
303GC	Illite	49.64	31.02	4.53	0.21	3.38	1.92	90.69
301GC	Illite	50.14	30.98	4.66	0.19	2.79	1.98	90.73
301GC	Altered Muscovite	47.79	33.59	9.55	0.03	2.70	0.98	94.64
301GC	Illite	49.95	23.68	3.11	0.44	5.10	3.93	86.20
301GC	Illite	48.06	34.49	7.84	0.01	1.62	1.04	93.05
301GC	Illite	51.02	28.78	3.72	0.29	2.62	3.15	89.57
301GC	Altered Muscovite	47.45	34.77	8.76	0.00	1.80	1.04	93.81
301GC	Altered Muscovite	46.87	23.32	7.44	0.44	2.87	3.63	84.58
301GC	Altered Muscovite	50.03	26.53	7.67	0.35	2.16	2.83	89.57
301GC	Illite	49.71	31.26	5.57	0.14	2.41	1.75	90.85
301GC	Illite	50.85	24.58	4.36	0.53	4.77	3.04	88.12
302GC	Illite	49.94	30.43	4.09	0.19	3.55	1.88	90.09
302GC	Illite	50.64	29.74	4.63	0.24	3.90	2.35	91.51
302GC	Altered Muscovite	47.27	33.25	8.82	0.04	1.90	1.26	92.54
302GC	Illite	50.24	32.52	6.83	0.08	2.29	1.77	93.74

Table B.6: Oxide weight percent data for silicate minerals from the Bong deposit, Thelon Basin, Nunavut, Canada

Sample	Mineral	SiO_2	Al_2O_3	K_2O	CaO	FeO	MgO	Total
302GC	Illite	53.30	29.73	3.54	0.33	2.85	2.59	92.33
302GC	Illite	49.68	29.65	5.81	0.19	3.06	2.24	90.61
302GC	Altered Muscovite	45.87	33.72	9.61	0.03	1.81	1.00	92.05
302GC	Altered Muscovite	46.86	33.69	7.07	0.08	1.98	1.21	90.89
302GC	Altered Muscovite	46.52	35.06	9.24	0.02	1.72	1.01	93.56
302GC	Altered Muscovite	47.65	33.27	8.34	0.02	2.13	1.56	92.97
302GC	Altered Muscovite	48.14	33.45	8.39	0.07	1.90	1.36	93.31
302GC	Illite	50.03	28.39	3.86	0.38	3.83	2.20	88.68

Table B.7: Elemental weight percent data for sulphide minerals from the Bong deposit, Thelon Basin, Nunavut, Canada

Sample	Mineral	S	Fe	Ni	Cu	As	Ag	Pb	Au	Total
303GC	Pyrite	53.56	45.36	<DL	0.39	0.06	<DL	0.26	<DL	99.62
303GC	Galena	11.97	0.32	<DL	0.46	<DL	<DL	68.44	<DL	81.18
303GC	Pyrite	53.47	45.01	<DL	0.78	0.06	0.04	0.30	<DL	99.65
303GC	Pyrite	53.55	44.35	<DL	1.03	<DL	<DL	0.26	<DL	99.20
303GC	Pyrite	35.02	30.08	<DL	34.14	<DL	<DL	0.09	<DL	99.33
303GC	Pyrite	53.04	46.01	<DL	0.72	<DL	<DL	0.20	<DL	99.96
303GC	Chalcopyrite	35.04	29.95	<DL	34.11	0.07	<DL	0.10	<DL	99.26
303GC	Pyrite	38.28	32.63	<DL	3.67	<DL	<DL	0.25	<DL	74.82
303GC	Chalcopyrite	30.04	25.50	<DL	29.73	<DL	<DL	0.07	<DL	85.34
303GC	Pyrite	53.33	45.80	<DL	0.86	0.06	<DL	0.10	<DL	100.15
303GC	Pyrite	53.31	45.57	<DL	1.06	0.07	<DL	0.25	<DL	100.25
303GC	Chalcopyrite	35.46	29.13	0.05	33.55	0.07	<DL	0.18	<DL	98.46
303GC	Pyrite	53.43	45.43	<DL	0.83	<DL	<DL	0.29	<DL	99.98
303GC	Chalcopyrite	34.72	28.15	0.07	32.09	<DL	0.04	0.21	<DL	95.27
303GC	Pyrite	48.95	40.26	0.25	<DL	<DL	<DL	0.31	<DL	89.76
303GC	Pyrite	40.13	32.33	0.55	<DL	<DL	0.04	0.87	<DL	73.91
303GC	Pyrite	53.63	44.62	<DL	1.70	<DL	<DL	0.38	<DL	100.33
303GC	Chalcopyrite	35.18	29.09	0.17	32.00	0.08	0.11	0.27	<DL	96.91
303GC	Pyrite	52.95	45.61	<DL	0.42	<DL	<DL	0.38	<DL	99.35
303GC	Chalcopyrite	31.65	25.96	0.18	30.53	<DL	0.08	0.15	<DL	88.54
303GC	Pyrite	53.53	45.67	<DL	0.66	0.11	<DL	0.29	<DL	100.26
303GC	Pyrite	53.50	45.49	<DL	0.58	<DL	<DL	0.57	<DL	100.15
301GC	Pyrite	53.88	46.32	<DL	<DL	0.07	<DL	0.12	<DL	100.39
301GC	Pyrite	52.77	45.44	<DL	<DL	0.07	<DL	0.19	<DL	98.46
301GC	Pyrite	53.49	45.87	<DL	<DL	0.08	<DL	0.21	<DL	99.65
301GC	Pyrite	53.21	46.06	<DL	<DL	<DL	<DL	0.59	<DL	99.86
301GC	Pyrite	47.66	41.29	<DL	<DL	<DL	<DL	0.26	<DL	89.21
301GC	Pyrite	53.22	45.28	<DL	<DL	<DL	<DL	0.19	<DL	98.69
301GC	Pyrite	53.85	45.86	<DL	0.04	<DL	0.04	0.52	<DL	100.30
301GC	Pyrite	52.76	45.82	<DL	<DL	<DL	<DL	0.83	<DL	99.42
301GC	Pyrite	54.03	45.55	<DL	<DL	0.07	<DL	0.13	<DL	99.77
301GC	Pyrite	53.46	45.30	<DL	<DL	0.07	<DL	0.58	<DL	99.40
301GC	Pyrite	53.64	45.49	<DL	<DL	0.07	<DL	0.17	<DL	99.37
301GC	Pyrite	53.47	45.72	<DL	<DL	<DL	<DL	0.07	<DL	99.26

Table B.7: Elemental weight percent data for sulphide minerals from the Bong deposit, Thelon Basin, Nunavut, Canada

Sample	Mineral	S	Fe	Ni	Cu	As	Ag	Pb	Au	Total
301GC	Pyrite	53.67	46.05	<DL	<DL	<DL	<DL	0.15	<DL	99.88
301GC	Pyrite	53.49	46.25	<DL	<DL	<DL	<DL	0.14	<DL	99.88
301GC	Pyrite	53.45	46.10	<DL	<DL	<DL	<DL	0.25	<DL	99.80
301GC	Pyrite	53.58	45.68	<DL	0.08	<DL	<DL	0.72	<DL	100.05
302GC	Pyrite	49.97	42.87	<DL	0.58	0.06	<DL	0.16	<DL	93.65
302GC	Pyrite	53.53	45.70	<DL	0.72	<DL	<DL	0.19	<DL	100.14
302GC	Chalcopyrite	35.02	29.14	<DL	33.21	0.08	<DL	0.11	<DL	97.57
302GC	Chalcopyrite	34.03	27.68	0.11	31.09	<DL	<DL	0.27	<DL	93.18
302GC	Pyrite	52.91	45.16	<DL	0.97	0.04	<DL	0.18	<DL	99.26
302GC	Pyrite	53.40	45.65	<DL	0.51	<DL	<DL	0.18	<DL	99.74
302GC	Chalcopyrite	25.52	21.20	<DL	25.00	<DL	<DL	0.25	<DL	71.96
302GC	Chalcopyrite	26.71	21.41	<DL	26.34	0.06	<DL	0.23	<DL	74.75
302GC	Pyrite	53.61	45.43	0.04	0.81	<DL	<DL	0.16	<DL	100.05
302GC	Pyrite	51.85	44.71	<DL	2.23	0.06	<DL	0.22	<DL	99.06
302GC	Pyrite	53.40	45.46	<DL	0.94	<DL	<DL	0.34	<DL	100.13
302GC	Chalcopyrite	34.88	29.24	<DL	33.93	0.08	<DL	0.17	<DL	98.30
302GC	Chalcopyrite	28.18	26.90	0.04	31.30	<DL	<DL	0.27	<DL	86.69
302GC	Chalcopyrite	35.07	29.71	0.04	33.92	<DL	<DL	0.24	<DL	98.98
302GC	Pyrite	52.80	44.86	<DL	0.63	<DL	<DL	0.38	<DL	98.66
302GC	Pyrite	51.84	43.50	0.04	0.66	<DL	0.06	0.39	<DL	96.50

Appendix C
Illite Mineral Chemical Compositions and Temperatures of Formation

Table C.1: Compositions and temperatures of formation of illite from the Bong deposit, Thelon Basin, Nunavut, Canada

Sample	303GC	303GC	303GC	303GC	303GC	303GC	303GC	303GC	303GC	301GC	301GC	301GC
Mineral	Illite	Illite	Illite	Illite	Illite	Illite	Illite	Illite	Illite	Illite	Illite	Illite
SiO_2	52.27	51.51	50.40	49.33	50.00	48.58	51.92	49.72	49.64	50.14	49.95	48.06
Al_2O_3	28.91	28.63	26.95	27.12	33.59	35.18	29.55	32.52	31.02	30.98	23.68	34.49
FeO	2.66	2.05	4.28	2.34	2.24	1.71	1.51	2.64	3.38	2.79	5.10	1.62
MgO	2.64	2.79	2.54	2.75	1.38	0.71	2.17	1.19	1.92	1.98	3.93	1.04
CaO	0.07	0.45	0.45	0.32	0.11	0.09	0.30	0.12	0.21	0.19	0.44	0.01
K_2O	6.26	4.58	3.98	4.14	5.02	5.28	6.69	6.03	4.53	4.66	3.11	7.84
Total	92.81	90.00	88.60	85.99	92.34	91.55	92.15	92.22	90.69	90.73	86.20	93.05
Fe	0.1474	0.1156	0.2481	0.1381	0.1239	0.0953	0.0841	0.1471	0.1906	0.1571	0.3038	0.0902
Mg	0.2612	0.2807	0.2622	0.2895	0.1359	0.0705	0.2156	0.1185	0.1929	0.1985	0.4175	0.1032
K	0.5294	0.3948	0.3518	0.3735	0.4223	0.4479	0.5685	0.5132	0.3904	0.3995	0.2830	0.6666
Temp (°C)	204	182	130	172	148	158	219	177	137	150	138	214

Sample	301GC	301GC	301GC	302GC	302GC	302GC	302GC	302GC	302GC	-	-	Average
Mineral	Illite	Illite	Illite	Illite	Illite	Illite	Illite	Illite	Illite	-	-	Illite
SiO_2	51.02	49.71	50.85	49.94	50.64	50.24	53.30	49.68	50.03	-	-	**50.33**
Al_2O_3	28.78	31.26	24.58	30.43	29.74	32.52	29.73	29.65	28.39	-	-	**29.89**
FeO	2.62	2.41	4.77	3.55	3.90	2.29	2.85	3.06	3.83	-	-	**2.93**
MgO	3.15	1.75	3.04	1.88	2.35	1.77	2.59	2.24	2.20	-	-	**2.19**
CaO	0.29	0.14	0.53	0.19	0.24	0.08	0.33	0.19	0.38	-	-	**0.24**
K_2O	3.72	5.57	4.36	4.09	4.63	6.83	3.54	5.81	3.86	-	-	**4.98**
Total	89.57	90.85	88.12	90.09	91.51	93.74	92.33	90.61	88.68	-	-	**90.56**
Fe	0.1483	0.1358	0.2797	0.2010	0.2190	0.1262	0.1558	0.1740	0.2207	-	-	**0.1668**
Mg	0.3176	0.1761	0.3172	0.1904	0.2356	0.1739	0.2524	0.2271	0.2256	-	-	**0.2220**
K	0.3211	0.4796	0.3898	0.3540	0.3965	0.5742	0.2958	0.5042	0.3390	-	-	**0.4283**
Temp (°C)	163	171	146	129	142	198	137	181	124	-	-	**163**

Appendix D
Iron Speciation Data

Table D.1: Whole rock fusion ICP-MS and ferrous iron titration results from core samples from the Bong Deposit, Thelon Basin, Nunavut, Canada

Analyte Symbol	SiO_2	Al_2O_3	Fe_2O_3-calc	MnO	MgO	CaO	Na_2O	K_2O	TiO_2	P_2O_5	LOI	LOI2	Total 2	Total	FeO	Fe_2O_3-Total
Unit Symbol	%	%	%	%	%	%	%	%	%	%	%	%	%	%	%	%
Detection Limit	0.01	0.01	0.01	0.001	0.01	0.01	0.01	0.01	0.001	0.01			0.01	0.01	0.01	0.01
Analysis Method	FUS-ICP	FUS-ICP	CALC	FUS-ICP	FUS-ICP	FUS-ICP	FUS-ICP	FUS-ICP	FUS-ICP	FUS-ICP	FUS-ICP	FUS-ICP	FUS-ICP	FUS-ICP	TITR	FUS-ICP
RS-11-003	98.21	1.18	< 0.01	0.005	0.07	0.06	0.03	0.35	0.025	< 0.01	0.31	0.28	100.4	100.5	0.21	0.21
RS-11-005	95.78	1.59	0.32	0.003	0.06	0.04	0.03	0.48	0.037	0.04	0.29	0.26	98.93	98.96	0.25	0.57
RS-11-007	95.23	1.91	0.11	0.004	0.06	0.03	0.04	0.56	0.047	< 0.01	0.3	0.28	98.52	98.54	0.21	0.32
RS-11-009	96.73	2.14	0.25	0.006	0.14	0.05	0.04	0.62	0.059	0.03	0.41	0.36	100.9	101	0.45	0.70
RS-11-011	96.04	0.97	< 0.01	0.006	0.09	0.05	0.02	0.23	0.027	< 0.01	0.25	0.14	98.47	98.58	0.97	0.97
RS-11-013	78.03	12.13	0.76	0.011	0.65	0.07	0.08	5.55	0.084	< 0.01	2.2	2.14	100.1	100.2	0.56	1.32
RS-11-015	68.17	16.2	1.61	0.075	0.56	0.87	0.05	4.97	0.459	0.61	4.18	4.12	98.29	98.35	0.54	2.15
RS-11-017	69.12	14.5	0.65	0.042	1.93	0.63	2.25	4.8	0.383	0.12	2.58	2.28	99.64	99.93	2.63	3.28
RS-11-019	62.97	15.49	1.01	0.091	1.98	3.22	2.19	3.35	0.537	0.17	3.95	3.36	100.2	100.8	5.23	6.24
RS-11-034	66.43	14.43	< 0.01	0.076	1.69	2.83	3.63	1.93	0.421	0.14	3.51	3.06	98.93	99.37	3.95	3.95
RS-11-036	73.14	12.86	0.38	0.049	1.36	0.76	2.96	2.87	0.349	0.11	1.95	1.62	99.76	100.1	2.98	3.36
RS-11-038	55.28	20.15	0.85	0.092	2.32	2.97	4.63	4.05	0.555	0.16	4.13	3.65	99.48	99.96	4.29	5.14
RS-11-040	65.64	15.76	0.24	0.085	2.28	1.9	4.17	1.9	0.469	0.15	2.59	2.01	100.4	101	5.19	5.43
RS-11-042	68.29	14.39	0.04	0.054	1.51	2.16	3.85	2.1	0.391	0.12	2.82	2.44	99.1	99.48	3.37	3.41
RS-11-044	68.48	15.48	0.49	0.045	1.31	1.1	4.87	2.13	0.376	0.12	1.6	1.23	99.24	99.6	3.25	3.74
RS-11-046	60.17	14.34	1.81	0.13	3.17	2.05	2.1	2.71	0.473	0.17	2	0.97	98.35	99.39	9.23	11.04
RS-11-048	67.68	14.33	0.66	0.051	1.26	2.85	3.22	3.74	0.371	0.1	2.72	2.45	99.39	99.65	2.4	3.06
RS-11-050	48.59	14.82	1.32	0.125	6.92	4.1	0.47	5.53	2.886	1.42	6.37	5.55	99.82	100.6	7.28	8.60
RS-11-052	66.39	16.31	0.96	0.065	1.69	2.01	3.34	2.86	0.438	0.12	2.61	2.23	100.1	100.5	3.33	4.29
RS-11-054	66.4	15.06	0.52	0.071	1.64	2.76	3.73	2.42	0.439	0.13	2.87	2.48	99.47	99.85	3.43	3.95
RS-11-056	58.51	19.79	0.46	0.081	2.44	1.57	2.64	4.41	0.677	0.17	3.37	2.78	99.44	100	5.31	5.77
RS-11-058	58.83	19.42	0.67	0.091	1.99	2.74	3.84	3.32	0.558	0.19	2.19	1.59	99.23	99.84	5.41	6.08
RS-11-060	69.58	15.09	0.43	0.047	1.17	1.56	3.61	2.29	0.396	0.1	1.48	1.17	98.54	98.85	2.78	3.21
RS-11-062	66.76	13.76	< 0.01	0.073	3	2.2	3.42	1.91	0.468	0.13	3.29	2.77	99.59	100.1	4.72	4.72
RS-11-064	58.21	12.68	2.36	0.087	2.31	5.37	1.76	7.34	0.658	0.79	4.25	3.95	98.56	98.87	2.75	5.11
RS-11-066	66.01	15.12	0.44	0.07	2.97	2.57	3.51	2.38	0.488	0.15	1.95	1.44	100.2	100.7	4.56	5.00

Table D.1: Whole rock fusion ICP-MS and ferrous iron titration results from core samples from the Bong Deposit, Thelon Basin, Nunavut, Canada

Analyte Symbol	SiO_2	Al_2O_3	Fe_2O_3-calc	MnO	MgO	CaO	Na_2O	K_2O	TiO_2	P_2O_5	LOI	LOI2	Total 2	Total	FeO	Fe_2O_3-total
Unit Symbol	%	%	%	%	%	%	%	%	%	%	%	%	%	%	%	%
Detection Limit	0.01	0.01	0.01	0.001	0.01	0.01	0.01	0.01	0.001	0.01			0.01	0.01	0.01	0.01
Analysis Method	FUS-ICP	FUS-ICP	CALC	FUS-ICP	FUS-ICP	FUS-ICP	FUS-ICP	FUS-ICP	FUS-ICP	FUS-ICP	FUS-ICP	FUS-ICP	FUS-ICP	FUS-ICP	TITR	FUS-ICP
RS-11-081	75.14	12.79	0.67	0.019	0.71	0.46	0.13	7.89	0.083	< 0.01	1.92	1.9	99.95	99.97	0.13	0.80
RS-11-083	77.06	12.87	1.37	0.007	0.57	0.08	0.26	4	0.4	0.03	2.14	2.12	98.94	98.96	0.17	1.54
RS-11-085	68.69	15.97	1.42	0.034	2.79	0.27	0.12	4.27	0.463	0.16	4.28	4.04	100.7	100.9	2.21	3.63
RS-11-087	65.36	16.03	0.67	0.046	1.62	2.97	2.5	4.29	0.342	0.12	3.93	3.7	99.88	100.1	2.01	2.68
RS-11-089	57.74	12.23	0.3	0.077	6.81	3.01	0.14	6.54	1.208	1.44	4.67	4.22	98.12	98.56	3.97	4.27
RS-11-091	71.79	16.01	1.32	0.026	1.25	0.16	0.18	4.63	0.281	0.09	2.66	2.53	99.56	99.69	1.16	2.48
RS-11-093	67.18	13.73	0.33	0.094	2.99	1.93	1.45	4.37	0.395	0.13	5.03	4.7	100.6	101	2.99	3.32
RS-11-095	67.72	13.86	0.37	0.081	1.85	2.6	3.92	1.6	0.435	0.13	2.79	2.36	99.2	99.63	3.84	4.21
RS-11-097	70.67	14.45	1.07	0.034	2.78	0.42	0.09	4.79	0.268	0.06	3.33	3.14	99.68	99.87	1.7	2.77
RS-11-099	67.64	14.19	0.26	0.073	2.39	0.65	3.31	2.51	0.463	0.14	2.61	2.13	98.52	98.99	4.27	4.53
RS-11-101	57.69	18.87	1.35	0.056	4.01	1.07	0.3	5.14	0.632	0.19	5.46	4.98	99.08	99.56	4.3	5.65
RS-11-103	71.85	13.42	1.07	0.027	2.36	0.24	0.06	4.05	0.421	0.13	3.02	2.76	98.98	99.24	2.34	3.41
RS-11-113	67.99	14.61	< 0.01	0.04	2.62	0.82	0.06	5.67	0.377	0.13	4.24	3.88	99.68	100	3.18	3.18
RS-11-115	64.88	13.84	0.73	0.062	4.31	1.84	0.04	4.6	0.363	0.11	5.91	5.66	98.97	99.23	2.29	3.02
RS-11-117	48.11	17.78	0.84	0.11	6.8	4.24	0.06	6.23	0.517	0.16	10.44	10.05	98.74	99.12	3.45	4.29
RS-11-119	66.07	11.6	0.32	0.084	3.95	2.47	0.06	4.96	0.344	0.11	6.28	5.97	99.04	99.36	2.79	3.11
RS-11-121	72.22	16.69	< 0.01	0.005	1.49	0.28	0.03	5.09	0.501	0.15	3.6	3.54	100.6	100.6	0.49	0.49
RS-11-123	37.96	16.4	0.72	0.038	1.44	18.11	0.05	5.19	0.586	0.21	16.81	16.71	98.41	98.51	0.89	1.61
RS-11-125	70.78	16.6	0.88	0.015	2.2	0.36	0.05	5.01	0.473	0.13	4.02	3.97	100.9	101	0.41	1.29
RS-11-127	65.23	16.59	0.87	0.017	4.29	0.39	0.05	3.92	0.516	0.14	4.88	4.57	99.68	100	2.79	3.66
RS-11-129	46.83	30.08	0.74	0.011	3.49	0.3	0.14	8.49	1.228	0.11	7.02	6.95	99.06	99.12	0.62	1.36
RS-11-131	69.41	17.58	0.17	0.012	2	0.52	0.14	5	0.547	0.12	4.34	4.23	100.8	100.9	0.94	1.11
RS-11-133	42.78	27.24	0.77	0.022	8.35	0.65	0.07	5.65	0.694	0.32	10.76	10.64	98.39	98.51	1.07	1.84
RS-11-135	70.47	12.34	0.23	0.04	4.77	0.25	0.02	3.04	0.448	0.09	3.73	3.28	99.48	99.94	4.06	4.29

Table D.2: Calculated molar percent Fe^{2+} and Fe^{3+} data, and Fe^{2+}/Fe^{3+} ratios for core samples from hole BONG-49, Thelon Basin, Nunavut, Canada

Lithology	Sample	Fe_2O_3-total	Fe_2O_3-calc	FeO	Ratio	Mol % Fe^{2+}	Mol % Fe^{3+}	Fe^{2+}/Fe^{3+}	Depth (m)
Qtz eye gneiss	RS-11-003	0.21	<DL	0.21	N/A	N/A	N/A	N/A	3
Qtz eye gneiss	RS-11-005	0.57	0.32	0.25	0.78	0.19	0.22	0.87	23
Qtz eye gneiss	RS-11-007	0.32	0.11	0.21	1.91	0.16	0.08	2.12	43
Qtz eye gneiss	RS-11-009	0.70	0.25	0.45	1.80	0.35	0.17	2.00	63
Qtz eye gneiss	RS-11-011	0.97	<DL	0.97	N/A	N/A	N/A	N/A	83
Qtz eye gneiss	RS-11-013	1.32	0.76	0.56	0.74	0.44	0.53	0.82	103
Qtz eye gneiss	RS-11-015	2.15	1.61	0.54	0.34	0.42	1.13	0.37	123
Metasediments	RS-11-017	3.28	0.65	2.63	4.05	2.04	0.45	4.50	143
Metasediments	RS-11-019	6.24	1.01	5.23	5.18	4.07	0.71	5.75	163
Metasediments	RS-11-034	3.95	<DL	3.95	N/A	N/A	N/A	N/A	183
Metasediments	RS-11-036	3.36	0.38	2.98	7.84	2.32	0.27	8.72	203
Metasediments	RS-11-038	5.14	0.85	4.29	5.05	3.33	0.59	5.61	223
Metasediments	RS-11-040	5.43	0.24	5.19	21.63	4.03	0.17	24.03	243
Metasediments	RS-11-042	3.41	0.04	3.37	84.25	2.62	0.03	93.63	263
Metasediments	RS-11-044	3.74	0.49	3.25	6.63	2.53	0.34	7.37	283
Metasediments	RS-11-046	11.04	1.81	9.23	5.10	7.17	1.27	5.67	303
Metasediments	RS-11-048	3.06	0.66	2.40	3.64	1.87	0.46	4.04	323
Metasediments	RS-11-050	8.60	1.32	7.28	5.52	5.66	0.92	6.13	343
Metasediments	RS-11-052	4.29	0.96	3.33	3.47	2.59	0.67	3.85	363
Metasediments	RS-11-054	3.95	0.52	3.43	6.60	2.67	0.36	7.33	383
Metasediments	RS-11-056	5.77	0.46	5.31	11.54	4.13	0.32	12.83	403
Metasediments	RS-11-058	6.08	0.67	5.41	8.07	4.21	0.47	8.97	423
Metasediments	RS-11-060	3.21	0.43	2.78	6.47	2.16	0.30	7.18	443
Metasediments	RS-11-062	4.72	<DL	4.72	N/A	N/A	N/A	N/A	463
Metasediments	RS-11-064	5.11	2.36	2.75	1.17	2.14	1.65	1.30	483
Metasediments	RS-11-066	5.00	0.44	4.56	10.36	3.54	0.31	11.52	503

Table D.3: Calculated molar percent Fe^{2+} and Fe^{3+} data, and Fe^{2+}/Fe^{3+} ratios for core samples from hole BONG-42, Thelon Basin, Nunavut, Canada

Lithology	Sample	Fe_2O_3-total	Fe_2O_3-calc	FeO	Ratio	Mol % Fe^{2+}	Mol % Fe^{3+}	Fe^{2+}/Fe^{3+}	Depth (m)
Qtz eye gneiss	RS-11-081	0.80	0.67	0.13	0.19	0.10	0.47	0.22	9
Qtz eye gneiss	RS-11-083	1.54	1.37	0.17	0.12	0.13	0.96	0.14	29
Metasediments	RS-11-085	3.63	1.42	2.21	1.56	1.72	0.99	1.73	49
Metasediments	RS-11-087	2.68	0.67	2.01	3.00	1.56	0.47	3.33	69
Metasediments	RS-11-089	4.27	0.30	3.97	13.23	3.09	0.21	14.71	89
Metasediments	RS-11-091	2.48	1.32	1.16	0.88	0.90	0.92	0.98	109
Metasediments	RS-11-093	3.32	0.33	2.99	9.06	2.32	0.23	10.07	129
Metasediments	RS-11-095	4.21	0.37	3.84	10.38	2.98	0.26	11.53	149
Metasediments	RS-11-097	2.77	1.07	1.70	1.59	1.32	0.75	1.77	169
Metasediments	RS-11-099	4.53	0.26	4.27	16.42	3.32	0.18	18.25	189
Metasediments	RS-11-101	5.65	1.35	4.30	3.19	3.34	0.94	3.54	209
Metasediments	RS-11-103	3.41	1.07	2.34	2.19	1.82	0.75	2.43	229
Metasediments	RS-11-113	3.18	<DL	3.18	N/A	N/A	N/A	N/A	249
Metasediments	RS-11-115	3.02	0.73	2.29	3.14	1.78	0.51	3.49	269
Metasediments	RS-11-117	4.29	0.84	3.45	4.11	2.68	0.59	4.56	289
Metasediments	RS-11-119	3.11	0.32	2.79	8.72	2.17	0.22	9.69	309
Altered Metased	RS-11-121	0.49	<DL	0.49	N/A	N/A	N/A	N/A	329
Altered Metased	RS-11-123	1.61	0.72	0.89	1.24	0.69	0.50	1.37	349
Altered Metased	RS-11-125	1.29	0.88	0.41	0.47	0.32	0.62	0.52	369
Altered Dyke	RS-11-127	3.66	0.87	2.79	3.21	2.17	0.61	3.56	389
Altered Metased	RS-11-129	1.36	0.74	0.62	0.84	0.48	0.52	0.93	409
Altered Metased	RS-11-131	1.11	0.17	0.94	5.53	0.73	0.12	6.15	429
Altered Metased	RS-11-133	1.84	0.77	1.07	1.39	0.83	0.54	1.54	449
Metasediments	RS-11-135	4.29	0.23	4.06	17.65	3.16	0.16	19.62	469

Appendix E
Secondary Ion Mass Spectrometry (SIMS)

Table E.1: Secondary Ion Mass Spectrometer analyses of mica standard and hydrogen-isotope ratios in illite, altered muscovite, and muscovite from the Bong Deposit, Thelon Basin, Nunavut, Canada

Sample Number	Sample Name	D/H	1σ	Fract. Factor	Mass Bias
3-19h08	MP-Mica Std	4.93321E-05	3.1	0.338726	-661.273757
3-19h09	MP-Mica Std	4.90192E-05	3.1	0.336578	-663.422205
3-19h10	MP-Mica Std	5.05195E-05	3.1	0.346879	-653.120640
Average				0.340728	-659.272201
Standard Deviation				0.005435	5.4

True V-SMOW D/H =1.5576 x 10^{4}

True MP Mica Std D/H = 1.456 x 10^{4}

Sample	Mineral	D/H	1σ	δD V-SMOW (‰)
RS-11-148-1	Illite	5.18421E-05	3.1	-23.2
RS-11-148-2	Illite	4.81789E-05	3.1	-92.2
RS-11-148-3	Illite	5.10362E-05	3.1	-38.4
RS-11-148-4	Illite	5.22907E-05	3.1	-14.7
RS-11-148-5	Illite	4.67184E-05	3.2	-119.7
RS-11-172-1	Illite	4.90836E-05	3.2	-75.1
RS-11-172-2	Illite	4.50744E-05	3.1	-150.7
RS-11-172-3	Illite	4.65441E-05	3.2	-123.0
RS-11-172-4	Illite	4.68245E-05	3.0	-117.7
303GCB-1	Illite	5.03343E-05	3.0	-51.6
303GCB-2	Illite	4.90078E-05	3.0	-76.6
303GCB-3	Illite	4.68798E-05	3.0	-116.7

Sample	Mineral	D/H	1σ	δD V-SMOW (‰)
303GCB-4	Altered Muscovite	4.76805E-05	3.1	-101.6
303GCB-5	Altered Muscovite	4.97025E-05	3.1	-63.5
RS-11-172-5	Altered Muscovite	4.64119E-05	3.2	-125.5
RS-11-172-6	Altered Muscovite	4.76933E-05	3.1	-101.3
RS-11-172-7	Altered Muscovite	4.96028E-05	3.2	-65.4
RS-11-172-8	Altered Muscovite	5.00576E-05	3.2	-56.8
RS-11-172-9	Altered Muscovite	4.81139E-05	3.2	-93.4

Table E.1: Secondary Ion Mass Spectrometer analyses of mica standard and hydrogen-isotope ratios in illite, altered muscovite, and muscovite from the Bong Deposit, Thelon Basin, Nunavut, Canada

Sample Number	Sample Name	D/H	1σ	Fract. Factor	Mass Bias
3-20H01	MP-Mica Std	4.87227E-05	3.1	0.334542	-665.457979
3-20H02	MP-Mica Std	4.92862E-05	3.1	0.338411	-661.589055
3-20H03	MP-Mica Std	4.9814E-05	3.0	0.342035	-657.964913
3-20H04	MP-Mica Std	4.94934E-05	3.1	0.339834	-660.166094
Average				0.338705	-661.294510
Standard Deviation				0.003151	3.2

True V-SMOW D/H =1.5576 x 10^4

True MP Mica Std D/H = 1.456 x 10^4

Sample	Mineral	D/H	1σ	δD V-SMOW (‰)
RS-068A-1	Muscovite	5.11864E-05	3.1	-29.8
RS-068A-2	Muscovite	4.92398E-05	3.1	-66.7
RS-068C-1	Muscovite	4.97031E-05	3.2	-57.9
RS-068C-2	Muscovite	5.08202E-05	3.1	-36.7
RS-068C-3	Muscovite	4.90922E-05	3.2	-69.5
RS-068B-1	Muscovite	5.04917E-05	3.2	-42.9
RS-068B-2	Muscovite	4.98192E-05	3.2	-55.7
RS-068B-3	Muscovite	5.06194E-05	4.2	-40.5

Table E.2: Secondary Ion Mass Spectrometer analyses of mica standard and oxygen-isotope ratios in illite, altered muscovite, and muscovite from the Bong Deposit, Thelon Basin, Nunavut, Canada

Sample Number	Sample Name	$^{18}O/^{16}O_{measured}$	Mass Bias	1σ	$\delta^{18}O$ V-SMOW (‰)
3-4o_Mica_MP-3	MP Mica Std	1.875482	0.928824	1.2	-71.2
3-4o_Mica_MP-4	MP Mica Std	1.874713	0.928443	1.2	-71.6
3-4o_Mica_MP-5	MP Mica Std	1.873015	0.927603	1.2	-72.4
3-4o_Mica_MP-6	MP Mica Std	1.876642	0.929399	1.2	-70.6
Average		1.875582	0.928874	1.2	-71.1
Standard Deviation		0.001710			0.8
Instrumental Mass Fractionation					1.862578

True V-SMOW $^{18}O/^{16}O$ = 2.0052

True MP Mica Std $^{18}O/^{16}O$ = 2.0192

Sample Number	Mineral	$^{18}O/^{16}O_{measured}$	1σ	$\delta^{18}O$ V-SMOW (‰)
RS-142-1	Altered Muscovite	1.880614	1.3	9.7
RS-142-2	Altered Muscovite	1.874181	1.3	6.2
RS-142-3	Altered Muscovite	1.866621	1.3	2.2
RS-142-4	Altered Muscovite	1.868440	1.3	3.1
RS-142-5	Altered Muscovite	1.860276	1.3	-1.2
RS-142-6	Altered Muscovite	1.869487	1.3	3.7
RS-142-7	Altered Muscovite	1.864186	1.3	0.9
RS-142-8	Altered Muscovite	1.858210	1.3	-2.3
RS-142-9	Altered Muscovite	1.867860	1.2	2.8
RS-142-10	Altered Muscovite	1.869175	1.3	3.5
RS-142-11	Altered Muscovite	1.866924	1.3	2.3

Sample Number	Mineral	$^{18}O/^{16}O_{measured}$	1σ	$\delta^{18}O$ V-SMOW (‰)
RS-147-1	Illite	1.847027	1.2	-8.3
RS-147-2	Illite	1.848253	1.2	-7.7
RS-147-3	Illite	1.855177	1.2	-4.0
RS-147-4	Illite	1.853247	1.2	-5.0
RS-147-5	Illite	1.854076	1.2	-4.6
RS-147-6	Illite	1.845548	1.3	-9.1
RS-147-7	Illite	1.872723	1.3	5.4
RS-147-8	Illite	1.869527	1.3	3.7
RS-147-9	Illite	1.864087	1.3	0.8
RS-147-10	Illite	1.856375	1.3	-3.3

Table E.2: Secondary Ion Mass Spectrometer analyses of mica standard and oxygen-isotope ratios in illite, altered muscovite, and muscovite from the Bong Deposit, Thelon Basin, Nunavut, Canada

Sample Number	Sample Name	$^{18}O/^{16}O_{measured}$	Mass Bias	1σ	$\delta^{18}O$ V-SMOW (‰)
6-5o_Mica_MP-2	MP Mica Std	1.856111	0.919231	1.2	-80.8
6-5o_Mica_MP-3	MP Mica Std	1.861757	0.922027	1.3	-78.0
6-5o_Mica_MP-4	MP Mica Std	1.856979	0.919661	1.2	-80.3
Average		1.858282	0.920306	1.2	-79.7
Standard Deviation		0.002482			1.2
Instrumental Mass Fractionation					1.845398

True V-SMOW $^{18}O/^{16}O$ = 2.0052

True MP Mica Std $^{18}O/^{16}O$ = 2.0192

Sample Number	Mineral	$^{18}O/^{16}O_{measured}$	1σ	$\delta^{18}O$ V-SMOW (‰)
RS-136-1	Muscovite	1.874684	1.3	15.9
RS-136-2	Muscovite	1.866337	1.2	11.3
RS-136-3	Muscovite	1.861612	1.2	8.8
RS-136-4	Muscovite	1.859636	1.3	7.7
RS-136-5	Muscovite	1.869725	1.3	13.2
RS-136-6	Muscovite	1.869984	1.2	13.3
RS-136-7	Muscovite	1.855123	1.2	5.3
RS-136-8	Muscovite	1.859524	1.2	7.7
RS-136-9	Muscovite	1.860114	1.3	8.0
RS-136-10	Muscovite	1.859758	1.2	7.8

Table E.3: Secondary Ion Mass Spectrometer analyses of UO_2 standard and oxygen-isotope ratios in uraninite from the Bong Deposit, Thelon Basin, Nunavut, Canada

Sample Number	Sample Name	$^{18}O/^{16}O_{measured}$	Mass Bias	1σ	$\delta^{18}O$ V-SMOW (‰)
4-11o-UO2-std-1	UO_2 std	1.904645	0.942222	1.1	-57.8
4-11o-UO2-std-2	UO_2 std	1.907025	0.943399	1.3	-56.6
4-11o-UO2-std-3	UO_2 std	1.906081	0.942932	1.2	-57.1
4-11o-UO2-std-5	UO_2 std	1.904586	0.942193	1.2	-57.8
Average		1.906466	0.942771	1.2	-57.3
Standard Deviation		0.001822			0.5
Instrumental Mass Fractionation					1.890275

True V-SMOW $^{18}O/^{16}O = 2.0052$

True UO_2 Std $^{18}O/^{16}O = 2.02144$

Sample Number	Mineral	$^{18}O/^{16}O_{measured}$	1σ	$\delta^{18}O$ V-SMOW (‰)
RS-143BO-1	Vein Uraninite	1.855572	1.2	-18.4
RS-143BO-2	Vein Uraninite	1.846531	1.2	-23.2
RS-143BO-3	Vein Uraninite	1.840645	1.2	-26.3
RS-143BO-4	Vein Uraninite	1.853023	1.2	-19.8
303GCO-1	Vein Uraninite	1.858671	1.2	-16.8
303GCO-2	Vein Uraninite	1.867876	1.2	-11.9
303GCO-3	Vein Uraninite	1.857581	1.2	-17.4
303GCO-4	Vein Uraninite	1.890157	1.2	-0.2
RS-143AO-1	Vein Uraninite	1.887129	1.2	-1.8
RS-143AO-2	Vein Uraninite	1.897731	1.2	3.9
RS-143AO-3	Vein Uraninite	1.890989	1.2	0.3
RS-143AO-4	Vein Uraninite	1.882809	1.2	-4.0
RS-143BO-5	Vein Uraninite	1.854619	1.2	-19.0
RS-143BO-6	Vein Uraninite	1.845956	1.2	-23.5
RS-172O-1	Vein Uraninite	1.878906	1.2	-6.1
RS-172O-2	Vein Uraninite	1.865603	1.2	-13.1
RS-172O-3	Vein Uraninite	1.858387	1.2	-17.0
RS-172O-4	Vein Uraninite	1.853578	1.2	-19.5
RS-172O-5	Vein Uraninite	1.866251	1.2	-12.8
RS-172O-6	Vein Uraninite	1.876478	1.2	-7.4
303GCB-1	Vein Uraninite	1.838614	1.2	-27.4
303GCB-2	Vein Uraninite	1.849991	1.2	-21.4
303GCB-3	Vein Uraninite	1.850111	1.2	-21.3
303GCB-4	Vein Uraninite	1.860268	1.2	-16.0

Table E.3: Secondary Ion Mass Spectrometer analyses of UO_2 standard and oxygen-isotope ratios in uraninite from the Bong Deposit, Thelon Basin, Nunavut, Canada

Sample Number	Sample Name	$^{18}O/^{16}O_{measured}$	Mass Bias	1σ	$\delta^{18}O$ V-SMOW (‰)
4-12o-UO2-std-6	UO_2 std	1.938893	0.959164	1.8	-40.8
4-12o-UO2-std-7	UO_2 std	1.941318	0.960364	1.8	-39.6
4-12o-UO2-std-8	UO_2 std	1.946386	0.962871	1.8	-37.1
4-12o-UO2-std-9	UO_2 std	1.943205	0.961297	1.8	-38.7
Average		1.942451	0.960924	1.8	-39.1
Standard Deviation		0.002738			1.4
Instrumental Mass Fractionation					1.926845

True V-SMOW $^{18}O/^{16}O$ = 2.0052

True UO_2 Std $^{18}O/^{16}O$ = 2.02144

Sample Number	Mineral	$^{18}O/^{16}O_{measured}$	1σ	$\delta^{18}O$ V-SMOW (‰)
RS-176CO-1	Roll Front Uraninite	1.846531	1.2	-41.7
RS-176CO-2	Roll Front Uraninite	1.840645	1.2	-44.7
RS-176CO-3	Roll Front Uraninite	1.853023	1.2	-38.3
RS-176CO-4	Roll Front Uraninite	1.858671	1.2	-35.4
RS-176CO-5	Roll Front Uraninite	1.867876	1.2	-30.6
RS-176CO-6	Roll Front Uraninite	1.857581	1.2	-35.9

Table E.4: Secondary Ion Mass Spectrometer analyses of UO_2 standard and uranium- & lead-isotope ratios in uraninite from the Bong Deposit, Thelon Basin, Nunavut, Canada

Sample Number	Sample Name	$^{206}Pb/^{204}Pb$	$^{207}Pb/^{206}Pb$	$^{206}Pb/^{238}U$	$^{207}Pb/^{235}U$
3-21U-TKK-1	UO_2 Standard	211806.3	0.073175	0.257521	2.497715
3-21U-TKK-2	UO_2 Standard	252756.2	0.073555	0.264483	2.577013
3-21U-TKK-3	UO_2 Standard	223706.4	0.073654	0.262420	2.568518
3-21U-TKK-4	UO_2 Standard	247933.9	0.073381	0.256718	2.492726
Average		234050.7	0.073441	0.260286	2.533993
True Value		684261.2	0.073382	0.170120	1.721285
Fractionation Factor		0.342049	1.000802	1.530011	1.472152

Sample Number	Mineral	$^{206}Pb/^{204}Pb$	$^{207}Pb/^{206}Pb$	$^{206}Pb/^{238}U$	$^{207}Pb/^{235}U$
RS-172U-1	Vein uraninite	4374.1	0.067102	0.009673	0.088511
RS-172U-2	Vein uraninite	16117.5	0.060535	0.007777	0.065094
RS-172U-3	Vein uraninite	14320.4	0.057965	0.007053	0.056196
RS-172U-4	Vein uraninite	22228.6	0.074258	0.018907	0.193318
303GCBU-1	Vein uraninite	25077.2	0.077363	0.106219	1.135763
303GCBU-2	Vein uraninite	101757.5	0.076421	0.114861	1.211645
303GCBU-3	Vein uraninite	33583.1	0.076651	0.093887	0.997500
303GCBU-4	Vein uraninite	42171.6	0.077155	0.075290	0.800796
RS-143BU-1	Vein uraninite	11108.9	0.074921	0.069363	0.714811
RS-143BU-2	Vein uraninite	95213.6	0.074804	0.141238	1.446595
RS-143BU-3	Vein uraninite	28728.3	0.075452	0.123795	1.293021
RS-143BU-4	Vein uraninite	23019.3	0.076161	0.082667	0.870503
RS-143AU-1	Vein uraninite	4399.6	0.077710	0.021926	0.235402
RS-143AU-2	Vein uraninite	12916.0	0.076536	0.068749	0.726475
RS-143AU-3	Vein uraninite	8027.8	0.078001	0.056707	0.610678
RS-143AU-4	Vein uraninite	9936.8	0.079183	0.058765	0.639219
303GCAU-1	Vein uraninite	108050.9	0.071683	0.109163	1.075189
303GCAU-2	Vein uraninite	12494.3	0.077785	0.056609	0.607590
303GCAU-3	Vein uraninite	39742.6	0.074172	0.082463	0.844106

Errors associated with measurements are <10% for 206Pb/204Pb and <1% for 207Pb/206Pb, 206Pb/238U & 207Pb/235U

Table E.4: Secondary Ion Mass Spectrometer analyses of UO_2 standard and uranium- & lead-isotope ratios in uraninite from the Bong Deposit, Thelon Basin, Nunavut, Canada

Sample Number	Sample Name	$^{206}Pb/^{204}Pb$	$^{207}Pb/^{206}Pb$	$^{206}Pb/^{238}U$	$^{207}Pb/^{235}U$
3-22U-LA-MNH-1	UO_2 Standard	66910.68	0.053945	0.049466	0.353673
3-22U-LA-MNH-2	UO_2 Standard	66673.44	0.053550	0.049396	0.351990
3-22U-LA-MNH-3	UO_2 Standard	57334.60	0.054683	0.052560	0.381998
3-22U-LA-MNH-4	UO_2 Standard	58379.73	0.054677	0.049335	0.355192
Average		62324.61	0.054214	0.050189	0.360713
True Value		50000.00	0.053807	0.002607	0.055333
Fractionation Factor		1.246492	1.007562	0.907034	0.879074

Sample Number	Mineral	$^{206}Pb/^{204}Pb$	$^{207}Pb/^{206}Pb$	$^{206}Pb/^{238}U$	$^{207}Pb/^{235}U$
RS-176BU-1	Roll-front uraninite	656.37	0.073090	0.012122	0.125008
RS-176BU-2	Roll-front uraninite	739.26	0.077452	0.006251	0.068383
RS-176BU-3	Roll-front uraninite	227.34	0.081231	0.001602	0.018675
RS-176BU-4	Roll-front uraninite	1166.69	0.072789	0.007760	0.078485
RS-176BU-5	Roll-front uraninite	77.89	0.085156	0.000711	0.008309
RS-176CU-1	Roll-front uraninite	149.84	0.076476	0.000828	0.009275
RS-176CU-2	Roll-front uraninite	55.24	0.111329	0.000246	0.003803
RS-176CU-3	Roll-front uraninite	221.42	0.098542	0.001191	0.015363
RS-176CU-4	Roll-front uraninite	238.72	0.089376	0.001242	0.014770

Errors associated with measurements are <20% for 206Pb/204Pb and <10% for 207Pb/206Pb, 206Pb/238U & 207Pb/235U

Table E.4: Secondary Ion Mass Spectrometer analyses of UO_2 standard and uranium- & lead-isotope ratios in uraninite from the Bong Deposit, Thelon Basin, Nunavut, Canada

Sample Number	Sample Name	$^{206}Pb/^{204}Pb$	$^{207}Pb/^{206}Pb$	$^{206}Pb/^{238}U$	$^{207}Pb/^{235}U$
3-30U-LA-MNH-4	UO_2 Standard	93237.95	0.053897	232.016000	0.073694
3-30U-LA-MNH-5	UO_2 Standard	87405.82	0.054123	205.288800	0.073787
3-30U-LA-MNH-6	UO_2 Standard	90573.04	0.053916	209.583600	0.069781
3-30U-LA-MNH-7	UO_2 Standard	100514.80	0.053481	259.038900	0.072604
Average		92932.90	0.053854	226.481825	0.072466
True Value		50000.00	0.053807	0.002607	0.055333
Fractionation Factor		1.858658	1.000883	1.309635	1.260936

Sample Number	Mineral	$^{206}Pb/^{204}Pb$	$^{207}Pb/^{206}Pb$	$^{206}Pb/^{238}U$	$^{207}Pb/^{235}U$
RS-176BU-6	Roll-front uraninite	497.13	0.075778	0.003280	0.034553
RS-176BU-7	Roll-front uraninite	136.69	0.062491	0.000783	0.006678
RS-176BU-8	Roll-front uraninite	135.22	0.088272	0.000694	0.008181
RS-176BU-9	Roll-front uraninite	53.95	0.093805	0.000463	0.006068
RS-176BU-10	Roll-front uraninite	676.68	0.076740	0.003267	0.035390
RS-176BU-11	Roll-front uraninite	202.36	0.088203	0.000921	0.011236
RS-176BU-12	Roll-front uraninite	392.05	0.076192	0.001799	0.019022
RS-176BU-13	Roll-front uraninite	168.87	0.087329	0.000962	0.011551
RS-176CU-5	Roll-front uraninite	89.71	0.086048	0.000610	0.007537
RS-176CU-6	Roll-front uraninite	353.61	0.086879	0.001767	0.021218
RS-176CU-7	Roll-front uraninite	23.11	0.104138	0.000168	0.002470
RS-176CU-8	Roll-front uraninite	123.17	0.085487	0.005676	0.006657
RS-176CU-9	Roll-front uraninite	72.03	0.113322	0.000479	0.007345
RS-176CU-10	Roll-front uraninite	50.78	0.091775	0.000273	0.003419
RS-176CU-11	Roll-front uraninite	316.24	0.084105	0.001887	0.022104
RS-176CU-12	Roll-front uraninite	946.05	0.091344	0.006657	0.084082
RS-176CU-13	Roll-front uraninite	408.88	0.100301	0.002370	0.032902
RS-176CU-14	Roll-front uraninite	660.96	0.085933	0.003389	0.040817
RS-176CU-15	Roll-front uraninite	160.30	0.088728	0.000827	0.010283
RS-176CU-16	Roll-front uraninite	187.02	0.097484	0.001596	0.021676

Errors associated with measurements are <20% for 206Pb/204Pb and <10% for 207Pb/206Pb, 206Pb/238U & 207Pb/235U

Appendix F
Carbon-Isotope Study

Table F.1: Carbon-isotope values from various hydrocarbon samples from the Bong deposit, Thelon Basin, Nunavut, Canada

Sample ID	Sample Description	Weight (mg)	% Carbon	δ^{13}C V-PBD (‰)
RS-11-142	OM associated with roll front	3.505	0.494	-25.5
RS-11-145	OM associated with roll front	10.790	0.206	-27.9
RS-11-159	Unmineralized OM	50.540	0.167	-48.3
RS-11-160	OM associated with roll front	10.370	0.369	-22.2
RS-11-173	Mineralized graphite nodule	0.260	55.150	-39.0
RS-11-190	OM associated with roll front	9.788	0.247	-21.1
RS-11-192	Unmineralized OM	56.013	0.138	-40.2

Abbreviations: OM = Organic matter

Appendix G
Chemical-Pb Ages

Table G.1: Chemical-Pb ages of uranium minerals from the Bong Deposit, Thelon Basin, Nunavut, Canada (U, Pb, and Th data in wt.% from EMPA)

Sample	Mineral	U	Pb	Th	Chemical Pb Age (Ma)
RS-11-172	Uraninite	27.58	3.94	<DL	885
RS-11-172	Altered Uraninite	23.69	0.16	<DL	43
RS-11-172	Altered Uraninite	23.79	0.17	<DL	44
RS-11-172	Uraninite	27.48	3.90	<DL	879
RS-11-172	Uraninite	27.77	3.76	<DL	840
RS-11-172	Altered Uraninite	23.29	0.08	<DL	21
RS-11-172	Altered Uraninite	23.31	<DL	<DL	N/A
RS-11-172	Altered Uraninite	21.16	0.46	<DL	135
RS-11-172	Altered Uraninite	22.96	<DL	<DL	N/A
RS-11-143	Altered Uraninite	20.38	1.02	<DL	309
RS-11-143	Altered Uraninite	24.26	<DL	<DL	N/A
RS-11-143	Altered Uraninite	22.67	0.59	<DL	163
RS-11-143	Altered Uraninite	23.88	<DL	<DL	N/A
RS-11-143	Altered Uraninite	23.62	<DL	<DL	N/A
RS-11-143	Uraninite	25.83	3.99	<DL	959
RS-11-143	Uraninite	27.78	4.63	<DL	1034
RS-11-143	Uraninite	26.54	4.03	<DL	943
RS-11-143	Uraninite	27.57	5.24	<DL	1179
RS-11-143	Uraninite	27.73	5.12	<DL	1145
RS-11-143	Uraninite	27.51	4.80	<DL	1082
RS-11-143	Uraninite	27.93	4.69	<DL	1041
RS-11-143	Uraninite	27.91	5.06	<DL	1125
RS-11-143	Uraninite	27.83	5.36	<DL	1195
RS-11-143	Altered Uraninite	22.49	<DL	<DL	N/A
RS-11-143	Altered Uraninite	22.56	<DL	<DL	N/A
RS-11-143	Altered Uraninite	22.18	<DL	<DL	N/A
RS-11-143	Altered Uraninite	23.06	<DL	<DL	N/A
RS-11-143	Altered Uraninite	23.29	<DL	<DL	N/A
RS-11-143	Altered Uraninite	23.08	<DL	<DL	N/A
RS-11-143	Altered Uraninite	22.52	<DL	<DL	N/A
RS-11-143	Altered Uraninite	24.30	<DL	<DL	N/A
RS-11-143	Altered Uraninite	24.56	<DL	<DL	N/A
RS-11-143	Altered Uraninite	23.24	<DL	<DL	N/A
301GC	Coffinite	12.03	0.41	<DL	211
301GC	Coffinite	12.05	<DL	<DL	N/A
301GC	Coffinite	13.91	<DL	<DL	N/A
301GC	Coffinite	13.36	0.08	<DL	37
301GC	Coffinite	8.21	<DL	<DL	N/A
301GC	Coffinite	12.93	0.04	<DL	19
301GC	Coffinite	14.20	<DL	<DL	N/A
301GC	Coffinite	13.15	<DL	<DL	N/A
301GC	Coffinite	9.31	0.03	<DL	20
301GC	Coffinite	14.88	<DL	<DL	N/A
301GC	Coffinite	13.77	<DL	<DL	N/A

Table G.1: Chemical-Pb ages of uranium minerals from the Bong Deposit, Thelon Basin, Nunavut, Canada (U, Pb, and Th data in wt.% from EMPA)

Sample	Mineral	U	Pb	Th	Chemical Pb Age (Ma)
301GC	Coffinite	12.23	<DL	<DL	N/A
301GC	Coffinite	9.15	0.05	<DL	34
301GC	Coffinite	10.27	<DL	<DL	N/A
RS-11-162	Altered Uraninite	22.78	0.14	<DL	38
RS-11-162	Altered Uraninite	22.62	0.12	<DL	33
RS-11-162	Altered Uraninite	23.76	0.20	<DL	52
RS-11-162	Altered Uraninite	23.80	0.16	<DL	42
RS-11-162	Altered Uraninite	23.99	0.19	<DL	49
RS-11-162	Altered Uraninite	24.18	0.18	<DL	46
RS-11-162	Altered Uraninite	24.20	0.20	<DL	51
RS-11-162	Altered Uraninite	23.86	0.17	<DL	44
RS-11-162	Altered Uraninite	24.15	0.19	<DL	49
RS-11-162	Altered Uraninite	24.49	0.25	<DL	63
RS-11-162	Altered Uraninite	25.03	0.16	<DL	40
RS-11-162	Altered Uraninite	25.11	0.16	<DL	40
RS-11-162	Altered Uraninite	24.91	0.18	<DL	45
RS-11-143	Uraninite	26.52	4.05	<DL	948
RS-11-143	Uraninite	27.10	4.53	<DL	1037
RS-11-143	Altered Uraninite	22.54	0.40	<DL	110
RS-11-143	Altered Uraninite	21.29	0.34	<DL	99
RS-11-143	Altered Uraninite	21.64	0.13	<DL	37
RS-11-143	Altered Uraninite	23.17	0.67	<DL	180
RS-11-143	Altered Uraninite	22.53	0.77	<DL	211
RS-11-143	Altered Uraninite	16.90	0.35	<DL	127
RS-11-143	Altered Uraninite	20.98	0.36	<DL	106
RS-11-143	Altered Uraninite	20.17	0.65	<DL	200
RS-11-143	Coffinite	16.29	0.03	<DL	10
RS-11-143	Altered Uraninite	20.05	0.28	<DL	86
RS-11-143	Coffinite	16.63	0.05	<DL	19
RS-11-143	Altered Uraninite	23.89	0.57	<DL	149
RS-11-143	Altered Uraninite	21.39	0.52	<DL	151
RS-11-143	Altered Uraninite	21.47	<DL	<DL	N/A
RS-11-143	Coffinite	18.19	0.08	<DL	27
RS-11-143	Altered Uraninite	23.21	<DL	<DL	N/A
RS-11-143	Altered Uraninite	18.36	<DL	<DL	N/A
RS-11-143	Altered Uraninite	22.95	<DL	<DL	N/A
RS-11-143	Altered Uraninite	22.66	0.06	<DL	17
RS-11-143	Altered Uraninite	23.80	2.42	<DL	630
RS-11-145	Altered Uraninite	17.68	0.42	<DL	146
RS-11-145	Altered Uraninite	20.49	0.98	<DL	296
RS-11-145	Coffinite	15.33	0.93	<DL	376
RS-11-145	Coffinite	13.34	<DL	<DL	N/A
RS-11-145	Coffinite	10.66	0.56	<DL	327
RS-11-172	Coffinite	12.14	0.44	<DL	226

Table G.1: Chemical-Pb ages of uranium minerals from the Bong Deposit, Thelon Basin, Nunavut, Canada (U, Pb, and Th data in wt.% from EMPA)

Sample	Mineral	U	Pb	Th	Chemical Pb Age (Ma)
RS-11-172	Coffinite	15.39	<DL	<DL	N/A
RS-11-172	Altered Uraninite	18.46	<DL	<DL	N/A
RS-11-172	Altered Uraninite	22.69	<DL	<DL	N/A
302GC	Altered Uraninite	23.17	<DL	<DL	N/A
302GC	Altered Uraninite	21.70	0.85	<DL	242
302GC	Coffinite	16.25	<DL	<DL	N/A
302GC	Altered Uraninite	23.12	<DL	<DL	N/A
302GC	Coffinite	16.94	<DL	<DL	N/A
302GC	Coffinite	13.19	<DL	<DL	N/A
302GC	Coffinite	18.48	<DL	<DL	N/A
302GC	Coffinite	12.94	0.03	<DL	17
302GC	Coffinite	16.42	0.11	<DL	42
302GC	Coffinite	18.86	<DL	<DL	N/A
302GC	Coffinite	14.25	<DL	<DL	N/A
302GC	Coffinite	15.38	<DL	<DL	N/A
302GC	Coffinite	16.99	<DL	<DL	N/A
302GC	Coffinite	16.42	0.10	<DL	38
302GC	Altered Uraninite	22.98	0.41	<DL	111
302GC	Coffinite	17.18	<DL	<DL	N/A
302GC	Altered Uraninite	21.41	0.21	<DL	61
302GC	Coffinite	16.27	0.35	<DL	133
301GC	Altered Uraninite	23.44	0.08	<DL	21
301GC	Coffinite	17.32	0.09	<DL	32
301GC	Coffinite	14.03	0.09	<DL	40
301GC	Altered Uraninite	21.84	0.09	<DL	26
301GC	Coffinite	13.29	<DL	<DL	N/A
301GC	Coffinite	17.74	<DL	<DL	N/A
301GC	Coffinite	13.44	0.04	<DL	18
301GC	Coffinite	17.42	0.07	<DL	25
301GC	Coffinite	13.26	0.05	<DL	23
301GC	Coffinite	12.79	0.06	<DL	29
301GC	Coffinite	14.55	0.04	<DL	17
301GC	Coffinite	13.99	0.05	<DL	22
303GC	Altered Uraninite	21.80	0.27	<DL	77
303GC	Altered Uraninite	20.43	0.10	<DL	30
303GC	Coffinite	18.08	<DL	<DL	N/A
303GC	Coffinite	11.43	<DL	<DL	N/A
303GC	Uraninite	27.42	4.51	<DL	1020
303GC	Altered Uraninite	21.51	0.49	<DL	141
303GC	Altered Uraninite	18.79	0.60	<DL	198
303GC	Uraninite	26.37	4.88	<DL	1148
303GC	Uraninite	27.96	4.57	<DL	1014
303GC	Altered Uraninite	24.13	2.16	<DL	555
303GC	Altered Uraninite	25.15	2.73	<DL	673

Table G.1: Chemical-Pb ages of uranium minerals from the Bong Deposit, Thelon Basin, Nunavut, Canada (U, Pb, and Th data in wt.% from EMPA)

Sample	Mineral	U	Pb	Th	Chemical Pb Age (Ma)
303GC	Altered Uraninite	20.88	1.44	<DL	428
303GC	Altered Uraninite	21.23	2.30	<DL	672
303GC	Altered Uraninite	18.00	1.04	<DL	358
303GC	Altered Uraninite	17.72	1.93	<DL	676
303GC	Altered Uraninite	19.05	1.78	<DL	580
303GC	Altered Uraninite	24.08	4.30	<DL	1108
303GC	Altered Uraninite	16.92	0.71	<DL	259
303GC	Altered Uraninite	24.57	3.98	<DL	1004
303GC	Coffinite	14.68	0.73	<DL	309
303GC	Coffinite	14.32	0.24	<DL	105
303GC	Coffinite	11.91	0.37	<DL	190
303GC	Altered Uraninite	23.47	2.68	<DL	708
303GC	Altered Uraninite	14.89	0.68	<DL	283
303GC	Altered Uraninite	25.73	3.13	<DL	754
303GC	Altered Uraninite	16.43	0.60	<DL	225
RS-11-172	Coffinite	14.15	0.66	<DL	291
RS-11-172	Coffinite	16.52	1.76	<DL	660
RS-11-172	Altered Uraninite	26.50	4.10	<DL	960
RS-11-172	Altered Uraninite	21.26	0.48	<DL	140
RS-11-144	Uraninite	21.52	0.18	<DL	52
RS-11-144	Altered Uraninite	19.24	0.10	<DL	33
RS-11-144	Altered Uraninite	23.08	0.15	<DL	41
303GC	Coffinite	15.95	<DL	<DL	N/A
303GC	Coffinite	15.83	<DL	<DL	N/A
303GC	Uraninite	27.35	5.27	<DL	1195
303GC	Altered Uraninite	19.26	<DL	<DL	N/A
303GC	Uraninite	28.12	5.06	<DL	1116
303GC	Altered Uraninite	25.15	3.95	<DL	973
RS-11-142	Coffinite	18.21	<DL	<DL	N/A
RS-11-142	Altered Uraninite	21.97	<DL	<DL	N/A
RS-11-142	Coffinite	14.92	<DL	<DL	N/A
RS-11-142	Altered Uraninite	22.97	<DL	<DL	N/A
RS-11-173	Altered Uraninite	14.15	0.66	<DL	289
RS-11-173	Altered Uraninite	16.52	1.76	<DL	661
RS-11-173	Uraninite	26.50	4.10	<DL	960

*Ages determined using equation [1] ($t = Pb \times 10^{10} / (1.612U + 4.95\ Th)$; Cameron-Schiman 1978)

Appendix H
Lead-Lead Ages for Uraninite

Table H.1: Pb-Pb ages for vein-type uraninite from the Bong Deposit, Thelon Basin, Nunavut, Canada

Sample	$^{207}Pb/^{206}Pb$	Age (Ma)	Error (Ma)
RS-172U-3	0.05797	529	5
RS-172U-2	0.06054	623	7
RS-172U-1	0.06710	841	10
303GCAU-1	0.07168	977	7
303GCAU-3	0.07417	1046	3
RS-172U-4	0.07426	1049	2
RS-143BU-2	0.07480	1063	3
RS-143BU-1	0.07492	1066	3
RS-143BU-3	0.07545	1081	3
RS-143BU-4	0.07616	1099	2
303GCBU-2	0.07642	1106	2
RS-143AU-2	0.07654	1109	3
303GCBU-3	0.07665	1112	6
303GCBU-4	0.07716	1125	3
303GCBU-1	0.07736	1130	3
RS-143AU-1	0.07771	1140	5
RS-143AU-3	0.07800	1147	3
303GCAU-2	0.07779	1147	5
RS-143AU-4	0.07918	1177	4

*Ages determined using equation [5] ($^{207}Pb/^{206}Pb = {}^{235}U/^{238}U * e^{\lambda 2t} - 1 / e^{\lambda 1t} - 1$; Nier 1941).

Table H.2: Pb-Pb ages for roll-front uraninite from the Bong Deposit, Thelon Basin, Nunavut, Canada

Sample	$^{207}Pb/^{206}Pb$	Age (Ma)	Error (Ma)
RS-176BU-7	0.06249	691	25
RS-176BU-4	0.07279	1008	27
RS-176BU-1	0.07309	1017	60
RS-176BU-6	0.07578	1089	27
RS-176BU-12	0.07619	1100	110
RS-176CU-1	0.07648	1108	38
RS-176BU-10	0.07674	1115	90
RS-176BU-2	0.07745	1133	74
RS-176BU-3	0.08123	1227	135
RS-176CU-11	0.08410	1295	38
RS-176BU-5	0.08516	1319	74
RS-176CU-8	0.08549	1327	53
RS-176CU-14	0.08593	1337	76
RS-176CU-5	0.08605	1339	110
RS-176CU-6	0.08688	1358	149
RS-176BU-13	0.08733	1368	88
RS-176BU-11	0.08820	1387	86
RS-176BU-8	0.08827	1389	110
RS-176CU-15	0.08873	1398	52
RS-176CU-4	0.08938	1412	212
RS-176CU-12	0.09134	1454	95
RS-176CU-10	0.09178	1463	123
RS-176BU-9	0.09380	1504	147
RS-176CU-16	0.09748	1576	63
RS-176CU-3	0.09854	1597	30
RS-176CU-13	0.10030	1630	60
RS-176CU-7	0.10414	1699	49
RS-176CU-2	0.11133	1821	104
RS-176CU-9	0.11332	1853	93

*Ages determined using equation [5] ($^{207}Pb/^{206}Pb = {}^{235}U/{}^{238}U * e^{\lambda 2t} - 1 / e^{\lambda 1t} - 1$; Nier 1941).